A NONLINEAR MODEL FOR THE DYNAMICS OF MOORED FLOATING PLATFORMS

Dissertation

submitted to and approved by the

Department of Architecture, Civil Engineering and Environmental Sciences
University of Braunschweig – Institute of Technology

and the

Department of Civil and Environmental Engineering
University of Florence

in candidacy for the degree of a
Doktor-Ingenieur (Dr.-Ing.) /
Dottore di Ricerca in Processes, Materials and Constructions in Civil and Environmental Engineering and for the Protection of the Historic-Monumental Heritage[*)]

by

Alessandro Giusti
born 30/01/1986
from Figline Valdarno, Italy

Submitted on	30/08/2016
Oral examination on	10/11/2016
Professorial advisors	Prof. Claudio Borri Prof. Klaus Thiele

2018

*) Either the German or the Italian form of the title may be used.

to my mum and my dad,
nothing would have been possible without them.

to my big twin brother,
the rational part of me.

Preface

Se venti anni fa mi avessero detto che avrei discusso una tesi di Dottorato probabilmente mi sarei congedato con una grassa risata. Poi la vecchiaia e l'insaziabile curiosità di sapere hanno fatto tutto il resto. Così mi sono catapultato in questa avventura con l'incoscienza del bambino che si tuffa per la prima volta in mare: l'attrazione primordiale dell'ignoto. Tanti i momenti in cui mi sono più volte chiesto se tutto quello che stavo facendo avesse avuto senso e altrettanti altri di vera esaltazione. L'unica certezza è che sono entrato in un processo iterativo che non può convergere, ogni volta che apprendo qualcosa di nuovo divento ancora più consapevole di tutto quello che ancora ignoro e che bramo di conoscere. Non si tratta di essere i migliori, ognuno lo è già a suo modo, si tratta di voler sapere. Spero che il momento in cui dovrò interrompere il processo arrivi il più tardi possibile. Non sempre si può fare ciò che si vuole e neppure ciò che gli altri si aspettano che tu faccia, bensì quello che si ritiene giusto fare. Il Dottorato è stata un'avventura appassionante fatta di atmosfere indimenticabili, di suoni, di odori, di colori, che porterò sempre con me. Ma soprattutto fatta di persone, persone che anche solo per un attimo hanno incrociato la mia vita lasciandone traccia indelebile. Quello che resta è una storia senza tempo, che vi voglio raccontare.

Reggello, 15 giugno 2016

Alessandro

Desidero ringraziare il Professore Claudio Borri per la fiducia incondizionata che mi ha dimostrato durante questo percorso. Un grazie di cuore anche ai Professori Klaus Thiele e Udo Peil che mi hanno supportato e accolto a Braunschweig non mancando mai di farmi sentire come a casa. Desidero inoltre esprimere la mia sincera gratitudine al Professore Olivier Brüls per il suo straordinario aiuto. Allo stesso modo vorrei ringraziare l'Ingegnere Enzo Marino che è stato senza dubbio uno dei punti di riferimento con i suoi suggerimenti e consigli. Il grazie speciale va a tutte le persone con cui ho condiviso tutti questi anni, amici prima che colleghi, hanno reso questa esperienza davvero straordinaria... Tommaso, Gabriele, Michele, Irene, Giovanni, Serena...

If twenty years ago someone had told me I would have defended a Doctorate thesis, probably I would have left him, laughing. Then, old age and curiosity of knowing something new did all the rest. So I catapulted myself into this adventure with the recklessness of the child who dives in the sea for the first time: the primordial attraction of the unknown. There were a lot of moments when I asked myself and asked myself again if what I was doing made sense, just as many moments of real exaltation. The only certainty is that I entered in an iterative process that cannot converge, whenever I learn something new I become more and more aware of what I ignore and I long to know. It is not about being the best, everyone is already the best in his own way, it is about wanting to know. I hope the time to interrupt the process will arrive as late as possible. You cannot always do what you want and not even what the others expect from you, but what you think is right to do. The Doctorate has been a fascinating adventure made of unforgettable atmospheres, of sounds, of smells, of colours, that I will always carry with me. But mostly made up of people, people that even just for a moment crossed my life leaving an indelible mark. What remains is a timeless story that I would like to tell you.

Reggello, June 15$^{\text{th}}$, 2016

Alessandro

I wish to express my gratitude to Professor Claudio Borri for the unconditional trust he demonstrated in me during this route. A big thank also to Professors Klaus Thiele and Udo Peil who supported and welcomed me in Braunschweig letting me feel at home. I wish also to express my sincere gratitude to Professor Olivier Brüls for his extraordinary help. In the same way I would like to thank Engineer Enzo Marino who was undoubtedly one of the reference points with his suggestions and advice. The special thanks goes to all the people with whom I shared all these years, friends before colleagues, they made this experience really amazing... Tommaso, Gabriele, Michele, Irene, Giovanni, Serena...

Abstract

"Questions are never indiscreet,
answers sometimes are."

Oscar Wilde

Among the renewable energies, the exploitation of offshore wind energy in deep waters is becoming more and more important, and it is expected to increase even more because of the intrinsic potential and the large availability of this resource. Deep-water wind turbines are usually installed over moored floating supports. Their dynamics depends on the complex interaction between the system and the environment making the use of numerical models almost inevitable for the design and optimization of such structures. In this context, a nonlinear model for the dynamics of moored floating platforms is developed.

The dynamic problem of the platform is formulated in the framework of the dynamics of rigid bodies, referring to the mixed representation of the motion, which consists in the simultaneous use of two different bases. The formulation is developed for a wide range of loads (forces and torques) with particular attention to the transformations of the state variables. Both follower and non-follower loads are considered. The differential problem is solved with a recently developed time integration algorithm that considers the Lie group structure of the configuration space overcoming some critical aspects associated with the typical use of nautical angles and their time derivatives. The resulting formulation is very general and in principle can be exploited for the study of every system modelled as a rigid body, such as ships and hulls.

The developed dynamic solver can be coupled with other models to study specific problems. In this work the assessment of the loads related to both the mooring system and the hydrodynamic action is addressed. In particular, mooring lines are modelled by means of a quasi-static formulation, whereas wave loads are evaluated with the linear hydrodynamic theory. In general, both the formulations guarantee a satisfying level of accuracy, even though in some specific cases the inertia and damping of the mooring lines as well as higher-order hydrodynamic terms should be included to improve the reliability of the model.

The numerical model is tested against a number of dynamic problems for which the exact analytic solution is known, allowing a detailed assessment of the capabilities of the method. The dynamics of moored floating platforms is then investigated discussing the effect of different strategies of simulation on the system response and the role of the main parameters affecting the motion.

Sommario

"Behind every problem
there is an opportunity."

Galileo Galilei

Tra le energie rinnovabili, lo sfruttamento dell'energia eolica offshore in acque profonde sta diventando sempre più importante e potrebbe crescere ancora visti il potenziale intrinseco e la grande disponibilità di questa risorsa. Gli aerogeneratori in acque profonde sono solitamente installati su supporti galleggianti ancorati al fondale. La loro dinamica dipende dalla complessa interazione tra il sistema e l'ambiente, che rende inevitabile il ricorso a modelli numerici per la progettazione e ottimizzazione di queste strutture. In quest'ambito, si presenta un modello non lineare per la dinamica di piattaforme galleggianti ancorate al fondale.

Il problema dinamico della piattaforma è formulato nell'ambito della dinamica dei corpi rigidi, con riferimento a una rappresentazione mista del moto che si basa sull'uso simultaneo di due diverse basi. La formulazione è sviluppata per un'ampia gamma di carichi (forze e coppie) con particolare attenzione alle trasformazioni delle variabili di stato. Sono considerati i carichi sia *follower* che *non-follower*. Il problema differenziale è risolto con un algoritmo di integrazione nel dominio del tempo recentemente sviluppato che sfrutta la struttura dei gruppi di Lie dello spazio delle configurazioni, superando alcune criticità associate al tipico uso degli angoli nautici e delle loro derivate. La formulazione risultante è molto generale e in principio può essere utilizzata per lo studio di qualsiasi sistema schematizzabile come corpo rigido, come barche e scafi.

Il solutore dinamico sviluppato può essere accoppiato con altri modelli per lo studio di problemi specifici. In questo lavoro sono valutati i carichi legati al sistema di ormeggio e all'azione idrodinamica. In particolare, gli ancoraggi sono modellati con una formulazione quasi-statica mentre per l'azione delle onde si fa riferimento alla teoria idrodinamica lineare. In generale, entrambe le formulazioni garantiscono un soddisfacente livello di accuratezza, sebbene in alcuni casi specifici l'inerzia e lo smorzamento dei cavi così come i termini idrodinamici di ordine superiore dovrebbero essere inclusi per migliorare l'affidabilità del modello.

Il modello numerico è testato su una serie di problemi dinamici per i quali è nota l'espressione analitica della soluzione, permettendo una dettagliata valutazione delle capacità del metodo. La dinamica delle piattaforme offshore ancorate al fondale è quindi studiata discutendo l'effetto di diverse strategie di simulazione sulla risposta del sistema e il ruolo dei principali parametri che condizionano il moto.

Kurzfassung

"If you can't explain it simply,
you don't understand it well enough."

Albert Einstein

Die Bedeutung von Offshore-Windenergie unter den erneuerbaren Energieträgern nimmt momentan stark zu und weitere Zuwächse werden aufgrund der weiten Verfügbarkeit dieser Energiequelle und ihres intrinsischen Potenzials erwartet. Windkraftanlagen in Tiefwasser werden normalerweise mittels schwimmenden Offshore-Fundamenten am Meeresboden verankert. Ihr dynamisches Verhalten hängt von der komplexen Interaktion zwischen dem System und der Umgebung ab, weshalb numerische Modelle unerlässlich für die Entwicklung und Optimierung solcher Strukturen sind. Daher wird ein nichtlineares Modell zur Beschreibung des dynamischen Verhaltens von schwimmenden Offshore-Fundamenten vorgestellt.

Dafür wird ein analytischer Ansatz aus dem Bereich der Dynamik starrer Körper unter Verwendung einer gemischten Darstellung der Bewegung entwickelt. Dieser Ansatz berücksichtigt eine große Bandbreite an Belastungen (Kräfte und Momente) unter Beachtung der Transformation der Zustandsvariablen. Dabei werden sowohl Lasten mit raumfesten als auch mit veränderlichen Wirkrichtungen berücksichtigt. Die Lösung des Differentialgleichungssystems erfolgt mittels eines Zeitintegrationsverfahrens, das die Struktur der Lie-Gruppe des betrachteten Raumes berücksichtigt und eine Vereinfachung in Bezug auf die allgemein verwendeten Eulerschen Winkel darstellt. Der resultierende Ansatz ist allgemeingültig und kann prinzipiell auf jedes beliebige, als starrer Körper modellierte System angewendet werden.

Der dynamische Gleichungslöser wird mit zusätzlichen Modellen zur Ermittlung der, von der Verankerung verursachten, Reaktionskräfte und -momente und der Beanspruchung durch hydrodynamische Lasten gekoppelt. Dabei werden die Ankertrossen mittels eines quasi-statischen Ansatzes modelliert und die Belastung durch Wellen wird nach der linearen hydrodynamischen Theorie bestimmt. Generell liefern beide Ansätze eine hohe Genauigkeit, in einigen Spezialfällen sollten die Massenträgheit und Dämpfung der Verankerung sowie hydrodynamische Terme höherer Ordnung zur Verbesserung des Modells berücksichtigt werden.

Das numerische Modell wird anhand einer Reihe dynamischer Problemstellungen mit exakten, analytischen Lösungen validiert, wodurch die allgemeingültige Anwendbarkeit der Methode belegt wird. Abschließend wird das dynamische Verhalten von schwimmenden Offshore-Fundamenten hinsichtlich verschiedener Simulationsstrategien

und des Einflusses der Hauptparameter auf die Bewegung untersucht.

Contents

List of symbols

The dimensions of the quantities listed below are indicated by a symbolic convention regardless of the system of measure adopted, namely: M = *mass;* L = *length;* T = *time;* F = *force;* R = *angle;* • = *the dimension depends on the element of the vector, tensor, matrix considered;* - = *dimensionless.*

Letters

a	length of the parallelepiped along the x'-axis	[L]
A	anchor	[-]
A_0	cut water-plane area	[L^2]
b	length of the parallelepiped along the y'-axis	[L]
B	center of buoyancy	[-]
c	length of the parallelepiped along the z'-axis	[L]
C	geometric center of an element of area	[-]
C	reference point of the hydrodynamic operators in the framework of the linear theory	[-]
d	water depth	[L]
D_c	diameter of the mooring line	[L]
EA	extensional stiffness	[F]
f	frequency	[T^{-1}]
f_p	peak frequency	[T^{-1}]
F	amplitude of the sinusoidal force	[F]
F	fairlead	[-]
g	gravity acceleration magnitude	[$\mathrm{L}\cdot\mathrm{T}^{-2}$]
G	center of mass	[-]
G_f	geometric center of the fairleads	[-]
G_p	geometric center of the parallelepiped platform	[-]
G_{wl}	projection of the center of mass onto the sea water plane	[-]
h	time step size	[T]
H_s	significant wave height	[L]
j	imaginary unit, $j^2 = -1$	[-]
k	wave number	[$\mathrm{R}\cdot\mathrm{L}^{-1}$]
l	length of the mooring line	[L]
l_b	portion of the mooring line resting on the seabed	[L]
l_s	suspended portion of the mooring line	[L]
m	mass of the body	[M]
m_η^n	spectral moment of order n	[•]

n	generic number of elements	[-]
N	arbitrary pole	[-]
N	number of superimposed regular waves	[-]
O	arbitrary reference point of a body	[-]
O	origin of the spatial (inertial) reference frame	[-]
O'	origin of the body-attached (non-inertial) reference frame	[-]
O''	origin of the local reference frame	[-]
p	pressure	$[\mathrm{F}\cdot\mathrm{L}^{-2}]$
P	material point of a body	[-]
r	radius	[L]
$R_{\eta\eta}$	autocorrelation of the wave elevation	$[\mathrm{L}^2]$
S	closed surface of an arbitrary region of the fluid	$[\mathrm{L}^2]$
S_0	wetted surface of the body	$[\mathrm{L}^2]$
S_{JS}	Jonswap spectrum	$[\mathrm{L}^2\cdot\mathrm{T}]$
S_{PM}	Pierson-Moskowitz spectrum	$[\mathrm{L}^2\cdot\mathrm{T}]$
$S_{\eta\eta}$	spectral density of the sea surface elevation	$[\mathrm{L}^2\cdot\mathrm{T}]$
t	time	[T]
T	amplitude of the sinusoidal torque	$[\mathrm{F}\cdot\mathrm{L}]$
T	period of the regular wave	[T]
T_1	average wave period	[T]
T_c	average period between response maxima	[T]
T_p	peak period	[T]
T_{sim}	total time of simulation	[T]
T_t	time window of the linear scaling procedure	[T]
T_z	mean zero-crossing wave period	[T]
U	potential of the gravitational field	$[\mathrm{L}^2\cdot\mathrm{T}^{-2}]$
V	volume of the rigid body	$[\mathrm{L}^3]$
V	volume of an arbitrary region of the fluid	$[\mathrm{L}^3]$
V_0	submerged volume of the body	$[\mathrm{L}^3]$
w	apparent weight in fluid per unit length	$[\mathrm{F}\cdot\mathrm{L}^{-1}]$
$X^{(\bullet)}$	Fourier coefficients of the quantity $(\bullet)$	$[\bullet]$
α_f	algorithmic parameter of the generalized-α method	[-]
α_m	algorithmic parameter of the generalized-α method	[-]
β	algorithmic parameter of the generalized-α method	[-]
β	wave direction	[R]
γ	algorithmic parameter of the generalized-α method	[-]
ϵ	spectral broadness	[-]
ε	random phase	[R]
ζ	wave amplitude	[L]
η	sea surface elevation	[L]
$\bar{\eta}$	mean wave amplitude	[L]
$\eta_{1/3}$	significant wave amplitude	[L]
μ	dynamic viscosity	$[\mathrm{M}\cdot\mathrm{L}^{-1}\cdot\mathrm{T}^{-1}]$
μ_c	mass per unit length of the mooring line	$[\mathrm{M}\cdot\mathrm{L}^{-1}]$
μ_η	mean value of the sea surface elevation	[L]
ν	damping factor	[-]
ξ_b	seabed friction coefficient	[-]

ρ	density	[M·L^{-3}]
ρ	spectral radius (control parameter of the numerical damping)	[-]
ρ_w	water density	[M·L^{-3}]
ϕ	amplitude of the rotation	[R]
Φ	velocity potential of inviscid-incompressible fluids with irrotational flow	[L^2·T^{-1}]
φ_i	Tait-Bryan (or nautical) angles, with $i = 1, 2, 3$	[R]
ω	circular frequency	[R·T^{-1}]
ω_n	undamped natural angular frequency	[R·T^{-1}]

Vectors

$\mathbf{a}$	acceleration of a material point	[L·T^{-2}]
$\mathbf{b}$	body forces per unit mass	[L·T^{-2}]
$\mathbf{e}_i$	orthonormal basis	[-]
$\mathbf{F}^{(\bullet)}_{(\diamond)}$	force applied to point ($\diamond$) and expressed with respect to the basis ($\bullet$)	[F]
$\mathbf{F}^{diff}$	first-order diffraction load (force and torque)	[$\bullet$]
$\mathbf{F}^{f}_{(\diamond)}$	follower force applied to point ($\diamond$)	[F]
$\mathbf{F}^{hyd}$	hydrodynamic load (force and torque)	[$\bullet$]
$\mathbf{F}^{hys}$	first-order hydrostatic load (force and torque)	[$\bullet$]
$\mathbf{F}^{moor}$	force exerted on the floating body by the mooring system	[F]
$\mathbf{F}^{nf}_{(\diamond)}$	non-follower force applied to point ($\diamond$)	[F]
$\mathbf{F}^{rad}$	first-order radiation load (force and torque)	[$\bullet$]
$\mathcal{F}$	resultant of external forces	[F]
$\mathbf{g}$	gravity acceleration	[L·T^{-2}]
$\mathbf{H}_{(\bullet)}$	angular momentum with respect to the pole ($\bullet$)	[M·L^2·T^{-1}]
$\mathbf{n}$	unit outward normal to a surface element dS	[-]
$\mathbf{p}$	generic vector quantity	[$\bullet$]
$\hat{\mathbf{q}}$	position state variable associated with the mixed representation of the motion ($\in \mathbb{R}^3 \times SO(3)$, non-vectorial nature)	[$\bullet$]
$\bar{\mathbf{q}}$	position state variable associated with the local representation of the motion (non-vectorial nature)	[$\bullet$]
$\mathbf{Q}$	linear momentum	[M·L·T^{-1}]
$\hat{\mathbf{r}}$	residual associated with the mixed representation of the motion	[$\bullet$]
$\bar{\mathbf{r}}$	residual associated with the local representation of the motion	[$\bullet$]
$\mathbf{T}^{(\bullet)}_{(\diamond)}$	torque about the point ($\diamond$) and expressed with respect to the basis ($\bullet$)	[F·L]
$\mathbf{T}^{f}_{(\diamond)}$	follower torque about the point ($\diamond$)	[F·L]
$\mathbf{T}^{moor}$	torque exerted on the floating body by the mooring system	[F·L]
$\mathbf{T}^{nf}_{(\diamond)}$	non-follower torque about the point ($\diamond$)	[F·L]
$\mathcal{T}_{(\diamond)}$	resultant torque of external forces about to the pole ($\diamond$)	[F·L]
$\mathbf{u}$	unit eigenvector of the rotation matrix	[-]
$\mathbf{v}$	velocity of a material point	[L·T^{-1}]

$\hat{\mathbf{v}}$	velocity state variable associated with the mixed representation of the motion	[•]
$\bar{\mathbf{v}}$	velocity state variable associated with the local representation of the motion	[•]
$\hat{\dot{\mathbf{v}}}$	acceleration state variable associated with the mixed representation of the motion	[•]
$\bar{\dot{\mathbf{v}}}$	acceleration state variable associated with the local representation of the motion	[•]
$\mathbf{w}$	generic vector quantity	[•]
$\mathbf{x}$	position of a material point	[L]
$\mathbf{X}$	transfer (complex) function of the wave-excitation load per unit wave amplitude	[•]
$\mathbf{z}$	generic vector quantity	[•]
$\boldsymbol{\theta}$	incremental rotation	[R]
$\boldsymbol{\psi}$	rotational vector	[R]
$\boldsymbol{\omega}$	angular velocity	[R·T^{-1}]
$\dot{\boldsymbol{\omega}}$	angular acceleration	[R·T^{-2}]

Matrices

$\mathbf{A}^{(\bullet)}$	matrix associated with a non-follower linear transformation of the quantity (•), i.e. defined in the spatial (inertial) frame	[•]
$\mathbf{A}^{(\bullet)}_{(\diamond)}$	matrix associated with a non-follower linear transformation of the quantity (•) applied to point ($\diamond$)	[•]
$\hat{\mathbf{A}}^{(\bullet)}$	matrix $\mathbf{A}^{(\bullet)}$ expressed in the framework of the mixed representation of the motion	[•]
$\bar{\mathbf{A}}^{(\bullet)}$	matrix $\mathbf{A}^{(\bullet)}$ expressed in the framework of the local representation of the motion	[•]
$\mathbf{B}^{(\bullet)}$	matrix associated with a follower linear transformation of the quantity (•), i.e. defined in the body-attached frame	[•]
$\mathbf{B}^{(\bullet)}_{(\diamond)}$	matrix associated with a follower linear transformation of the quantity (•) applied to point ($\diamond$)	[•]
$\hat{\mathbf{B}}^{(\bullet)}$	matrix $\mathbf{B}^{(\bullet)}$ expressed in the framework of the mixed representation of the motion	[•]
$\bar{\mathbf{B}}^{(\bullet)}$	matrix $\mathbf{B}^{(\bullet)}$ expressed in the framework of the local representation of the motion	[•]
$\mathbf{C}^t$	tangent damping operator	[•]
$\mathbf{D}$	hydrodynamic damping matrix	[•]
$\mathbf{D}^{ker}$	radiation-retardation kernel	[•]
$\mathbf{J}$	tensor of inertia of the body	[M·L^2]
$\mathbf{K}^{hys}$	hydrostatic stiffness matrix	[•]
$\mathbf{K}^t$	tangent stiffness operator	[•]
$\mathbf{M}^A$	hydrodynamic added mass matrix	[•]
$\mathbf{M}^t$	tangent inertia operator	[•]
$\mathbf{R}$	rotation operator	[-]

$\mathbf{T}$	tangent operator of the Lie group $SO(3)$	[-]
$\mathbf{T}$	stress tensor of the fluid	[F·L^{-2}]
$\hat{\mathbf{T}}^{(\bullet)}_{(\diamond)}$	transport transformation of the operator $(\bullet)$ applied to point $(\diamond)$, in the framework of the mixed representation of the motion	[$\bullet$]
$\bar{\mathbf{T}}^{(\bullet)}_{(\diamond)}$	transport transformation of the operator $(\bullet)$ applied to point $(\diamond)$, in the framework of the local representation of the motion	[$\bullet$]

Operators

$\dot{(\bullet)}$	first time derivative of the quantity $(\bullet)$	[T^{-1}]
$\ddot{(\bullet)}$	second time derivative of the quantity $(\bullet)$	[T^{-2}]
$\widetilde{(\bullet)}$	skew-symmetric matrix associated with the vector cross product of the quantity $(\bullet)$	[-]
$(\bullet)^T$	transpose of the matrix (vector) $(\bullet)$	[-]
$D_{(\bullet)}(\diamond)$	directional derivative of the quantity $(\diamond)$ with respect to the quantity $(\bullet)$	[$\bullet$]
∇	differential vector operator	[L^{-1}]

Symbol conventions

$(\bullet)_0$	initial value of the quantity $(\bullet)$
$(\bullet)_0$	quantity $(\bullet)$ in the reference configuration
$(\bullet)^B$	quantity $(\bullet)$ observed in the body-attached (non-inertial) frame
$(\bullet)^I$	quantity $(\bullet)$ observed in the spatial (inertial) frame
$(\bullet)^L$	quantity $(\bullet)$ observed in the local frame
$(\bullet)^{\mathcal{L}}$	quantity $(\bullet)$ expressed with respect to the basis $\mathcal{L}$
$(\bullet)^{\mathcal{M}}$	quantity $(\bullet)$ expressed with respect to the (rotating) basis $\mathcal{M}$
$(\bullet)^{\mathcal{S}}$	quantity $(\bullet)$ expressed with respect to the (fixed) basis $\mathcal{S}$
$(\bullet)^{(\diamond),(\circ)}$	quantity $(\bullet)$ observed in the frame $(\diamond)$ and expressed with respect to the basis $(\circ)$
$(\bullet)_{(\diamond)}$	quantity $(\bullet)$ referred to point $(\diamond)$
$(\bullet)_{(\diamond),i}$	i-th component of the quantity $(\bullet)$ referred to point $(\diamond)$
$(\bullet)_{i:j}$	subvector of the vector $(\bullet)$ with elements $(\bullet)_k$, such that $k = i, i+1, \ldots, j$
$(\bullet)_{i:j\times l:m}$	submatrix of the matrix $(\bullet)$ with elements $(\bullet)_{hk}$, such that $h = i, i+1, \ldots, j$ and $k = l, l+1, \ldots, m$
$\mathcal{C}$	configuration of the body
$\mathcal{C}_0$	reference configuration
$\mathcal{C}_v$	varied configuration of the body
$\mathcal{L}$	basis of the local reference frame
$\mathcal{M}$	basis of the body-attached (non-inertial) reference frame
$\mathcal{S}$	basis of the spatial (inertial) reference frame

Chapter 1

Introduction

"I am always ready to learn,
although I do not always like being taught."

Winston Churchill

The topic of the research activity is presented and discussed in the context of offshore wind energy in deep waters. The chapter aims at addressing the reader to the dissertation.

Global warming is more and more attracting interest of many researchers as well as many governments all over the world. The common objective is to reduce the gas emissions responsible of the greenhouse effect, in particular the emissions related to the combustion of fossil fuels, widely used to produce energy (electrical, mechanical, etc.) since the Industrial Revolution. Renewable energies are promising alternatives to traditional sources (fossil fuels and nuclear power) and limit the emissions of greenhouse gases. The most common renewable resources used to produce energy include sunlight, wind, waves, tides, flowing water, geothermal heat, biomass and biological processes. However, the exploitation of these alternative sources requires the development of specific as well as efficient and economic technologies. In this scenario, wind energy is very promising and gained over the years a primary role.

This research concerns offshore wind turbines in deep waters and is focused on the numerical modelling of moored floating devices, widely used as supports of the wind turbines for deep-water purposes. In the following, first of all, offshore wind turbines are introduced describing their main features, with particular attention to the supports, the dynamic analysis, and the design problem. The topic of the research is finally discussed.

1.1 Offshore wind turbines

Wind energy is one of the most important resources in the renewable energy sector as confirmed by the almost constant growth of the installed power during the last decade [28, 38], and it is expected to maintain a primary role for many years in the future. Recent statistics [28] on the total installed power capacity in Europe, highlight wind energy as the first renewable energy technology (15.6%) and the absolute third energy resource after gas (21.1%) and coal (17.5%). Offshore wind energy is registering a very fast growth. In 2015 new installations and investments doubled with respect to 2014, whereas the onshore market decreased [28]. This is probably due to both the saturation of onshore available sites and the perspective of offshore wind energy exploitation. Offshore sites usually guarantee higher mean wind speeds and less turbulent fields than onshore sites. Moreover, if wind farms are built quite far from the shore, also the visual and noise pollution can be mitigated. However, the ocean (marine) ecosystem is inevitably perturbed.

The exploitation of shallow-water wind energy is not always possible and feasible both for geographic (morphology of the sites) and environmental reasons. In fact, a lot of available sites all around the Europe, but not only, are characterized by either a continental slope close to the coast or a very steep continental shelf, so that the available shallow-water sites are a very narrow stripe. Since the construction of an offshore wind farm very close to the shore is rarely feasible, mainly for the environmental impact of such constructions, the only chance is to move into deep-water sites. Depending on the water depth, several concepts of offshore support structures were proposed for wind engineering purposes. The floating platform concept (with mooring lines) was evaluated to be the most economical type of support for deep-water installations [46], whereas other concepts, such as bottom-fixed wind turbines, are only feasible in shallow waters.

For these reasons, the study of the dynamics of moored floating platforms has a prominent importance in the renewable energy scenario and requires tools able to face the complex problem of interaction between the system and the loads (environment). The main sources of load on an offshore wind turbine (see Figure 1.1) are generally

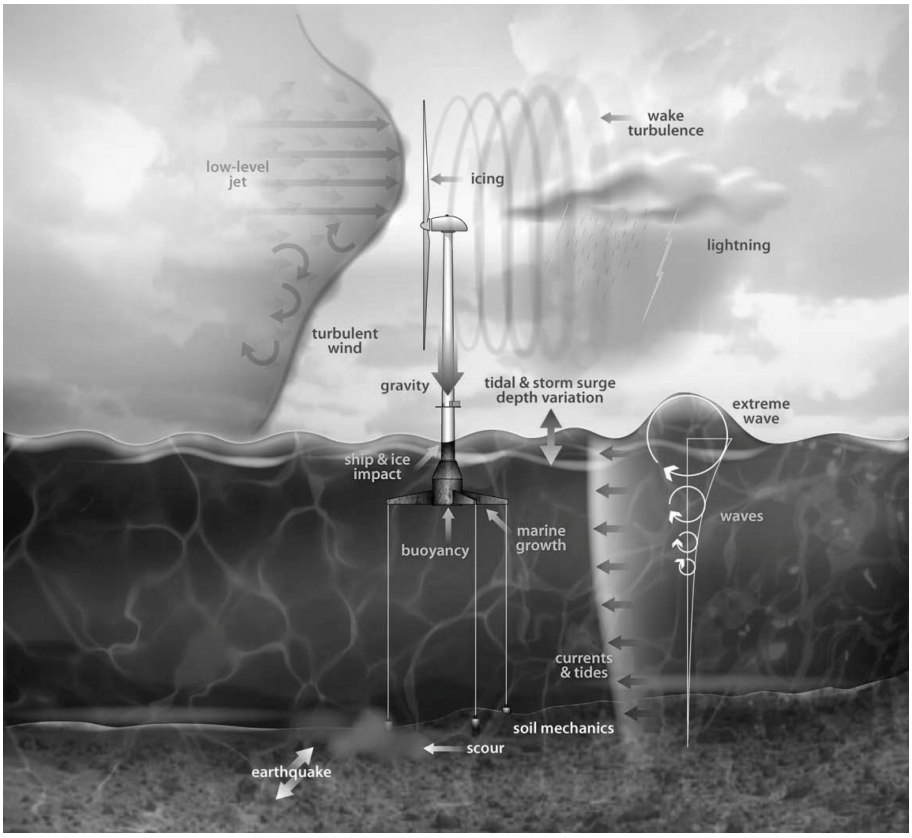

Figure 1.1: Loads on an offshore wind turbine. Source: NREL [58, 67].

gravity, waves, and wind[1] actions, but other environmental loads could also be relevant, such as marine currents, earthquakes, tides, ice, lighting. These loads should be included in the models considering the reciprocal interaction with the structure as well as the correlation between different actions (like wind and waves).

1.1.1 Wind turbine components

Wind turbines are systems designed to convert the kinetic energy of an air flow, like the wind, into mechanical energy of a rotating shaft, which can eventually be converted in electrical power through the so called generator. On the basis of the orientation of the rotor axis, wind turbines can be classified into two main concepts that refer to different technical and technological solutions, i.e. vertical-axis and horizontal-axis wind turbines. Vertical-axis wind turbines usually permit to place the generator close to the ground and do not need any yaw mechanism [27]. However, they have some drawbacks that make this concept less attractive than horizontal-axis wind turbines. In

[1]Wind action and aerodynamic effects are significant in operational conditions. By contrast, if the wind turbine is in parked condition, as it happens in extreme wind and sea states, the loads acting on the structure above the sea water level (tower, nacelle, rotor) are very limited because of the safety configuration of the blades that limits the overall thrust on the rotor.

particular, the maintenance of the main bearing requires the disassembly of the whole turbine and the rotor is too much close to the ground where the wind is of poor quality [27]. Horizontal-axis wind turbines are the most widespread and consist of the following main parts:

- *rotor*. This is the device that converts the kinetic energy into mechanical energy. It consists of a number of blades with a particular streamlined asymmetrical shape (like the wings of an aircraft) twisted along the blade axis. Upwind rotors (most common) face the wind in front of the tower, whereas downwind rotors are placed on the tower shade so that the incoming flow is affected by the wake due to the presence of the tower and nacelle [27]. The number of blades can vary from one to several (rotors with high solidity); however, the three-bladed concept is the most widely used because it allows the limitation of both the fluctuation of the loads (inertia effects) and the thrust at high wind speeds [27]. Horizontal-axis rotors should be aligned with the main direction of the wind, so that the wind is orthogonal to the rotor plane [27];

- *nacelle*. This part of the wind turbine is placed on the top of the tower and encloses the devices for the transmission and conversion of mechanical energy, i.e. the main shaft, the main bearing and the generator, and other apparatuses such as the gearbox, the breaking system, and the control system;

- *tower*. This is the structure that keeps the rotor several meters above the sea (or more in general the ground) where the wind properties, in terms of mean velocity and turbulence, are better than near the sea surface. The tower is the support of both the rotor and the nacelle and should withstand all the loads transmitted by the supported devices. It is usually made of steel, but there are also cases of concrete structures. Towers can be either tubular or lattice structures, but tubular conic towers are undoubtedly the most common [27];

- *foundation*. This is the part of the system that supports the tower and transfers the loads to the ground. Onshore wind turbines usually have slab or pile reinforced concrete foundations (depending on the geotechnical properties of the soil), whereas for offshore employments the foundations are much more complex because they should withstand the hydrodynamic loads keeping the tower in a stable position. Depending on the water depth, several support concepts were developed, like piled structures or moored floating platforms (see Section 1.1.2). The foundation of offshore wind turbines can be split into two main subsystems: the actual foundation, i.e. the structure inside or close to the ground, and the submerged (or semi-submerged) support;

- *control system*. This is an almost invisible part of the device, it consists of a set of sensors and algorithms that control the operational state of the wind turbine on the basis of both environmental conditions and system response. The main objectives of the control system are the optimization of the power conversion and the safety of structures and devices. In particular, wind turbines are usually designed to optimize the power for low wind speeds, which represent the ordinary condition, whereas high wind speeds generally require a limitation of the power to avoid damages on the system [27]. The main strategies of power control are

the stall control, pitch control, and active stall control [27]. For instance, the modification of the pitch angle of blades changes the angle of attack between the wind and the chord line, and thus the lift and drag coefficients. Moreover, the control system has an active role for the safety of wind turbines. It monitors a set of parameters, such as the wind speed, rotor speed, vibrations, temperatures, and, in case of failure, it activates the protection procedures to ensure that all the parameters stay within their design range. For further discussions on the control system the reader is addressed to the references [14, 27].

The focus of this thesis is on the analysis of moored floating supports. Therefore, in the following a more comprehensive description of the supports is given, whereas for further details regarding the structure above the sea level (tower, nacelle, rotor), which is not a specific object of this work, the reader is addressed to the references [14, 26, 27, 41, 42], among others.

1.1.2 Supports

Offshore wind turbines should be properly connected to the seabed in order to achieve the stability of the system under a wide range of environmental loads. Foundations are usually either piled or gravity based, or a combination of them. The piles are drilled on the seabed reaching the soil layers with adequate mechanical characteristics to withstand the loads transmitted by the support by means of the pile tip resistance and the friction along the pile walls. By contrast, gravity foundations withstand the loads with their own dead weight and are designed to avoid tensile loads at the seabed-foundation interface.

Support concepts for offshore wind turbines are usually identified by the technical solution used for achieving the stability of the system. In particular, the most common solutions include piled structures (monopile, tripod, lattice), gravity-based structures, skirt and bucket structures, moored floating structures [26]. The floating concept is the most suitable for deep-water employments [46] and, under certain depths, it is the only feasible kind of support. In fact, the other typical substructures, widely used in shallow-water sites, for depth larger than about fifty meters (even less) have technical difficulties and require non-competitive economical efforts.

1.1.2.1 Floating platform concepts

Floating supports basically are platforms anchored to the seabed by mooring lines and can be classified into three main concepts (see Figure 1.2) on the basis of the strategy used for achieving the stability, namely [15, 46, 48]:

- *ballast stabilized*. The stability is achieved by means of ballast weights, placed below a central buoyancy tank, that lower the location of the overall center of mass so that pitch and roll motions are opposed by both righting moments and inertial resistance. Heave motions are generally offset by the buoyancy, whereas sway, surge, and yaw displacements can be constrained only with a mooring system (catenary). For instance, spar-buoy platforms refer to this concept;

- *mooring line stabilized*. The stability is achieved by means of the mooring line tension. This kind of support does not require large or heavy platforms, and moorings are usually shorter than the lines used for the other concepts, even if they have to withstand higher tensile stresses, which affect also the design of

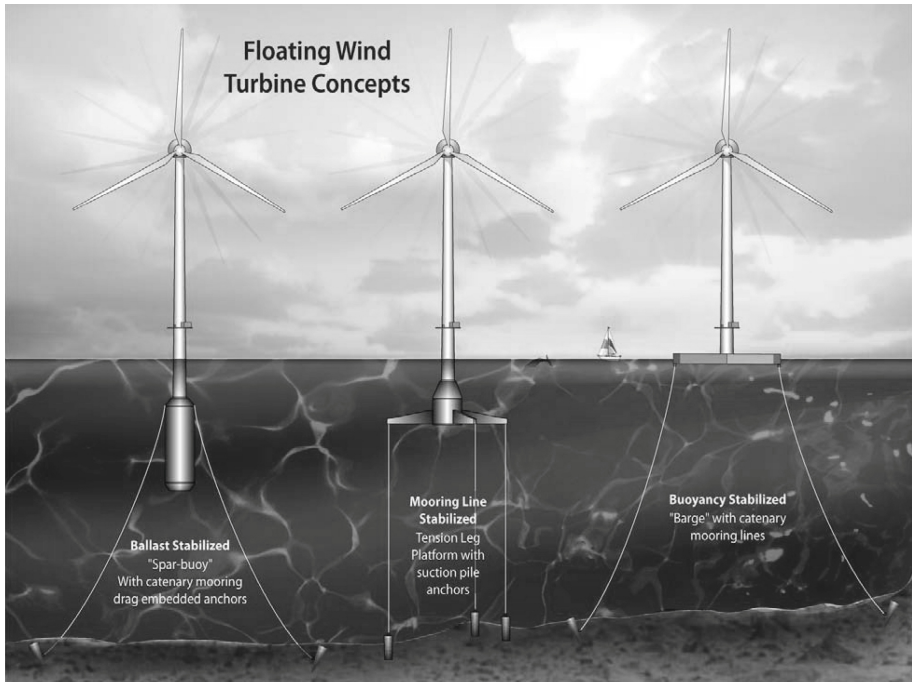

Figure 1.2: Floating support concepts for offshore wind turbines. Source: NREL [45, 49].

platform and anchors. For instance tension leg platforms (TLP) refer to this concept;

- *buoyancy stabilized*. The stability is achieved by means of the distributed buoyancy. Roll and pitch motions are opposed by the righting moment related to the extension of the platform on the water plane. Mooring lines should provide the station-keeping. This kind of support is sensitive to waves and can experience large motions (especially rotations), which can affect the design of the turbine. For instance barge floating platforms refer to this concept.

The designed platform is usually a hybrid solution, i.e. a combination of these main concepts (principles), which minimizes the costs respecting the technical requirements; hence, it is necessarily a compromise [15]. This research is focused on the analysis of moored floating platforms mainly based on the buoyancy stabilized concept, even if the models introduced can also be used for the study of the other floating support concepts.

1.1.2.2 Design of the support concept

The design of an offshore wind turbine is mainly driven by economic targets, which are not only related to the cost of the turbine itself but should also account for the higher costs associated with the support (foundation), the operation, and maintenance as well as the grid connection [15, 65]. The economical feasibility is usually assessed on the basis of the overall architecture of the floating platform roughly established with a first-order static stability analysis [15]. Many aspects contribute to the final design:

support, mooring lines, anchors, installation, decommissioning, maintainability, corrosion resistance, depth independence, sensitivity to bottom condition, wave sensitivity, minimum footprint [15].

The support should guarantee that the displacements (oscillations) of the rotor are within the design range. This is a complex task of wind-wave-structure interaction, which requires accurate tools to be properly evaluated. For this reason, even the choice of design tools and methods could affect the final solution and should then be properly weighed up. Moreover, since also the weight of the supported structure (tower, nacelle, rotor) influences the size of the support, many research studies are focused on the design of lighter structures as well as on the increase of the admissible displacements [15]. A very interesting aspect is the use of control procedures, i.e. active variation of the configuration of the system, to reduce both the loads and the displacements [15]. For further discussions on design challenges of offshore wind turbines the reader is addressed to the references [15, 65].

1.1.3 Numerical analyses

As introduced in the previous section, the analysis of a floating wind turbine is a complex problem of wind-wave-structure interaction and requires advanced numerical tools able to properly understand the fully coupled response. Design standards, for instance IEC 61400 [41, 42], require the analysis of several design load cases that should reproduce particular situations during the life of the turbine, both normal and extreme conditions. The study of such load cases implies a high number of simulations (hundreds, even thousands) that should be carried out in a reasonable time. The computational effort is a basilar aspect since the simulations are necessary not only for the optimization of the project but also for the certification procedure [23]. The dynamic analysis of a floating wind turbine can be performed by means of two different but not equivalent approaches, namely:

- *frequency-domain analyses.* They can be useful for a preliminary feasibility study. The main limit relates to the impossibility of gathering nonlinear dynamic characteristics or properly modelling the transients associated with some loading procedures (such as start and stop) [23, 46, 58];

- *time-domain analyses.* They can capture the nonlinear nature of the dynamics of floating wind turbines with a level of accuracy that mainly depends on the approach (formulation) used to model the dynamic problem.

Time-domain solvers are based on three main approaches or a combination of them[2], namely: modal representation, multibody systems, finite elements [23]. Modal representation requests the lower computational effort but has some drawbacks that make the approach unreliable for offshore applications. In particular, the method cannot properly capture large motions since the structural response is obtained as a linear combination of modal shapes, and the number of degrees of freedom is usually too low [23]. By contrast, a multibody approach, based on the subdivision of the structure into a number of rigid and flexible bodies coupled to each other, permits to increase the degrees of freedom and to consider the nonlinearity of the system dynamics, while maintaining

[2]The FAST model employs a combined modal and multibody dynamic formulation, using both rigid bodies and flexible bodies [47].

a good computational efficiency. Finite element modelling allows the achievement of the highest level of detail (also material nonlinearities can be considered) but needs a substantial computational effort [23].

1.1.3.1 Available computational tools

Many computational tools are available for time-domain analyses of offshore wind turbines. The most popular is FAST (Fatigue, Aerodynamics, Structures, and Turbulence) developed by NREL [47], widely used by the scientific research community. A non-exhaustive list of available codes can be found in [23] with some details on the theoretical approaches used for modelling structural dynamics, aerodynamics, hydrodynamics, and mooring lines, and a very interesting code-to-code comparison. Moreover, many research groups all over the world have their own code developed for addressing specific problems with a higher level of detail. However, their field of application is either very limited or not well-defined.

Generally, all such codes are almost equivalent in terms of hydrodynamic formulation since they are mostly based on the linear theory (in some cases associated with Morison's equations) with some corrective factors. By contrast, moorings are modelled in several ways, either with a finite element model or with a quasi-static theory, or simply by means of a nonlinear spring placed at the fairlead locations. All these codes appear like a black-box, and they can be safely used only for the specific problems they were designed for. The absence of detailed information regarding the implementation and the use of some loose assumptions make the application or the extension of such codes to the solution of new fundamental problems quite difficult, with the high risk of generating huge errors.

Important limitations are present both in the basic assumptions of formulations, for example the assumption of small rotations of the floating support (for instance, in FAST) is not consistent with the intrinsic nature of such devices, and in the algorithms addressing the dynamic problem. The latter is for example the case of the use, quite common in naval engineering, of Euler angles that leads to less efficient computational tools. In fact, the use of Euler angles (three parameters) is always associated with mathematical singularities[3] in the description of rotations and, more important, leads to highly nonlinear dynamic equations, completely far from the intrinsic nature of the motion[4] [86]. The use of redundant parameters (i.e. overall number greater than three) allows us to remove the singularities and to reduce the degree of nonlinearity [86].

However, the best way of improving the whole formulation seems to be the use of the so called geometric methods. These methods, in spite of the use of a global minimal parametrization, do not alter the dynamic equations and do not suffer all the drawbacks related to the introduction of redundant parameters, in particular the increase of the number of equations [86]. As detailed in the following, this research activity aims at developing a nonlinear numerical model for the dynamics of floating platforms based on such innovative approach that considers the structure of Lie groups [11, 87], i.e. the space $SO(3)$ of finite rotations.

[3] The presence of such singularities is not always a computational problem if the rotations are limited to a given range, as typically happens for offshore wind turbines.

[4] Since the rotation operator and the angular velocity are related to the parametrization by transcendental functions, the original differential dynamic problem is transformed.

1.1.3.2 Small-displacement hypothesis

In civil engineering, structures usually have a prevalent static behaviour and are usually assessed by means of the infinitesimal strain theory (or small deformation theory), based on the assumption that both the strains and the displacements of the bodies are small. This approach permits to confuse the deformed configuration with the undeformed one. However, specific nonlinear problems require the use of more accurate models able to handle finite deformations and displacements; thus, other theories and methods were developed in past.

Offshore platforms are quite far from a classic civil structure since their operational condition is prevalently dynamic. Only in absence of environmental loads (waves, wind, earthquakes, currents, etc.) the structure can be considered in static condition. However, this case is in general not interesting. The dynamic analysis of floating bodies should consider that the system can undergo large displacements without any restriction[5]. The small-displacement assumption, especially for rotations, could lead to relevant inaccuracies in the evaluation of extreme load conditions, mainly related to the strong first-order approximation of sine and cosine terms in the formulation of the rotation operators.

1.1.4 Design problems

An offshore wind turbine is a very complex system made of many specific parts (see Section 1.1.1) and is subjected at least to wind and wave actions[6]. The loads should be treated with a statistical approach considering their correlation. The peculiarities of the dynamic problem, in particular the variability in time and space of the loads (with an established probabilistic model) together with the nonlinearity of the system, make time-domain analyses fundamental. In order to properly define the system response from a statistical point of view (in terms of displacement or load distribution), a high number of simulations is required. The overall computational effort could be a restrictive limitation.

The open issues are both the reliability of dynamic models and the characterization of the system response. The first issue is related to the development of a numerical tool able to properly carry out time-domain dynamic analyses. Many aspects should be accounted for, for instance hydrodynamics, aerodynamics, control functions, load models, foundation (supports) concepts. The second issue consists in choosing the better time-domain simulation strategy[7] to obtain a significant statistical sample to built the response distribution or identify the proper characteristic loads. The design of an offshore wind turbine is a very arduous task because of such a stochastic nature of the system. Statistical methods are usually employed to evaluate the dynamic response (design loads), both in normal load conditions and in extreme load conditions, on the

[5] Floating offshore wind turbines can undergo large displacements, especially in extreme load conditions [44, 70].

[6] Although wind and waves are the main sources of loads, it is always necessary to evaluate the occurrence of all the other possible environmental actions, such as earthquake, ice, marine currents, etc.

[7] Wind and waves conditions are usually correlated to each other. The joint probability distribution depends at least on three parameters, namely the mean wind speed, significant wave height, and the peak spectral period [42]. Since it is not feasible to explore all the joint probability domain, a limited set of combinations of environmental loads should be selected so that it is representative of the most severe conditions.

basis of different possible approaches. The most widely used are the ones related to the direct integration method (high computational effort) and those related to the Inverse First-Order Reliability Method (IFORM) [3, 30, 94]. Each method requires time-domain simulations, i.e. a dynamic numerical model. The accuracy of such models is a very important target since the numerical tool could affect the whole process and invalidate the design procedure.

This research activity is focused on the dynamic model of floating supports for offshore wind engineering purposes; the characterization of design loads, even if important, is therefore left to future works. For further discussions on load extrapolation procedures and the environmental contour method (IFORM) the reader is addressed to the references [1, 2, 21, 31, 34, 62, 63, 75, 76], among others, where statistical methods are used both for the selection of the relevant load conditions and for the post-process of the time histories of structural loads. Many researches discussed the response of a floating wind turbine, for instance [43, 44, 70, 72], with a number of limitations mainly related to the strong case dependence of such systems, the code used for the dynamic simulations, and the formulations adopted to model the loads.

1.2 Objectives and present contributions

As discussed in the previous sections, the analysis of offshore wind turbines needs advanced computational tools able to properly model the complex interactions between the structure and the various environmental loads, in particular waves and wind. The main objective of this research activity is the development of a nonlinear numerical model[8] for the dynamic analysis of systems undergoing large displacements (both translations and rotations) in the offshore wind engineering framework. In particular, rigid-body dynamics is considered since the most floating supports for offshore wind turbines can be modelled as rigid bodies[9].

The nonlinear[10] differential problem is solved with the so called geometric method [11, 13, 86, 87], which considers the Lie group structure of the configuration space without the necessity of introducing a parametrization to handle the kinematic compatibility, thus avoiding the drawbacks associated with classical methods (strong nonlinearities and singularities) [86]. The approach is rather innovative in the maritime engineering framework where nautical angles (or Euler angles) and their time derivatives are widely used for the formulation of the differential problem [68]. Such formulations are strongly nonlinear because of the transcendental functions that relate the parametrization of rotations to the quantities characterizing the rotational motion, i.e. the rotation operator, the angular velocity, and angular acceleration. By contrast, geometric methods solve the equations directly on the Lie group [13] preserving the structure of original equations with reduced nonlinearities and no singularity [86]. This new approach is also interesting for real-time applications, for instance in the monitoring or in a control

[8] The numerical codes developed in this research activity are implemented in Matlab environment. Matlab is widely used in the scientific community being a high-level language with a set of useful tools, like functions for statistical analyses or optimization problems.

[9] The platform is considered strong and inflexible so that direct hydro-elastic effects can be neglected [46].

[10] Nonlinearities arise from the nature of the rotational motion and cannot be avoided (only few cases can be described by linear equations, like the homogeneous sphere). Other sources of nonlinearities could be associated with the system features and the loads, which are generally an arbitrary function of time and state variables, i.e. configuration, velocity, and acceleration of the system.

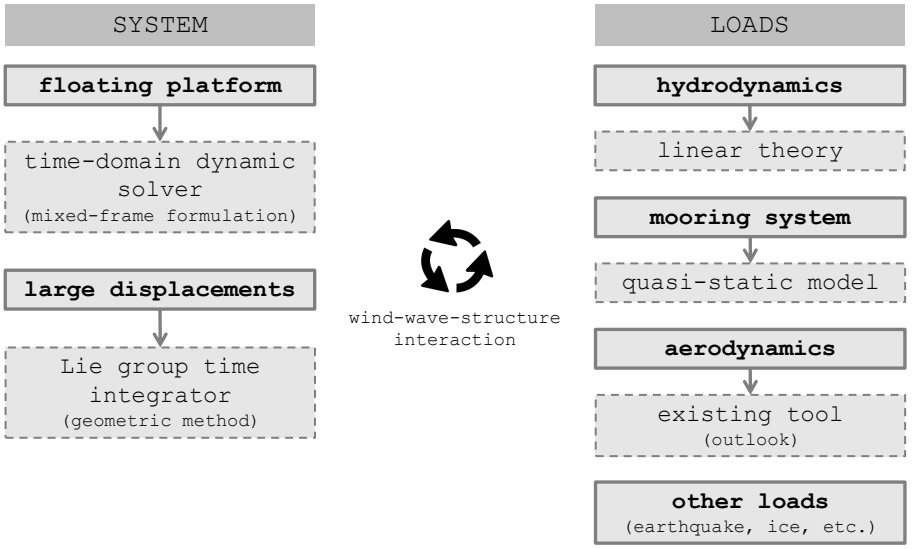

Figure 1.3: Wind-wave-structure interaction: the case of a moored floating platform.

procedure.

This research contributes also to the systematic analysis of different typologies of loads and their formulation in the framework of the Lie group time integrator. In particular, both follower and non-follower loads are considered including also the special case of transformations of the state variables. Moreover, another important aspect faced in this activity is the evaluation of the method for the study of moored floating bodies (buoyancy stabilized) with interesting suggestions on the approaches for the coupling of the dynamic model with load models and possible strategies to reduce the computational effort.

Figure 1.3 illustrates the main framework of the thesis. The long-term objective, pursued over the years inside the department through several research projects [53, 54, 55, 56], is the assessment of wind-wave-structure interaction, which is a complex problem of reciprocal interaction between the system and the loads (environment), and gets further complicated in the case of large displacements both in terms of system dynamics and interaction models. In this context, the focus of this research is mainly on the dynamic model of the system with the aim of developing an advanced dynamic solver to be used as a basis for future researches and integration with improved load models. The dynamic formulation of the rigid body is developed referring to the mixed representation of the motion[11], also referred to as the *mixed-frame* formulation or the *mixed-vision* formulation, which consists in the simultaneous use of two different bases. The translations of the center of mass are expressed with respect to the basis that defines the inertial (fixed) reference frame, whereas the rotational motion (and thus all the torques) is referred to the basis that defines the body-attached (non-inertial) frame, and therefore a basis that changes its orientation during the motion of the body[12].

[11] Sometimes this approach is indicated as the direct product $\mathbb{R}^3 \times SO(3)$ [64].

[12] In the body-attached frame the most operators associated with the rotational motion are constant,

The dynamic model (see Figure 1.4), also referred to as *dynamic solver*, or *main solver*, or *main code*, should be regarded as the core of the overall model, which interfaces the system with the loads. It can analyse the dynamics of a rigid body in the Euclidean space for several load typologies. Any configuration of the body is defined by six parameters (as many as the degrees of freedom considered): the three components of the position vector of the center of mass and the three parameters that determine the rotation (orientation) of the body. The system is modelled in terms of inertia, damping, and stiffness properties[13,14]. The possible loads include forces and torques, both follower and non-follower, applied to the center of mass or to any other point of the body. In particular, the code permits to consider sources of load related to transformations of the state variables ($\mathbf{A}^{(\bullet)}$ and $\mathbf{B}^{(\bullet)}$), i.e. stiffness-like, damping-like, and inertia-like loads. Moreover, the parameters of the algorithm, like the simulation time, the time step size, the numerical damping, the tolerances on the residual of the iterative processes, and their maximum number of iterations can be set on the basis of the specific users' requirements. The outputs of the code are the time histories of the vectors that define the configuration of the body, its velocity, and its acceleration. The main solver is not only suitable for the analysis of moored floating platforms but could also be used to analyse other kind of floating systems like ships, slabs, hulls.

Such main code can be coupled with other models that address specific issues, for instance the evaluation of external loads. In particular (see Figure 1.3), in this context mooring system and wave loads are assessed respectively by means of a quasi-static theory [29, 46] and the linear hydrodynamic theory [46]. By contrast, aerodynamic and aeroelastic loads, related to the interaction of the structure with the wind, as well as other sources of loads such as earthquakes, ice, currents, are not considered. As far as aerodynamic loads are concerned, their state of the art is rather advanced [39, 40], and the detail got with existing models can be considered satisfactory. However, their implementation is not simple and requires advanced expertise, from mechanical and aerospatial engineering to robotics, to electronics and automation (control system). The aeroelastic problem can be integrated in future, even using existing tools.

It goes without saying that the coupled model has its own limitations, mainly associated with the theories used to model the loads, which restrict the field of employment. Moreover, the dynamic response of a floating system is strongly case-dependent because of the features of the environment and the system itself that make any case of study almost unique. However, the method presented can be widely used. All the limitations will be highlighted and summarized in the dissertation in order to specifically address future research in this topic. This research does not pretend to develop a complete numerical solver like existing ones (for instance, FAST [47]), but the first milestones can be achieved as the bases for further research activities in order to obtain a reliable tool, more accurate than existing ones, useful for both research activities and design tasks.

for instance the inertia tensor of a rigid body.

[13]The damping and stiffness properties could also be regarded as loads related respectively to the velocity and the configuration of the body. By contrast, the parallelism between inertia and transformation of the acceleration is misleading and could lead to neglect some apparent forces.

[14]Damping and stiffness properties could also be time-dependent without introducing significant issues. By contrast, time-dependent inertia properties modify the basic formulation of the dynamic problem since they should be properly considered in the evaluation of the time derivatives of the linear momentum and angular momentum.

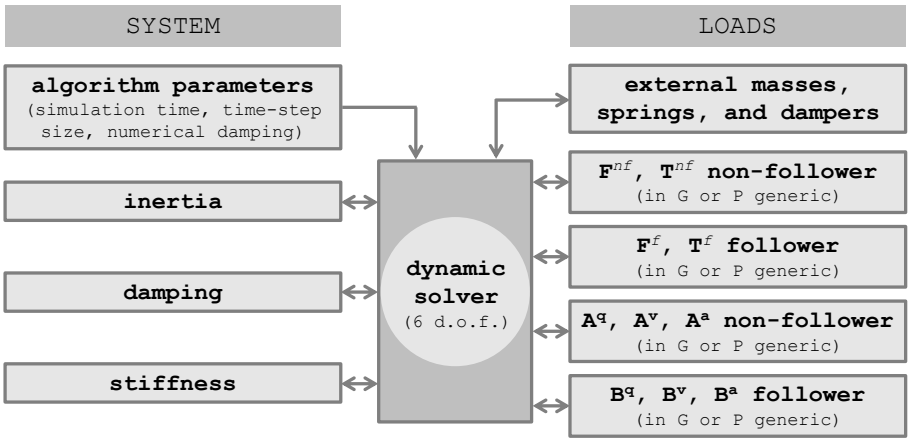

Figure 1.4: Dynamic solver framework.

1.2.1 Research activity outline

The development of the code inspired several discussions concerning theoretical aspects of finite motions as well as issues much more related to numerical modelling. The dissertation aims at explaining the whole process with a rigorous approach based on a comprehensive discussion of the fundamentals behind any model employed. The dissertation is organized as follows.

Chapter 1. The topic of the research activity is presented and discussed in the context of offshore wind energy in deep waters. The chapter aims at addressing the reader to the dissertation.

Chapter 2. The dynamics of rigid bodies in the Euclidean space is discussed with a rigorous approach providing the reader with an original point of view on different representations of the motion related to the observer, i.e. the reference frame, and the mathematical basis used to express the physical quantities. Finite rotations are presented as elements of the Lie group of proper orthogonal transformations $SO(3)$ whose structure is the core of the numerical algorithm. Moreover, the fundamentals of fluid dynamics are briefly reviewed and potential flows are introduced. The chapter aims at introducing the reader in the theoretical framework of the dissertation.

Chapter 3. The formulation of the dynamics of rigid bodies is presented in the mixed-frame context, with a meticulous analysis of different typologies of loads. In particular both follower and non-follower loads are considered including the important case of transformations of the state variables. The algorithm [11] used for solving the differential problem is briefly described. The approach is tested on a number of cases whose analytic solution is known, like the homogeneous sphere with follower torque or the axially symmetric rigid body with follower torque, proving the convergence of the method. Other interesting comparisons with classic oscillators (simple, damped, forced) are discussed in Appendix B. The formulation is also compared with an alternative approach based on a complete local representation of the motion, and the possibility of truncating the tangent stiffness operator is discussed. The chapter aims at providing the reader with the details on the formulation of the rigid-body dynamic problem in the

framework of the mixed representation of the motion, for various typologies of loads.

Chapter 4. The hydrodynamic model is presented in the framework of the linear theory, widely used for deep-water purposes. The reliability of the small-displacement hypothesis is discussed for hydrostatic loads on the basis of an alternative approach developed to account for large motions. Both regular and irregular waves are described together with their formulations in terms of hydrodynamic loads on the submerged structure. Some interesting remarks about higher-order effects and the use of the linear hydrodynamic theory are finally illustrated. The chapter aims at providing the reader with the fundamentals of hydrodynamic loads based on the linear theory.

Chapter 5. The loads associated with the mooring system are discussed in the framework of quasi-static models. Two different formulations are presented and compared to each other in terms of tension on the single cable and loads on the whole mooring system, with parametric analyses on the role of the different parameters that characterize the models. The chapter aims at providing the reader with a critique overview of the models used in this research to assess the mooring line loads.

Chapter 6. The coupled response of a moored floating platform is assessed by coupling the main solver with the load models. Different coupling and simulation strategies are introduced and discussed in order to reduce the computational effort. The coupled code is evaluated with a series of perturbation tests to ensure the correct functionality of the system in restoring the equilibrium. The dynamics of a moored floating platform is finally analysed with the main objective to better understand the role of some parameters as the wave period, wave amplitude, mass of the platform, length of the cables. The chapter aims at discussing the potentiality of the method together with some applications to floating offshore platforms.

Chapter 7. A summary of the main achievements of the present research is given together with conclusions and final remarks for future research activities.

Appendix A. The use of a mixed representation of the motion is not the unique possibility to formulate the dynamic problem of a rigid body. A complete local representation of the motion is a suitable alternative approach, especially in multibody dynamics [86]. All the operators defined in Chapter 3 are redefined in this alternative framework. The appendix aims at providing the reader with another point of view on the dynamics of rigid bodies.

Appendix B. The numerical model based on the mixed-frame formulation is tested on a series of oscillators whose exact analytic solution is well known. Several cases are analysed, which differ to each other on the excited degree of freedom (translational or rotational), or on the stiffness and damping properties of the system, or on the forcing load. The appendix aims at providing the reader with some additional details on the reliability of the numerical dynamic model.

Chapter 2

Background and theoretical framework

"Once you have experienced the exhilaration of flying,
when you will be back down to the ground,
you will continue to look at the sky."

Leonardo da Vinci

The dynamics of rigid bodies in the Euclidean space is discussed with a rigorous approach providing the reader with an original point of view on different representations of the motion related to the observer, i.e. the reference frame, and the mathematical basis used to express the physical quantities. Finite rotations are presented as elements of the Lie group of proper orthogonal transformations $SO(3)$ whose structure is the core of the numerical algorithm. Moreover, the fundamentals of fluid dynamics are briefly reviewed and potential flows are introduced. The chapter aims at introducing the reader in the theoretical framework of the dissertation.

2.1 Kinematics of rigid bodies

The kinematics of rigid bodies is presented in an uncommon way providing the reader with an interesting point of view, very useful for the next developments. For further discussions on the topics presented in this section the reader is addressed to the references [7, 16, 37, 68] or every book of classical mechanics.

2.1.1 Reference frames

The description of the rigid-body motion varies according to the reference frame adopted in the mathematical formulation. There is not a general rule in the choice of the frames providing that only an observer attached to an inertial reference frame can have an exhaustive view of the motion. The formulations reported hereafter refer to the following right-handed orthogonal Cartesian systems (see Figure 2.1):

- spatial (fixed) inertial reference frame $\{O; x, y, z\}$ defined by the orthonormal basis $\mathcal{S} = \{\mathbf{e}_i^I\}$. The physical quantities $(\bullet)$ observed in this frame are indicated with the notation $(\bullet)^I$;
- body-attached (non-inertial) reference frame $\{O'; x', y', z'\}$ defined by the orthonormal basis $\mathcal{M} = \{\mathbf{e}_i^B\}$. This frame can translate and rotate with respect to the fixed frame according to the motion of the rigid body. Therefore, the associated basis generally changes its orientation during the motion. An observer solidal with the body-attached frame sees the rigid body fixed. The physical quantities $(\bullet)$ observed in this frame are indicated with the notation $(\bullet)^B$;
- local (non-inertial) reference frame $\{O''; x'', y'', z''\}$ defined by the orthonormal basis $\mathcal{L} = \{\mathbf{e}_i^L\}$. This frame can translate and rotate not only with respect to the fixed frame but also with respect to the body. The associated basis can therefore change its orientation in time. The physical quantities $(\bullet)$ observed in this frame are indicated with the notation $(\bullet)^L$.

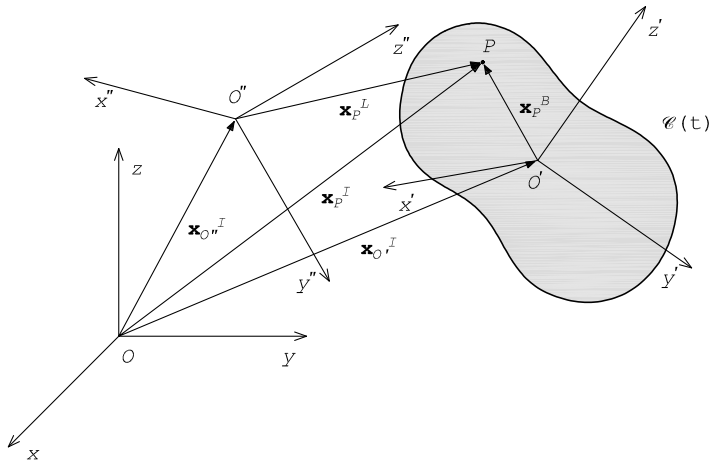

Figure 2.1: Reference frames adopted for the kinematic description of the motion.

2.1.2 Position, velocity, and acceleration

Given a rigid body in the Euclidean space, let's focus on its generic point P. The position, velocity, and acceleration vectors, seen by an observer placed in the spatial inertial frame, can be related to the kinematic physical quantities observed in a moving frame (non-inertial), as follows[1]:

$$\mathbf{x}_P^I = (P - O'') + (O'' - O) = \mathbf{x}_P^L + \mathbf{x}_{O''}^I = x_{P,i}^L \mathbf{e}_i^L + x_{O'',i}^I \mathbf{e}_i^I \tag{2.1}$$

$$\mathbf{v}_P^I = \dot{\mathbf{x}}_P^I = \mathbf{v}_P^L + \boldsymbol{\omega} \times \mathbf{x}_P^L + \mathbf{v}_{O''}^I \tag{2.2}$$

$$\mathbf{a}_P^I = \dot{\mathbf{v}}_P^I = \mathbf{a}_P^L + 2\boldsymbol{\omega} \times \mathbf{v}_P^L + \dot{\boldsymbol{\omega}} \times \mathbf{x}_P^L + \boldsymbol{\omega} \times (\boldsymbol{\omega} \times \mathbf{x}_P^L) + \mathbf{a}_{O''}^I \tag{2.3}$$

If the moving frame is attached to the rigid body, i.e. the point P is fixed with respect to the non-inertial frame, the previous relations simplify as follows:

$$\mathbf{x}_P^I = (P - O') + (O' - O) = \mathbf{x}_P^B + \mathbf{x}_{O'}^I = x_{P,i}^B \mathbf{e}_i^B + x_{O',i}^I \mathbf{e}_i^I \tag{2.4}$$

$$\mathbf{v}_P^I = \dot{\mathbf{x}}_P^I = \boldsymbol{\omega} \times \mathbf{x}_P^B + \mathbf{v}_{O'}^I \tag{2.5}$$

$$\mathbf{a}_P^I = \dot{\mathbf{v}}_P^I = \dot{\boldsymbol{\omega}} \times \mathbf{x}_P^B + \boldsymbol{\omega} \times (\boldsymbol{\omega} \times \mathbf{x}_P^B) + \mathbf{a}_{O'}^I \tag{2.6}$$

The vector $\boldsymbol{\omega}$, called angular velocity, does not depend on the orientation of the body-attached reference frame (i.e. on the choice of its basis), but it is an intrinsic property of the rigid-body motion.

2.1.3 The rotation operator

The equations introduced in the previous section are not easy to manage since they contain physical quantities expressed with respect to different bases. It is necessary to develop a formulation that considers the reciprocal orientation of the frames. Let's focus on the spatial (inertial) reference frame and the body-attached frame, whose bases are respectively $\mathcal{S} = \{\mathbf{e}_i^I\}$ and $\mathcal{M} = \{\mathbf{e}_i^B\}$. The physical quantity $(\bullet)$ observed in the frame $(\diamond)$, with $(\diamond) = I, B, L$, and expressed with respect to the basis of the inertial frame is indicated with the notation $(\bullet)^{(\diamond),\mathcal{S}}$, whereas if the quantity is expressed with respect to the basis of the body-attached frame (also called material frame), the notation is $(\bullet)^{(\diamond),\mathcal{M}}$. If the basis indication is omitted, the operator is expressed with respect to

[1] It is used the index notation (or Einstein notation). If an index is not repeated, i.e. it appears once in a formula (free index), it can freely takes the values 1, 2, 3; on the other hand, if an index appears twice (dummy index) it implies the summation over all the possible values of the index, namely for a vector $\mathbf{p}$:

$$\mathbf{p} = \sum_{i=1}^{3} p_i \mathbf{e}_i = p_i \mathbf{e}_i$$

$$p_i = \mathbf{p} \cdot \mathbf{e}_i, \qquad i = 1, 2, 3$$

Furthermore, let $\mathbf{p} = p_i \mathbf{e}_i$ be a vector, its time derivatives are indicated with the following notation:

$$\frac{d}{dt}\mathbf{p} = \dot{\mathbf{p}} = \dot{p}_i \mathbf{e}_i + p_i \dot{\mathbf{e}}_i$$

$$\frac{d^2}{dt^2}\mathbf{p} = \frac{d}{dt}\dot{\mathbf{p}} = \ddot{\mathbf{p}}$$

the basis that defines the reference frame adopted. The change of basis can be seen as a linear transformation[2] (rotation about the origin) of the reference frame that preserves the distance between different points and their reciprocal orientation (relative angles). In other words, it is a change of reference frame that maintains the location of the origin. Let $\mathbf{R} : \mathcal{M} \to \mathcal{S}$ be the matrix associated with the transformation from the basis of the material frame to the basis of the spatial frame, namely[3]:

$$\mathbf{e}_i^{B,\mathcal{S}} = \mathbf{R}\mathbf{e}_i^{I,\mathcal{S}} = \mathbf{R}\mathbf{e}_i^{B,\mathcal{M}} \tag{2.7}$$

$$\mathbf{x}_P^{B,\mathcal{S}} = \mathbf{R}\mathbf{x}_P^{B,\mathcal{M}}, \qquad \mathbf{x}_P^{B,\mathcal{M}} = \mathbf{R}^T\mathbf{x}_P^{B,\mathcal{S}} \tag{2.8}$$

Since the transformation $\mathbf{R}$ should preserve the distances between any arbitrary pair of points fixed in the material frame, i.e. attached to the body, and the angles between any arbitrary pair of directions, $\mathbf{R}$ should be a proper orthogonal matrix[4] [37]. It is interesting to notice, as demonstrated in [37], that the matrix $\mathbf{R}$ admits at least one unit eigenvector $\mathbf{u}$ that is unaffected by the transformation, namely:

$$\mathbf{R}\mathbf{u} = \mathbf{u} \tag{2.9}$$

The matrix $\mathbf{R}$ is called *rotation operator* and the associated unit eigenvector $\mathbf{u}$ represents the *rotation axis*. The rotation operator can be expressed in terms of the rotation axis

[2]The basis $\mathcal{M}$ changes its orientation in time according to the motion of the rigid body; hence, the linear transformation $\mathbf{R} : \mathcal{M} \to \mathcal{S}$ is in general time-dependent, namely $\mathbf{R} = \mathbf{R}(t)$.

[3]It is used a matrix representation of vector and tensor operations, as also done in [37]. Let $\mathbf{p}$ and $\{\mathbf{e}_i\}$ be respectively a vector and a basis of the Euclidean space, the matrix representation of the vector is given by:

$$\mathbf{p} = p_i\mathbf{e}_i = [p_1 \ p_2 \ p_3]^T$$

Given the vectors $\mathbf{p}$ and $\mathbf{w}$ expressed with respect to the same basis $\{\mathbf{e}_i\}$, it is used the following matrix notation:

$$\mathbf{p} \cdot \mathbf{w} = \mathbf{p}^T\mathbf{w}$$

$$\mathbf{p} \otimes \mathbf{w} = \mathbf{p}\mathbf{w}^T$$

$$\mathbf{p} \times \mathbf{w} = \widetilde{\mathbf{p}}\mathbf{w}$$

In the cross product, $\mathbf{p}$ is the vector part of $\widetilde{\mathbf{p}}$, i.e. they are linked together by a biunivocal relation, namely [16, 37]:

$$\mathbf{p} = \mathrm{vect}(\widetilde{\mathbf{p}}) = \frac{1}{2}\epsilon_{ijk}\widetilde{p}_{kj}\mathbf{e}_i$$

$$\widetilde{\mathbf{p}} = \mathrm{spin}(\mathbf{p}) = -\epsilon_{ijk}p_k\mathbf{e}_i \otimes \mathbf{e}_j$$

where ϵ_{ijk} are the components of the Ricci's tensor (third-order tensor) that can be easily determined remembering these three simple rules [37]:

1. $\epsilon_{ijk} = 1$ if ijk is an even permutation (cyclic);
2. $\epsilon_{ijk} = -1$ if ijk is an odd permutation;
3. $\epsilon_{ijk} = 0$ in all the other cases (that is when there is a repeated index).

[4]A matrix is said to be *proper orthogonal* if [37]:

$$\mathbf{R}\mathbf{R}^T = \mathbf{I}$$

$$\det(\mathbf{R}) = 1$$

and the amplitude of the rotation ϕ, as follows [16, 37, 52, 84]:

$$\mathbf{R} = \mathbf{I}\cos\phi + (1-\cos\phi)\mathbf{u}\mathbf{u}^T + \widetilde{\mathbf{u}}\sin\phi = \exp(\widetilde{\mathbf{u}}\phi) \tag{2.10}$$

which has the following linear invariants [37]:

$$\mathrm{tr}(\mathbf{R}) = 1 + 2\cos\phi \tag{2.11}$$
$$\mathrm{vect}(\mathbf{R}) = \mathbf{u}\sin\phi \tag{2.12}$$

The rotation operator is further discussed in Section 2.3, as element of $SO(3)$, whereas in Section 2.4 some of its possible representations are presented. By using the rotation operator $\mathbf{R}$, the position of the generic point P of the rigid body, expressed by the Equation (2.4), can be rewritten as follows:

$$\mathbf{x}_P^{I,\mathcal{S}} = \mathbf{x}_{O'}^{I,\mathcal{S}} + \mathbf{R}\mathbf{x}_P^{B,\mathcal{M}} = \mathbf{x}_{O'}^{I,\mathcal{S}} + \mathbf{x}_P^{B,\mathcal{S}} \tag{2.13}$$

which relates, with respect to the basis $\mathcal{S}$, the position vectors observed (measured) in the material and spatial frames.

2.1.4 Analysis of the velocity

Let P be a generic point of a rigid body in the Euclidean space, its velocity vector, given by the Equation (2.5), can be rewritten in terms of the rotation operator $\mathbf{R}$ in order to get a relation formulated with respect to the same basis, or alternatively, as the time derivative of the Equation (2.13), namely[5]:

$$\mathbf{v}_P^{I,\mathcal{S}} = \mathbf{R}(\boldsymbol{\omega}^{\mathcal{M}} \times \mathbf{x}_P^{B,\mathcal{M}}) + \mathbf{v}_{O'}^{I,\mathcal{S}} = \mathbf{R}\mathbf{v}_P^{I,\mathcal{M}} \tag{2.14}$$
$$\mathbf{v}_P^{I,\mathcal{S}} = \mathbf{v}_{O'}^{I,\mathcal{S}} + \dot{\mathbf{R}}\mathbf{x}_P^{B,\mathcal{M}} = \mathbf{v}_{O'}^{I,\mathcal{S}} + \mathbf{v}_P^{A,\mathcal{S}} = \mathbf{v}_{O'}^{I,\mathcal{S}} + \mathbf{R}\mathbf{v}_P^{A,\mathcal{M}} \tag{2.15}$$

where the physical quantities $(\bullet)$ indicated with the notation $(\bullet)^A$ represent apparent quantities due to the non-inertial nature of the body-attached frame, and they cannot be directly observed (except in the particular case of spherical motion) neither in the spatial frame nor in the material frame. In order to get useful relations for the angular velocity vectors, let's focus on the spherical motion described by the Equation (2.8), as

[5] The time derivative of the position vector observed in the body-attached frame is given by:

$$\frac{d}{dt}(x_i^{B,\mathcal{S}}\mathbf{e}_i^{I,\mathcal{S}}) = \frac{d}{dt}(x_i^{B,\mathcal{M}}\mathbf{e}_i^{B,\mathcal{S}}) = \frac{d}{dt}(x_j^{B,\mathcal{M}}R_{ij}\mathbf{e}_i^{B,\mathcal{M}}) = x_j^{B,\mathcal{M}}\dot{R}_{ij}\mathbf{e}_i^{B,\mathcal{M}} = \dot{\mathbf{R}}\mathbf{x}_P^{B,\mathcal{M}}$$

where $x_i^{B,\mathcal{S}}$ and $x_i^{B,\mathcal{M}}$ are respectively the components of the vector $\mathbf{x}^B$ with respect to the basis $\mathcal{S} = \{\mathbf{e}_i^I\}$ and $\mathcal{M} = \{\mathbf{e}_i^B\}$.

follows[6] [37]:

$$\mathbf{v}_P^{A,\mathcal{S}} = \dot{\mathbf{R}}\mathbf{x}_P^{B,\mathcal{M}} = \dot{\mathbf{R}}\mathbf{R}^T\mathbf{x}_P^{B,\mathcal{S}} = \widetilde{\boldsymbol{\omega}}^{\mathcal{S}}\mathbf{x}_P^{B,\mathcal{S}} \tag{2.16}$$

$$\widetilde{\boldsymbol{\omega}}^{\mathcal{S}} = \dot{\mathbf{R}}\mathbf{R}^T, \qquad \boldsymbol{\omega}^{\mathcal{S}} = \mathrm{vect}(\widetilde{\boldsymbol{\omega}}^{\mathcal{S}}) \tag{2.17}$$

$$\mathbf{v}_P^{A,\mathcal{M}} = \mathbf{R}^T\dot{\mathbf{R}}\mathbf{x}_P^{B,\mathcal{M}} = \widetilde{\boldsymbol{\omega}}^{\mathcal{M}}\mathbf{x}_P^{B,\mathcal{M}} \tag{2.18}$$

$$\widetilde{\boldsymbol{\omega}}^{\mathcal{M}} = \mathbf{R}^T\dot{\mathbf{R}}, \qquad \boldsymbol{\omega}^{\mathcal{M}} = \mathrm{vect}(\widetilde{\boldsymbol{\omega}}^{\mathcal{M}}) \tag{2.19}$$

The angular velocity vectors and the associated skew-symmetric tensors transform with the rule of the change of basis confirming their tensorial nature, namely:

$$\widetilde{\boldsymbol{\omega}}^{\mathcal{M}} = \mathbf{R}^T\widetilde{\boldsymbol{\omega}}^{\mathcal{S}}\mathbf{R} \tag{2.20}$$

$$\boldsymbol{\omega}^{\mathcal{S}} = \mathbf{R}\boldsymbol{\omega}^{\mathcal{M}} \tag{2.21}$$

2.1.4.1 Explicit expressions

The angular velocity vectors can be expressed in terms of the invariants of the rotation ($\mathbf{u}$ and ϕ) and their time derivatives, namely[7] [37]:

$$\boldsymbol{\omega}^{\mathcal{S}} = \big[\mathbf{I}\sin\phi + (1-\cos\phi)\widetilde{\mathbf{u}}\big]\dot{\mathbf{u}} + \mathbf{u}\dot{\phi} \tag{2.22}$$

$$\boldsymbol{\omega}^{\mathcal{M}} = \big[\mathbf{I}\sin\phi - (1-\cos\phi)\widetilde{\mathbf{u}}\big]\dot{\mathbf{u}} + \mathbf{u}\dot{\phi} \tag{2.23}$$

[6] The matrices associated with the tensors $\dot{\mathbf{R}}\mathbf{R}^T$ and $\dot{\mathbf{R}}^T\mathbf{R}$ are skew-symmetric, namely [37]:

$$\frac{d}{dt}(\mathbf{R}\mathbf{R}^T) = \mathbf{0} = \dot{\mathbf{R}}\mathbf{R}^T + \mathbf{R}\dot{\mathbf{R}}^T = \dot{\mathbf{R}}\mathbf{R}^T + (\dot{\mathbf{R}}\mathbf{R}^T)^T$$

$$\frac{d}{dt}(\mathbf{R}^T\mathbf{R}) = \mathbf{0} = \dot{\mathbf{R}}^T\mathbf{R} + \mathbf{R}^T\dot{\mathbf{R}} = (\mathbf{R}^T\dot{\mathbf{R}})^T + \mathbf{R}^T\dot{\mathbf{R}}$$

[7] The Equations (2.21) and (2.22) are definitely equivalent, in fact, the last one can be obtained by combining the Equations (2.10) and (2.23) with the Equation (2.21), namely:

$$\begin{aligned}
\boldsymbol{\omega}^{\mathcal{S}} =& \mathbf{R}\Big[\big(\mathbf{I}\sin\phi - (1-\cos\phi)\widetilde{\mathbf{u}}\big)\dot{\mathbf{u}} + \mathbf{u}\dot{\phi}\Big] = \mathbf{R}\big[\mathbf{I}\sin\phi - (1-\cos\phi)\widetilde{\mathbf{u}}\big]\dot{\mathbf{u}} + \mathbf{u}\dot{\phi} = \\
=& \mathbf{I}\cos\phi\big[\mathbf{I}\sin\phi - (1-\cos\phi)\widetilde{\mathbf{u}}\big]\dot{\mathbf{u}} + (1-\cos\phi)\mathbf{u}\mathbf{u}^T\big[\mathbf{I}\sin\phi - (1-\cos\phi)\widetilde{\mathbf{u}}\big]\dot{\mathbf{u}} + \\
&+ \widetilde{\mathbf{u}}\sin\phi\big[\mathbf{I}\sin\phi - (1-\cos\phi)\widetilde{\mathbf{u}}\big]\dot{\mathbf{u}} + \mathbf{u}\dot{\phi} = \\
=& \big[\mathbf{I}\cos\phi\sin\phi - \cos\phi(1-\cos\phi)\widetilde{\mathbf{u}}\big]\dot{\mathbf{u}} + \big[\sin\phi(1-\cos\phi)\mathbf{u}\mathbf{u}^T - (1-\cos\phi)^2\mathbf{u}\mathbf{u}^T\widetilde{\mathbf{u}}\big]\dot{\mathbf{u}} + \\
&+ \big[(\sin\phi)^2\widetilde{\mathbf{u}} - \sin\phi(1-\cos\phi)\widetilde{\mathbf{u}}\widetilde{\mathbf{u}}\big]\dot{\mathbf{u}} + \mathbf{u}\dot{\phi} = \\
=& \big[\mathbf{I}\cos\phi\sin\phi - \cos\phi(1-\cos\phi)\widetilde{\mathbf{u}}\big]\dot{\mathbf{u}} + \big[\sin\phi(1-\cos\phi)(\mathbf{I}+\widetilde{\mathbf{u}}\widetilde{\mathbf{u}})\big]\dot{\mathbf{u}} + \\
&+ \big[(1+\cos\phi)(1-\cos\phi)\widetilde{\mathbf{u}} - \sin\phi(1-\cos\phi)\widetilde{\mathbf{u}}\widetilde{\mathbf{u}}\big]\dot{\mathbf{u}} + \mathbf{u}\dot{\phi} = \\
=& \big[\mathbf{I}\sin\phi + (1-\cos\phi)\widetilde{\mathbf{u}}\big]\dot{\mathbf{u}} + \mathbf{u}\dot{\phi}
\end{aligned}$$

provided the following identities:

$$\mathbf{u}\mathbf{u}^T\widetilde{\mathbf{u}} = \mathbf{0}$$

$$\mathbf{I} + \widetilde{\mathbf{u}}\widetilde{\mathbf{u}} = \mathbf{u}\mathbf{u}^T$$

2.1.5 Analysis of the acceleration

Let P be a generic point of a rigid body in the Euclidean space, its acceleration vector, given by the Equation (2.6), can be rewritten in terms of the rotation operator $\mathbf{R}$ in order to get a relation formulated with respect to the same basis, or alternatively, as the time derivative of the Equation (2.15), namely[8]:

$$\mathbf{a}_P^{I,\mathcal{S}} = \mathbf{R}(\dot{\boldsymbol{\omega}}^{\mathcal{M}} \times \mathbf{x}_P^{B,\mathcal{M}}) + \mathbf{R}\big[\boldsymbol{\omega}^{\mathcal{M}} \times (\boldsymbol{\omega}^{\mathcal{M}} \times \mathbf{x}_P^{B,\mathcal{M}})\big] + \mathbf{a}_{O'}^{I,\mathcal{S}} = \mathbf{R}\mathbf{a}_P^{I,\mathcal{M}} \tag{2.24}$$

$$\mathbf{a}_P^{I,\mathcal{S}} = \mathbf{a}_{O'}^{I,\mathcal{S}} + \ddot{\mathbf{R}}\mathbf{x}_P^{B,\mathcal{M}} = \mathbf{a}_{O'}^{I,\mathcal{S}} + \mathbf{a}_P^{A,\mathcal{S}} = \mathbf{a}_{O'}^{I,\mathcal{S}} + \mathbf{R}\mathbf{a}_P^{A,\mathcal{M}} \tag{2.25}$$

In order to get useful relations for the angular acceleration vectors, let's focus on the spherical motion described by the Equation (2.8), as follows[9] [37]:

$$\begin{aligned}\mathbf{a}_P^{A,\mathcal{S}} &= \ddot{\mathbf{R}}\mathbf{x}_P^{B,\mathcal{M}} = \ddot{\mathbf{R}}\mathbf{R}^T\mathbf{x}_P^{B,\mathcal{S}} = \big[\frac{d}{dt}(\dot{\mathbf{R}}\mathbf{R}^T) - \dot{\mathbf{R}}\dot{\mathbf{R}}^T\big]\mathbf{x}_P^{B,\mathcal{S}} = \\ &= \big[\dot{\widetilde{\boldsymbol{\omega}}}^{\mathcal{S}} + \widetilde{\boldsymbol{\omega}}^{\mathcal{S}}\widetilde{\boldsymbol{\omega}}^{\mathcal{S}}\big]\mathbf{x}_P^{B,\mathcal{S}}\end{aligned} \tag{2.26}$$

$$\dot{\widetilde{\boldsymbol{\omega}}}^{\mathcal{S}} = \frac{d}{dt}(\dot{\mathbf{R}}\mathbf{R}^T), \qquad \dot{\boldsymbol{\omega}}^{\mathcal{S}} = \mathrm{vect}(\dot{\widetilde{\boldsymbol{\omega}}}^{\mathcal{S}}) = \mathrm{vect}(\ddot{\mathbf{R}}\mathbf{R}^T) \tag{2.27}$$

$$\mathbf{a}_P^{A,\mathcal{M}} = \mathbf{R}^T\ddot{\mathbf{R}}\mathbf{x}_P^{B,\mathcal{M}} = \big[\frac{d}{dt}(\mathbf{R}^T\dot{\mathbf{R}}) - \dot{\mathbf{R}}^T\dot{\mathbf{R}}\big]\mathbf{x}_P^{B,\mathcal{M}} = \big[\dot{\widetilde{\boldsymbol{\omega}}}^{\mathcal{M}} + \widetilde{\boldsymbol{\omega}}^{\mathcal{M}}\widetilde{\boldsymbol{\omega}}^{\mathcal{M}}\big]\mathbf{x}_P^{B,\mathcal{M}} \tag{2.28}$$

$$\dot{\widetilde{\boldsymbol{\omega}}}^{\mathcal{M}} = \frac{d}{dt}(\mathbf{R}^T\dot{\mathbf{R}}), \qquad \dot{\boldsymbol{\omega}}^{\mathcal{M}} = \mathrm{vect}(\dot{\widetilde{\boldsymbol{\omega}}}^{\mathcal{M}}) = \mathrm{vect}(\mathbf{R}^T\ddot{\mathbf{R}}) \tag{2.29}$$

As discussed for the angular velocity vectors, also the angular acceleration vectors and the associated skew-symmetric tensors transform with the rule of the change of basis confirming their tensorial nature, namely:

$$\dot{\widetilde{\boldsymbol{\omega}}}^{\mathcal{M}} = \mathbf{R}^T\dot{\widetilde{\boldsymbol{\omega}}}^{\mathcal{S}}\mathbf{R} \tag{2.30}$$

$$\dot{\boldsymbol{\omega}}^{\mathcal{S}} = \mathbf{R}\dot{\boldsymbol{\omega}}^{\mathcal{M}} \tag{2.31}$$

2.1.5.1 Explicit expressions

The angular acceleration vectors can be expressed in terms of the invariants of the rotation ($\mathbf{u}$ and ϕ) and their time derivatives, and can be directly obtained by derivating the Equations (2.22) and (2.23) [37]:

$$\dot{\boldsymbol{\omega}}^{\mathcal{S}} = \big[\mathbf{I}\sin\phi + (1-\cos\phi)\widetilde{\mathbf{u}}\big]\ddot{\mathbf{u}} + \mathbf{u}\ddot{\phi} + \big[\mathbf{I}\cos\phi + \sin\phi\widetilde{\mathbf{u}}\big]\dot{\mathbf{u}}\dot{\phi} + \dot{\mathbf{u}}\dot{\phi} \tag{2.32}$$

$$\dot{\boldsymbol{\omega}}^{\mathcal{M}} = \big[\mathbf{I}\sin\phi - (1-\cos\phi)\widetilde{\mathbf{u}}\big]\ddot{\mathbf{u}} + \mathbf{u}\ddot{\phi} + \big[\mathbf{I}\cos\phi - \sin\phi\widetilde{\mathbf{u}}\big]\dot{\mathbf{u}}\dot{\phi} + \dot{\mathbf{u}}\dot{\phi} \tag{2.33}$$

[8] Let $\mathbf{R}$ be a proper orthogonal matrix, given the vectors $\mathbf{p}$ and $\mathbf{w}$, the orthogonal transformation (rotation) is distributive with respect to their vector cross product, namely:

$$\mathbf{R}(\mathbf{p}\times\mathbf{w}) = \mathbf{R}\mathbf{p}\times\mathbf{R}\mathbf{w}$$

[9] Given the skew-symmetric tensor $\widetilde{\boldsymbol{\omega}}^{\mathcal{S}}$, it follows that:

$$(\widetilde{\boldsymbol{\omega}}^{\mathcal{S}})^T = -\widetilde{\boldsymbol{\omega}}^{\mathcal{S}} = (\dot{\mathbf{R}}\mathbf{R}^T)^T = \mathbf{R}\dot{\mathbf{R}}^T$$

$$\widetilde{\boldsymbol{\omega}}^{\mathcal{S}}\widetilde{\boldsymbol{\omega}}^{\mathcal{S}} = \dot{\mathbf{R}}\mathbf{R}^T\dot{\mathbf{R}}\mathbf{R}^T = -\dot{\mathbf{R}}\mathbf{R}^T\mathbf{R}\dot{\mathbf{R}}^T = -\dot{\mathbf{R}}\dot{\mathbf{R}}^T$$

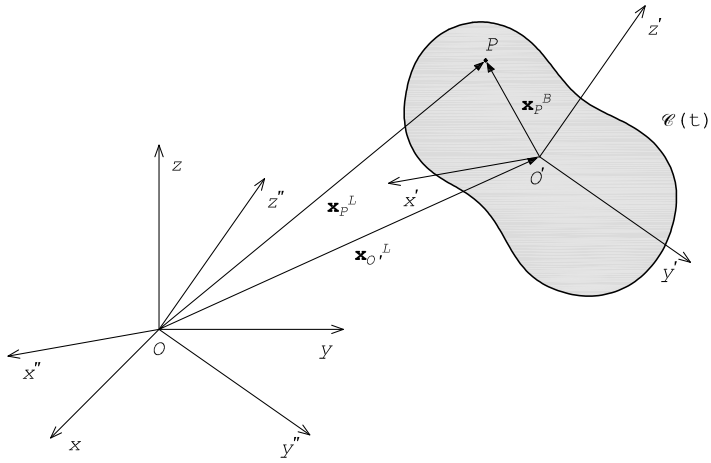

Figure 2.2: Local reference frame.

2.1.6 Local kinematic formulation

Let $\{O; x'', y'', z''\}$ be a local (non-inertial) reference frame (see Figure 2.2) whose origin coincides with that of the spatial (inertial) frame, and assume that this local frame rotates with the same law of the rigid body, i.e. they have the same orthogonal basis $\mathcal{M} = \{\mathbf{e}_i^L\} = \{\mathbf{e}_i^B\}$. Let's focus on the origin O' of the material frame, the kinematic vectors of the point O' can be expressed by means of the Equations (2.1), (2.2), and (2.3), where $P \equiv O'$ and $O'' \equiv O$, namely:

$$\mathbf{x}_{O'}^{I,\mathcal{S}} = \mathbf{R}\mathbf{x}_{O'}^{L,\mathcal{M}} \tag{2.34}$$

$$\mathbf{v}_{O'}^{I,\mathcal{S}} = \mathbf{R}(\mathbf{v}_{O'}^{L,\mathcal{M}} + \widetilde{\boldsymbol{\omega}}^{\mathcal{M}}\mathbf{x}_{O'}^{L,\mathcal{M}}) = \mathbf{R}\mathbf{v}_{O'}^{I,\mathcal{M}} \tag{2.35}$$

$$\begin{aligned}\mathbf{a}_{O'}^{I,\mathcal{S}} &= \mathbf{R}\big[\mathbf{a}_{O'}^{L,\mathcal{M}} + 2\widetilde{\boldsymbol{\omega}}^{\mathcal{M}}\mathbf{v}_{O'}^{L,\mathcal{M}} + \dot{\widetilde{\boldsymbol{\omega}}}^{\mathcal{M}}\mathbf{x}_{O'}^{L,\mathcal{M}} + \widetilde{\boldsymbol{\omega}}^{\mathcal{M}}(\widetilde{\boldsymbol{\omega}}^{\mathcal{M}}\mathbf{x}_{O'}^{L,\mathcal{M}})\big] = \\ &= \mathbf{R}(\dot{\mathbf{v}}_{O'}^{I,\mathcal{M}} + \widetilde{\boldsymbol{\omega}}^{\mathcal{M}}\mathbf{v}_{O'}^{I,\mathcal{M}}) = \mathbf{R}\mathbf{a}_{O'}^{I,\mathcal{M}}\end{aligned} \tag{2.36}$$

If the Equations (2.35) and (2.36) are substituted respectively in the Equations (2.15) and (2.25), the second members of the resulting relations express the velocity and acceleration vectors in a local view of the motion, namely:

$$\mathbf{v}_P^{I,\mathcal{S}} = \mathbf{v}_{O'}^{I,\mathcal{S}} + \mathbf{R}\mathbf{v}_P^{A,\mathcal{M}} = \mathbf{R}(\mathbf{v}_{O'}^{I,\mathcal{M}} + \mathbf{v}_P^{A,\mathcal{M}}) = \mathbf{R}(\mathbf{v}_{O'}^{I,\mathcal{M}} + \widetilde{\boldsymbol{\omega}}^{\mathcal{M}}\mathbf{x}_P^{B,\mathcal{M}}) \tag{2.37}$$

$$\begin{aligned}\mathbf{a}_P^{I,\mathcal{S}} &= \mathbf{a}_{O'}^{I,\mathcal{S}} + \mathbf{R}\mathbf{a}_P^{A,\mathcal{M}} = \mathbf{R}(\mathbf{a}_{O'}^{I,\mathcal{M}} + \mathbf{a}_P^{A,\mathcal{M}}) = \\ &= \mathbf{R}\big[\dot{\mathbf{v}}_{O'}^{I,\mathcal{M}} + \widetilde{\boldsymbol{\omega}}^{\mathcal{M}}\mathbf{v}_{O'}^{I,\mathcal{M}} + (\dot{\widetilde{\boldsymbol{\omega}}}^{\mathcal{M}} + \widetilde{\boldsymbol{\omega}}^{\mathcal{M}}\widetilde{\boldsymbol{\omega}}^{\mathcal{M}})\mathbf{x}_P^{B,\mathcal{M}}\big]\end{aligned} \tag{2.38}$$

2.2 Dynamics of rigid bodies

The dynamics of rigid bodies in the Euclidean space is presented starting from the cardinal equations of dynamics, i.e. conservation of linear momentum $\mathbf{Q}$ and angular momentum $\mathbf{H}$, and the kinematic description of the motion developed in the previous

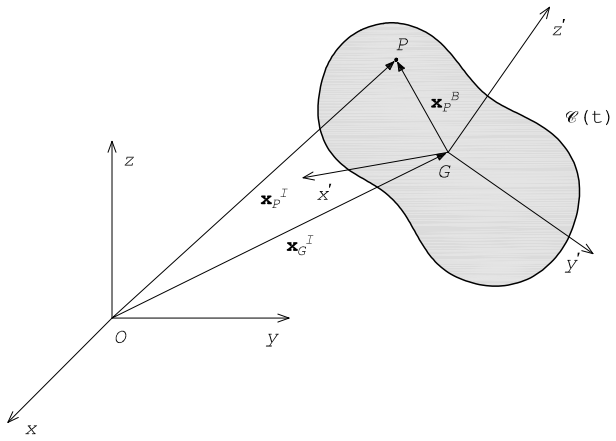

Figure 2.3: Reference frames adopted for the dynamic description of the motion.

section. For further discussions on the topics presented in this section the reader is addressed to the references [7, 16, 37, 68, 86] or every book of classical mechanics.

2.2.1 Reference frames

The description of the rigid-body dynamics varies according to the reference frame adopted in the mathematical formulation. The formulations reported hereafter refer to the following right-handed orthogonal Cartesian systems (see Figure 2.3), which have a further assumption with respect to the frames adopted in the previous section. In particular, the origin of the body-attached frame coincides with the center of mass of the rigid body:

- spatial (fixed) inertial reference frame $\{O; x, y, z\}$ defined by the orthonormal basis $\mathcal{S} = \{\mathbf{e}_i^I\}$. The physical quantities $(\bullet)$ observed in this frame are indicated with the notation $(\bullet)^I$;

- body-attached (non-inertial) reference frame $\{G; x', y', z'\}$ defined by the orthonormal basis $\mathcal{M} = \{\mathbf{e}_i^B\}$. This frame can translate and rotate with respect to the fixed frame according to the motion of the rigid body. Therefore, the associated basis generally changes its orientation during the motion. An observer solidal with the body-attached frame sees the rigid body fixed. The physical quantities $(\bullet)$ observed in this frame are indicated with the notation $(\bullet)^B$.

2.2.2 Dynamics of the center of mass

The motion of the center of mass is governed by the first cardinal equation of dynamics that expresses the conservation of the linear momentum $\mathbf{Q}$, namely:

$$\mathbf{Q}^{I,\mathcal{S}} = \int_V \rho \mathbf{v}_P^{I,\mathcal{S}} dV = m\mathbf{v}_G^{I,\mathcal{S}} \tag{2.39}$$

$$\dot{\mathbf{Q}}^{I,\mathcal{S}} = m\mathbf{a}_G^{I,\mathcal{S}} = \mathcal{F}^{\mathcal{S}} \tag{2.40}$$

where $\mathcal{F}$ is the resultant of external forces. If the acceleration vector of the center of mass is expressed by using the Equation (2.38), where $P \equiv O' \equiv G$, the Equation (2.40) assumes a local vision, namely:

$$\left(\dot{\mathbf{Q}}^{I,\mathcal{S}}\right)^{\mathcal{M}} = m\dot{\mathbf{v}}_G^{I,\mathcal{M}} + m\widetilde{\boldsymbol{\omega}}^{\mathcal{M}}\mathbf{v}_G^{I,\mathcal{M}} = \mathbf{R}^T\mathcal{F}^{\mathcal{S}} = \mathcal{F}^{\mathcal{M}} \tag{2.41}$$

The last equation is nonlinear, since it contains the product of the velocity components (apparent forces), and generally requires to know (or to predict) the updated configuration at any time instant as the body rotates. Moreover, because of the apparent forces, the dynamic problem of the center of mass is coupled with the dynamics about the center of mass. Note also that all the physical quantities in the Equation (2.40) are expressed with respect to the basis of the spatial frame, whereas the quantities in the Equation (2.41) are expressed with respect to the basis of the body-attached frame, which changes its orientation in the Euclidean space according to the motion of the body.

2.2.3 Dynamics about the center of mass

The motion about the center of mass is governed by the second cardinal equation of dynamics that states the conservation of the angular momentum $\mathbf{H}_N$ about an arbitrary point N (pole) of the Euclidean space, namely:

$$\mathbf{H}_N^{I,\mathcal{S}} = \int_V (P - N) \times \rho\mathbf{v}_P^{I,\mathcal{S}} dV \tag{2.42}$$

$$\dot{\mathbf{H}}_N^{I,\mathcal{S}} = -\mathbf{v}_N^{I,\mathcal{S}} \times \mathbf{Q}^{I,\mathcal{S}} + \mathcal{T}_N^{\mathcal{S}} \tag{2.43}$$

where $\mathcal{T}_N$ is the resultant torque of external forces about the pole N. If the pole N coincides either with a fixed point of the body (if exists) or with the center of mass, the first term of the second member of the Equation (2.43) vanishes. Let's assume that the pole N coincides with the center of mass G and let's express the velocity vector with the Equation (2.14), where $O' \equiv G$, the angular momentum can be written in terms of tensor of inertia $\mathbf{J}$[10], namely:

$$\begin{aligned}\mathbf{H}_G^{I,\mathcal{S}} &= \int_V (P - G) \times \rho\mathbf{v}_P^{I,\mathcal{S}} dV = \int_V (P - G) \times \rho(\mathbf{v}_G^{I,\mathcal{S}} + \boldsymbol{\omega}^{\mathcal{S}} \times \mathbf{x}_P^{B,\mathcal{S}}) dV = \\ &= \rho\Big[\int_V \mathbf{x}_P^{B,\mathcal{S}} dV\Big] \times \mathbf{v}_G^{I,\mathcal{S}} + \int_V \rho\mathbf{x}_P^{B,\mathcal{S}} \times (\boldsymbol{\omega}^{\mathcal{S}} \times \mathbf{x}_P^{B,\mathcal{S}}) dV = \\ &= \mathbf{0} + \mathbf{J}^{B,\mathcal{S}}\boldsymbol{\omega}^{\mathcal{S}} = \mathbf{J}^{B,\mathcal{S}}\boldsymbol{\omega}^{\mathcal{S}}\end{aligned} \tag{2.44}$$

The last relation allows us to write the conservation of the angular momentum as follows:

$$\dot{\mathbf{H}}_G^{I,\mathcal{S}} = \frac{d}{dt}(\mathbf{J}^{B,\mathcal{S}}\boldsymbol{\omega}^{\mathcal{S}}) = \dot{\mathbf{J}}^{B,\mathcal{S}}\boldsymbol{\omega}^{\mathcal{S}} + \mathbf{J}^{B,\mathcal{S}}\dot{\boldsymbol{\omega}}^{\mathcal{S}} = \mathcal{T}_G^{\mathcal{S}} \tag{2.45}$$

[10] Given a body of volume V in the Euclidean space and a reference frame $\{O; x, y, z\}$ with orthonormal basis $\{\mathbf{e}_i\}$, the tensor of inertia is given by:

$$\mathbf{J} = \begin{bmatrix} \int_V \rho(x_2^2 + x_3^2)dV & -\int_V \rho x_1 x_2 dV & -\int_V \rho x_1 x_3 dV \\ -\int_V \rho x_1 x_2 dV & \int_V \rho(x_1^2 + x_3^2)dV & -\int_V \rho x_2 x_3 dV \\ -\int_V \rho x_1 x_3 dV & -\int_V \rho x_2 x_3 dV & \int_V \rho(x_1^2 + x_2^2)dV \end{bmatrix} = -\int_V \rho\widetilde{\mathbf{x}}\widetilde{\mathbf{x}} dV$$

Following the evolution in time of the inertia tensor $\mathbf{J}^{B,\mathcal{S}}$ and, in particular, keeping track of its time derivative is not easy in a spatial vision, i.e. with the physical quantities expressed with respect to the basis $\mathcal{S}$, even when the inertial frame initially coincides with the principal inertia frame of the body, because the inertia properties vary with time (only in the very special case of a homogeneous sphere they are constant regardless of the choice of the reference system).

If the rotational motion is referred to the basis $\mathcal{M}$ of the body-attached frame (non-inertial), the formulation assumes a local vision and generally it is easier to solve even if it embeds the contribution of the apparent forces, namely[11]:

$$\begin{aligned}\dot{\mathbf{H}}_G^{I,\mathcal{S}} &= \frac{d}{dt}(\mathbf{R}\mathbf{R}^T\mathbf{J}^{B,\mathcal{S}}\mathbf{R}\mathbf{R}^T\boldsymbol{\omega}^{\mathcal{S}}) = \frac{d}{dt}(\mathbf{R}\mathbf{J}^{B,\mathcal{M}}\boldsymbol{\omega}^{\mathcal{M}}) = \\ &= \mathbf{R}\mathbf{J}^{B,\mathcal{M}}\dot{\boldsymbol{\omega}}^{\mathcal{M}} + \mathbf{R}\widetilde{\boldsymbol{\omega}}^{\mathcal{M}}\mathbf{J}^{B,\mathcal{M}}\boldsymbol{\omega}^{\mathcal{M}} = \mathcal{T}_G^{\mathcal{S}}\end{aligned} \tag{2.46}$$

$$\left(\dot{\mathbf{H}}_G^{I,\mathcal{S}}\right)^{\mathcal{M}} = \mathbf{J}^{B,\mathcal{M}}\dot{\boldsymbol{\omega}}^{\mathcal{M}} + \widetilde{\boldsymbol{\omega}}^{\mathcal{M}}\mathbf{J}^{B,\mathcal{M}}\boldsymbol{\omega}^{\mathcal{M}} = \mathbf{R}^T\mathcal{T}_G^{\mathcal{S}} = \mathcal{T}_G^{\mathcal{M}} \tag{2.47}$$

The last equation is nonlinear, since it contains the product of the angular velocity components. Note also that all the physical quantities of the Equation (2.47) are expressed with respect to the basis of the body-attached frame, which generally changes its orientation in the Euclidean space according to the motion of the body.

2.2.4 Dynamic problem

The dynamic problem of a rigid body consists in establishing the evolution in time of the configuration of the system. The set of dynamic equilibrium equations should be associated with the kinematic equations, which relate the velocity of the center of mass and the angular velocity with the actual rotation and its time derivative [86]. Depending on the orthonormal basis used for expressing the physical quantities, different equivalent formulations of the dynamic problem can be obtained.

2.2.4.1 Mixed representation

In the mixed representation, also referred to as the *mixed-frame* formulation or the *mixed-vision* formulation, the motion of the center of mass is described with respect to the basis $\mathcal{S}$ of the inertial frame, whereas the motion about the center of mass is described with respect to the basis $\mathcal{M}$ of the body-attached frame, which changes its orientation during the motion. The set of equations that solve the dynamic problem is

[11] The angular momentum with respect to the pole G can be expressed in a local vision as follows:

$$\begin{aligned}\mathbf{H}_G^{I,\mathcal{S}} &= \int_V (P-G)\times\rho\mathbf{v}_P^{I,\mathcal{S}}dV = \int_V (P-G)\times\rho(\mathbf{R}\mathbf{v}_G^{I,\mathcal{M}} + \mathbf{R}\boldsymbol{\omega}^{\mathcal{M}}\times\mathbf{R}\mathbf{x}_P^{B,\mathcal{M}})dV = \\ &= \rho\mathbf{R}\Big[\int_V \mathbf{x}_P^{B,\mathcal{M}}dV\Big]\times\mathbf{v}_G^{I,\mathcal{M}} + \mathbf{R}\int_V \rho\mathbf{x}_P^{B,\mathcal{M}}\times(\boldsymbol{\omega}^{\mathcal{M}}\times\mathbf{x}_P^{B,\mathcal{M}})dV = \\ &= \mathbf{0} - \mathbf{R}\int_V \rho\widetilde{\mathbf{x}}_P^{B,\mathcal{M}}\widetilde{\mathbf{x}}_P^{B,\mathcal{M}}\boldsymbol{\omega}^{\mathcal{M}}dV = \mathbf{R}\mathbf{J}^{B,\mathcal{M}}\boldsymbol{\omega}^{\mathcal{M}}\end{aligned}$$

given by[12] [86]:

$$\begin{cases} \mathbf{v}_G^{I,\mathcal{S}} = \dot{\mathbf{x}}_G^{I,\mathcal{S}} \\ \dot{\mathbf{R}} = \mathbf{R}\widetilde{\boldsymbol{\omega}}^{\mathcal{M}} \\ m\mathbf{a}_G^{I,\mathcal{S}} = \mathcal{F}^{\mathcal{S}} \\ \mathbf{J}^{B,\mathcal{M}}\dot{\boldsymbol{\omega}}^{\mathcal{M}} + \widetilde{\boldsymbol{\omega}}^{\mathcal{M}}\mathbf{J}^{B,\mathcal{M}}\boldsymbol{\omega}^{\mathcal{M}} = \mathcal{T}_G^{\mathcal{M}} \end{cases}$$

The resultant force and resultant torque of external loads can be functions both of time and of the kinematic quantities; therefore, the dynamic equilibrium equation that describes the motion of the center of mass is not independent from the equation that describes the motion of the body about the center of mass. Only in particular cases, for instance when the external loads vanish, it is possible to solve the two problems separately and without having to know the actual configuration of the body (independence of kinematic and dynamic problems).

2.2.4.2 Local representation

In the local representation of the motion, also referred to as the *local-frame* formulation or the *local-vision* formulation, all the physical quantities are expressed with respect to the basis $\mathcal{M}$ of the body-attached frame, which changes its orientation during the motion. The set of equations that solve the dynamic problem is given by [86]:

$$\begin{cases} \mathbf{v}_G^{I,\mathcal{S}} = \mathbf{R}\mathbf{v}_G^{I,\mathcal{M}} \\ \dot{\mathbf{R}} = \mathbf{R}\widetilde{\boldsymbol{\omega}}^{\mathcal{M}} \\ m\dot{\mathbf{v}}_G^{I,\mathcal{M}} + m\widetilde{\boldsymbol{\omega}}^{\mathcal{M}}\mathbf{v}_G^{I,\mathcal{M}} = \mathcal{F}^{\mathcal{M}} \\ \mathbf{J}^{B,\mathcal{M}}\dot{\boldsymbol{\omega}}^{\mathcal{M}} + \widetilde{\boldsymbol{\omega}}^{\mathcal{M}}\mathbf{J}^{B,\mathcal{M}}\boldsymbol{\omega}^{\mathcal{M}} = \mathcal{T}_G^{\mathcal{M}} \end{cases}$$

If the external loads vanish (free rigid body), the dynamic equilibrium equations are independent from the kinematic ones, i.e. they can be solved without having to know the actual configuration of the body [86]. However, in the most general case of forced motions, the dynamic and kinematic problems are coupled to each other.

2.3 Finite rotation manifold

If the hypothesis of small displacements fails, a proper description of the motion that includes both large displacements and large rotations becomes fundamental. Finite rotations are described from a mathematical point of view in order to provide the reader with the most important fundamentals. For further discussions on the topics presented in this section the reader is addressed to the references [11, 16, 20, 52, 84, 89].

2.3.1 Continuous groups

Let U be a set of elements that depend on a number of real continuous parameters $\mathbf{a}$, such that $U(\mathbf{a}) = U(a_1, a_2, \ldots, a_n)$ with $\mathbf{a} \in G$, with a binary composition rule (also

[12] If the origin of the reference frame is located at the center of mass of the body, it is possible to get simpler formulations since all the first moments of volume are null. In this case, the use of a mixed representation of the velocities ensures the simplest form of the dynamic problem. In fact, the motion of the center of mass is described by the second Newton's law, whereas the motion about the center of mass is described by the Euler's equations.

called *multiplication* or *translation*); these elements form a continuous group if they satisfy the following properties:

- closure under composition, i.e. the composition of two arbitrary elements of U is still an element of U, or rather $U(\mathbf{c}) = U(\mathbf{a})U(\mathbf{b})$ with $\mathbf{a}, \mathbf{b}, \mathbf{c} \in G$;
- associativity of the composition rule, i.e. $[U(\mathbf{a})U(\mathbf{b})]U(\mathbf{c}) = U(\mathbf{a})[U(\mathbf{b})U(\mathbf{c})]$ for every $\mathbf{a}, \mathbf{b}, \mathbf{c} \in G$;
- existence of the identity I, such that $U(\mathbf{a})I = IU(\mathbf{a}) = U(\mathbf{a})$ for every $\mathbf{a} \in G$;
- existence of the inverse $U(\mathbf{a}')$ for any element $U(\mathbf{a})$, such that $U(\mathbf{a}')U(\mathbf{a}) = U(\mathbf{a})U(\mathbf{a}') = I$ with $\mathbf{a}, \mathbf{a}' \in G$;
- continuity, i.e. for every $\mathbf{a}, \mathbf{b}, \mathbf{c} \in G$, if $U(\mathbf{c}) = U(\mathbf{a})U(\mathbf{b})$ then $\mathbf{c} = \mathbf{f}(\mathbf{a}, \mathbf{b})$, where $\mathbf{f}$ is a continuous real function.

The last property makes a group continuous and establishes that a small change on the elements $U(\mathbf{a})$ and $U(\mathbf{b})$, i.e. on the parameters $\mathbf{a}, \mathbf{b} \in G$, produces a small change also in their product. If the function $\mathbf{f}$ admits a convergent Taylor series expansion in the domain G (analytic function), the group is called (n-parameter) Lie group. Note that the requirements of a continuous group do not include a commutative composition rule.

2.3.2 Special orthogonal group $SO(3)$

As seen in a previous section, a finite rotation is a linear orthogonal transformation between two vector spaces isomorphic to $\mathbb{R}^3$. The rotation operator fulfils all the requirements of a continuous group and, in particular, belongs to the special Lie group of proper orthogonal transformations $SO(3)$, defined as follows[13] [52, 84]:

$$SO(3) := \{\mathbf{R} : \mathbb{R}^3 \to \mathbb{R}^3 \text{ linear} | \mathbf{R}^T\mathbf{R} = \mathbf{I},\ \det(\mathbf{R}) = 1\} \tag{2.48}$$

Since the transformation should preserve the length, the set of elements that form the Lie group depends on three independent parameters, for example the components of the rotational vector $\boldsymbol{\psi}$[14]. The rotation operator can be defined through the exponential map [52, 84]:

$$\mathbf{R} = \exp(\widetilde{\boldsymbol{\psi}}) = \mathbf{I} + \widetilde{\boldsymbol{\psi}} + \frac{1}{2!}\widetilde{\boldsymbol{\psi}}^2 + \frac{1}{3!}\widetilde{\boldsymbol{\psi}}^3 + \cdots + \frac{1}{n!}\widetilde{\boldsymbol{\psi}}^n \tag{2.49}$$

2.3.2.1 Composition rule

There are two equivalent ways to define compound rotations, which refer either to a material description or to a spatial description of the incremental rotation. Let's focus

[13] If $\det(\mathbf{R}) = -1$ the rotation is said *improper*, and the orthogonal transformation changes the parity of the reference frame.

[14] Two parameters define the direction, i.e. the rotation axis, and the third one defines the modulus, i.e. the amplitude of the rotation.

on the material description and the associated composition rule called *left translation map*[15], namely [52]:

$$\mathbf{R}^{new} = \mathbf{R}\mathbf{R}^{left} = \mathbf{R}\exp(\widetilde{\boldsymbol{\theta}}^{\mathcal{M}}) \tag{2.50}$$

One of the most important property of finite rotations is their non-commutative character, which implies that finite rotations cannot be treated as vector quantities, i.e. the parallelogram composition rule is no longer valid.

2.3.2.2 Tangent space

Let's introduce the space $so(3)$ of skew-symmetric tensors, isomorphic to $\mathbb{R}^3$ defined as follows [52, 84]:

$$so(3) := \{\widetilde{\boldsymbol{\psi}} : \mathbb{R}^3 \to \mathbb{R}^3 \text{ linear} | \widetilde{\boldsymbol{\psi}}^T + \widetilde{\boldsymbol{\psi}} = \mathbf{0}\} \tag{2.51}$$

Let's focus on the directional (Fréchet) derivative of the exponential map at the identity $\mathbf{R}(\mathbf{0}) = \mathbf{I}$ and at the generic point $\mathbf{R}(\boldsymbol{\psi})$, which defines the tangent vector spaces at the respective base point, namely [16, 52]:

$$\frac{d}{d\varepsilon}\exp(\varepsilon\widetilde{\boldsymbol{\psi}})\bigg|_{\varepsilon=0} = \widetilde{\boldsymbol{\psi}}, \qquad \widetilde{\boldsymbol{\psi}} \in \mathbf{T}_{\mathbf{I}}SO(3) \equiv so(3) \tag{2.52}$$

$$\frac{d}{d\varepsilon}\mathbf{R}(\boldsymbol{\psi})\exp(\varepsilon\widetilde{\boldsymbol{\theta}})\bigg|_{\varepsilon=0} = \mathbf{R}\widetilde{\boldsymbol{\theta}}, \qquad {}_{\text{left}}\mathbf{T}_{\mathbf{R}}SO(3) := \{\mathbf{R}\widetilde{\boldsymbol{\theta}} | \widetilde{\boldsymbol{\theta}} \in so(3)\} \tag{2.53}$$

The skew-symmetric tensors $\widetilde{\boldsymbol{\psi}}$ and $\widetilde{\boldsymbol{\theta}}$ can be seen as an infinitesimal rotation about the eigenvector associated with the zero eigenvalue, and are indissolubly associated with the base point, i.e. with the corresponding tangent space. The tangent spaces have a great importance in Lie groups because of their vector nature; thus, rotational vectors belonging to the same tangent space can be summed (parallelogram rule). Let's focus on the composition rule defined by the left translation map, the relation between the tangent space at the identity, $\mathbf{T}_{\mathbf{I}}SO(3)$, and the tangent space at the base point $\mathbf{R}$, ${}_{\text{left}}\mathbf{T}_{\mathbf{R}}SO(3)$, can be expressed through the tangent operator $\mathbf{T}(\boldsymbol{\psi})$ as follows [16, 52]:

$$\exp(\widetilde{\boldsymbol{\psi}} + \varepsilon\delta\widetilde{\boldsymbol{\psi}}) = \exp(\widetilde{\boldsymbol{\psi}})\exp(\varepsilon\delta\widetilde{\boldsymbol{\theta}}) \tag{2.54}$$

$$\frac{d}{d\varepsilon}\exp(\widetilde{\boldsymbol{\psi}} + \varepsilon\delta\widetilde{\boldsymbol{\psi}})\bigg|_{\varepsilon=0} = \frac{d}{d\varepsilon}\exp(\widetilde{\boldsymbol{\psi}})\exp(\varepsilon\delta\widetilde{\boldsymbol{\theta}})\bigg|_{\varepsilon=0} \quad \to \quad \delta\widetilde{\boldsymbol{\theta}} = \mathbf{T}(\boldsymbol{\psi})\delta\widetilde{\boldsymbol{\psi}} \tag{2.55}$$

$$\mathbf{T}(\boldsymbol{\psi}) = \mathbf{I} - \frac{1}{2!}\widetilde{\boldsymbol{\psi}} + \frac{1}{3!}\widetilde{\boldsymbol{\psi}}^2 + \cdots + \frac{(-1)^n}{(n+1)!}\widetilde{\boldsymbol{\psi}}^n \tag{2.56}$$

[15] The incremental rotation represents the change of orientation of the basis $\mathcal{M}$ of the body-attached frame with respect to the basis $\mathcal{S}$ of the spatial frame. In the material description, the composition rule implies that the incremental rotation is expressed with respect to the basis $\mathcal{M}$. By contrast, the composition rule associated with the spatial description, called *right translation map*, is given by [52]:

$$\mathbf{R}^{new} = \mathbf{R}^{right}\mathbf{R} = \exp(\widetilde{\boldsymbol{\theta}}^{\mathcal{S}})\mathbf{R}$$
$$\widetilde{\boldsymbol{\theta}}^{\mathcal{S}} = \mathbf{R}\widetilde{\boldsymbol{\theta}}^{\mathcal{M}}\mathbf{R}^T$$

and implies that the incremental rotation $\boldsymbol{\theta}$ is expressed with respect to the basis $\mathcal{S}$. For further discussions the reader is addressed to the references [16, 52, 84].

Hence, compound rotations can be obtained either through the left translation map or as a composition of rotational vectors, provided that they are defined in the same tangent space, for instance at the identity.

2.3.2.3 Lie algebra

A Lie algebra is a vector space $\mathfrak{g}$ over some field F with a binary operation $[\cdot,\cdot] : \mathfrak{g}\times\mathfrak{g} \to \mathfrak{g}$, called the Lie bracket, such that satisfies the following axioms:

- bilinearity, $[\alpha x + \beta y, z] = \alpha[x, z] + \beta[y, z]$ and $[z, \alpha x + \beta y] = \alpha[z, x] + \beta[z, y]$ for every $\alpha, \beta \in F$ and $x, y, z \in \mathfrak{g}$;
- Jacobi identity, $\big[[x, y], z\big] + \big[[z, x], y\big] + \big[[y, z], x\big] = 0$ for every $x, y, x \in \mathfrak{g}$;
- antisymmetry, $[x, y] = -[y, x]$ for every $x, y \in \mathfrak{g}$.

2.4 Rotation operator representations

The rotation is a linear transformation that preserves the distances and the reciprocal orientation between different points of the same body. The rotation operator is thus a proper orthogonal matrix and depends on three independent parameters. The choice of the set of parameters is not unique and relates to the specific issue. Several kinds of parametrization were proposed over the years, which can differ for independence, mathematical form, existence of singularities, computational efficiency, composition law, geometric interpretation, etc. [37], as follows:

- *Euler angles.* It results from the application of three consecutive principal rotations referred either to the updated axes or to the initial ones; the Euler angle convention depends on the order (twelve different choices) of successive rotations [6];
- *Tait-Bryan (or nautical) angles.* It is a particular Euler angle convention widely used both in nautical and aeronautical applications;
- *rotational vector.* It directly refers to the axis of the rotation and its amplitude, invariants of the rotation;
- *Euler parameters.* It consists of a purely algebraic set of four dependent parameters that can be obtained by introducing a change of variables in the Euler's representation of the rotation operator [37];
- *Rodrigues parameters.* It consists of a set of three independent parameters related and somehow similar to the rotational vector;
- *Quaternions.* It results equivalent to Euler parameters, but the quaternion algebra makes this parametrization much more attractive;
- *conformal rotation vector.* It consists of a set of three independent parameters obtained through a conformal transformation applied to Euler parameters [37].

Euler angles (and Tait-Bryan angles), and in general all the geometric parameters, have a straightforward physical interpretation which can offer an immediate view of the motion, but, because of their trigonometric nature, these parameters lead to singularities

and low computational efficiency, especially when the rotations are arbitrarily large [37]. For these reasons, the algebraic approach, which is based on the invariants of the rotation, is preferable even mandatory.

2.4.1 Rotational vector

The rotational vector parametrization consists of a set of three independent parameters with an easy geometric interpretation and without any kinematic singularities [37]. The rotational vector is defined as the vector with the same direction of the rotation axis and magnitude equal to the rotation amplitude [37], namely:

$$\boldsymbol{\psi} = \mathbf{u}\phi \tag{2.57}$$

The rotation operator can be expressed either in trigonometric form or through the exponential map, and admits a series expansion, namely [11, 16, 37, 52]:

$$\mathbf{R} = \mathbf{I} + \frac{\sin\phi}{\phi}\widetilde{\boldsymbol{\psi}} + \frac{1-\cos\phi}{\phi^2}\widetilde{\boldsymbol{\psi}}\widetilde{\boldsymbol{\psi}} = \exp(\widetilde{\boldsymbol{\psi}}) \tag{2.58}$$

$$\mathbf{R} = \mathbf{I} + \widetilde{\boldsymbol{\psi}} + \frac{1}{2!}\widetilde{\boldsymbol{\psi}}^2 + \frac{1}{3!}\widetilde{\boldsymbol{\psi}}^3 + \cdots + \frac{1}{n!}\widetilde{\boldsymbol{\psi}}^n \tag{2.59}$$

The tangent operator and its series expansion, associated with the rotational vector representation, are given by [11, 16, 37]:

$$\mathbf{T}(\boldsymbol{\psi}) = \mathbf{I} + \frac{\cos\phi - 1}{\phi^2}\widetilde{\boldsymbol{\psi}} + \left(1 - \frac{\sin\phi}{\phi}\right)\frac{\widetilde{\boldsymbol{\psi}}\widetilde{\boldsymbol{\psi}}}{\phi^2} \tag{2.60}$$

$$\mathbf{T}(\boldsymbol{\psi}) = \mathbf{I} - \frac{1}{2!}\widetilde{\boldsymbol{\psi}} + \frac{1}{3!}\widetilde{\boldsymbol{\psi}}^2 + \cdots + \frac{(-1)^n}{(n+1)!}\widetilde{\boldsymbol{\psi}}^n \tag{2.61}$$

The angular velocity and acceleration vectors, in terms of rotational vector parameters, are given by [37]:

$$\boldsymbol{\omega}^{\mathcal{S}} = \mathbf{T}^T(\boldsymbol{\psi})\dot{\boldsymbol{\psi}} \tag{2.62}$$

$$\boldsymbol{\omega}^{\mathcal{M}} = \mathbf{T}(\boldsymbol{\psi})\dot{\boldsymbol{\psi}} \tag{2.63}$$

$$\dot{\boldsymbol{\omega}}^{\mathcal{S}} = \mathbf{T}^T(\boldsymbol{\psi})\ddot{\boldsymbol{\psi}} + \dot{\mathbf{T}}^T(\boldsymbol{\psi})\dot{\boldsymbol{\psi}} \tag{2.64}$$

$$\dot{\boldsymbol{\omega}}^{\mathcal{M}} = \mathbf{T}(\boldsymbol{\psi})\ddot{\boldsymbol{\psi}} + \dot{\mathbf{T}}(\boldsymbol{\psi})\dot{\boldsymbol{\psi}} \tag{2.65}$$

Note that the apparent singularity in the Equations (2.58) and (2.60) for $\phi = 0$, can be removed by noticing that both the expressions in the neighbourhood of $\boldsymbol{\psi} = \mathbf{0}$ tend to the identity matrix [37].

2.4.1.1 Logarithmic map

The so called *logarithmic map* is the inverse function of the exponential map and gives the rotational vector $\boldsymbol{\psi}$ associated with the rotation operator $\mathbf{R}(\boldsymbol{\psi})$, namely [86]:

$$\widetilde{\boldsymbol{\psi}} = \log_{SO(3)}(\mathbf{R}) = \frac{\vartheta}{2\sin\vartheta}(\mathbf{R} - \mathbf{R}^T), \qquad \vartheta = \cos^{-1}\left[\frac{\mathrm{tr}(\mathbf{R}) - 1}{2}\right] \tag{2.66}$$

with $|\vartheta| < \pi$. Such limitation is necessary because of the non-injectivity of the exponential map; otherwise, the logarithmic map would be multivalued [86]. Note that the apparent singularity for $\vartheta = 0$ can be removed by noticing that ϑ is zero if and only if the rotation operator is the identity matrix, i.e. $\mathbf{R} = \mathbf{I}$. In this case the corresponding rotational vector is the null vector, i.e. $\boldsymbol{\psi} = \mathbf{0}$ [86].

2.4.2 Tait-Bryan angles

The Tait-Bryan (or nautical[16]) angles parametrization is widely used in nautical fields because of its immediate and useful geometric interpretation. It consists in three successive principal rotations about the axes of the body-attached frame[17], namely:

- a rotation φ_1 about the x'-axis, also called *roll*;
- a rotation φ_2 about the y'-axis, also called *pitch*;
- a rotation φ_3 about the z'-axis, also called *yaw*.

The rotation operator associated with the Tait-Bryan angles is given by [6, 37]:

$$\mathbf{R} = \begin{bmatrix} \cos\varphi_2\cos\varphi_3 & -\cos\varphi_1\sin\varphi_3 + \sin\varphi_1\sin\varphi_2\cos\varphi_3 & \sin\varphi_1\sin\varphi_3 + \cos\varphi_1\sin\varphi_2\cos\varphi_3 \\ \cos\varphi_2\sin\varphi_3 & \cos\varphi_1\cos\varphi_3 + \sin\varphi_1\sin\varphi_2\sin\varphi_3 & -\sin\varphi_1\cos\varphi_3 + \cos\varphi_1\sin\varphi_2\sin\varphi_3 \\ -\sin\varphi_2 & \sin\varphi_1\cos\varphi_2 & \cos\varphi_1\cos\varphi_2 \end{bmatrix} \tag{2.67}$$

The angular velocity vectors, in terms of Tait-Bryan parameters and their time derivatives, are given by [37]:

$$\boldsymbol{\omega}^{\mathcal{S}} = \begin{bmatrix} \cos\varphi_2\cos\varphi_3 & -\sin\varphi_3 & 0 \\ \cos\varphi_2\sin\varphi_3 & \cos\varphi_3 & 0 \\ -\sin\varphi_2 & 0 & 1 \end{bmatrix} \begin{bmatrix} \dot{\varphi}_1 \\ \dot{\varphi}_2 \\ \dot{\varphi}_3 \end{bmatrix} \tag{2.68}$$

$$\boldsymbol{\omega}^{\mathcal{M}} = \begin{bmatrix} 1 & 0 & -\sin\varphi_2 \\ 0 & \cos\varphi_1 & \sin\varphi_1\cos\varphi_2 \\ 0 & -\sin\varphi_1 & \cos\varphi_1\cos\varphi_2 \end{bmatrix} \begin{bmatrix} \dot{\varphi}_1 \\ \dot{\varphi}_2 \\ \dot{\varphi}_3 \end{bmatrix} \tag{2.69}$$

2.4.2.1 Inverse formulae

In some applications the rotation operator $\mathbf{R} = R_{ij}\mathbf{e}_i \otimes \mathbf{e}_j$ is known but not the corresponding Tait-Bryan angles, which can be found by inverting the Equation (2.67),

[16] In the nautical context a specific terminology of motions is usually used. Let's consider a Cartesian reference frame $\{O; x, y, z\}$ with the z-axis pointing vertically upwards and the x-axis aligned with the longitudinal direction of the floating body. *Roll*, *pitch*, and *yaw* are respectively the rotations about the x, y, and z-axis, while *surge*, *sway*, and *heave* are respectively the motions along the longitudinal, transverse, and vertical axes.

[17] Nautical angles can also be interpreted in terms of principal rotations about the axes of the spatial frame.

namely [6]:

$$
\begin{aligned}
R_{31} &\neq \pm 1 \\
&\varphi_2 = \text{asin}(-R_{31}), \qquad -\pi/2 < \varphi_2 < \pi/2 \\
&\varphi_1 = \text{atan2}(R_{32}, R_{33}) \\
&\varphi_3 = \text{atan2}(R_{21}, R_{11}) \\
\\
&\varphi_2 = \text{asin}(-R_{31}), \qquad \pi/2 < \varphi_2 < 3\pi/2 \\
&\varphi_1 = \text{atan2}(-R_{32}, -R_{33}) \\
&\varphi_3 = \text{atan2}(-R_{21}, -R_{11}) \\
R_{31} &= -1 \\
&\varphi_2 = \pi/2 \\
&\varphi_1 = \text{atan2}(R_{12}, R_{13}) + \varphi_3 \\
&\varphi_3 = \text{any value} \\
R_{31} &= +1 \\
&\varphi_2 = -\pi/2 \\
&\varphi_1 = \text{atan2}(-R_{12}, -R_{13}) - \varphi_3 \\
&\varphi_3 = \text{any value}
\end{aligned}
$$

2.5 Fluid dynamics

The hydrodynamic actions are probably the main source of loads that can affect the static and dynamic behaviour of a floating body, together with the aerodynamic loads due to the interaction of the structure placed above the floating body (wind turbine, sail, etc.) with the wind. The present work is much more focused on the dynamics of floating bodies regardless of the supported device. However, aerodynamic loads can be added in future by means of proper models based on the specific features of the supported structure. The basics of hydrodynamics are briefly reminded here. For further discussions on the topics presented in this section the reader is addressed to the references [29, 61, 66, 68].

2.5.1 Fundamental law assumptions

The fundamental fluid dynamics laws are presented in the Eulerian specification of the flow field, i.e. the particle of fluid is not followed in time and space, but the observer is focused on specific locations of the motion field. Let's consider a spatial (fixed) inertial reference frame $\{O; x, y, z\}$ with the z-axis pointing vertically upwards and defined by the orthonormal basis $\mathcal{S} = \{\mathbf{e}_i^I\}$. All the physical quantities are observed in this frame and expressed with respect to the canonical basis[18].

[18] In order to not weigh the notation down, the indication of both the reference frame and the basis is removed, namely:

$$\mathbf{x} = \mathbf{x}^{I,\mathcal{S}}$$

2.5.1.1 Continuity equation

Given an arbitrary region V of the fluid with closed surface S, the principle of mass conservation, also known in fluid dynamics as continuity equation, states that the mass m enclosed by the surface S is constant with respect to time[19,20], namely [61]:

$$\frac{Dm}{Dt} = \int_V \frac{\partial \rho}{\partial t} dV + \int_S \rho \mathbf{v} \cdot \mathbf{n} dS = 0 \tag{2.70}$$

Since the Equation (2.70) is valid in all the regions V of the fluid, the continuity equation can be written in differential terms rather than in integral terms[21] [61]:

$$\frac{\partial \rho}{\partial t} + \nabla \cdot (\rho \mathbf{v}) = \frac{D\rho}{Dt} + \rho \nabla \cdot \mathbf{v} = 0 \tag{2.71}$$

If the fluid can be considered incompressible, i.e. the density ρ is constant, the continuity equation can be rewritten as follows [66, 68]:

$$\nabla \cdot \mathbf{v} = 0 \tag{2.72}$$

In most of maritime hydraulic problems, such as the dynamics of floating bodies, the fluid is usually considered incompressible.

2.5.1.2 Cauchy equation

Let $\mathbf{T}$ be the stress tensor, the Cauchy momentum equation describes the momentum transport (conservation) in an arbitrary region of the fluid, namely [61]:

$$\nabla \cdot \mathbf{T} + \rho \mathbf{b}(\mathbf{x}, t) - \rho \frac{D\mathbf{v}(\mathbf{x}, t)}{Dt} = \mathbf{0} \tag{2.73}$$

[19] Let $f(\mathbf{x}, t)$ be a scalar function and $\mathbf{f}(\mathbf{x}, t)$ a vector field, which describe some properties of the fluid, the *material derivatives* are given by [61, 68]:

$$\frac{Df}{Dt} = \frac{\partial f}{\partial t} + \mathbf{v} \cdot \nabla f$$
$$\frac{D\mathbf{f}}{Dt} = \frac{\partial \mathbf{f}}{\partial t} + (\mathbf{v} \cdot \nabla)\mathbf{f}$$

[20] Let $f(\mathbf{x}, t)$ be a scalar function and $\mathbf{f}(\mathbf{x}, t)$ a vector field, which describe some properties of the fluid, the Reynold transport theorem states that [61]:

$$\frac{D}{Dt} \int_V f dV = \int_V \left[\frac{\partial f}{\partial t} + \nabla \cdot (f\mathbf{v}) \right] dV$$
$$\frac{D}{Dt} \int_V \mathbf{f} dV = \int_V \left[\frac{\partial \mathbf{f}}{\partial t} + \nabla \cdot (\mathbf{f}\mathbf{v}) \right] dV$$

[21] The vector differential operator ∇ in a Cartesian coordinate system in $\mathbb{R}^n$ with standard basis $\{\mathbf{e}_1, \ldots, \mathbf{e}_n\}$ is defined in terms of partial derivative operators, namely:

$$\nabla = \sum_{i=1}^{n} \mathbf{e}_i \frac{\partial}{\partial x_i}$$

If the fluid is incompressible and Newtonian[22], the Cauchy equation is given by [61]:

$$-\nabla p + \mu\nabla^2\mathbf{v} + \rho\mathbf{b}(\mathbf{x},t) - \rho\frac{D\mathbf{v}(\mathbf{x},t)}{Dt} = \mathbf{0} \tag{2.74}$$

2.5.1.3 Navier-Stokes and Euler equations

The Navier-Stokes equations describe the dynamics of a fluid. Given an incompressible and Newtonian fluid, they can be obtained by combining Equations (2.72) and (2.74), namely [61]:

$$\begin{cases} -\nabla p + \mu\nabla^2\mathbf{v} + \rho\mathbf{b}(\mathbf{x},t) - \rho\frac{D\mathbf{v}(\mathbf{x},t)}{Dt} = \mathbf{0} \\ \nabla\cdot\mathbf{v} = 0 \end{cases}$$

If the fluid is also inviscid, the Navier-Stokes equations are called Euler equations, namely [61]:

$$\begin{cases} -\nabla p + \rho\mathbf{b}(\mathbf{x},t) - \rho\frac{D\mathbf{v}(\mathbf{x},t)}{Dt} = \mathbf{0} \\ \nabla\cdot\mathbf{v} = 0 \end{cases}$$

These equations make up a system of nonlinear partial differential equations that can be solved only numerically. In this context, computational fluid dynamics (CFD) methods are very attractive also for civil engineering purposes.

2.5.2 Potential flows

Given an inviscid-incompressible Newtonian fluid and an irrotational[23] flow, it is possible to define a scalar function $\Phi(\mathbf{x},t)$, called potential, such that [29, 66, 68]:

$$\mathbf{v} = \nabla\Phi \tag{2.75}$$

The Laplace equation can be obtained by combining the Equations (2.72) and (2.75), namely [66, 68]:

$$\nabla^2\Phi = 0 \tag{2.76}$$

This equation, associated with proper boundary conditions, completely defines the motion of the fluid.

[22] Let $\mathbf{D}$ be the symmetric part of the gradient of the velocity vector and p be a scalar function (pressure). The constitutive relation of an incompressible Newtonian fluid is given by [61]:

$$\mathbf{T} = -p\mathbf{I} + 2\mu\mathbf{D}$$

[23] A flow is irrotational if [29, 66, 68]:

$$\nabla\times\mathbf{v} = \mathbf{0}$$

2.5.2.1 Bernoulli equation

Given an homogeneous, inviscid-incompressible Newtonian fluid subjected only to the gravity acceleration $\mathbf{g}$, which is a conservative vector field defined by the gradient of the scalar function U (potential), namely:

$$\mathbf{g} = \nabla U = \nabla(-gx_3) \tag{2.77}$$

the Euler equations can be written in a form well known as Bernoulli equation, namely [68]:

$$\frac{\partial \mathbf{v}}{\partial t} + (\nabla \times \mathbf{v}) \times \mathbf{v} = -\nabla\left(\frac{p}{\rho} + \frac{1}{2}\mathbf{v} \cdot \mathbf{v} - U\right) \tag{2.78}$$

If the flow is irrotational, the Bernoulli equation can be written as follows [29, 68]:

$$\frac{p}{\rho} + \frac{\partial \Phi}{\partial t} + \frac{1}{2}\nabla\Phi \cdot \nabla\Phi + gx_3 = C \tag{2.79}$$

Given the potential function of the fluid, the Bernoulli equation defines the pressure in the whole motion field; therefore, the resultant forces exerted by the fluid on any submerged body can be computed as the integral of such pressures.

Chapter 3

Nonlinear dynamic model

"If you cannot convince them,
confuse them."

Harry S. Truman

The formulation of the dynamics of rigid bodies is presented in the mixed-frame context, with a meticulous analysis of different typologies of loads. In particular both follower and non-follower loads are considered including the important case of transformations of the state variables. The algorithm used for solving the differential problem is briefly described. The approach is tested on a number of cases whose analytic solution is known, like the homogeneous sphere with follower torque or the axially symmetric rigid body with follower torque, proving the convergence of the method. Other interesting comparisons with classic oscillators (simple, damped, forced) are discussed in Appendix B. The formulation is also compared with an alternative approach based on a complete local representation of the motion, and the possibility of truncating the tangent stiffness operator is discussed. The chapter aims at providing the reader with the details on the formulation of the rigid-body dynamic problem in the framework of the mixed representation of the motion, for various typologies of loads.

3.1 Dynamic problem

The dynamics of rigid bodies assumes a great importance in a wide range of applied problems, such as the analysis of the motion of floating platforms, ships, hulls, etc., whenever the system features and the boundary conditions make the inflexibility hypothesis acceptable. The dynamic problem aims at establishing the configuration[1] of the rigid body at any time instant and consists in solving the set of differential equations that defines the motion of the center of mass and the motion about the center of mass. The problem analysed hereafter refers to the mixed-frame formulation (see Section 2.2.4.1).

3.1.1 Reference frames

The choice of the reference frames used for describing either the displacements of the center of mass or the rotational motion of the body can lead to different mathematical formulations of the dynamic problem, formally equivalent. The code is designed to work simultaneously with two different bases relating to two different reference frames[2] (see Figure 3.1):

- inertial (spatial or fixed) reference frame $\{O; x, y, z\}$ defined by the orthonormal basis $\mathcal{S} = \{\mathbf{e}_i^I\}$. The physical quantities $(\bullet)$ observed in this frame are indicated with the notation $(\bullet)^I$;
- non-inertial (body-attached) reference frame[3] $\{G; x', y', z'\}$ defined by the orthonormal basis $\mathcal{M} = \{\mathbf{e}_i^B\}$. This frame can translate and rotate with respect to the fixed frame according to the motion of the rigid body. Therefore, the associated basis generally changes its orientation during the motion. An observer solidal with the body-attached frame sees the rigid body fixed. The physical quantities $(\bullet)$ observed in this frame are indicated with the notation $(\bullet)^B$.

The motion of the center of mass is described with respect to the orthonormal basis $\mathcal{S}$, whereas the motion about the center of mass is described with respect to the orthonormal basis $\mathcal{M}$, resulting in a mixed formulation. This approach avoids considering the apparent forces in the translational problem. Furthermore, since in the body-attached frame the most operators (inertia tensor) are time-invariant, the conservation of the angular momentum is simplified. By contrast, some complications arise from the coupling of the translational and rotational problems, for instance due to the hydrodynamic action (extra-diagonal terms of the hydrodynamic added mass and damping matrices)

[1] In the most cases the configuration of the body, in terms of displacement of the center of mass and orientation, is much more of interest. In this dissertation the various methods are therefore compared referring to the time histories of the state variable $\hat{\mathbf{q}}$ that defines the configuration of the body. The equivalence of the evolution in time between different records of the variable $\hat{\mathbf{q}}$ implies also the equivalence of the time histories of both velocities and accelerations. However, the numerical model can return all the time series of the kinematic quantities.

[2] As introduced in the previous chapter, the notation $(\bullet)^{(\diamond),(\circ)}$ indicates a physical quantity $(\bullet)$ observed in the frame $(\diamond)$ and expressed with respect to the basis $(\circ)$, with $(\diamond) = I, B$ and $(\circ) = \mathcal{S}, \mathcal{M}$. Alternatively, if the indication of the reference frame is not significant (for instance for forces and torques), the superscript is limited to the information about the basis, i.e. $(\bullet)^{(\circ)}$.

[3] The origin of the body-attached frame is located at the center of mass of the body. This assumption simplifies the expressions of the linear momentum and angular momentum since all the first moments of volume are zero. However, it is possible to obtain formulations similar to those developed in this work also for generic reference frames.

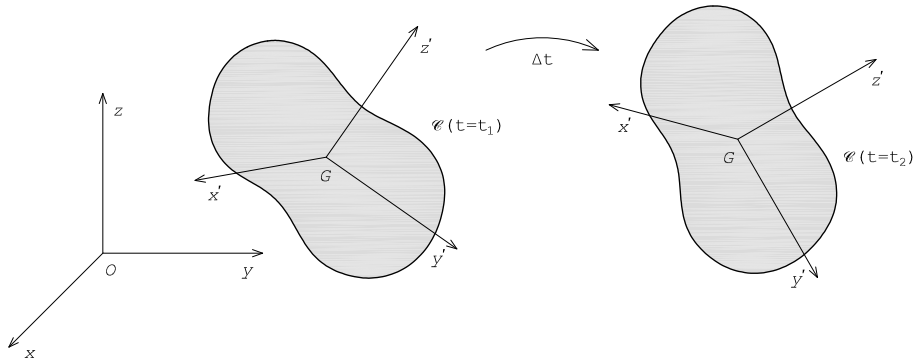

Figure 3.1: Mixed reference frame.

and follower forces. This implies, at any time instant, the loss of symmetry of all the main system linear operators (damping and stiffness) and their dependence on the actual rotation. However, the loss of symmetry cannot be avoided even using a total local formulation because of the gyroscopic (apparent) loads.

3.1.2 Linear operators

Let $\hat{\mathbf{q}} = [\mathbf{x}_G^{I,\mathcal{S}}; \boldsymbol{\psi}]$ be the position state vector[4], collecting the position vector of the center of mass and the rotational vector, let $\hat{\mathbf{v}} = [\mathbf{v}_G^{I,\mathcal{S}}; \boldsymbol{\omega}^{\mathcal{M}}]$ be the velocity state vector, collecting the velocity vector of the center of mass and the angular velocity vector, let $\hat{\dot{\mathbf{v}}} = [\mathbf{a}_G^{I,\mathcal{S}}; \dot{\boldsymbol{\omega}}^{\mathcal{M}}]$ be the acceleration state vector, collecting the acceleration vector of the center of mass and the angular acceleration vector, these three quantities can be regarded as state variables and completely describe the rigid-body motion. In other words, the evolution in time of the state variables offers a complete knowledge about the dynamics of the body. The dynamic equilibrium equations can be written in terms of the state variables, defining the residual vector $\hat{\mathbf{r}}$, as follows:

$$\hat{\mathbf{r}} = \begin{bmatrix} m\mathbf{I}_3 & \mathbf{0}_{3\times3} \\ \mathbf{0}_{3\times3} & \mathbf{J}^{B,\mathcal{M}} \end{bmatrix} \hat{\dot{\mathbf{v}}} + \begin{bmatrix} \mathbf{0}_{3\times1} \\ \widetilde{\hat{\mathbf{v}}}_{4:6}\mathbf{J}^{B,\mathcal{M}}\hat{\mathbf{v}}_{4:6} \end{bmatrix} - \begin{bmatrix} \mathcal{F}^{\mathcal{S}}(\hat{\mathbf{q}}, \hat{\mathbf{v}}, \hat{\dot{\mathbf{v}}}, t) \\ \mathcal{T}_G^{\mathcal{M}}(\hat{\mathbf{q}}, \hat{\mathbf{v}}, \hat{\dot{\mathbf{v}}}, t) \end{bmatrix} = \mathbf{0}_{6\times1} \quad (3.1)$$

[4]Even if the state variable associated with the configuration of the body is expressed as a vector $\hat{\mathbf{q}} \in \mathbb{R}^6$, do not confuse the nature of the rotational vector $\boldsymbol{\psi}$, which is a parametrization of the rotation operator $\mathbf{R} \in SO(3)$. The position state vector should therefore be treated as an element $\hat{q}$ of the Lie group $\mathbb{R}^3 \times SO(3)$, namely $\hat{q} \in \mathbb{R}^3 \times SO(3)$, together with the left translation map.

The linearisation of the Equation (3.1) with respect to the state variables defines the tangent (stiffness, damping, and mass) operators, namely[5]:

$$\mathbf{K}^t \cdot \Delta\hat{\mathbf{q}} = D_{\mathbf{q}}\hat{\mathbf{r}} \cdot \Delta\hat{\mathbf{q}} \tag{3.2}$$

$$\mathbf{C}^t \cdot \Delta\hat{\mathbf{v}} = D_{\mathbf{v}}\hat{\mathbf{r}} \cdot \Delta\hat{\mathbf{v}} \tag{3.3}$$

$$\mathbf{M}^t \cdot \Delta\hat{\dot{\mathbf{v}}} = D_{\dot{\mathbf{v}}}\hat{\mathbf{r}} \cdot \Delta\hat{\dot{\mathbf{v}}} \tag{3.4}$$

3.1.3 Rotation derivatives

The rotation operator can be seen as a linear transformation and, in the dynamics of rigid bodies, it is usually applied to vectors or to a composition of matrices and vectors, i.e. to another vector. Hence, the derivative of the resulting vector with respect to the rotational vector (state variable) becomes of particular interest. Let $\mathbf{z}$ be a vector[6]:

$$\begin{aligned} \mathbf{R}^T(\boldsymbol{\psi})\mathbf{z}^{\mathcal{S}}, \qquad D(\mathbf{R}^T\mathbf{z}^{\mathcal{S}}) \cdot \widetilde{\boldsymbol{\theta}}^{\mathcal{M}} &= \big[D(\mathbf{R}^T) \cdot \widetilde{\boldsymbol{\theta}}^{\mathcal{M}}\big]\mathbf{z}^{\mathcal{S}} = -\widetilde{\boldsymbol{\theta}}^{\mathcal{M}}\mathbf{R}^T\mathbf{z}^{\mathcal{S}} = \\ &= -\boldsymbol{\theta}^{\mathcal{M}} \times (\mathbf{R}^T\mathbf{z}^{\mathcal{S}}) = \widetilde{\mathbf{R}^T\mathbf{z}^{\mathcal{S}}}\boldsymbol{\theta}^{\mathcal{M}} \end{aligned} \tag{3.5}$$

$$\begin{aligned} \mathbf{R}(\boldsymbol{\psi})\mathbf{z}^{\mathcal{M}}, \qquad D(\mathbf{R}\mathbf{z}^{\mathcal{M}}) \cdot \widetilde{\boldsymbol{\theta}}^{\mathcal{M}} &= \big[D(\mathbf{R}) \cdot \widetilde{\boldsymbol{\theta}}^{\mathcal{M}}\big]\mathbf{z}^{\mathcal{M}} = \mathbf{R}\widetilde{\boldsymbol{\theta}}^{\mathcal{M}}\mathbf{z}^{\mathcal{M}} = \\ &= \mathbf{R}(\boldsymbol{\theta}^{\mathcal{M}} \times \mathbf{z}^{\mathcal{M}}) = -\mathbf{R}\widetilde{\mathbf{z}}^{\mathcal{M}}\boldsymbol{\theta}^{\mathcal{M}} \end{aligned} \tag{3.6}$$

3.2 Inertial loads

An accelerating body can be transformed into an equivalent static system by means of the so called inertial loads (D'Alembert's principle), i.e. external forces and torques associated with the accelerating masses, namely:

$$\mathbf{F}_G^{\mathcal{S}} = -m\hat{\dot{\mathbf{v}}}_{1:3} \tag{3.7}$$

$$\mathbf{T}_G^{\mathcal{M}} = -\mathbf{J}^{B,\mathcal{M}}\dot{\boldsymbol{\omega}}^{\mathcal{M}} - \boldsymbol{\omega}^{\mathcal{M}} \times \mathbf{J}^{B,\mathcal{M}}\boldsymbol{\omega}^{\mathcal{M}} = -\mathbf{J}^{B,\mathcal{M}}\hat{\dot{\mathbf{v}}}_{4:6} - \hat{\mathbf{v}}_{4:6} \times \mathbf{J}^{B,\mathcal{M}}\hat{\mathbf{v}}_{4:6} \tag{3.8}$$

[5] The directional derivative with respect to the position state variable $\hat{\mathbf{q}} = [\mathbf{x}_G^{I,\mathcal{S}}; \boldsymbol{\psi}]$ requires somehow attention because of the nature of the rotational vector $\boldsymbol{\psi}$, which represents elements of the special orthogonal group of finite rotations $SO(3)$. The infinitesimal increment of the rotational vector should therefore be referred to the proper tangent space, in fact $\mathbf{R}(\boldsymbol{\psi} + \delta\boldsymbol{\psi}) \neq \mathbf{R}(\boldsymbol{\psi})\mathbf{R}(\delta\boldsymbol{\psi})$. In particular, in the framework of the mixed-frame formulation, compound rotations are defined by the left translation map (see Section 2.3.2.1), which is associated with a material (body-attached) representation of the rotational motion. Because of the structure of the algorithm [11], the directional derivative of the rotation is computed with respect to the increment $\boldsymbol{\theta}^{\mathcal{M}}$ of the current rotation operator $\mathbf{R}(\boldsymbol{\psi})$ that is related to the increment of the rotational vector through the tangent operator, namely $\boldsymbol{\theta}^{\mathcal{M}} = \mathbf{T}(\boldsymbol{\psi})\delta\boldsymbol{\psi}$. By contrast, the position vector of the center of mass does not introduce any significant issues.

[6] These derivatives can easily be verified. Let $\delta\boldsymbol{\psi}$ be an infinitesimal rotation belonging to the tangent space at the identity, for any finite rotation $\boldsymbol{\psi}$ and any vector $\mathbf{z}$ it follows that:

$$[\mathbf{R}^T(\boldsymbol{\psi} + \delta\boldsymbol{\psi}) - \mathbf{R}^T(\boldsymbol{\psi})]\mathbf{z} \approx [\widetilde{\mathbf{R}^T(\boldsymbol{\psi})\mathbf{z}}]\mathbf{T}(\boldsymbol{\psi})\delta\boldsymbol{\psi}$$

$$[\mathbf{R}(\boldsymbol{\psi} + \delta\boldsymbol{\psi}) - \mathbf{R}(\boldsymbol{\psi})]\mathbf{z} \approx -\mathbf{R}(\boldsymbol{\psi})\widetilde{\mathbf{z}}\mathbf{T}(\boldsymbol{\psi})\delta\boldsymbol{\psi}$$

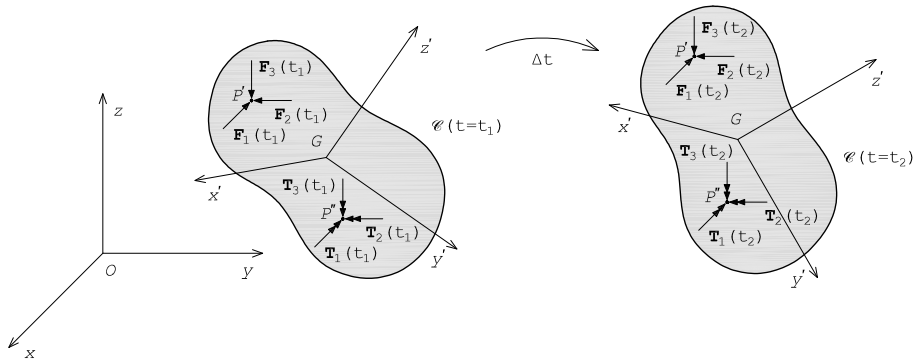

Figure 3.2: Non-follower loads.

The tangent operators associated with the inertial loads are given by:

$$\mathbf{M}^t_{1:3\times 1:3} = m\mathbf{I}_3 \tag{3.9}$$

$$\mathbf{M}^t_{4:6\times 4:6} = \mathbf{J}^{B,\mathcal{M}} \tag{3.10}$$

$$\mathbf{C}^t_{4:6\times 4:6} = \widetilde{\hat{\mathbf{v}}}_{4:6}\mathbf{J}^{B,\mathcal{M}} - \widetilde{(\mathbf{J}^{B,\mathcal{M}}\hat{\mathbf{v}}_{4:6})} \tag{3.11}$$

3.3 Non-follower loads

A load is said non-follower (see Figure 3.2) if its orientation does not depend on the orientation of the body. The classic example is the gravity force, which is always directed downward regardless of the configuration of the body. The components of a non-follower load, both forces and torques, are referred to the basis $\mathcal{S}$ of the inertial (fixed) frame. Because of the mixed-frame formulation, the components of non-follower loads should be properly modified in order to be coherent with the bases adopted in the formulation of the dynamic problem[7].

3.3.1 Force

Let $\mathbf{F}^{nf}_P$ be a non-follower force, applied to the location (point) P of the rigid body, that can depend on time but not on the state variables. Its contribution to the loads acting on the system in the mixed-frame formulation is given by:

$$\mathbf{F}^{\mathcal{S}}_G = \mathbf{F}^{nf}_P \tag{3.12}$$

$$\mathbf{T}^{\mathcal{M}}_G = (P-G)\times\mathbf{R}^T\mathbf{F}^{nf}_P = \widetilde{\mathbf{x}}^{B,\mathcal{M}}_P\mathbf{R}^T\mathbf{F}^{nf}_P \tag{3.13}$$

The tangent operator associated with the non-follower force is given by:

$$\mathbf{K}^t_{4:6\times 4:6} = -\widetilde{\mathbf{x}}^{B,\mathcal{M}}_P\widetilde{\left(\mathbf{R}^T\mathbf{F}^{nf}_P\right)} \tag{3.14}$$

[7]In the formulations developed in this section, the rotation operator $\mathbf{R}$ is considered a function of the rotational vector $\boldsymbol{\psi}$ through the exponential map, i.e. $\mathbf{R} = \mathbf{R}(\boldsymbol{\psi})$. Such dependence should be taken into account in the derivation of the tangent stiffness operators.

3.3.2 Torque

Let $\mathbf{T}_P^{nf}$ be a non-follower moment, applied to the location (point) P of the rigid body, that can depend on time but not on the state variables. Its contribution to the loads acting on the system in the mixed-frame formulation is given by:

$$\mathbf{F}_G^{\mathcal{S}} = \mathbf{0} \tag{3.15}$$

$$\mathbf{T}_G^{\mathcal{M}} = \mathbf{R}^T \mathbf{T}_P^{nf} \tag{3.16}$$

The tangent operator associated with the non-follower torque is given by:

$$\mathbf{K}_{4:6\times 4:6}^{t} = -\big(\widetilde{\mathbf{R}^T \mathbf{T}_P^{nf}}\big) \tag{3.17}$$

3.3.3 Transformations of the state variables

An interesting case is when the loads acting on the rigid body can be modelled as linear transformations of the state variables[8], $\mathbf{q}$, $\mathbf{v}$, $\dot{\mathbf{v}}$, defined with respect to the basis $\mathcal{S}$ of the inertial frame. The matrices associated with the linear transformations should be properly converted in order to consider that the motion of the center of mass and the rotational motion of the body are defined with respect to different bases, according to the mixed representation of the velocities. The transformation $\mathbf{A}^{(\bullet)}$ of the state variable $(\bullet)$ associated with the mixed-frame formulation is indicated with the notation $\hat{\mathbf{A}}^{(\bullet)}$.

3.3.3.1 Configuration operators

Let $\mathbf{A}^{\mathbf{q}}$ be the square matrix of order six associated with a linear transformation of the displacements defined as follows[9]:

$$\begin{bmatrix} \mathbf{F}_G^{\mathcal{S}} \\ \mathbf{T}_G^{\mathcal{S}} \end{bmatrix} = -\mathbf{A}^{\mathbf{q}} \begin{bmatrix} \mathbf{x}_G^{I,\mathcal{S}} \\ \boldsymbol{\psi} \end{bmatrix} \tag{3.18}$$

[8] For instance, in the case of a floating body, the hydrodynamic operators (added mass and damping matrices) are usually defined with respect to an inertial frame.

[9] The rotational vector $\boldsymbol{\psi}$ represents the orientation of the rigid body, and then of the body-attached reference frame $\{G; x', y', z'\}$, with respect to the spatial frame $\{O; x, y, z\}$. In this sense, it is an absolute physical quantity with a non-vector nature, since it is the parametrization of an element of the space $SO(3)$. Its representation is therefore always the same regardless of the basis considered. From another point of view, the rotational vector is the eigenvector of the rotational matrix, i.e. $\mathbf{R}(\boldsymbol{\psi})\boldsymbol{\psi} = \mathbf{R}^T(\boldsymbol{\psi})\boldsymbol{\psi} = \boldsymbol{\psi}$. On the other hand, the angular velocity $\boldsymbol{\omega}$ and angular acceleration $\dot{\boldsymbol{\omega}}$ are still absolute quantities characteristic of the motion of the body, but because of their vector nature, they have different representations with respect to different bases. Note also that the rotation of a rigid body seen by an observer attached to the body itself is always null.

The transformation expressed in the framework of the mixed representation of the motion is given by:

$$\begin{bmatrix} \mathbf{F}_G^{\mathcal{S}} \\ \mathbf{T}_G^{\mathcal{M}} \end{bmatrix} = -\hat{\mathbf{A}}^{\mathbf{q}} \begin{bmatrix} \hat{\mathbf{q}}_{1:3} \\ \hat{\mathbf{q}}_{4:6} \end{bmatrix} \tag{3.19}$$

$$\hat{\mathbf{A}}^{\mathbf{q}}_{1:3\times 1:3} = \mathbf{A}^{\mathbf{q}}_{1:3\times 1:3} \tag{3.20}$$

$$\hat{\mathbf{A}}^{\mathbf{q}}_{1:3\times 4:6} = \mathbf{A}^{\mathbf{q}}_{1:3\times 4:6} \tag{3.21}$$

$$\hat{\mathbf{A}}^{\mathbf{q}}_{4:6\times 1:3} = \mathbf{R}^T \mathbf{A}^{\mathbf{q}}_{4:6\times 1:3} \tag{3.22}$$

$$\hat{\mathbf{A}}^{\mathbf{q}}_{4:6\times 4:6} = \mathbf{R}^T \mathbf{A}^{\mathbf{q}}_{4:6\times 4:6} \tag{3.23}$$

The new transformation is nonlinear with respect to the state variable $\boldsymbol{\psi}$, through the rotation operator $\mathbf{R}$. The tangent operators associated with the transformation $\hat{\mathbf{A}}^{\mathbf{q}}$ are given by[10]:

$$\mathbf{K}^t_{1:3\times 1:3} = \hat{\mathbf{A}}^{\mathbf{q}}_{1:3\times 1:3} \tag{3.24}$$

$$\mathbf{K}^t_{1:3\times 4:6} = \hat{\mathbf{A}}^{\mathbf{q}}_{1:3\times 4:6} \big[\mathbf{T}(\hat{\mathbf{q}}_{4:6})\big]^{-1} \tag{3.25}$$

$$\mathbf{K}^t_{4:6\times 1:3} = \hat{\mathbf{A}}^{\mathbf{q}}_{4:6\times 1:3} \tag{3.26}$$

$$\mathbf{K}^t_{4:6\times 4:6} = \hat{\mathbf{A}}^{\mathbf{q}}_{4:6\times 4:6} \big[\mathbf{T}(\hat{\mathbf{q}}_{4:6})\big]^{-1} + \big(\widetilde{\hat{\mathbf{A}}^{\mathbf{q}}_{4:6\times 1:3}\hat{\mathbf{q}}_{1:3}}\big) + \big(\widetilde{\hat{\mathbf{A}}^{\mathbf{q}}_{4:6\times 4:6}\hat{\mathbf{q}}_{4:6}}\big) \tag{3.27}$$

3.3.3.2 Velocity operators

Let $\mathbf{A}^{\mathbf{v}}$ be the square matrix of order six associated with a linear transformation of the velocities defined as follows:

$$\begin{bmatrix} \mathbf{F}_G^{\mathcal{S}} \\ \mathbf{T}_G^{\mathcal{S}} \end{bmatrix} = -\mathbf{A}^{\mathbf{v}} \begin{bmatrix} \mathbf{v}_G^{I,\mathcal{S}} \\ \boldsymbol{\omega}^{\mathcal{S}} \end{bmatrix} \tag{3.28}$$

[10] The transformation by means of the operator $\big[\mathbf{T}(\hat{\mathbf{q}}_{4:6})\big]^{-1}$ (defined by the Equation (2.60)), applied to the first term of the Equations (3.25) and (3.27), is due to the structure of the Lie group time integrator. In particular, the algorithm is structured so that the tangent stiffness operators are defined with respect to the increment $\boldsymbol{\theta}^{\mathcal{M}}$ and then projected on the tangent space at $\mathbf{R}(\boldsymbol{\psi}_n)$, since the Newton-Raphson scheme updates the vector $\mathbf{y}$ with a classic composition rule. However, the transformation $\hat{\mathbf{A}}^{\mathbf{q}}$ operates directly on the rotational vector $\boldsymbol{\psi}$ and its increments. Let $\widetilde{\boldsymbol{\theta}}^{\mathcal{M}}$ be an infinitesimal rotation imposed to the current configuration $\boldsymbol{\psi}_{n+1}$, the new rotation operator is given by:

$$\mathbf{R}(\boldsymbol{\psi}_{n+1} + d\boldsymbol{\psi}) = \mathbf{R}(\boldsymbol{\psi}_{n+1})\mathbf{R}(\boldsymbol{\theta}^{\mathcal{M}}) = \mathbf{R}(\boldsymbol{\psi}_n)\mathbf{R}(\mathbf{y}_{4:6})\mathbf{R}(\boldsymbol{\theta}^{\mathcal{M}}) = \mathbf{R}(\boldsymbol{\psi}_n)\mathbf{R}(\mathbf{y}_{4:6} + d\mathbf{y}_{4:6})$$

$$\boldsymbol{\theta}^{\mathcal{M}} = \mathbf{T}(\mathbf{y}_{4:6})d\mathbf{y}_{4:6} = \mathbf{T}(\boldsymbol{\psi}_{n+1})d\boldsymbol{\psi}$$

The transformation expressed in the framework of the mixed representation of the motion is given by:

$$\begin{bmatrix} \mathbf{F}_G^{\mathcal{S}} \\ \mathbf{T}_G^{\mathcal{M}} \end{bmatrix} = -\hat{\mathbf{A}}^{\mathbf{v}} \begin{bmatrix} \hat{\mathbf{v}}_{1:3} \\ \hat{\mathbf{v}}_{4:6} \end{bmatrix} \tag{3.29}$$

$$\hat{\mathbf{A}}^{\mathbf{v}}_{1:3\times 1:3} = \mathbf{A}^{\mathbf{v}}_{1:3\times 1:3} \tag{3.30}$$

$$\hat{\mathbf{A}}^{\mathbf{v}}_{1:3\times 4:6} = \mathbf{A}^{\mathbf{v}}_{1:3\times 4:6}\mathbf{R} \tag{3.31}$$

$$\hat{\mathbf{A}}^{\mathbf{v}}_{4:6\times 1:3} = \mathbf{R}^T\mathbf{A}^{\mathbf{v}}_{4:6\times 1:3} \tag{3.32}$$

$$\hat{\mathbf{A}}^{\mathbf{v}}_{4:6\times 4:6} = \mathbf{R}^T\mathbf{A}^{\mathbf{v}}_{4:6\times 4:6}\mathbf{R} \tag{3.33}$$

The new transformation is nonlinear with respect to the state variable $\boldsymbol{\psi}$. The tangent operators associated with the transformation $\hat{\mathbf{A}}^{\mathbf{v}}$ are given by:

$$\mathbf{C}^t = \hat{\mathbf{A}}^{\mathbf{v}} \tag{3.34}$$

$$\mathbf{K}^t_{1:3\times 4:6} = -\hat{\mathbf{A}}^{\mathbf{v}}_{1:3\times 4:6}\widetilde{\hat{\mathbf{v}}}_{4:6} \tag{3.35}$$

$$\mathbf{K}^t_{4:6\times 4:6} = \big(\widetilde{\hat{\mathbf{A}}^{\mathbf{v}}_{4:6\times 1:3}\hat{\mathbf{v}}_{1:3}}\big) + \big(\widetilde{\hat{\mathbf{A}}^{\mathbf{v}}_{4:6\times 4:6}\hat{\mathbf{v}}_{4:6}}\big) - \hat{\mathbf{A}}^{\mathbf{v}}_{4:6\times 4:6}\widetilde{\hat{\mathbf{v}}}_{4:6} \tag{3.36}$$

3.3.3.3 Acceleration operators

Let $\mathbf{A}^{\dot{\mathbf{v}}}$ be the square matrix of order six associated with a linear transformation of the accelerations defined as follows:

$$\begin{bmatrix} \mathbf{F}_G^{\mathcal{S}} \\ \mathbf{T}_G^{\mathcal{S}} \end{bmatrix} = -\mathbf{A}^{\dot{\mathbf{v}}} \begin{bmatrix} \mathbf{a}_G^{I,\mathcal{S}} \\ \dot{\boldsymbol{\omega}}^{\mathcal{S}} \end{bmatrix} \tag{3.37}$$

The transformation expressed in the framework of the mixed representation of the motion is given by:

$$\begin{bmatrix} \mathbf{F}_G^{\mathcal{S}} \\ \mathbf{T}_G^{\mathcal{M}} \end{bmatrix} = -\hat{\mathbf{A}}^{\dot{\mathbf{v}}} \begin{bmatrix} \hat{\dot{\mathbf{v}}}_{1:3} \\ \hat{\dot{\mathbf{v}}}_{4:6} \end{bmatrix} \tag{3.38}$$

$$\hat{\mathbf{A}}^{\dot{\mathbf{v}}}_{1:3\times 1:3} = \mathbf{A}^{\dot{\mathbf{v}}}_{1:3\times 1:3} \tag{3.39}$$

$$\hat{\mathbf{A}}^{\dot{\mathbf{v}}}_{1:3\times 4:6} = \mathbf{A}^{\dot{\mathbf{v}}}_{1:3\times 4:6}\mathbf{R} \tag{3.40}$$

$$\hat{\mathbf{A}}^{\dot{\mathbf{v}}}_{4:6\times 1:3} = \mathbf{R}^T\mathbf{A}^{\dot{\mathbf{v}}}_{4:6\times 1:3} \tag{3.41}$$

$$\hat{\mathbf{A}}^{\dot{\mathbf{v}}}_{4:6\times 4:6} = \mathbf{R}^T\mathbf{A}^{\dot{\mathbf{v}}}_{4:6\times 4:6}\mathbf{R} \tag{3.42}$$

The new transformation is nonlinear with respect to the state variable $\boldsymbol{\psi}$. The tangent operators associated with the transformation $\hat{\mathbf{A}}^{\dot{\mathbf{v}}}$ are given by:

$$\mathbf{M}^t = \hat{\mathbf{A}}^{\dot{\mathbf{v}}} \tag{3.43}$$

$$\mathbf{K}^t_{1:3\times 4:6} = -\hat{\mathbf{A}}^{\dot{\mathbf{v}}}_{1:3\times 4:6}\widetilde{\hat{\dot{\mathbf{v}}}}_{4:6} \tag{3.44}$$

$$\mathbf{K}^t_{4:6\times 4:6} = \big(\widetilde{\hat{\mathbf{A}}^{\dot{\mathbf{v}}}_{4:6\times 1:3}\hat{\mathbf{v}}_{1:3}}\big) + \big(\widetilde{\hat{\mathbf{A}}^{\dot{\mathbf{v}}}_{4:6\times 4:6}\hat{\dot{\mathbf{v}}}_{4:6}}\big) - \hat{\mathbf{A}}^{\dot{\mathbf{v}}}_{4:6\times 4:6}\widetilde{\hat{\dot{\mathbf{v}}}}_{4:6} \tag{3.45}$$

3.3.3.4 Eccentric transformations

Let's suppose that the linear transformations $\mathbf{A}_P^{(\bullet)}$ of the state variable $(\bullet)$ return a load that is applied to a generic point P of the rigid body. The formulation should account for the torque about the center of mass due to the resultant eccentric force. Given the position vector $\mathbf{x}_P^{B,\mathcal{M}}$ of the point P, the linear operator $\hat{\mathbf{A}}_P^{(\bullet)}$, computed with the formulations described in the previous sections, transforms as follows:

$$\hat{\mathbf{A}}^{(\bullet)} = \hat{\mathbf{T}}_P^{\mathbf{A}} \hat{\mathbf{A}}_P^{(\bullet)} \tag{3.46}$$

$$\hat{\mathbf{T}}_P^{\mathbf{A}} = \begin{bmatrix} \mathbf{I}_3 & \mathbf{0}_{3\times 3} \\ \widetilde{(\mathbf{x}_P^{B,\mathcal{M}})}\mathbf{R}^T & \mathbf{I}_3 \end{bmatrix} \tag{3.47}$$

The operator $\hat{\mathbf{T}}_P^{\mathbf{A}}$ operates as a linear transformation that transports the load applied to point P into a load applied to the center of mass. The associated linear operators $\mathbf{M}_P^t$, $\mathbf{C}_P^t$, $\mathbf{K}_P^t$ transform with the same rule, namely:

$$\mathbf{M}^t = \hat{\mathbf{T}}_P^{\mathbf{A}} \mathbf{M}_P^t \tag{3.48}$$

$$\mathbf{C}^t = \hat{\mathbf{T}}_P^{\mathbf{A}} \mathbf{C}_P^t \tag{3.49}$$

$$\mathbf{K}^t = \hat{\mathbf{T}}_P^{\mathbf{A}} \mathbf{K}_P^t \tag{3.50}$$

Furthermore, since the Equation (3.47) depends on the current orientation through the rotation operator $\mathbf{R}$, there is an additional contribution to the tangent stiffness operator given by:

$$\mathbf{K}_{4:6\times 4:6}^t = \widetilde{\mathbf{x}}_P^{B,\mathcal{M}} \big(\mathbf{R}^T \widetilde{\hat{\mathbf{A}}_{P,1:3\times 1:3}^{(\bullet)}} (\bullet)_{1:3}\big) + \widetilde{\mathbf{x}}_P^{B,\mathcal{M}} \big(\mathbf{R}^T \widetilde{\hat{\mathbf{A}}_{P,1:3\times 4:6}^{(\bullet)}} (\bullet)_{4:6}\big) \tag{3.51}$$

3.4 Follower loads

A load is said follower (see Figure 3.3) if it is dragged by the body during the motion (it rotates with the body). The components of a follower load, both forces and torques, are referred to the basis $\mathcal{M}$ of the non-inertial frame. Because of the mixed-frame formulation, the components of follower loads should be properly modified in order to be coherent with the bases adopted in the formulation of the dynamic problem[11].

3.4.1 Force

Let $\mathbf{F}_P^f$ be a follower force, applied to the location (point) P of the rigid body, that can depend on time but not on the state variables. Its contribution to the loads acting on the system in the mixed-frame formulation is given by:

$$\mathbf{F}_G^{\mathcal{S}} = \mathbf{R}\mathbf{F}_P^f \tag{3.52}$$

$$\mathbf{T}_G^{\mathcal{M}} = (P - G) \times \mathbf{F}^f = \widetilde{\mathbf{x}}_P^{B,\mathcal{M}} \mathbf{F}_P^f \tag{3.53}$$

[11] As specified in the previous section, the rotation operator $\mathbf{R}$ is considered a function of the rotational vector $\boldsymbol{\psi}$ through the exponential map (see Note 7).

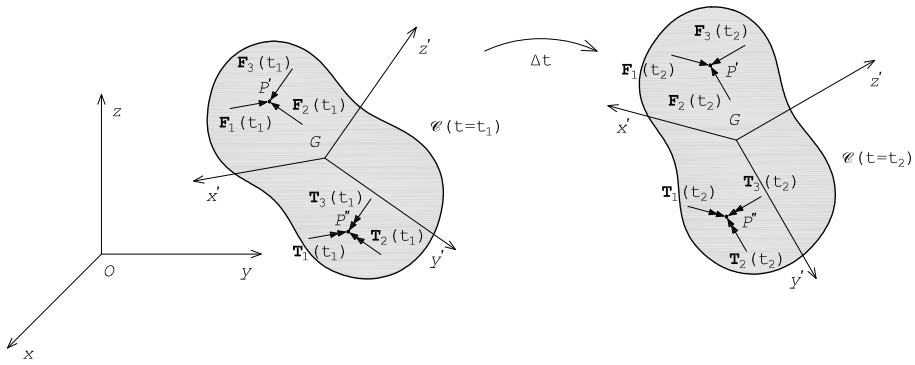

Figure 3.3: Follower loads.

The tangent operator associated with the follower force is given by:

$$\mathbf{K}^t_{1:3\times 4:6} = \mathbf{R}\widetilde{\mathbf{F}}^f_P \tag{3.54}$$

3.4.2 Torque

Let $\mathbf{T}^f_P$ be a follower moment, applied to the location (point) P of the rigid body, that can depend on time but not on the state variables. Its contribution to the loads acting on the system in the mixed-frame formulation is given by:

$$\mathbf{F}^{\mathcal{S}}_G = \mathbf{0} \tag{3.55}$$

$$\mathbf{T}^{\mathcal{M}}_G = \mathbf{T}^f_P \tag{3.56}$$

The follower torque gives no contribution to the tangent operators of the system.

3.4.3 Transformations of the state variables

Many practical problems refer to loads applied to the rigid body as linear transformations of the state variables $\mathbf{q}$, $\mathbf{v}$, $\dot{\mathbf{v}}$. An interesting case is when the transformation is defined with respect to the basis $\mathcal{M}$ of the body-attached frame[12]. The matrices associated with the linear transformations should be properly converted in order to consider that the motion of the center of mass and the rotational motion of the body are defined with respect to different bases. The transformation $\mathbf{B}^{(\bullet)}$ of the state variable $(\bullet)$ associated with the mixed-frame formulation is indicated with the notation $\hat{\mathbf{B}}^{(\bullet)}$.

3.4.3.1 Configuration operators

Let $\mathbf{B}^{\mathbf{q}}$ be the square matrix of order six associated with a linear transformation of the displacements defined as follows:

$$\begin{bmatrix} \mathbf{F}^{\mathcal{M}}_G \\ \mathbf{T}^{\mathcal{M}}_G \end{bmatrix} = -\mathbf{B}^{\mathbf{q}} \begin{bmatrix} \mathbf{x}^{I,\mathcal{M}}_G \\ \boldsymbol{\psi} \end{bmatrix} \tag{3.57}$$

[12]For instance, if the hydrodynamic operators are computed with respect to the current configuration of the floating body, they should be considered as follower transformations.

The transformation expressed in the framework of the mixed representation of the motion is given by:

$$\begin{bmatrix} \mathbf{F}_G^{\mathcal{S}} \\ \mathbf{T}_G^{\mathcal{M}} \end{bmatrix} = -\hat{\mathbf{B}}^{\mathbf{q}} \begin{bmatrix} \hat{\mathbf{q}}_{1:3} \\ \hat{\mathbf{q}}_{4:6} \end{bmatrix} \tag{3.58}$$

$$\hat{\mathbf{B}}^{\mathbf{q}}_{1:3\times 1:3} = \mathbf{R}\mathbf{B}^{\mathbf{q}}_{1:3\times 1:3}\mathbf{R}^T \tag{3.59}$$

$$\hat{\mathbf{B}}^{\mathbf{q}}_{1:3\times 4:6} = \mathbf{R}\mathbf{B}^{\mathbf{q}}_{1:3\times 4:6} \tag{3.60}$$

$$\hat{\mathbf{B}}^{\mathbf{q}}_{4:6\times 1:3} = \mathbf{B}^{\mathbf{q}}_{4:6\times 1:3}\mathbf{R}^T \tag{3.61}$$

$$\hat{\mathbf{B}}^{\mathbf{q}}_{4:6\times 4:6} = \mathbf{B}^{\mathbf{q}}_{4:6\times 4:6} \tag{3.62}$$

The new transformation is nonlinear with respect to the state variable $\boldsymbol{\psi}$. The tangent operators associated with the transformation $\hat{\mathbf{B}}^{\mathbf{q}}$ are given by:

$$\mathbf{K}^t_{1:3\times 1:3} = \hat{\mathbf{B}}^{\mathbf{q}}_{1:3\times 1:3} \tag{3.63}$$

$$\begin{aligned}\mathbf{K}^t_{1:3\times 4:6} = {} & \hat{\mathbf{B}}^{\mathbf{q}}_{1:3\times 4:6}\big[\mathbf{T}(\hat{\mathbf{q}}_{4:6})\big]^{-1} - \mathbf{R}\big(\widetilde{\mathbf{B}^{\mathbf{q}}_{1:3\times 1:3}\mathbf{R}^T\hat{\mathbf{q}}_{1:3}}\big) + \\ & + \mathbf{R}\mathbf{B}^{\mathbf{q}}_{1:3\times 1:3}\big(\widetilde{\mathbf{R}^T\hat{\mathbf{q}}_{1:3}}\big) - \mathbf{R}\big(\widetilde{\mathbf{B}^{\mathbf{q}}_{1:3\times 4:6}}\hat{\mathbf{q}}_{4:6}\big)\end{aligned} \tag{3.64}$$

$$\mathbf{K}^t_{4:6\times 1:3} = \hat{\mathbf{B}}^{\mathbf{q}}_{4:6\times 1:3} \tag{3.65}$$

$$\mathbf{K}^t_{4:6\times 4:6} = \hat{\mathbf{B}}^{\mathbf{q}}_{4:6\times 4:6}\big[\mathbf{T}(\hat{\mathbf{q}}_{4:6})\big]^{-1} + \mathbf{B}^{\mathbf{q}}_{4:6\times 1:3}\big(\widetilde{\mathbf{R}^T\hat{\mathbf{q}}_{1:3}}\big) \tag{3.66}$$

3.4.3.2 Velocity operators

Let $\mathbf{B}^{\mathbf{v}}$ be the square matrix of order six associated with a linear transformation of the velocities defined as follows:

$$\begin{bmatrix} \mathbf{F}_G^{\mathcal{M}} \\ \mathbf{T}_G^{\mathcal{M}} \end{bmatrix} = -\mathbf{B}^{\mathbf{v}} \begin{bmatrix} \mathbf{v}_G^{I,\mathcal{M}} \\ \boldsymbol{\omega}^{\mathcal{M}} \end{bmatrix} \tag{3.67}$$

The transformation expressed in the framework of the mixed representation of the motion is given by:

$$\begin{bmatrix} \mathbf{F}_G^{\mathcal{S}} \\ \mathbf{T}_G^{\mathcal{M}} \end{bmatrix} = -\hat{\mathbf{B}}^{\mathbf{v}} \begin{bmatrix} \hat{\mathbf{v}}_{1:3} \\ \hat{\mathbf{v}}_{4:6} \end{bmatrix} \tag{3.68}$$

$$\hat{\mathbf{B}}^{\mathbf{v}}_{1:3\times 1:3} = \mathbf{R}\mathbf{B}^{\mathbf{v}}_{1:3\times 1:3}\mathbf{R}^T \tag{3.69}$$

$$\hat{\mathbf{B}}^{\mathbf{v}}_{1:3\times 4:6} = \mathbf{R}\mathbf{B}^{\mathbf{v}}_{1:3\times 4:6} \tag{3.70}$$

$$\hat{\mathbf{B}}^{\mathbf{v}}_{4:6\times 1:3} = \mathbf{B}^{\mathbf{v}}_{4:6\times 1:3}\mathbf{R}^T \tag{3.71}$$

$$\hat{\mathbf{B}}^{\mathbf{v}}_{4:6\times 4:6} = \mathbf{B}^{\mathbf{v}}_{4:6\times 4:6} \tag{3.72}$$

The new transformation is nonlinear with respect to the state variable $\boldsymbol{\psi}$. The tangent operators associated with the transformation $\hat{\mathbf{B}}^{\mathbf{v}}$ are given by:

$$\mathbf{C}^t = \hat{\mathbf{B}}^{\mathbf{v}} \tag{3.73}$$

$$\mathbf{K}^t_{1:3\times 4:6} = -\mathbf{R}\big(\widetilde{\mathbf{B}^{\mathbf{v}}_{1:3\times 1:3}\mathbf{R}^T\hat{\mathbf{v}}_{1:3}}\big) + \mathbf{R}\mathbf{B}^{\mathbf{v}}_{1:3\times 1:3}\big(\widetilde{\mathbf{R}^T\hat{\mathbf{v}}_{1:3}}\big) - \mathbf{R}\big(\widetilde{\mathbf{B}^{\mathbf{v}}_{1:3\times 4:6}}\hat{\mathbf{v}}_{4:6}\big) \tag{3.74}$$

$$\mathbf{K}^t_{4:6\times 4:6} = \mathbf{B}^{\mathbf{v}}_{4:6\times 1:3}\big(\widetilde{\mathbf{R}^T\hat{\mathbf{v}}_{1:3}}\big) \tag{3.75}$$

3.4.3.3 Acceleration operators

Let $\mathbf{B}^{\dot{\mathbf{v}}}$ be the square matrix of order six associated with a linear transformation of the accelerations defined as follows:

$$\begin{bmatrix} \mathbf{F}_G^{\mathcal{M}} \\ \mathbf{T}_G^{\mathcal{M}} \end{bmatrix} = -\mathbf{B}^{\dot{\mathbf{v}}} \begin{bmatrix} \mathbf{a}_G^{I,\mathcal{M}} \\ \dot{\boldsymbol{\omega}}^{\mathcal{M}} \end{bmatrix} \tag{3.76}$$

The transformation expressed in the framework of the mixed representation of the motion is given by:

$$\begin{bmatrix} \mathbf{F}_G^{\mathcal{S}} \\ \mathbf{T}_G^{\mathcal{M}} \end{bmatrix} = -\hat{\mathbf{B}}^{\dot{\mathbf{v}}} \begin{bmatrix} \hat{\mathbf{v}}_{1:3} \\ \hat{\mathbf{v}}_{4:6} \end{bmatrix} \tag{3.77}$$

$$\hat{\mathbf{B}}^{\dot{\mathbf{v}}}_{1:3\times 1:3} = \mathbf{R}\mathbf{B}^{\dot{\mathbf{v}}}_{1:3\times 1:3}\mathbf{R}^T \tag{3.78}$$

$$\hat{\mathbf{B}}^{\dot{\mathbf{v}}}_{1:3\times 4:6} = \mathbf{R}\mathbf{B}^{\dot{\mathbf{v}}}_{1:3\times 4:6} \tag{3.79}$$

$$\hat{\mathbf{B}}^{\dot{\mathbf{v}}}_{4:6\times 1:3} = \mathbf{B}^{\dot{\mathbf{v}}}_{4:6\times 1:3}\mathbf{R}^T \tag{3.80}$$

$$\hat{\mathbf{B}}^{\dot{\mathbf{v}}}_{4:6\times 4:6} = \mathbf{B}^{\dot{\mathbf{v}}}_{4:6\times 4:6} \tag{3.81}$$

The new transformation is nonlinear with respect to the state variable $\boldsymbol{\psi}$. The tangent operators associated with the transformation $\hat{\mathbf{B}}^{\dot{\mathbf{v}}}$ are given by:

$$\mathbf{M}^t = \hat{\mathbf{B}}^{\dot{\mathbf{v}}} \tag{3.82}$$

$$\mathbf{K}^t_{1:3\times 4:6} = -\mathbf{R}\big(\mathbf{B}^{\dot{\mathbf{v}}}_{1:3\times 1:3}\widetilde{\mathbf{R}^T\hat{\mathbf{v}}_{1:3}}\big) + \mathbf{R}\mathbf{B}^{\dot{\mathbf{v}}}_{1:3\times 1:3}\big(\widetilde{\mathbf{R}^T\hat{\mathbf{v}}_{1:3}}\big) - \mathbf{R}\big(\mathbf{B}^{\dot{\mathbf{v}}}_{1:3\times 4:6}\widetilde{\hat{\mathbf{v}}_{4:6}}\big) \tag{3.83}$$

$$\mathbf{K}^t_{4:6\times 4:6} = \mathbf{B}^{\dot{\mathbf{v}}}_{4:6\times 1:3}\big(\widetilde{\mathbf{R}^T\hat{\mathbf{v}}_{1:3}}\big) \tag{3.84}$$

3.4.3.4 Eccentric transformations

Let's suppose that the linear transformations $\mathbf{B}_P^{(\bullet)}$ of the state variable $(\bullet)$ return a load that is applied to a generic point P of the rigid body. The formulation should account for the torque about the center of mass due to the resultant eccentric force. Given the position vector $\mathbf{x}_P^{B,\mathcal{M}}$ of the point P, the linear operator $\hat{\mathbf{B}}_P^{(\bullet)}$, computed with the formulations described in the previous sections, transforms as follows[13]:

$$\hat{\mathbf{B}}^{(\bullet)} = \hat{\mathbf{T}}_P^{\mathbf{B}}\hat{\mathbf{B}}_P^{(\bullet)} \tag{3.85}$$

$$\hat{\mathbf{T}}_P^{\mathbf{B}} = \begin{bmatrix} \mathbf{I}_3 & \mathbf{0}_{3\times 3} \\ \widetilde{(\mathbf{x}_P^{B,\mathcal{M}})}\mathbf{R}^T & \mathbf{I}_3 \end{bmatrix} \tag{3.86}$$

The operator $\hat{\mathbf{T}}_P^{\mathbf{B}}$ operates as a linear transformation that transports the load applied to point P into a load applied to the center of mass. The associated linear operators

[13]The formulation is the same described for non-follower loads. In effect both the operators $\hat{\mathbf{A}}_P^{(\bullet)}$ and $\hat{\mathbf{B}}_P^{(\bullet)}$ return a load expressed in the framework of the mixed representation of the motion, which should be transformed in the same way, i.e. $\hat{\mathbf{T}}_P^{\mathbf{B}} \equiv \hat{\mathbf{T}}_P^{\mathbf{A}}$.

$\mathbf{M}_P^t$, $\mathbf{C}_P^t$, $\mathbf{K}_P^t$ transform with the same rule, namely:

$$\mathbf{M}^t = \hat{\mathbf{T}}_P^{\mathbf{B}} \mathbf{M}_P^t \tag{3.87}$$

$$\mathbf{C}^t = \hat{\mathbf{T}}_P^{\mathbf{B}} \mathbf{C}_P^t \tag{3.88}$$

$$\mathbf{K}^t = \hat{\mathbf{T}}_P^{\mathbf{B}} \mathbf{K}_P^t \tag{3.89}$$

Furthermore, since the Equation (3.86) depends on the current orientation through the rotation operator $\mathbf{R}$, there is an additional contribution to the tangent stiffness operator given by:

$$\mathbf{K}_{4:6\times 4:6}^t = \widetilde{\mathbf{x}}_P^{B,\mathcal{M}} \big(\mathbf{R}^T \widetilde{\hat{\mathbf{B}}_{P,1:3\times 1:3}^{(\bullet)}} (\bullet)_{1:3} \big) + \widetilde{\mathbf{x}}_P^{B,\mathcal{M}} \big(\mathbf{R}^T \widetilde{\hat{\mathbf{B}}_{P,1:3\times 4:6}^{(\bullet)}} (\bullet)_{4:6} \big) \tag{3.90}$$

3.4.3.5 Remarks

The linear transformation of a state variable is a particular case of a more general transformation that could nonlinearly combine all the state variables, namely the position, velocity, and acceleration vectors. The formulations developed in this chapter are longer valid if at each time step the nonlinear law is linearised about the equilibrium configuration. Otherwise, the directional derivatives that define the tangent operators should include also the terms related to the nonlinear relation. Moreover, only transformations that return vectors expressed with respect to the same basis of the transformed vector were considered. However, if the transformation involves a mix of reference vector bases, the operators can be rightly expressed according to the mixed-frame convention by properly adapting the formulations developed in these sections. Basically, the problem consists in successive projections from one basis to another one.

3.5 Time integration algorithm

The dynamic differential problem of the rigid body in the Euclidean space (six degrees of freedom) is solved with an efficient Lie group time integrator [10, 11, 12, 13], suitable both for constrained and unconstrained rigid bodies[14]. At each time step, the scheme solves the set of differential equations with an extension of the classical generalized-α method combined with the Newton-Raphson scheme, necessary for computing the increment of the state variable $\hat{\mathbf{q}}$ (and then $\hat{\mathbf{v}}$, $\hat{\dot{\mathbf{v}}}$) that provides the dynamic equilibrium. The Newton-Raphson algorithm involves the linearisation of the nonlinear differential problem around the previous equilibrium configuration by means of the tangent operators. The algorithm operates directly in the special Lie group of proper orthogonal transformations and rotations are parametrized by the rotational vector, in place of the more common Euler angles (or Tait-Bryan angles).

Let $\hat{\mathbf{q}} = [\mathbf{x}_G^{I,\mathcal{S}}; \boldsymbol{\psi}]$ be the position state vector, where $\mathbf{x}_G^{I,\mathcal{S}}$ is the position vector of the center of mass and $\boldsymbol{\psi}$ is the rotational vector, and let $\hat{\mathbf{v}}$ and $\hat{\dot{\mathbf{v}}}$ be respectively the corresponding velocity vector and acceleration vector expressed in the framework of the mixed representation of the motion. The state variables at time t_{n+1} can be computed

[14] As a suggestion, the original algorithm can be improved with the introduction of a penalty coefficient and a scaling factor in order to guarantee a better numerical conditioning and to generate system matrices of the same order of amplitude (update suitable only for constrained systems) [37].

with the Algorithm 3.1[15] [11]. For further discussions on other possible numerical approaches the reader is addressed to the references [16, 17, 18, 52, 82, 83, 84, 89].

3.5.1 Numerical damping

The Newmark algorithm, as well as the generalized-α scheme, could lose the unconditional stability property, especially in the case of constrained systems because of the introduction of constraint equations in the differential dynamic problem [37]. In order to avoid instability, a numerical damping should be introduced by a modification of the parameters β and γ of the Newmark scheme. As suggested in [11], the parameters of the algorithm are selected with the following expressions [22][16]:

$$\alpha_f = \frac{\rho}{\rho+1} \tag{3.91}$$

$$\alpha_m = \frac{2\rho-1}{\rho+1} \tag{3.92}$$

$$\beta = \frac{1}{4}(1+\alpha_f-\alpha_m)^2 \tag{3.93}$$

$$\gamma = \frac{1}{2}+\alpha_f-\alpha_m \tag{3.94}$$

The control parameter is ρ that defines the level of damping; if $\rho = 1$ there is not numerical damping, on the contrary, $\rho = 0.6$ is a significant numerical damping.

3.5.2 Mappings

The algorithms proposed in [11] are a family of Lie group time integrators defined by the mappings used for updating the state variable $\hat{\mathbf{q}}$, i.e. $\hat{\mathbf{q}}_{n+1} = \varphi_h(\hat{\mathbf{q}}_n, \hat{\mathbf{v}}_n, \mathbf{a}_n, \mathbf{a}_{n+1})$. Unless otherwise specified, it is employed the integrator associated with the mappings φ^i_{h*} and φ^i_{hx} given by [11]:

$$\mathbf{q}_{n+1} = \varphi^i_h(\mathbf{q}_n, \mathbf{v}_n, \mathbf{a}_n, \mathbf{a}_{n+1}) = \varphi^i_{h*} \circ \exp(\widetilde{\varphi}^i_{hx}), \qquad i = 1,2,3 \tag{3.95}$$

$$\varphi^1_{h*}(\mathbf{q}_n, \mathbf{v}_n, \mathbf{a}_n) = \mathbf{q}_n \tag{3.96}$$

$$\varphi^1_{hx}(\mathbf{v}_n, \mathbf{a}_n, \mathbf{a}_{n+1}) = h\mathbf{v}_n + h^2(0.5-\beta)\mathbf{a}_n + \beta h^2 \mathbf{a}_{n+1} \tag{3.97}$$

[15] If the rotational motion is expressed with respect to the basis $\mathcal{S}$ of the inertial frame, i.e. considering $\boldsymbol{\omega}^{\mathcal{S}}$ and $\dot{\boldsymbol{\omega}}^{\mathcal{S}}$, the composition rule changes, and compound rotations should be computed by means of the right translation map. Moreover, given a vector $\mathbf{z}$, also the directional derivatives change as follows:

$$\mathbf{R}^T(\boldsymbol{\psi})\mathbf{z}^{\mathcal{S}}, \qquad D(\mathbf{R}^T\mathbf{z}^{\mathcal{S}})\cdot\widetilde{\boldsymbol{\theta}}^{\mathcal{S}} = \mathbf{R}^T\widetilde{\mathbf{z}}^{\mathcal{S}}\boldsymbol{\theta}^{\mathcal{S}}$$

$$\mathbf{R}(\boldsymbol{\psi})\mathbf{z}^{\mathcal{M}}, \qquad D(\mathbf{R}\mathbf{z}^{\mathcal{M}})\cdot\widetilde{\boldsymbol{\theta}}^{\mathcal{S}} = -\widetilde{\mathbf{R}\mathbf{z}^{\mathcal{M}}}\boldsymbol{\theta}^{\mathcal{S}}$$

[16] Numerical damping can be achieved in several ways, for instance, in [16] β and γ are directly modified as follows:

$$\beta = 0.25(1+\alpha)^2$$
$$\gamma = 0.5+\alpha$$

with $\alpha = 0.05$ (small numerical damping).

Algorithm 3.1: Scheme (single time step) for the solution of the mixed-frame formulation of the dynamic problem (adapted from [11]).

input : h, α_f, α_m, β, γ, tol, n_{max}, m, $\mathbf{J}$, $\mathbf{g}$, $\hat{\mathbf{q}}_n$, $\hat{\mathbf{v}}_n$, $\hat{\dot{\mathbf{v}}}_n$, $\mathbf{a}_n$, $\mathbf{F}^{(\bullet)}$, $\mathbf{T}^{(\bullet)}$, $\mathbf{A}^{(\bullet)}$, $\mathbf{B}^{(\bullet)}$, ...

output: $\hat{\mathbf{q}}_{n+1}$, $\hat{\mathbf{v}}_{n+1}$, $\hat{\dot{\mathbf{v}}}_{n+1}$, $\mathbf{a}_{n+1}$

$\beta' = \frac{1-\alpha_m}{\beta h^2(1-\alpha_f)}$;
$\gamma' = \frac{\gamma}{\beta h}$;
$\hat{\dot{\mathbf{v}}}_{n+1} = \mathbf{0}$;
$\mathbf{a}_{n+1} = \frac{\alpha_f \hat{\dot{\mathbf{v}}}_n - \alpha_m \mathbf{a}_n}{1-\alpha_m}$;
$\hat{\mathbf{v}}_{n+1} = \hat{\mathbf{v}}_n + h(1-\gamma)\mathbf{a}_n + \gamma h \mathbf{a}_{n+1}$;
$\mathbf{q}^* = \varphi^a_{h^*}(\hat{\mathbf{q}}_n, \hat{\mathbf{v}}_n, \mathbf{a}_n, h, \beta), \qquad a = 1,2,3;$
$\mathbf{y} = \varphi^a_{hy}(\hat{\mathbf{v}}_n, \mathbf{a}_n, \mathbf{a}_{n+1}, h, \beta), \qquad a = 1,2,3;$
for $i \leftarrow 1$ **to** n_{max} **do**
  $\hat{\mathbf{q}}_{n+1,1:3} = \mathbf{x}_{n+1} = \mathbf{q}^*_{1:3} + \mathbf{y}_{1:3}$;
  $\hat{\mathbf{q}}_{n+1,4:6} = \boldsymbol{\psi}_{n+1} = \log_{\mathbf{R}}\big(\mathbf{R}(\mathbf{q}^*_{4:6})\mathbf{R}(\mathbf{y}_{4:6})\big)$;
  $\hat{(\diamond)}^{(\bullet)} = \hat{(\diamond)}^{(\bullet)}(\boldsymbol{\psi}_{n+1}, t_{n+1}), \qquad (\diamond) = \mathbf{F}, \mathbf{T}, \mathbf{A}, \mathbf{B};$
  $\mathbf{res} = \hat{\mathbf{r}}(\hat{\mathbf{q}}_{n+1}, \hat{\mathbf{v}}_{n+1}, \hat{\dot{\mathbf{v}}}_{n+1}, t_{n+1})$;
  if $||\mathbf{res}|| < tol$ **then**
    break;
  end
  $\mathbf{M}^t = \mathbf{M}^t(\hat{\mathbf{q}}_{n+1}, \hat{\mathbf{v}}_{n+1}, \hat{\dot{\mathbf{v}}}_{n+1}, t_{n+1})$;
  $\mathbf{C}^t = \mathbf{C}^t(\hat{\mathbf{q}}_{n+1}, \hat{\mathbf{v}}_{n+1}, \hat{\dot{\mathbf{v}}}_{n+1}, t_{n+1})$;
  $\mathbf{K}^t = \mathbf{K}^t(\hat{\mathbf{q}}_{n+1}, \hat{\mathbf{v}}_{n+1}, \hat{\dot{\mathbf{v}}}_{n+1}, t_{n+1})$;
  $\mathbf{T}^\dagger_{1:3\times 1:3} = \mathbf{I}_3$;
  $\mathbf{T}^\dagger_{4:6\times 4:6} = \mathbf{I}_3 + \frac{\cos\phi - 1}{\phi^2}\widetilde{\mathbf{y}}_{4:6} + \left(1 - \frac{\sin\phi}{\phi}\right)\frac{\widetilde{\mathbf{y}}_{4:6}\widetilde{\mathbf{y}}_{4:6}}{\phi^2}, \qquad \phi = |\mathbf{y}_{4:6}|;$
  $\mathbf{S}_t = \beta'\mathbf{M}^t + \gamma'\mathbf{C}^t + \mathbf{K}^t\mathbf{T}^\dagger$;
  $\Delta\mathbf{y} = -\mathbf{S}_t^{-1}\mathbf{res}$;
  $\mathbf{y} = \mathbf{y} + \Delta\mathbf{y}$;
  $\hat{\mathbf{v}}_{n+1} = \hat{\mathbf{v}}_{n+1} + \gamma'\Delta\mathbf{y}$;
  $\hat{\dot{\mathbf{v}}}_{n+1} = \hat{\dot{\mathbf{v}}}_{n+1} + \beta'\Delta\mathbf{y}$;
end
$\mathbf{a}_{n+1} = \mathbf{a}_{n+1} + \frac{1-\alpha_f}{1-\alpha_m}\hat{\dot{\mathbf{v}}}_{n+1}$;

kind of load	non-follower	follower	app. to G	app. to P	time-dependent
force	x	x	x	x	x
torque	x	x	x	x	x
linear trans. of $\mathbf{q}$	x	x	x	x	x
linear trans. of $\mathbf{v}$	x	x	x	x	x
linear trans. of $\dot{\mathbf{v}}$	x	x	x	x	x

Table 3.1: Topologic map of the admissible loads applied to the rigid body.

For the sake of completeness, the other possible operators proposed in [11] are given by:

$$\varphi^2_{h*}(\mathbf{q}_n, \mathbf{v}_n, \mathbf{a}_n) = \mathbf{q}_n \circ \exp(h\widetilde{\mathbf{v}}_n) \tag{3.98}$$

$$\varphi^2_{hx}(\mathbf{v}_n, \mathbf{a}_n, \mathbf{a}_{n+1}) = h^2(0.5-\beta)\mathbf{a}_n + \beta h^2 \mathbf{a}_{n+1} \tag{3.99}$$

$$\varphi^3_{h*}(\mathbf{q}_n, \mathbf{v}_n, \mathbf{a}_n) = \mathbf{q}_n \circ \exp(h\widetilde{\mathbf{v}}_n) \circ \exp(h^2(0.5-\beta)\widetilde{\mathbf{a}}_n) \tag{3.100}$$

$$\varphi^3_{hx}(\mathbf{v}_n, \mathbf{a}_n, \mathbf{a}_{n+1}) = \beta h^2 \mathbf{a}_{n+1} \tag{3.101}$$

3.5.3 Admissible loads

A rigid body can be subjected to a very wide range of loads so that it is almost impossible to consider every possible case. As a consequence, each code should be designed on the basis of the specific task. The dynamic solver is implemented with the formulations developed in this chapter; thus, it can cover a satisfying range of admissible loads (see Table 3.1). However, the list is not mandatory and it is always possible to implement other kinds of loads.

3.5.3.1 Code coupling

The code can be coupled with other modules addressing specific problems, such as the hydrodynamic action or the mooring system loads, in terms of external loads, with a wide range of possible formulations and combinations. However, if the coupling requires a more complex load formulation, for instance a nonlinear transformations of different state variables, it is always possible to properly rewrite the part of the algorithm dealing with the dynamic differential problem and its linearisation (tangent operators). This version of the code does not allow to perfectly constrain the system degrees of freedom, but they can be conveniently limited through a stiffness-like load, i.e. a transformation of the displacements (external springs).

3.5.4 On the rotation representation

The code is written by using the rotational vector representation, but some operators, directly related to the rotations of the body as their linear or nonlinear transformations, can refer to other representations, such as the Euler angles (Tait-Bryan or nautical angles) [6]. This mismatch could lead to very rough errors if neglected. In this section the use of different representations is discussed.

3.5.4.1 Numerical comparison

In order to compare the two rotation representations (rotational vector and Tait-Bryan angles), a three component random vector is generated and scaled by a multiplication

factor of an opportune power of ten, which can be interpreted as the "order" of magnitude of the rotation. The formulations are compared in terms of absolute value of each component (see Figure 3.4(a)) and maximum relative error (see Figure 3.4(b)), given by:

$$\%\,\text{error} = 100\left[\max_i\left(\frac{\psi_i - \varphi_i}{\max_j |\psi_j|}\right)\right] \tag{3.102}$$

If the rotation is small (in modulus), the rotational vector components can be confused with the nautical angles without any significant loss of accuracy. In fact, if the order is smaller than 10^{-1} (see Figure 3.4), there is a perfect match of the components, also confirmed by the corresponding almost null relative error.

3.5.4.2 Remarks

The equivalence between Tait-Bryan angles and the components of the rotational vector is no longer valid for infinitesimal increments about an arbitrary configuration. Such increments should be transformed by a tangent operator proper of the reference configuration, i.e. the configuration where the incremental rotation is applied. Nevertheless, the rotational vector representation can be equivalent to the Tait-Bryan (or Euler) angles if and only if the angles are small, with magnitude of the order of 10^{-2} or smaller. This result could be directly applied to the numerical code. Let's consider a load formulated as a transformation of the rotations expressed with the Tait-Bryan representation. At each time step, if the time step size is sufficiently small to ensure small rotation increments in the neighbourhood of the previous equilibrium configuration and if the overall rotation is conveniently small, the Newton-Raphson iterations could be performed without converting the operator from the Tait-Bryan angle representation into the rotational vector formulation. Anyway, the actual loads due to the overall rotation should be computed referring to the right rotation representation[17]. With such procedure, the convergence of the Newton-Raphson iterations is not strongly deteriorated. However, for large rotations either a conversion of the operators or the use of a proper tangent operator is recommended, sometimes mandatory.

3.6 Numerical examples

In this section a number of numerical examples is presented in order to prove the effectiveness of the approach. Unluckily, exact analytic solutions are available only for few simple problems, as the one degree-of-freedom oscillator[18] (free, damped, and forced) or the sphere in the Euclidean space. The solution of the most practical problems can be obtained only by means of numerical procedures, which should be validated and calibrated against known cases.

[17] For instance, the operators associated with the first-order hydrodynamic problem (hydrostatic matrix) are usually referred to the nautical angles, even if it depends on the code used for generating the hydrodynamic, or any other, operators.

[18] For the sake of completeness, the oscillators are discussed in Appendix B where the numerical solutions obtained with the model developed in this research are compared with the corresponding exact analytic solutions. The analyses revealed a satisfactory level of accuracy for a wide range of cases, including both translational and rotational oscillators (free, damped, forced).

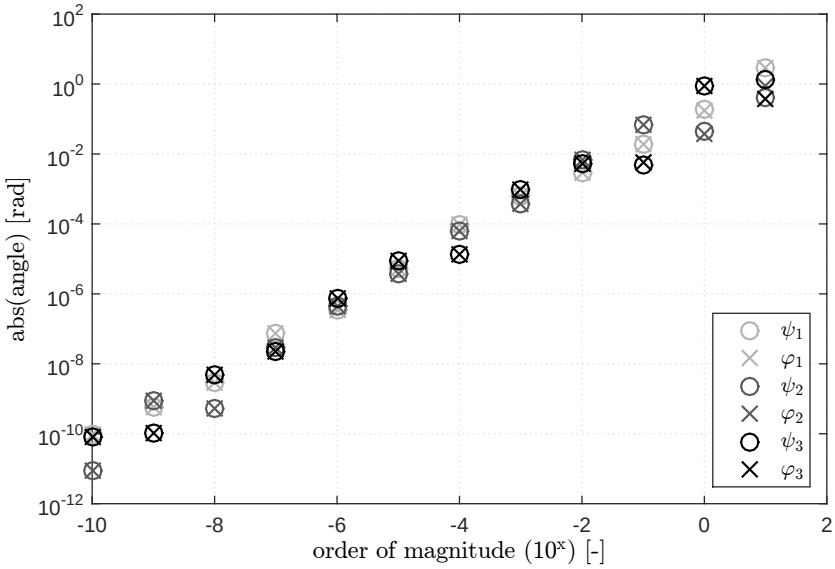

(a) angles' components

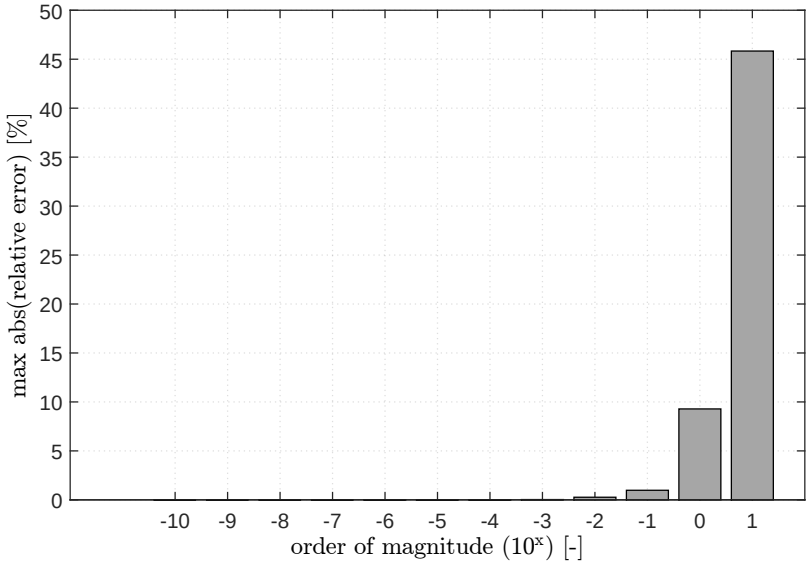

(b) relative error

Figure 3.4: Comparison between the rotational vector components and the Tait-Bryan angles for different orders of magnitude of the rotation.

environment		
gravity acceleration, g	0.00	m/s^2
rigid body		
inertia, $\mathbf{J}$	diag(3 3 3)	kg·m^2
reference point, $\mathbf{x}_P^{B,\mathcal{M}}$	$[0\ 0\ -0.6]^T$	m
loads		
torque, $\mathbf{T}_G^f$	$[0\ 0\ 30]^T$	N·m
initial conditions		
displacement, $\boldsymbol{\psi}\|_{t=0}$	$[0\ 0\ 0]^T$	rad
velocity, $\hat{\mathbf{v}}\|_{t=0}$	$[0\ 0\ 0\ 10\ 15\ 20]^T$	m/s|rad/s

Table 3.2: Sphere with follower torque; parameters used for the analysis.

3.6.1 Sphere with follower torque

Let's consider a rigid body with spherical ellipsoid of inertia in the Euclidean space in absence of gravity, i.e. with a null gravitational field, and subjected to a constant follower torque[19]; the features of the system and of loads are reported in Table 3.2. Since there are not external net forces applied to the body, the system rotates about the center of mass (which does not translate). This example allows to validate the part of the code that deals with finite rotations by means of a direct comparison with the exact analytic solution developed in [73][20].

3.6.1.1 Error evaluation

The numerical and analytic solutions are compared in terms of mean absolute error evaluated on the displacement of the reference point $\mathbf{x}_P^{B,\mathcal{M}}$ at a set of specified times t_k, namely [11]:

$$\text{error} = \frac{1}{n_{step}} \sum_{k=1}^{n_{step}} ||\mathbf{x}_P^{I,\mathcal{S}(\text{num})}(t_k) - \mathbf{x}_P^{I,\mathcal{S}(\text{ref})}(t_k)|| \tag{3.103}$$

$$\mathbf{x}_P^{I,\mathcal{S}}(t_k) = \mathbf{x}_G^{I,\mathcal{S}}(t_k) + \mathbf{R}\big(\boldsymbol{\psi}(t_k)\big)\mathbf{x}_P^{B,\mathcal{M}} \tag{3.104}$$

3.6.1.2 Results

The algorithm (see Figure 3.5), as expected, exhibits a quadratic convergence with a good level of accuracy even for large time step sizes. Coherently with the external torque and the initial conditions, the reference point depicts a curved trajectory about a variable axis. The numerical damping does not significantly affect the accuracy of the numerical solution[21].

[19] The dynamic problem addressed in this section is the same studied in [11] and it is used as a benchmark.

[20] This is one of the few cases (see also the next section) for which an exact analytic solution is available for a three dimensional rotational motion.

[21] Further analyses, not reported here, evaluated the other possible mappings of the algorithm proposed in [11]; the level of accuracy is the same described in [11], confirming the correct implementation of the code.

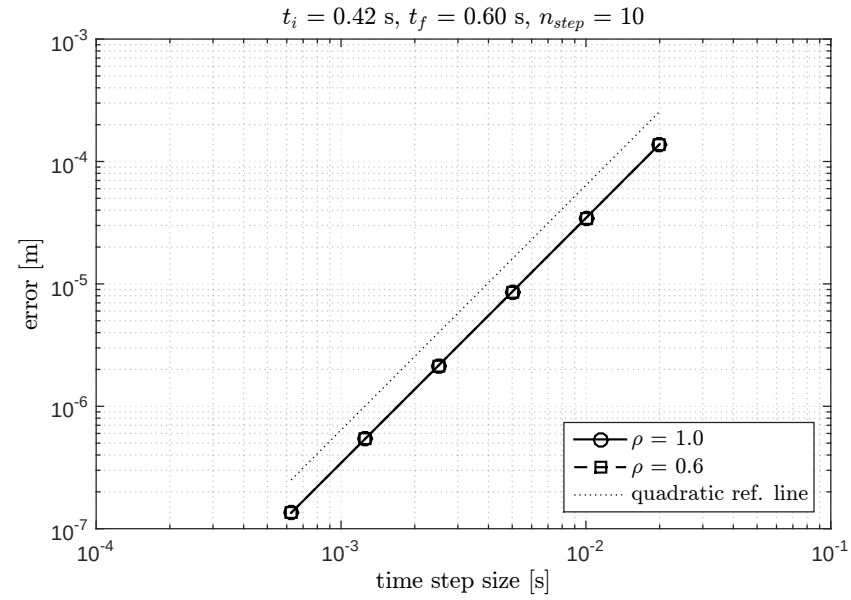

(a) error

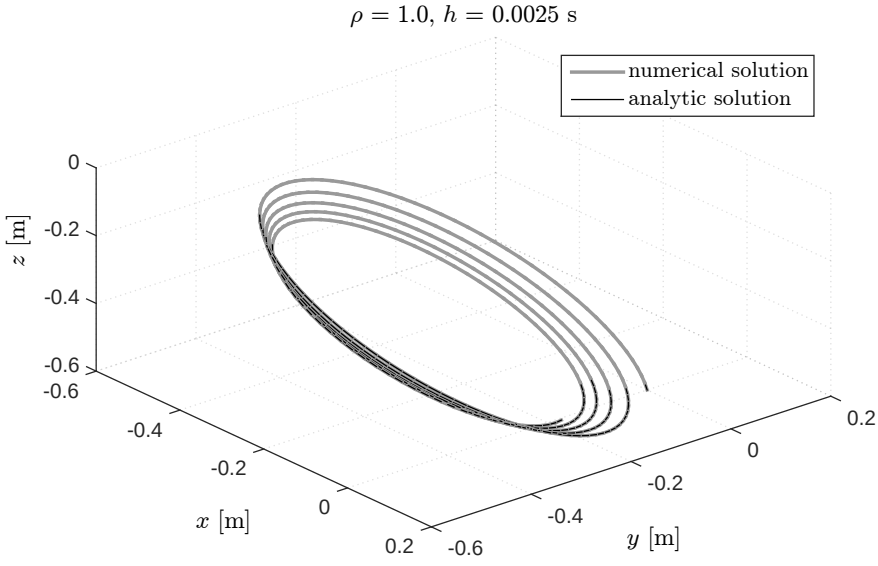

(b) trajectory

Figure 3.5: Sphere with follower torque; comparison between the numerical solution and the exact analytic solution.

environment		
gravity acceleration, g	0.00	m/s^2
rigid body		
inertia, $\mathbf{J}$	diag(20 20 7)	$kg{\cdot}m^2$
reference point, $\mathbf{x}_P^{B,\mathcal{M}}$	$[0\ 0\ -0.6]^T$	m
loads		
torque, $\mathbf{T}_G^f$	$[0\ 0\ 30]^T$	N·m
initial conditions		
displacement, $\boldsymbol{\psi}\|_{t=0}$	$[0\ 0\ 0]^T$	rad
velocity, $\hat{\mathbf{v}}\|_{t=0}$	$[0\ 0\ 0\ 1.0\ 2.0\ 3.0]^T$	m/s|rad/s

Table 3.3: Axially symmetric rigid body; parameters used for the analysis.

3.6.1.3 Remarks

The error trend matches exactly the results reported in [11], where the same system is analysed with the same initial and boundary conditions; therefore, the algorithm is well implemented. Regardless of the numerical damping, it is possible to get a good level of accuracy for a wide range of time step sizes.

3.6.2 Axially symmetric rigid body

Let's consider an axially symmetric rigid body in the Euclidean space in absence of gravity and subjected to a constant follower torque about the axis of symmetry[22]; the features of the system and of loads are reported in Table 3.3. Since there are not external net forces applied to the body, the system rotates about the center of mass (which does not translate). The exact analytic solution is developed in [74].

3.6.2.1 Results

The numerical and analytic solutions are compared in terms of mean absolute error evaluated on the displacement of the reference point $\mathbf{x}_P^{B,\mathcal{M}}$ at a set of specified times t_k, by using the Equation (3.103). The numerical error (see Figure 3.6(a)) obeys the second power of the time step size, typical of a second-order convergence. The numerical damping slightly modifies the accuracy of the algorithm, in particular, the larger the damping the larger the error. Moreover, if the system rotates faster (see Figure 3.6(b), initial velocity doubled), the error is larger. Therefore, in the case of very large velocities, only small time step sizes can guarantee high levels of accuracy.

3.6.2.2 Remarks

The algorithm can properly describe the motion of a rotating body with a satisfying level of accuracy, which depends on both the numerical damping and the features of the motion. In particular, if the system rotates very fast, the error can increase even of some orders of magnitude. In this condition, a good level of accuracy can be achieved only with very small time step sizes. However, floating platforms for wind engineering

[22] Also the problem addressed in this section is studied in [11] but with different inertia properties as well as different initial and boundary conditions.

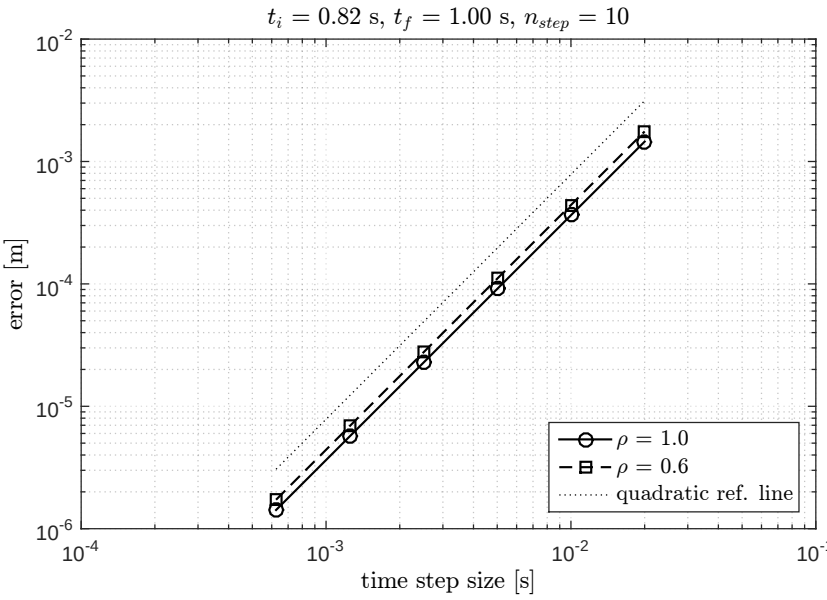

(a) error

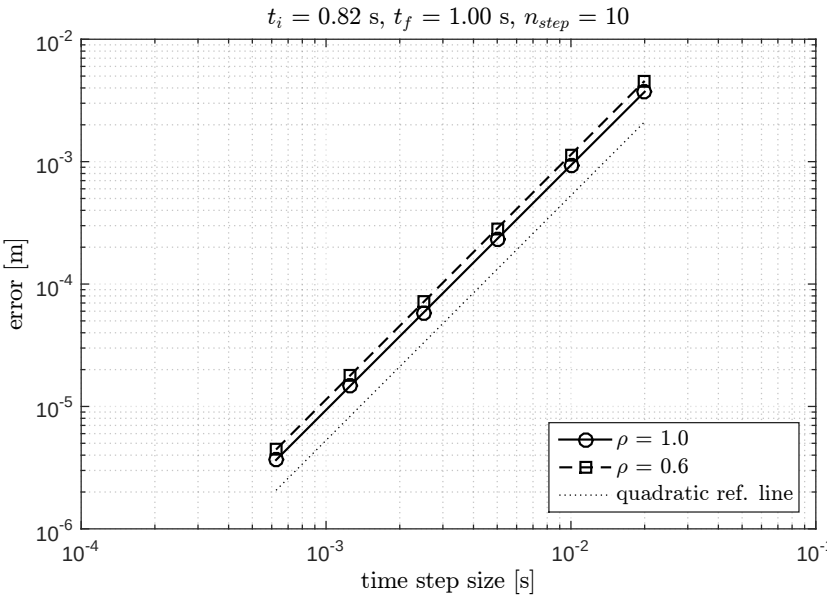

(b) error, initial velocity doubled

Figure 3.6: Axially symmetric rigid body; comparison between the numerical solution and the exact analytic solution.

	environment	
gravity acceleration, g	9.81	m/s^2
	rigid body	
mass, m	1.0	kg
inertia, $\mathbf{J}$	diag(20 20 10)	kg·m^2
	loads	
stiffness, $\mathbf{B}^{\mathbf{q}}$	10^{-3}sym[rand(6, 6)]	•
damping, $\mathbf{B}^{\mathbf{v}}$	10^{-3}sym[rand(6, 6)]	•
added inertia, $\mathbf{B}^{\dot{\mathbf{v}}}$	10^{-3}sym[rand(6, 6)]	•
force, $\mathbf{F}_G^f$	$10^{-1}\sin(\pi/5 \cdot t)[1\ 0\ 0]^T$	N
force, $\mathbf{F}_G^{nf}$	$mg[0\ 0\ 1]^T$	N
torque, $\mathbf{T}_G^f$	$10^{-1}\sin(\pi/10 \cdot t)[0\ 1\ 0]^T$	N·m
	initial conditions	
displacement, $\hat{\mathbf{q}}\|_{t=0}$	$[0\ 0\ 0\ 0\ 0\ 0]^T$	m|rad
velocity, $\hat{\mathbf{v}}\|_{t=0}$	$[0\ 0\ 0\ 0\ 0\ 0]^T$	m/s|rad/s

Table 3.4: Rigid body with follower loads; parameters used for the analysis.

purposes (but also ships) usually have low rotational speeds. The simulations of such systems can be performed using rather large time step sizes (for instance 0.05 s).

The numerical damping, usually associated with a loss of energy, can increase the error but without significantly affecting the accuracy. Moreover, other tests carried out using different mappings of the algorithm revealed that it is not possible to establish a priori which mapping criteria of the Lie group time integration scheme guarantees the higher level of accuracy because the problem is strongly case dependent.

3.6.3 Rigid body with follower loads

Let's consider a rigid body in the Euclidean space forced by a set of follower loads, i.e. sinusoidal force and torque, linear transformations of the state variables (displacement, velocity, and acceleration vectors); the features of the system and of loads are illustrated in Table 3.4. An additional constant non-follower force is considered to balance the weight associated with the gravitational field. In this section, the truncation of the tangent stiffness operator is discussed and proposed as an alternative approach that can guarantee a lesser computational effort.

3.6.3.1 Truncation

The time integration algorithm involves, at each time step, the linearisation of the dynamic differential problem around the previous equilibrium configuration by means of the tangent operators, which depend, among others, on the current orientation of the body. However, the convergence of the Newton-Raphson iterations could be achieved without computing the exact form of the tangent operators (stiffness, damping, and mass). In particular, the terms of the tangent stiffness matrix related to the directional derivative of the rotation operator could be neglected, with a positive impact on the

computational effort[23]. This approach can be explained with a truncation of the series expansion of the exponential map.

3.6.3.2 Results

The operators associated with the linear transformations of the state variables, expressed in the body-attached (non-inertial) reference frame, were randomly generated and converted into symmetric matrices simply by taking the mean value of the extra-diagonal terms, namely:

$$B^{\bullet}_{ij} = B^{\bullet}_{ji} = \frac{1}{2}(B^{\text{rand}}_{ij} + B^{\text{rand}}_{ji}) \qquad \text{for} \quad i \neq j \tag{3.105}$$

The operators used for the simulations are the following:

$$\mathbf{B^q} = 10^{-4} \begin{bmatrix} 7.6885 & & & & & \\ 3.7764 & 1.5475 & & & sym & \\ 8.2597 & 2.5919 & 5.3406 & & & \\ 8.3426 & 4.5107 & 1.3983 & 4.9501 & & \\ 6.8257 & 6.5463 & 5.2066 & 4.2214 & 5.8279 & \\ 8.8165 & 9.0725 & 0.6841 & 4.6021 & 7.1398 & 9.8995 \end{bmatrix} \tag{3.106}$$

$$\mathbf{B^v} = 10^{-4} \begin{bmatrix} 3.4771 & & & & & \\ 1.9639 & 4.4240 & & & sym & \\ 6.3475 & 6.9592 & 4.4231 & & & \\ 2.6621 & 2.7814 & 4.2065 & 4.2992 & & \\ 4.0678 & 5.6657 & 5.6969 & 8.2142 & 3.7740 & \\ 7.7267 & 6.7201 & 3.7594 & 5.3122 & 3.2733 & 8.3350 \end{bmatrix} \tag{3.107}$$

$$\mathbf{B^{\dot{v}}} = 10^{-4} \begin{bmatrix} 3.1807 & & & & & \\ 3.3197 & 6.4731 & & & sym & \\ 5.7925 & 3.2484 & 1.0970 & & & \\ 5.0568 & 7.4228 & 3.4574 & 7.7198 & & \\ 3.3575 & 3.3068 & 5.5042 & 5.1334 & 5.2540 & \\ 7.5023 & 7.3928 & 4.2091 & 8.2209 & 6.3580 & 5.2005 \end{bmatrix} \tag{3.108}$$

The truncated algorithm (see Figure 3.7) returns a numerical solution definitely equivalent to the solution obtained with the algorithm that uses the complete tangent stiffness matrix. The trajectory of the center of mass and the components of the rotational vector are qualitatively the same regardless of the algorithm employed. The absolute error (see Figure 3.8) confirms that the algorithms, in particular the Newton-Raphson schemes, converge to the same solution. However, such equivalence is not sufficient to consider the truncation of the tangent stiffness operator an effective strategy, also the number of iterations required by the Newton-Raphson schemes should be evaluated for every specific case. Note that the choice of plotting the absolute error in place of the relative error is mainly due to the fact that in the first seconds of the simulation the state variables are very close to zero, and therefore a slight difference near to the machine precision ($2.2204 \cdot 10^{-16}$) can produce a high relative error.

[23] In practical terms, the elements of the tangent stiffness operator in sub-matrices $[1:3 \times 4:6]$ and $[4:6 \times 4:6]$ can be computed neglecting the terms related to the variation of the rotation operator $\mathbf{R}$, or sometimes, more simply, they can be considered zero.

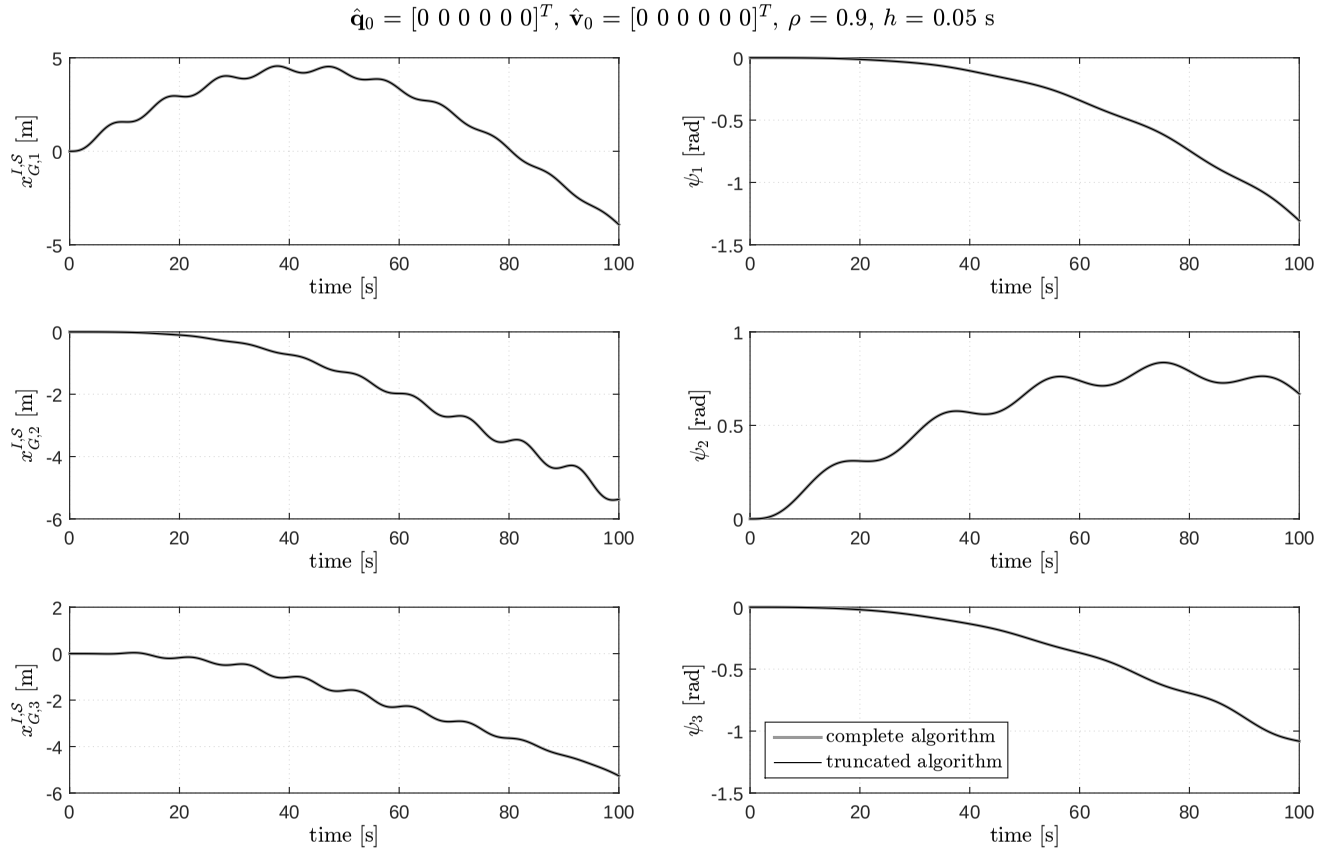

Figure 3.7: Rigid body with follower loads (including transformations of the state variables); comparison between the complete algorithm and the algorithm based on the truncation of the tangent stiffness operator.

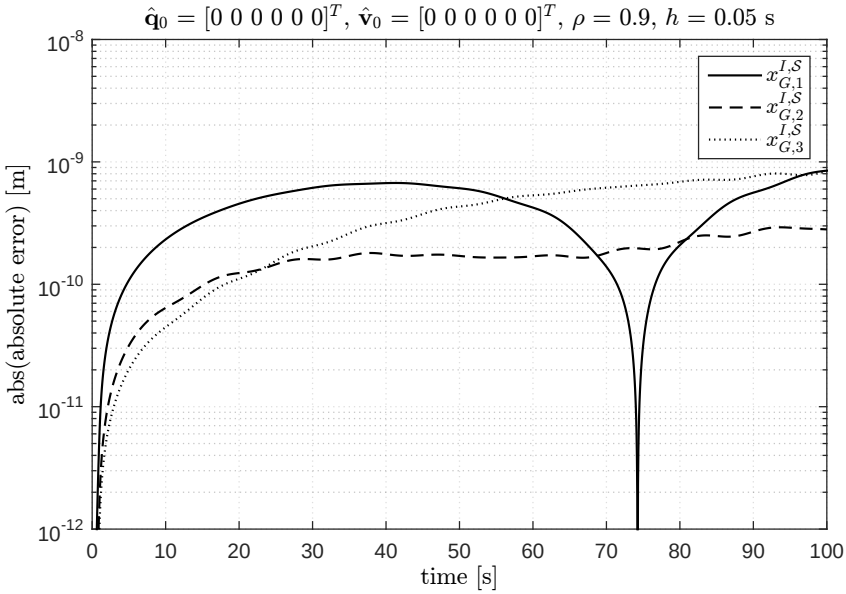

(a) trajectory of the center of mass

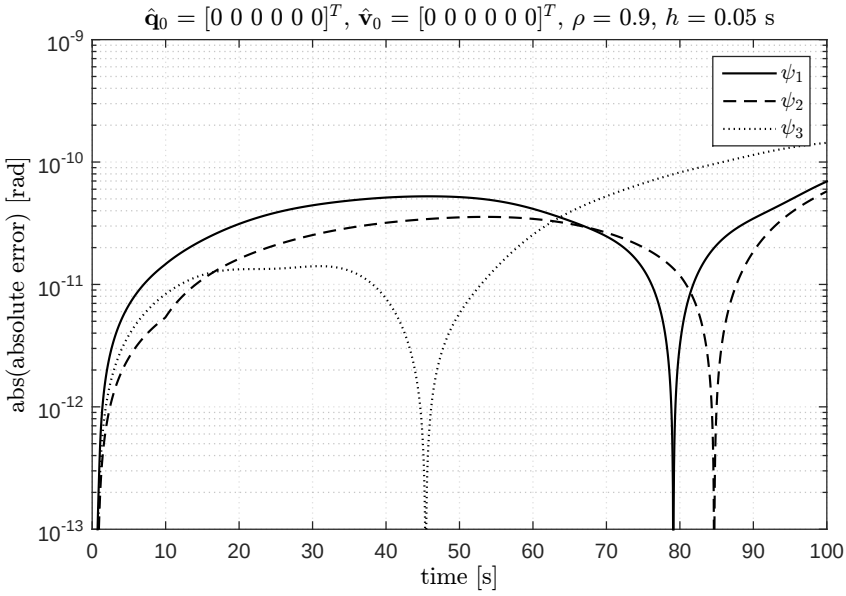

(b) rotation

Figure 3.8: Rigid body with follower loads (including transformations of the state variables); absolute value of the absolute error between the numerical solutions of the complete and truncated algorithms.

3.6.3.3 Remarks

In this section, two different versions of the algorithms based on the mixed-frame formulation are employed for the dynamic analysis of a very general system: a rigid body forced by external time-dependent loads (sinusoidal force and torque) and transformations of the system state variables. The algorithms converge to the same solution with the same level of accuracy; in these terms they can be considered definitely equivalent.

It is very interesting the possibility to truncate the tangent stiffness operators (for instance, those associated with the transformations of the state variables) by neglecting the terms related to the rotation of the body-attached frame with respect to the inertial (fixed) reference frame, paying it just with a very small increase of the total number of Newton-Raphson iterations. The truncation should be justified if the terms neglected in the Taylor's expansion of the dynamic equilibrium equations are higher-order infinitesimal, at least until the increment of the rotation at each time step is relatively small. In fact, for the system analysed, the truncated algorithm required about 0.5% more Newton-Raphson cycles to achieve the convergence on the residual magnitude, it is a slight increase of the computational effort with respect to the benefits obtained in the computation of the truncated tangent stiffness matrices. However, whenever the rotational motion is dominant, the truncation should be used very carefully because it could either produce rough errors, if the tangent hyperplanes are completely wrong, or require a high number of Newton-Raphson iterations to achieve the convergence.

3.6.4 Rigid body with non-follower loads

Let's consider a rigid body in the Euclidean space forced by a set of non-follower loads, i.e. sinusoidal force and torque, linear transformations of the state variables (displacement, velocity, and acceleration vectors); the features of the system and of loads are illustrated in Table 3.5. An additional constant non-follower force is considered to balance the weight associated with the gravitational field.

The use of a mixed-frame formulation does not represent the unique possibility for solving the equations of motion. There are some possible alternatives to model a rigid body motion, depending on the choice of the bases, i.e. reference frames, used for describing the translation of the center of mass and the rotational motion about the center of mass; either local (body-attached) frames or spatial (inertial) frames can be used. A complete local formulation [86] represents a reliable alternative approach (see Appendix A). In this section the algorithms based on both the approaches are evaluated.

3.6.4.1 Results

The transformations of the state variables used in the numerical simulations have the same values of the operators used in the previous example, but they are considered non-follower transformations $\mathbf{A}^{(\bullet)}$. The two formulations (see Figure 3.9) return the same numerical results in terms of trajectory of the center of mass and components of the rotational vector, with a negligible difference ascribing to the different dynamic (and kinematic) formulations and the consequent different time integration procedure. The dotted line in the plot highlights the different dynamic behaviour of the system subjected to the same loads but considered follower (as in the previous section). The relative error (see Figure 3.10) is limited by an upper threshold of about $10^{-3}\%$; therefore, the two approaches (and algorithms) can be considered equivalent not only from a

	environment	
gravity acceleration, g	9.81	m/s^2
	rigid body	
mass, m	1.0	kg
inertia, $\mathbf{J}$	diag(20 20 10)	kg·m^2
	loads	
stiffness, $\mathbf{A}^{\mathbf{q}}$	10^{-3}sym[rand(6, 6)]	•
damping, $\mathbf{A}^{\mathbf{v}}$	10^{-3}sym[rand(6, 6)]	•
added inertia, $\mathbf{A}^{\dot{\mathbf{v}}}$	10^{-3}sym[rand(6, 6)]	•
force (1), $\mathbf{F}_G^{nf}$	$10^{-1}\sin(\pi/5 \cdot t)[1\ 0\ 0]^T$	N
force (2), $\mathbf{F}_G^{nf}$	$mg[0\ 0\ 1]^T$	N
torque, $\mathbf{T}_G^{nf}$	$10^{-1}\sin(\pi/10 \cdot t)[0\ 1\ 0]^T$	N·m
	initial conditions	
displacement, $\hat{\mathbf{q}}\|_{t=0}$	$[0\ 0\ 0\ 0\ 0\ 0]^T$	m|rad
velocity, $\hat{\mathbf{v}}\|_{t=0}$	$[0\ 0\ 0\ 0\ 0\ 0]^T$	m/s|rad/s

Table 3.5: Rigid body with non-follower loads; parameters used for the analysis.

qualitative point of view. Although the plots are not reported here, also the velocity and acceleration vectors are equivalent, after all it would be impossible to obtain the same position state vector.

3.6.4.2 Remarks

The algorithms based on the mixed-frame formulation and on the local-frame formulation can be considered equivalent in terms of numerical result (dynamics of the system); as far as the computational effort is concerned, it should be properly investigated. Since both the algorithms, as expected, return the same dynamic behaviour, an implementation error of the dynamic solver should be considered very unlikely.

Another test of a system with the same mass and inertia features of the rigid body analysed in this section but subjected to follower loads modelled as linear non-symmetric transformations (randomly generated) of the state variables and with non-zero initial conditions (see Figure 3.11)[24], confirms the equivalence of the algorithms based either on the mixed-frame formulation, or on the local-frame formulation, or on the truncation of the tangent stiffness operator.

[24]The curves of the components of the rotational vectors have some discontinuities that occur when the magnitude of the rotation reaches the value of π rad because the algorithm is set up to return a magnitude in the interval $[-\pi,\ \pi]$. For this reason, for very large rotations it could be necessary to keep track of the actual rotation by adding (or subtracting) 2π rad to the modulus of the rotational vector whenever such a discontinuity occurs; otherwise, the definition of the stiffness-like loads related to the rotation becomes misleading. For instance a positive rotation of $3/2 \cdot \pi$ rad would be associated with the load corresponding to $-\pi/2$ rad. However, in the case of floating bodies for offshore wind engineering, the magnitude of rotations is always smaller than $\pi/2$ rad for sure. Moreover, note that the time series of the velocities (see Figure 3.12) and accelerations are not affected by the discontinuities in the time history of the components of the rotational vector.

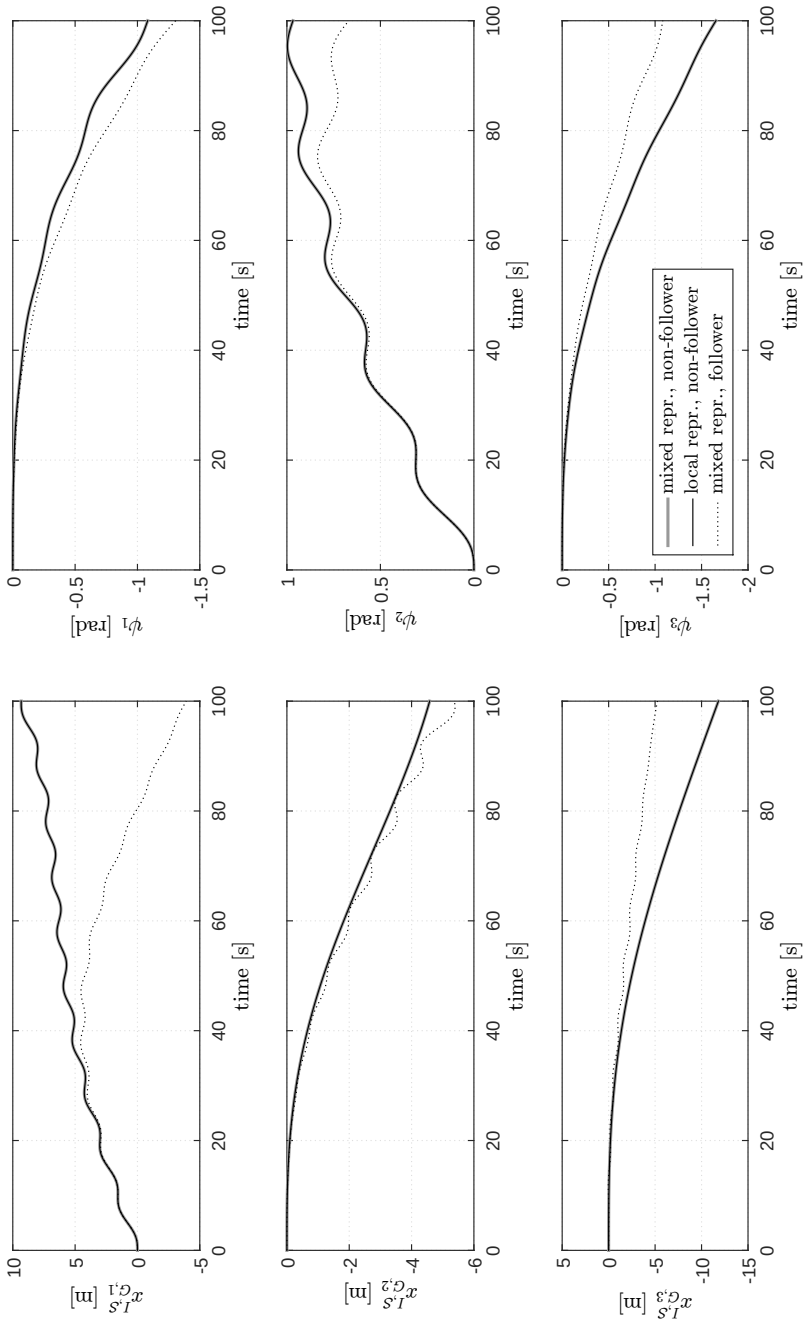

Figure 3.9: Rigid body with non-follower loads (including transformations of the state variables); comparison between the algorithm based on the mixed-frame formulation and the algorithm based on the local-frame formulation.

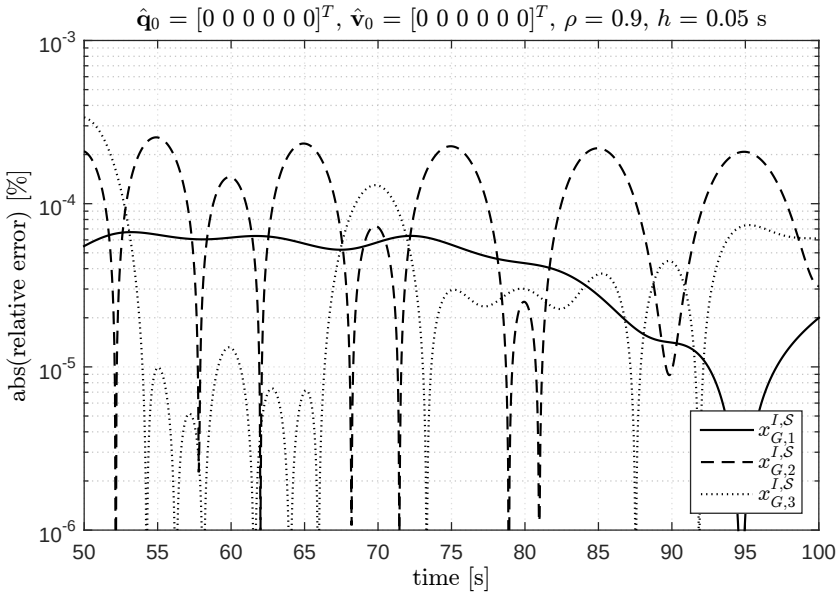

(a) trajectory of the center of mass

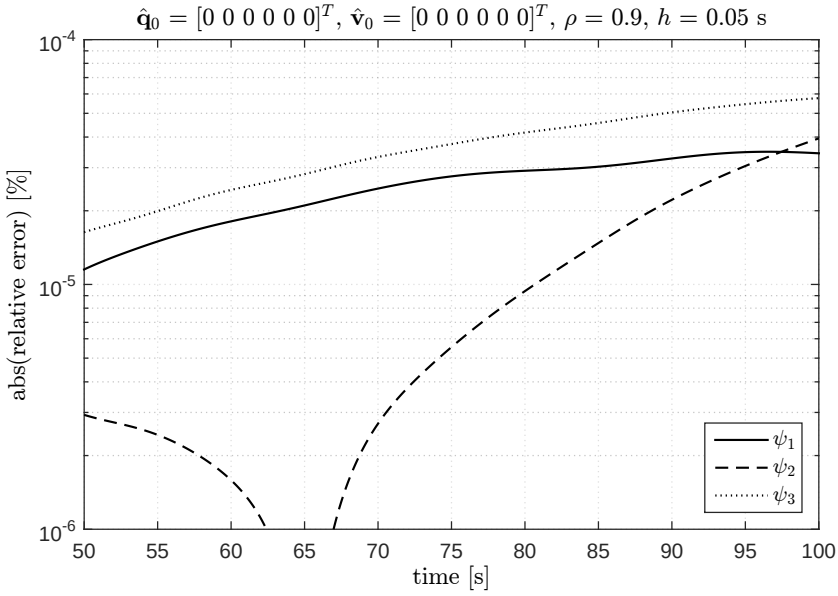

(b) rotation

Figure 3.10: Rigid body with non-follower loads (including transformations of the state variables); absolute value of the relative error between the numerical solutions of the algorithm based on the mixed-frame formulation and the algorithm based on the local-frame formulation.

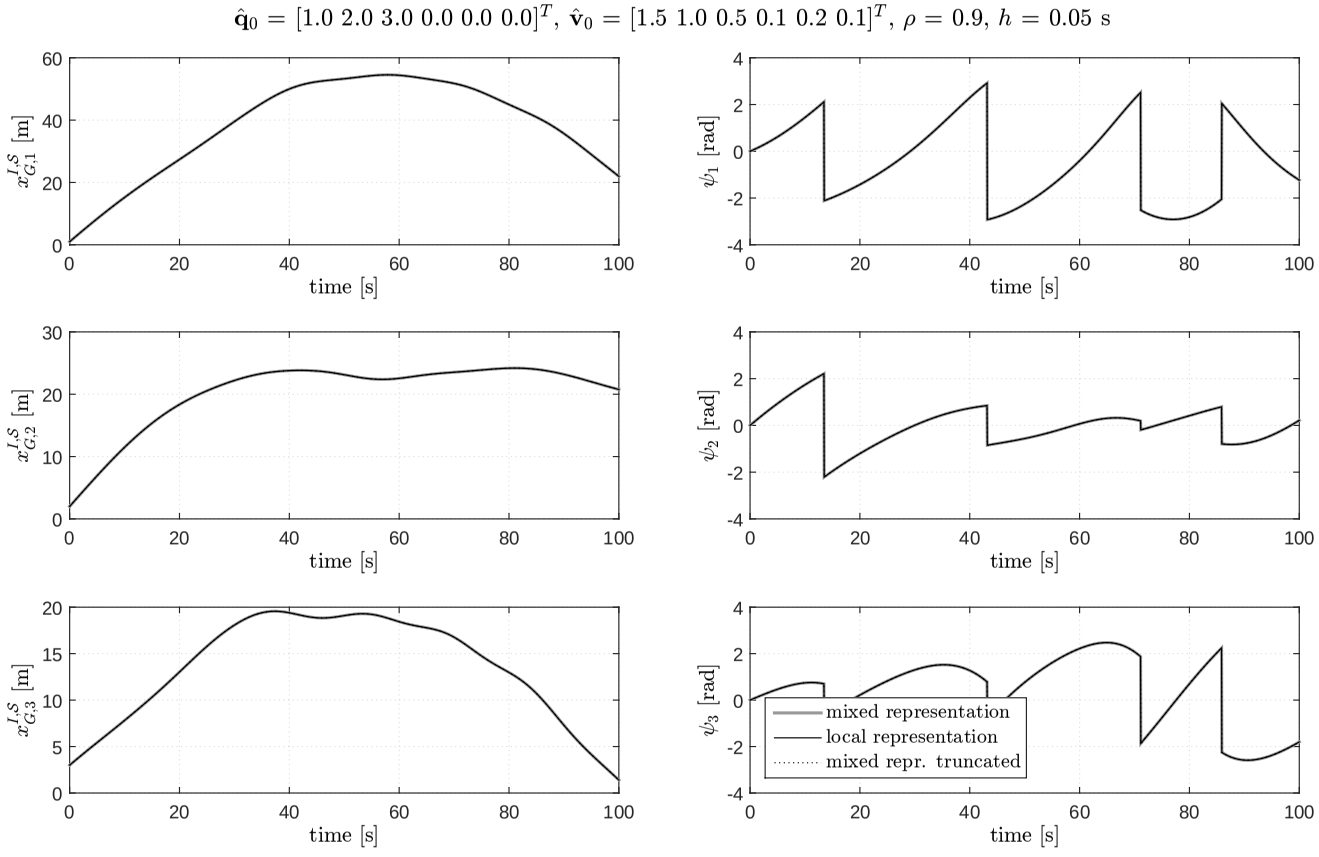

Figure 3.11: Rigid body with follower loads (as transformations of the state variables); comparison between the algorithms based either on the mixed-frame formulation, or on the local-frame formulation, or on the truncation of the tangent stiffness operator.

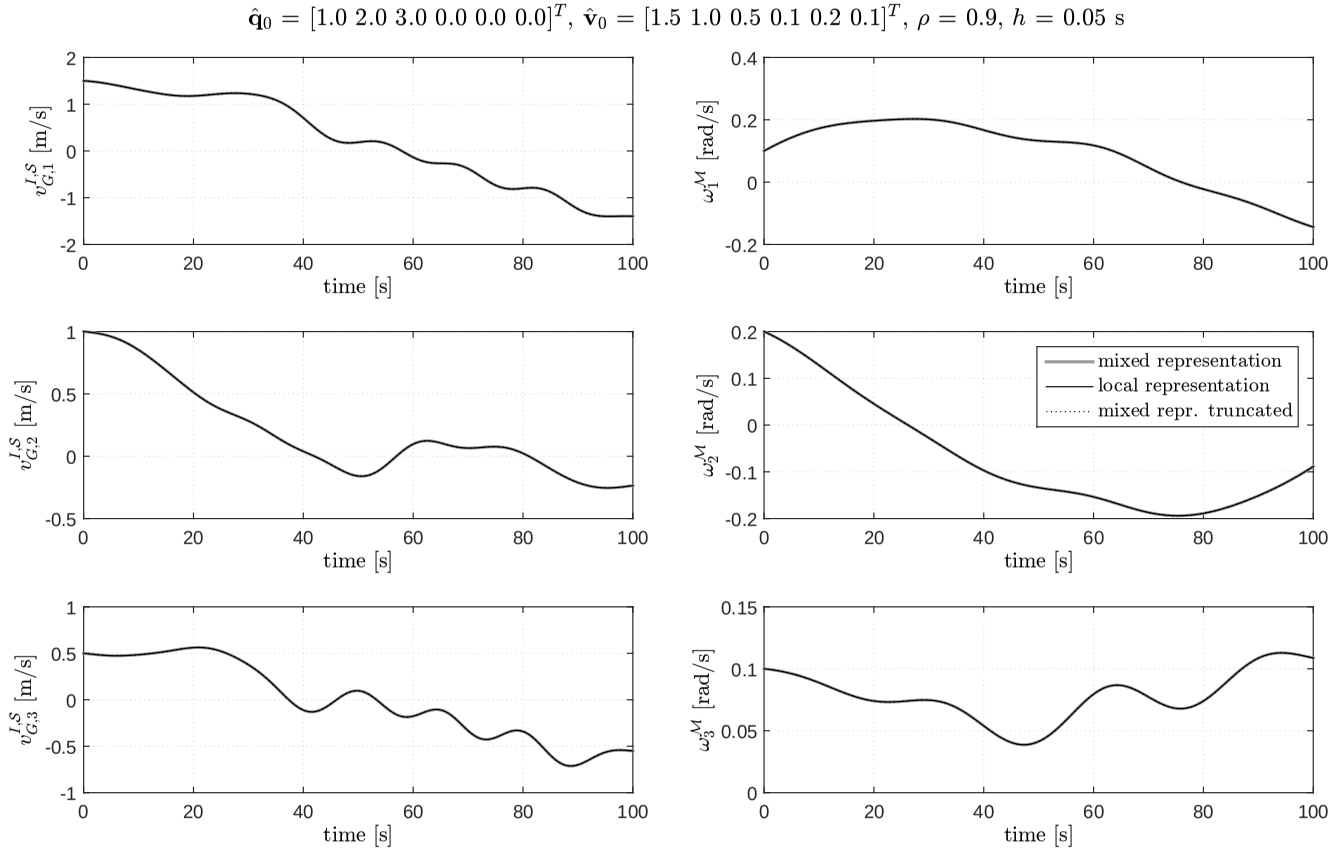

Figure 3.12: Rigid body with follower loads (as transformations of the state variables); comparison between the time histories of the velocity components obtained with the algorithms based either on the mixed-frame formulation, or on the local-frame formulation, or on the truncation of the tangent stiffness operator.

Chapter 4

Hydrodynamic model

"Millions saw the apple fall,
but Newton was the one who asked why."

Bernard M. Baruch

The hydrodynamic model is presented in the framework of the linear theory, widely used for deep-water purposes. The reliability of the small-displacement hypothesis is discussed for hydrostatic loads on the basis of an alternative approach developed to account for large motions. Both regular and irregular waves are described together with their formulations in terms of hydrodynamic loads on the submerged structure. Some interesting remarks about higher-order effects and the use of the linear hydrodynamic theory are finally illustrated. The chapter aims at providing the reader with the fundamentals of hydrodynamic loads based on the linear theory.

4.1 Hydrostatics

When a rigid body is placed in water (or any other fluid), the system can either float or sink, depending on the weight of displaced fluid with respect to the overall vertical force acting on the body (its weight but also external loads). The hydrostatics aims at studying the equilibrium of floating bodies in still water, i.e. the resultant force exerted by the fluid and the equilibrium configuration. For further discussions on the topics presented in this section the reader is addressed to the references [5, 46] or every book of fluid mechanics.

4.1.1 Reference frame

As previously introduced, the hydrostatic problem aims at establishing the equilibrium configuration (if exists) of a semi-submerged body. Since the specific mathematical formulation is indissolubly related to the observer, the choice of an appropriate reference frame can strongly simplify the formalisms of the problem. Let's consider a spatial (fixed) inertial reference frame $\{O; x, y, z\}$ defined by the orthonormal basis $\mathcal{S} = \{\mathbf{e}_i^I\}$. The origin O is located in the (mean) sea surface, and the z-axis points vertically upwards. The physical quantity $(\bullet)$ observed in this frame is indicated with the notation $(\bullet)^I$ and is always implicitly expressed with respect to the canonical basis[1] $\mathcal{S}$. On the other hand, when the indication of the reference frame is not as important as the information about the basis (for instance for forces), the physical quantity $(\bullet)$ expressed with respect to the basis of the inertial frame is indicated with the notation $(\bullet)^{\mathcal{S}}$.

4.1.2 Static equilibrium conditions

A body semi-submerged in a fluid is subjected to interaction forces all over the submerged contour (surface), associated with the fluid pressure, directed normal to the surface and pointing inwards. The system is in static equilibrium if the resultant force and the resultant moment, with respect to an arbitrary point, acting on the system are both zero (cardinal equations of statics). Given the geometry of the body, its weight, and the features of the fluid (density), the balance of forces and torques univocally defines the equilibrium configuration. If the only loads acting on the system are the gravity and the hydrostatic pressures, the net hydrostatic load, called buoyancy, should balance the weight of the body, and therefore is a force pointing upwards and passing through the center of mass. By contrast, if additional external loads act on the semi-submerged body, the net hydrostatic load is not generally aligned with the center of mass.

Given a floating body[2] in static equilibrium in the configuration $\mathcal{C}_0$[3], let P be a point

[1] In order to not weigh the notation down, the double indication of the reference frame and the basis is removed, namely:

$$\mathbf{x}^I = \mathbf{x}^{I,\mathcal{S}}$$

[2] In the framework of this research, it is of much more interest to study hydrostatic forces in the neighbourhood of the equilibrium configuration. The equilibrium on a free submerged body is possible only if the body has the same weight of the displaced fluid. Moreover, if the body is completely submerged in the fluid and is anchored to the seabed with tension moorings, for instance tension leg platforms, the hydrostatic load simply consists in the weight of the displaced fluid (of the same volume of the body).

[3] The quantities $(\bullet)$ associated with the equilibrium configuration are indicated with the notation

on the wetted surface S_0 of the body and let $\mathbf{n}$ be the unit normal vector of the body surface pointing outwards, the water-plane area A_0 cut by the body and the submerged volume V_0 are given by [5]:

$$A_0 = -\int_{S_0} n_3 dS \tag{4.1}$$

$$V_0 = \int_{S_0} x^I_{P,3} n_3 dS \tag{4.2}$$

When the equilibrium configuration is perturbed, the floating body can remain in the new configuration (neutral), or can move farther away (unstable), or can return in its original configuration after a transient (stable). In the case of a free floating body, the equilibrium is always neutral for sway, surge, and yaw motions and stable for heave (piercing) motions, whereas for roll and pitch motions the quality of the equilibrium depends on the specific characteristics of the body (geometry, weight, and mass distribution) and the fluid (density). In particular, if the metacenter is below the center of mass, the equilibrium is unstable, otherwise it is stable.

4.1.3 Hydrostatic stiffness matrix

The hydrostatic load can be seen as a vector function of the variables that define the configuration of the rigid-body, namely six parameters, as the number of degrees of freedom. The first-order Taylor series about the equilibrium configuration defines the tangent stiffness matrix $\mathbf{K}^{hys}$ associated with the hydrostatic problem. Let P be a point on the wetted surface S_0 of the body, let B be the center of buoyancy[4], and let G be the center of mass of the rigid body. The non-null components of the hydrostatic stiffness matrix about the equilibrium configuration are given by [5, 46]:

$$K^{hys}_{33} = -\rho_w g \int_{S_0} n_3 dS = \rho_w g A_0 \tag{4.3}$$

$$K^{hys}_{34} = K^{hys}_{43} = -\rho_w g \int_{S_0} (x^I_{P,2} - x^I_{G,2}) n_3 dS \tag{4.4}$$

$$K^{hys}_{35} = K^{hys}_{53} = \rho_w g \int_{S_0} (x^I_{P,1} - x^I_{G,1}) n_3 dS \tag{4.5}$$

$$K^{hys}_{44} = -\rho_w g \int_{S_0} (x^I_{P,2} - x^I_{G,2})^2 n_3 dS + \rho_w g (x^I_{B,3} - x^I_{G,3}) V_0 \tag{4.6}$$

$$K^{hys}_{45} = K^{hys}_{54} = -\rho_w g \int_{S_0} (x^I_{P,1} - x^I_{G,1})(x^I_{P,2} - x^I_{G,2}) n_3 dS \tag{4.7}$$

$$K^{hys}_{55} = -\rho_w g \int_{S_0} (x^I_{P,1} - x^I_{G,1})^2 n_3 dS + \rho_w g (x^I_{B,3} - x^I_{G,3}) V_0 \tag{4.8}$$

$$K^{hys}_{46} = -\rho_w g (x^I_{B,1} - x^I_{G,1}) V_0 \tag{4.9}$$

$$K^{hys}_{56} = -\rho_w g (x^I_{B,2} - x^I_{G,2}) V_0 \tag{4.10}$$

$(\bullet)_0$.

[4]The center of buoyancy is the centroid of the displaced volume of fluid.

Alternatively, the components of the hydrostatic stiffness operator can be defined with respect to the water-plane area A_0 cut by the floating body, in place of the wetted surface S_0, as follows [46]:

$$K_{33}^{hys} = \rho_w g \int_{A_0} dA = \rho_w g A_0 \tag{4.11}$$

$$K_{34}^{hys} = K_{43}^{hys} = \rho_w g \int_{A_0} (x_{P,2}^I - x_{G,2}^I) dA \tag{4.12}$$

$$K_{35}^{hys} = K_{53}^{hys} = -\rho_w g \int_{A_0} (x_{P,1}^I - x_{G,1}^I) dA \tag{4.13}$$

$$K_{44}^{hys} = \rho_w g \int_{A_0} (x_{P,2}^I - x_{G,2}^I)^2 dA + \rho_w g (x_{B,3}^I - x_{G,3}^I) V_0 \tag{4.14}$$

$$K_{45}^{hys} = K_{54}^{hys} = \rho_w g \int_{A_0} (x_{P,1}^I - x_{G,1}^I)(x_{P,2}^I - x_{G,2}^I) dA \tag{4.15}$$

$$K_{55}^{hys} = \rho_w g \int_{A_0} (x_{P,1}^I - x_{G,1}^I)^2 dA + \rho_w g (x_{B,3}^I - x_{G,3}^I) V_0 \tag{4.16}$$

$$K_{46}^{hys} = -\rho_w g (x_{B,1}^I - x_{G,1}^I) V_0 \tag{4.17}$$

$$K_{56}^{hys} = -\rho_w g (x_{B,2}^I - x_{G,2}^I) V_0 \tag{4.18}$$

If no external loads act on the body, the center of gravity is always aligned with the center of buoyancy along a vertical straight line; hence, the terms K_{46}^{hys} and K_{56}^{hys} are null and the hydrostatic stiffness matrix is symmetric [5].

4.1.4 Hydrostatic loads

The hydrostatic loads in the neighbourhood $\mathcal{C}_n$ of the equilibrium configuration $\mathcal{C}_0$, whose corresponding physical quantities are briefly indicated with the notation $(\bullet)_0$, can be successfully estimated by the first-order expansion (Taylor series) of the hydrostatic loads about $\mathcal{C}_0$, namely:

$$\begin{bmatrix} \mathbf{F}^{\mathcal{S},hys}|_{\mathcal{C}=\mathcal{C}_n} \\ \mathbf{T}^{\mathcal{S},hys}|_{\mathcal{C}=\mathcal{C}_n} \end{bmatrix} = \begin{bmatrix} \mathbf{F}_0^{\mathcal{S},hys} \\ \mathbf{T}_0^{\mathcal{S},hys} \end{bmatrix} - \mathbf{K}^{hys}|_{\mathcal{C}=\mathcal{C}_0} (\mathbf{q}|_{\mathcal{C}=\mathcal{C}_n} - \mathbf{q}_0) \tag{4.19}$$

It is of some interest to better understand how big could be this neighbourhood. Generally (see the next section), the translations do not significantly restrict the domain where the first-order expansion is sufficiently reliable. By contrast, the rotation of the rigid body could invalidate the approximation. However, if the rotational vector has a magnitude lower than 10^{-2} rad the linearisation of the hydrostatic problem can be considered accurate enough.

4.1.4.1 On the rotation representation

The rotation of the body can be parametrized in several ways, and any operator should refer to the proper representation. However, if the rotation remains small, the rotational vector components and the Tait-Bryan angles (or Euler angles) can be considered equivalent without any necessity of converting the tangent stiffness operator (for further discussions see Section 3.5.4), conversion that could not be easy.

4.2 Large-displacement hydrostatics

As discussed in the previous section, the hydrostatic problem of a semi-submerged floating platform consists in estimating the overall loads (forces and moments) due to the surface interaction of the fluid (water) with the solid body. Let's assume that the body moves from the initial configuration $\mathcal{C}_0$ to the varied configuration $\mathcal{C}_v$. If the body undergoes large displacements, the current configuration cannot be confused with the initial one, not even in terms of a first-order approximation; thus, all the static loads should be evaluated with respect to the varied configuration. This section presents a large-displacement numerical approach for the hydrostatic problem, suitable for very large floating platforms.

4.2.1 Hypotheses

The numerical approach presented in this section is not exact but can achieve a very good approximation, as better as the system is close to the basic assumptions of the mathematical formulation, namely:

- the overall center of mass in free floating conditions is aligned with the platform barycentre along a vertical straight line. The algorithm is not able to properly calculate the initial configuration due to an eccentricity of the center of mass. If the eccentricity is small, the formulation can be considered accurate enough;
- the body is semi-submerged, the upper surface is always considered completely dry as well as the lower one completely wet;
- the semi-submerged body is a parallelepiped rigid body, an equivalent formulation can be derived also for other shapes;
- the edge-effects are neglected (very large platform). All the quantities are calculated with respect to the lower wet surface and its projection to the still water level neglecting the contribution due to the wetted lateral surface of the floating body; thus, the larger is the platform the more reliable is the formulation.

4.2.2 Reference frames

The hydrostatic problem of a semi-submerged floating body undergoing large displacements should be formulated with respect to the current configuration. Since the specific mathematical formulation is indissolubly related to the observer, the choice of an appropriate reference frame can strongly simplify the formalisms of the problem. Let's consider the following right-handed orthogonal Cartesian systems:

- spatial (fixed) inertial reference frame $\{O; x, y, z\}$ with the z-axis pointing vertically upwards and defined by the orthonormal basis $\mathcal{S} = \{\mathbf{e}_i^I\}$. The physical quantities $(\bullet)$ observed in this frame are indicated with the notation $(\bullet)^I$ and are implicitly expressed with respect to the canonical basis $\mathcal{S}$;
- body-attached (non-inertial)[5] reference frame $\{G; x', y', z'\}$ defined by the orthonormal basis $\mathcal{M} = \{\mathbf{e}_i^B\}$. The origin is located in the center of mass of the

[5]The hydrostatics studies the body in static conditions; hence, the time derivative of the system configuration does not have any role, and all the reference frames can be assumed to be inertial even if the body can arbitrarily move in the Euclidean space.

floating body. This frame can translate and rotate with respect to the spatial frame, and an observer solidal with the body-attached frame sees the rigid body fixed. The physical quantities $(\bullet)$ observed in this frame are indicated with the notation $(\bullet)^B$ and are implicitly expressed with respect to the canonical basis $\mathcal{M}$.

When the indication of the reference frame is not as important as the information about the basis (for instance for forces), the physical quantity $(\bullet)$ expressed with respect to the basis of the inertial frame is indicated with the notation $(\bullet)^{\mathcal{S}}$, whereas if the quantity is expressed with respect to the basis of the body-attached frame, the notation is $(\bullet)^{\mathcal{M}}$.

4.2.3 Finite area formulation

Generally, the configuration of a rigid body is completely defined by six parameters, describing the translation of a reference point and the rotation about it, despite the magnitude of the displacements. However, if the system undergoes large displacements, the hydrostatic problem cannot be easily formulated with a closed formula able to describe the loads due to the fluid-structure interaction for all the admissible configurations; a numerical approach is therefore addressed. If the semi-submerged body is large enough, the major part of the interaction forces are exchanged at the lower surface; this is the case of the so called two-dimensional bodies where the height is at least one order of magnitude smaller than the other two dimensions, i.e. very large platforms.

Let's suppose to discretize the platform lower surface (bottom) into a finite number of rectangular sub-surfaces, for instance $(i \cdot j)$, and consequently $(i+1) \cdot (j+1)$ nodes, which define a finite grid to evaluate all the physical quantities. Let P_i be the points located at the corners of each rectangle, and let C_i be their geometric center. Let G and G_{wl} be respectively the overall center of mass and the projection of G onto the sea-water plane. Let's consider the state vector[6] $\hat{\mathbf{q}} = [\mathbf{x}_G^I; \boldsymbol{\psi}]$ describing the configuration of the parallelepiped platform with base $(a \cdot b)$ and height c. In the undisplaced configuration the weight[7] of the system is balanced by the buoyancy; the depth h_{imm} of the submerged portion of the body is given by:

$$h_{imm} = \frac{m}{\rho_w A_{base}} = \frac{m}{\rho_w ab} \tag{4.20}$$

Let's focus on the ij-th sub-surface element. Its contributions to the overall force and the overall torque with respect to the pole P' are given by:

$$F^{\mathcal{S}}_{P',1,ij} = 0 \tag{4.21}$$

$$F^{\mathcal{S}}_{P',2,ij} = 0 \tag{4.22}$$

$$F^{\mathcal{S}}_{P',3,ij} = -\rho_w g (x^I_{C_{ij},3} - x^I_{G_{wl},3}) dA \tag{4.23}$$

$$\mathbf{T}^{\mathcal{S}}_{P',ij} = (C_{ij} - P') \times \mathbf{F}^{\mathcal{S}}_{P',ij} = (\mathbf{x}^I_{C_{ij}} - \mathbf{x}^I_{P'}) \times \mathbf{F}^{\mathcal{S}}_{P',ij} \tag{4.24}$$

[6] The rotations can be parametrized by means of either the rotational vector representation or the Euler angles (or other conventions) provided that the proper rotation operator $\mathbf{R}$ is used.

[7] It is considered a free floating body, but if other external loads act on the body, the expression of the submerged portion should be properly modified; for instance, if there is an additional vertical force $F^{\mathcal{S}}_3$, the height of the submerged part is given by:

$$h_{imm} = \frac{mg - F^{\mathcal{S}}_3}{\rho_w gab}$$

where the current element of area dA and the position vectors $\mathbf{x}^I_{P_{ij}}$ are defined as follows:

$$\mathbf{x}^I_{P_{ij}} = (P_{ij} - O) = \mathbf{x}^I_G + \mathbf{R}(\boldsymbol{\psi})\mathbf{x}^B_{P_{ij}} \tag{4.25}$$

$$d\mathbf{x} = \mathbf{x}^I_{P_{(i+1)j}} - \mathbf{x}^I_{P_{ij}} \qquad \text{with} \quad dx_3 = 0 \tag{4.26}$$

$$d\mathbf{y} = \mathbf{x}^I_{P_{i(j+1)}} - \mathbf{x}^I_{P_{ij}} \qquad \text{with} \quad dy_3 = 0 \tag{4.27}$$

$$dA = |d\mathbf{x} \times d\mathbf{y}| \tag{4.28}$$

Of course, the overall loads are simply given by:

$$\mathbf{F}^{\mathcal{S}}_{P'} = \sum_{ij} \mathbf{F}^{\mathcal{S}}_{P',ij} \tag{4.29}$$

$$\mathbf{T}^{\mathcal{S}}_{P'} = \sum_{ij} \mathbf{T}^{\mathcal{S}}_{P',ij} \tag{4.30}$$

4.2.3.1 Hydrostatic stiffness matrix

For each current configuration it is possible to define a tangent stiffness matrix; this linear operator can well approximate the hydrostatic loads in the neighbourhood of the configuration by means of a first-order expansion. Let's assume that the pole P' coincides with the center of mass G of the floating body, the contribution of each sub-surface to the overall stiffness is given by:

$$K^{hys}_{33,ij} = \rho_w g dA \tag{4.31}$$

$$K^{hys}_{44,ij} = \rho_w g (x^I_{C_{ij},2} - x^I_{G,2})^2 dA \tag{4.32}$$

$$K^{hys}_{55,ij} = \rho_w g (x^I_{C_{ij},1} - x^I_{G,1})^2 dA \tag{4.33}$$

$$K^{hys}_{34,ij} = K^{hys}_{43,ij} = \rho_w g (x^I_{C_{ij},2} - x^I_{G,2}) dA \tag{4.34}$$

$$K^{hys}_{35,ij} = K^{hys}_{53,ij} = -\rho_w g (x^I_{C_{ij},1} - x^I_{G,1}) dA \tag{4.35}$$

$$K^{hys}_{45,ij} = K^{hys}_{54,ij} = \rho_w g (x^I_{C_{ij},1} - x^I_{G,1})(x^I_{C_{ij},2} - x^I_{G,2}) dA \tag{4.36}$$

Moreover, since the change of orientation of the center of buoyancy with respect to the center of mass causes the variation of the overall torque, four additional contributions should be considered [5, 46]. In particular, the additional tangent stiffness terms are given by:

$$K^{hys}_{44} = F^{\mathcal{S}}_{G,3}(x^I_{B,3} - x^I_{G,3}) \tag{4.37}$$

$$K^{hys}_{55} = F^{\mathcal{S}}_{G,3}(x^I_{B,3} - x^I_{G,3}) \tag{4.38}$$

$$K^{hys}_{46} = -F^{\mathcal{S}}_{G,3}(x^I_{B,1} - x^I_{G,1}) \tag{4.39}$$

$$K^{hys}_{56} = -F^{\mathcal{S}}_{G,3}(x^I_{B,2} - x^I_{G,2}) \tag{4.40}$$

4.2.4 Example: platform with $x^I_{G,3} \equiv x^I_{G_{wl},3}$

Let's consider a free parallelepiped rigid body semi-submerged in still water without any external load except the weight and the action of the fluid, and assume that the

environment		
gravity acceleration, g	9.81	m/s^2
water density, ρ_w	1 000	kg/m^3
rigid body		
mass, m	$1.15 \cdot 10^7$	kg
location of the platform geometric center, $\mathbf{x}^I_{G_p}$	$[0\ 0\ 1.8056]^T$	m
parallelepiped platform		
width, a	60	m
length, b	60	m
height, c	10	m
submerged height, h_{imm}	3.1944	m
grid		
width	201	nodes
length	201	nodes

Table 4.1: Platform with $x^I_{G,3} \equiv x^I_{G_{wl},3}$; parameters used for the analysis.

geometric center of the body, the center of mass, and the center of buoyancy are aligned along the same vertical line. Moreover, let's assume that the center of mass lies on the water plane; the features of the system are reported in Table 4.1[8]. In these conditions, a pure rotation about G does not imply a variation of the submerged volume.

The hydrostatic loads due to the interaction between the body and the fluid are evaluated for a set of admissible configurations obtained by perturbing the free equilibrium configuration with imposed simple displacements, either rotations or translations, namely:

- pitch, $\varphi_2 = \{10^{-4},\ 5 \cdot 10^{-4},\ 10^{-3},\ 5 \cdot 10^{-3},\ 10^{-2},\ 5 \cdot 10^{-2},\ 10^{-1}\}$ rad;
- roll, $\varphi_1 = \{10^{-4},\ 5 \cdot 10^{-4},\ 10^{-3},\ 5 \cdot 10^{-3},\ 10^{-2},\ 5 \cdot 10^{-2},\ 10^{-1}\}$ rad;
- heave, $-x^I_{G,3} = \{10^{-4},\ 5 \cdot 10^{-4},\ 10^{-3},\ 5 \cdot 10^{-3},\ 10^{-2},\ 5 \cdot 10^{-2},\ 10^{-1}\}$ m.

Note that the hydrostatic loads are not sensitive to the yaw, sway, and surge motions, i.e. the hydrostatics does not restore yaw, sway, and surge perturbations.

4.2.4.1 Results

The formulations based either on the small-displacement hypothesis or on the large-displacement approach, presented in this section, are evaluated in terms of hydrostatic loads. The torque is computed with respect to the center of mass G. The two formulations can be considered equivalent (see Figures 4.1, 4.2, and 4.3) if the rotations are on the order of 10^{-2} rad or smaller. However, if the rotations are larger, the torque obtained with the small-displacement hypothesis is still a good approximation. On the

[8]For both the examples reported in this section, let's consider an inertial reference frame with origin in the center of mass in its undisplaced configuration.

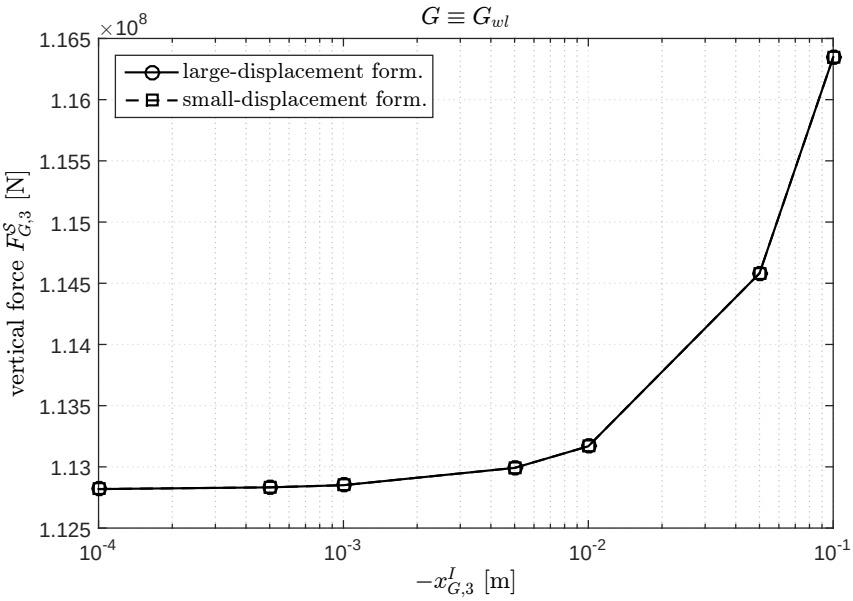

Figure 4.1: Platform with $x^I_{G,3} \equiv x^I_{G_{wl},3}$; comparison between the hydrostatic loads calculated with the small-displacement formulation and the large-displacement formulation in the case of heave perturbations.

other hand, the vertical force returned by the large-displacement formulation is affected by the error due to the neglected edge effects; in particular, the code cannot consider the hydrostatic thrust acting on the submerged lateral surface. When the rotation is very big, these forces appear not exactly negligible. If the body is subjected to pure heave motions (without any rotations, see Figure 4.1), the two formulations are equivalent regardless of the magnitude of the displacement.

4.2.5 Example: platform with eccentric masses

Let's consider a free parallelepiped rigid body semi-submerged in still water without any external load except the weight and the action of the fluid, and assume that the geometric center of the body, the center of mass, and the center of buoyancy are aligned along the same vertical line. Moreover, let's assume that the center of mass lies quite far above the water plane[9]; the features of the system are reported in Table 4.2. In these conditions, a pure rotation about G implies a variation of the submerged volume.

The hydrostatic loads due to the interaction between the body and the fluid are evaluated for a set of admissible configurations obtained by perturbing the free equilibrium configuration with imposed simple displacements, either rotations or translations, namely[10]:

- pitch, $\varphi_2 = \{10^{-4},\ 5 \cdot 10^{-4},\ 10^{-3},\ 5 \cdot 10^{-3},\ 10^{-2},\ 5 \cdot 10^{-2},\ 10^{-1}\}$ rad;

[9] For instance, this could be the scenario when a further rigid body is rigidly connected to the platform.

[10] The perturbations are the same considered in the previous example.

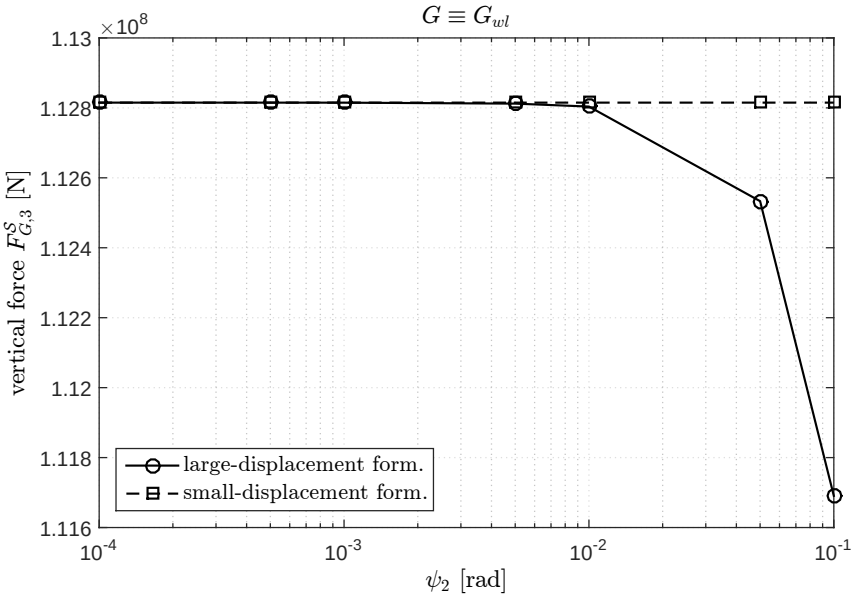

(a) force

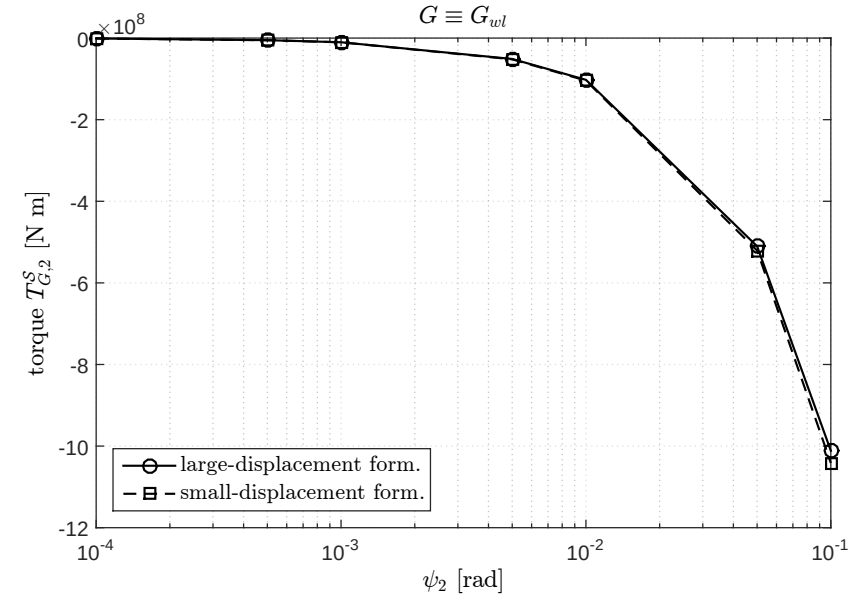

(b) torque

Figure 4.2: Platform with $x^I_{G,3} \equiv x^I_{G_{wl},3}$; comparison between the hydrostatic loads calculated with the small-displacement formulation and the large-displacement formulation in the case of pitch perturbations.

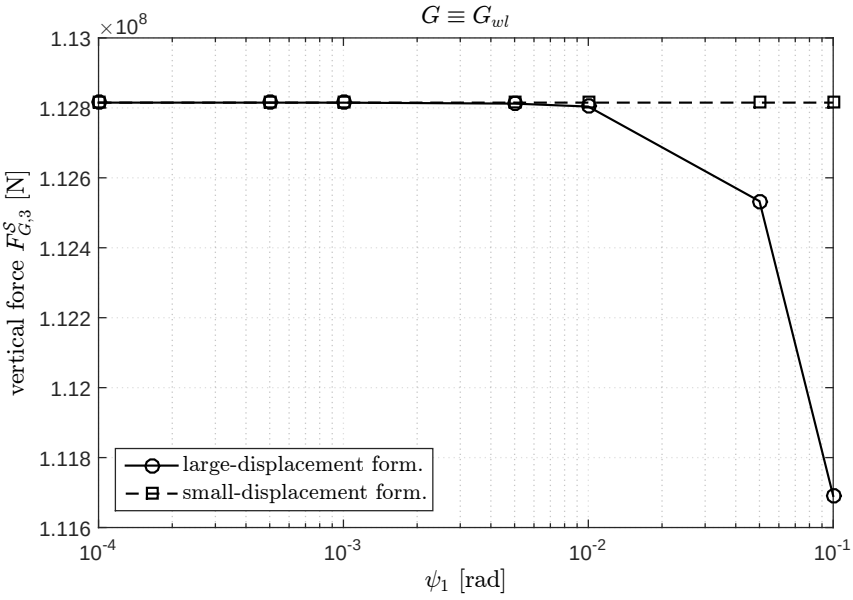

(a) force

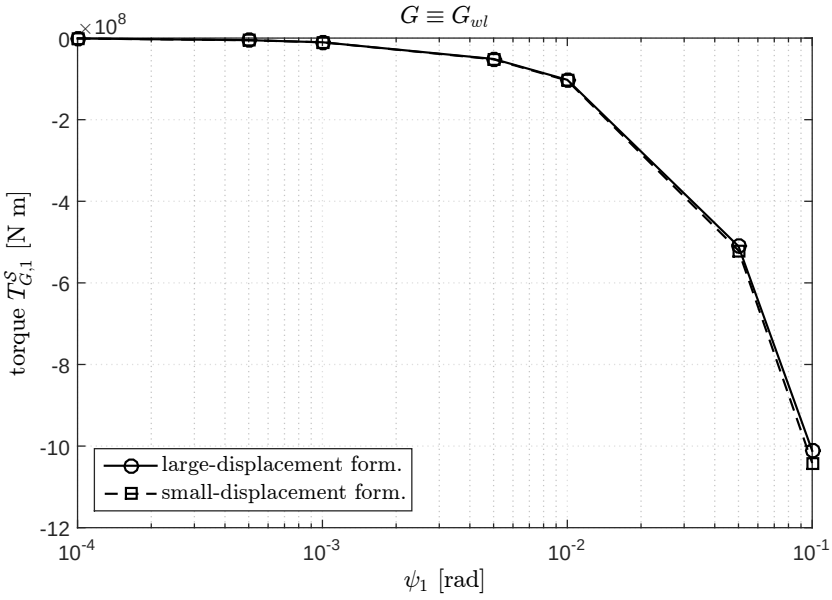

(b) torque

Figure 4.3: Platform with $x^I_{G,3} \equiv x^I_{G_{wl},3}$; comparison between the hydrostatic loads calculated with the small-displacement formulation and the large-displacement formulation in the case of roll perturbations.

environment		
gravity acceleration, g	9.81	m/s^2
water density, ρ_w	1 000	kg/m^3
rigid body		
mass, m	$1.25 \cdot 10^7$	kg
location of the platform geometric center, $\mathbf{x}^I_{G_p}$	$[0\ 0\ -5]^T$	m
parallelepiped platform		
width, a	60	m
length, b	60	m
height, c	10	m
submerged height, h_{imm}	3.4722	m
grid		
width	201	nodes
length	201	nodes

Table 4.2: Platform with eccentric masses; parameters used for the analysis.

- roll, $\varphi_1 = \{10^{-4},\ 5 \cdot 10^{-4},\ 10^{-3},\ 5 \cdot 10^{-3},\ 10^{-2},\ 5 \cdot 10^{-2},\ 10^{-1}\}$ rad;
- heave, $-x^I_{G,3} = \{10^{-4},\ 5 \cdot 10^{-4},\ 10^{-3},\ 5 \cdot 10^{-3},\ 10^{-2},\ 5 \cdot 10^{-2},\ 10^{-1}\}$ m.

4.2.5.1 Results

The formulations based either on the small-displacement hypothesis or on the large-displacement approach, presented in this section, are evaluated in terms of hydrostatic loads. The torque is computed with respect to the center of mass G. The two formulations can be considered equivalent (see Figures 4.4, 4.5, and 4.6) if the rotations are on the order of 10^{-2} rad or smaller. When the rotations are larger, the torque obtained with the small-displacement hypothesis is a good approximation, whereas the vertical force is affected by two kinds of errors: the first one, as discussed above, affects the large-displacement code since it neglects the edge effects; the second one regards the small-displacement formulation because it neglects the variation of the submerged volume due to a pure rotation about the center of mass. Also in this case the two approaches are equivalent when only heave motions occur (see Figure 4.4).

4.2.6 Remarks

The small-displacement hypothesis, used for solving the hydrostatic problem, leads to a good approximation until the rotations have a magnitude of the order of 10^{-2} rad. For larger values, the torque is well approximated, but the vertical force does not consider the variation of the submerged volume due to the rotation of the body about the center of mass[11]. This approximation can lead to some inaccuracies. On the other hand, the proposed approach, which considers the possibility that the body can undergo large

[11] Let's think to the first-order expansion of sine and cosine functions.

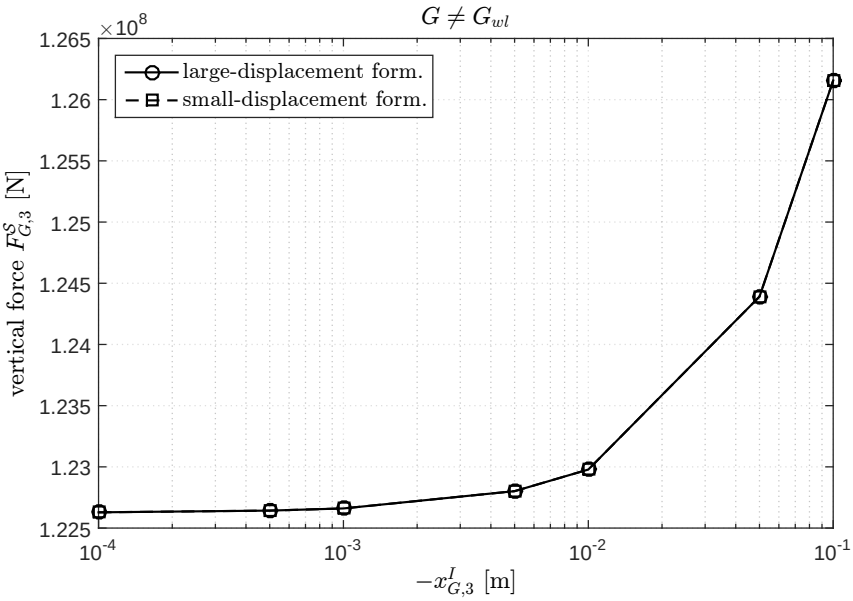

Figure 4.4: Platform with eccentric masses; comparison between the hydrostatic loads calculated with the small-displacement formulation and the large-displacement formulation in the case of heave perturbations.

displacements, appears definitely equivalent to the small-displacement formulation if the magnitude of the rotation does not exceed 10^{-2} rad; this could be considered a threshold above that the rotations cannot be considered small. However, the code exhibits a problem on the accuracy due to the neglected edge effects; the consequent error appears not exactly negligible when the rotations are larger than 10^{-2} rad (of magnitude), which is also the threshold of reliability of the small-displacement formulation. This error is anyway comparable, even lower, to the inaccuracies associated with the small-displacement approach, especially for the analysis of floating supports with eccentric masses (for instance, let's compare Figures 4.2 and 4.5), as an offshore wind turbine.

4.3 Statistical wave description

Regular waves, also called monochromatic, propagate with only one frequency. Although they are relatively simple to manage, they do not exhaustively represent a real sea state, which can be better described with a superimposition of a large number of monochromatic waves [25]. Ocean waves are random processes, both in time and in space, that require a stochastic approach. Since for engineering purposes it is of interest to describe the sea state over a limited area without considering the transients for the development of the waves, the stochastic process can be assumed stationary [66, 68]; this is the case of the so called *fully developed* seas.

In this section, the basics of the stochastic description of sea states are illustrated for waves that propagate only in one direction (for instance, the dominant wind direction); this is the case of the so called *long-crested* irregular seas. For further discussions on

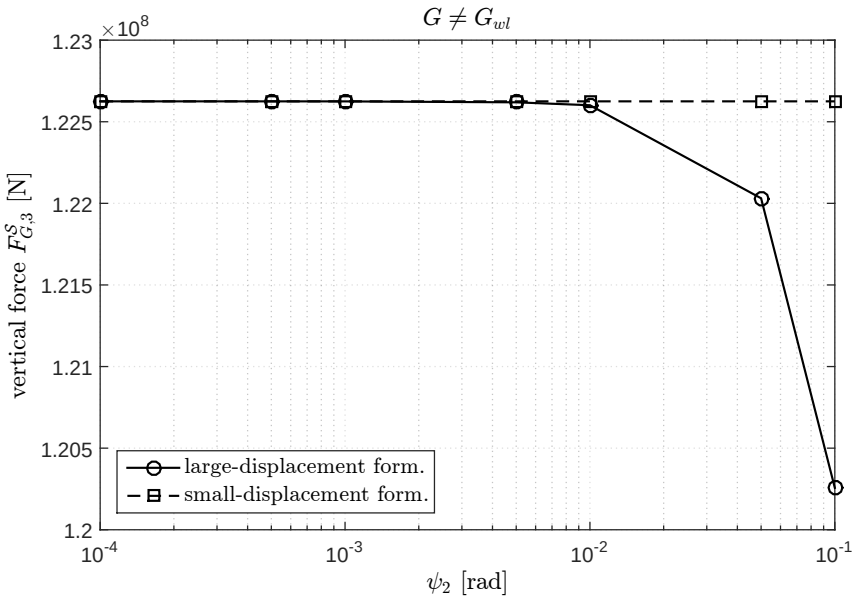

(a) force

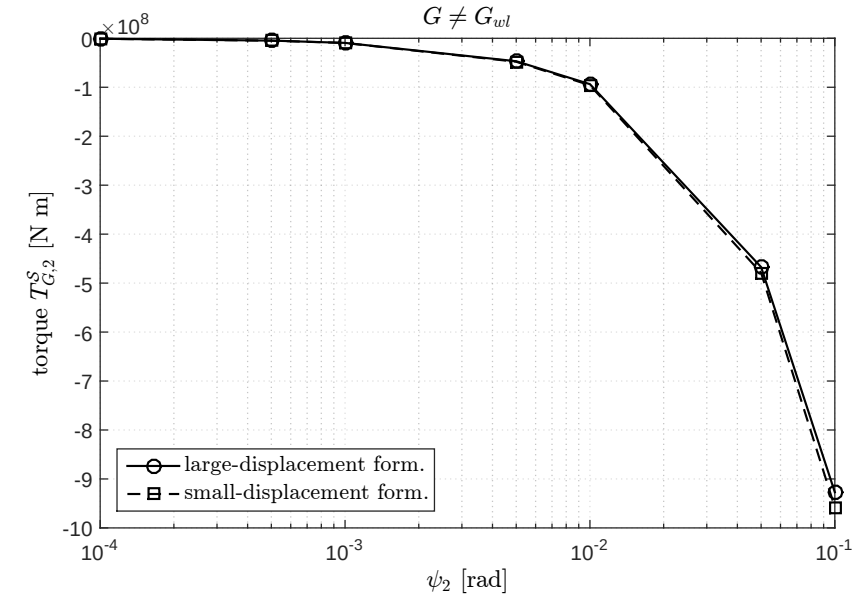

(b) torque

Figure 4.5: Platform with eccentric masses; comparison between the hydrostatic loads calculated with the small-displacement formulation and the large-displacement formulation in the case of pitch perturbations.

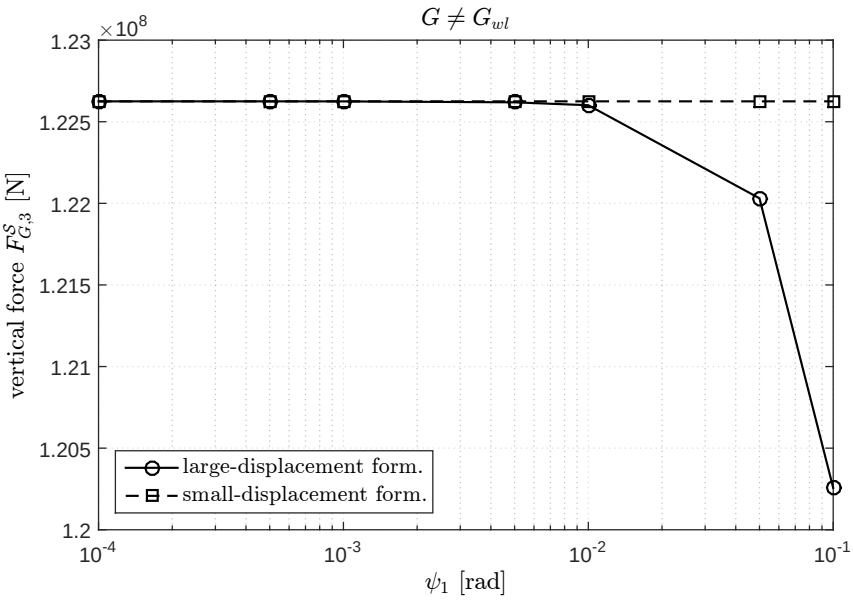

(a) force

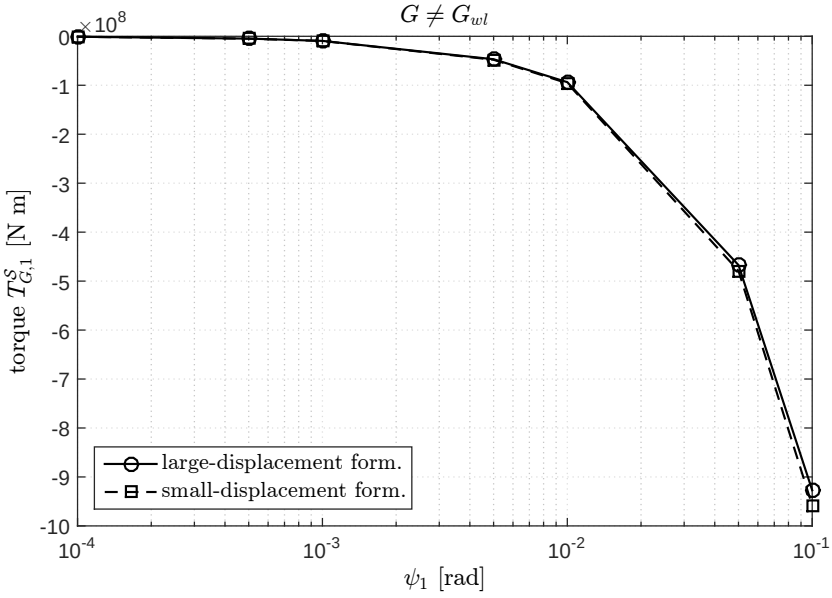

(b) torque

Figure 4.6: Platform with eccentric masses; comparison between the hydrostatic loads calculated with the small-displacement formulation and the large-displacement formulation in the case of roll perturbations.

the topics presented in this section the reader is addressed to the references [25, 29, 50, 66, 68].

4.3.1 Spectrum

Let's focus on the sea surface at a certain location and for short periods of time, and assume that the wave elevation is a *realisation of a stationary and homogeneous zero mean Gaussian stochastic process* [68]. Therefore, the process is exhaustively characterized by the power spectral density, i.e. the Fourier transform of the autocorrelation function; in particular, the mean value μ_η of the wave elevation and its variance σ_η^2 are given by[12]:

$$\mu_\eta = 0 \tag{4.41}$$

$$\sigma_\eta^2 = \int_0^\infty S_{\eta\eta}(\omega) d\omega \tag{4.42}$$

For deep-water purposes, the sea surface elevation can be considered Gaussian for all the admissible sea states, whereas in shallow waters the range of validity depends both on the period and on the significant wave height [68]. Moreover, the wave elevation spectrum is generally a function of both the circular frequency and the direction, but in many applications the waves are assumed to propagate in only one direction.

4.3.1.1 Time series

For time-domain analyses it is necessary a realization (time history) of the stochastic process that fulfils all the statistical properties of the process; in particular, the time series should have the same energy density spectrum [50]. The signal can be generated as the superimposition of a number of waves with different frequency (Fourier series). The wave elevation of a long-crested irregular sea propagating along the x-direction is given by [29, 50]:

$$\eta(t) = \sum_{i=1}^{N} \zeta_i \cos(k_i x_1 - \omega_i t + \varepsilon_i) \tag{4.43}$$

Since the area surrounded by the spectrum in the neighbourhood of the frequency ω_i, for instance of width $\Delta\omega_i$, is the variance of the wave component, the amplitude ζ_i is given by [29, 50]:

$$\zeta_i = \sqrt{2 S_{\eta\eta}(\omega_i) \Delta\omega_i} \tag{4.44}$$

If the spectrum is sampled at regular spaced intervals of amplitude $\Delta\omega$, the consequent time history is a periodic function of period $2\pi/\Delta\omega$ [50]. For further details see also Section 4.4.

[12] The equations presented here are valid for the so called one-sided spectrum, which is defined only for positive circular frequencies. In the case of two-sided spectra the expression of the variance modifies as follows:

$$\sigma_\eta^2 = \int_{-\infty}^{\infty} S_{\eta\eta}^{2-sided}(\omega) d\omega$$

4.3.2 Wave features

The features of the wave elevation stochastic process $\eta(t)$ can be defined through its statistical moments. In particular, in this section the quantities related to the statistics of the wave period and maxima are introduced. The spectral moments m_η^n of order n are defined as follows [68]:

$$m_\eta^n = \int_0^\infty \omega^n S_{\eta\eta}(\omega) d\omega \tag{4.45}$$

The average wave period T_1 (mean centroid wave period), the mean zero-crossing wave period T_z, and the average period between response maxima T_c are given by [50, 68]:

$$\bar{T} = T_1 = 2\pi \frac{m_\eta^0}{m_\eta^1} \tag{4.46}$$

$$T_z = 2\pi \sqrt{\frac{m_\eta^0}{m_\eta^2}} \tag{4.47}$$

$$T_c = 2\pi \sqrt{\frac{m_\eta^2}{m_\eta^4}} \tag{4.48}$$

The distribution of maxima, i.e. their probability density function, is related to the value of the so called *spectral broadness* ϵ [68]:

$$\epsilon = \sqrt{1 - \frac{T_c}{T_z}} \tag{4.49}$$

The spectral broadness measures the probability to have multiple maxima (and minima) within an excursion of a realisation of the process above or below zero. If ϵ is close (ideally equal) to zero, the spectrum is said *narrow-banded* and has not any multiple maxima (and minima) [68]. In this case the probability density function of maxima can be well approximated by a Rayleigh distribution [68]. By contrast, if ϵ equals to one, the spectrum is said *broad-banded* and exhibits a large number of maxima (and minima). In this case the probability density function of maxima is Gaussian [68]. The statistics of maxima are usually calculated assuming that the wave spectrum is narrow-banded [68]. In particular the mean value of the wave amplitude $\bar{\eta}$, the significant wave amplitude $\eta_{1/3}$, and the significant wave height[13] H_s are defined as follows [50, 68]:

$$\bar{\eta} = 1.5\sqrt{m_\eta^0} \tag{4.50}$$

$$\eta_{1/3} = 2\sqrt{m_\eta^0} \tag{4.51}$$

$$H_s = 4\sqrt{m_\eta^0}\sqrt{1-\epsilon^2} \tag{4.52}$$

[13]The significant wave height is defined as the average of the highest one-third of waves.

4.3.2.1 Standard wave spectra

In literature several standard wave spectra[14] are documented for fully developed long-crested seas. These spectra are generally defined as nonlinear functions of the statistical quantities associated with the stochastic process; in particular, the significant wave height and an average wave period. A standard spectrum, of course, is an approximation of the real environmental conditions. For instance, widely used families are the *Bretschneither* spectrum, the *Pierson-Moskowitz* spectrum, the *Modified Pierson-Moskovitz* spectrum, the *Jonswap* spectrum [50, 68]. Anyway, if experimental records are available for a certain site, the spectrum can be built by means of statistical procedures.

4.3.3 IEC 61400-3 spectra

For offshore wind engineering purposes all over the Europe the reference code is the IEC 61400-3 [42], which defines (annex B of the code) the wave spectrum formulations to be used for the design of such systems. It is assumed a two-parameter wave spectrum model, function of the significant wave height H_s and the peak period T_p. Although the spectral features are strongly case-dependent and should be ever investigated for each particular site, in absence of much more details, the code proposes the Pierson-Moskowitz (PM) spectrum for a fully developed sea and the Jonswap (JS) spectrum for a developing sea.

4.3.3.1 Pierson-Moskowitz spectrum

The Pierson-Moskowitz spectrum is used to describe a fully developed sea, i.e. when the fetch does not limit the growth of the waves. The spectral density of the sea surface elevation is given by [42]:

$$S_{PM}(f) = 0.3125 H_S^2 f_p^4 f^{-5} \exp\left[-1.25\left(\frac{f_p}{f}\right)^4\right] \tag{4.53}$$

4.3.3.2 Jonswap spectrum

The Jonswap spectrum is formulated as a modification of the PM spectrum by means of a peak-shape parameter γ and a normalising factor $C(\gamma)$, which generate a narrower spectrum with a higher peak (see Figure 4.7), namely [42]:

$$S_{JS} = C(\gamma) S_{PM}(f) \gamma^{\alpha} \tag{4.54}$$

The normalising factor $C(\gamma)$ is given by [42]:

$$C(\gamma) = \frac{\int_0^\infty S_{PM}(f) df}{\int_0^\infty S_{PM}(f) \gamma^{\alpha} df} \tag{4.55}$$

[14] Note that the standard spectra proposed in literature do not usually account for the effective spectrum (*wave encounter spectra*) seen by a floating body that is moving with a non-null mean speed, like non-moored ships. In these cases the spectrum observed stationary should be properly modified [68].

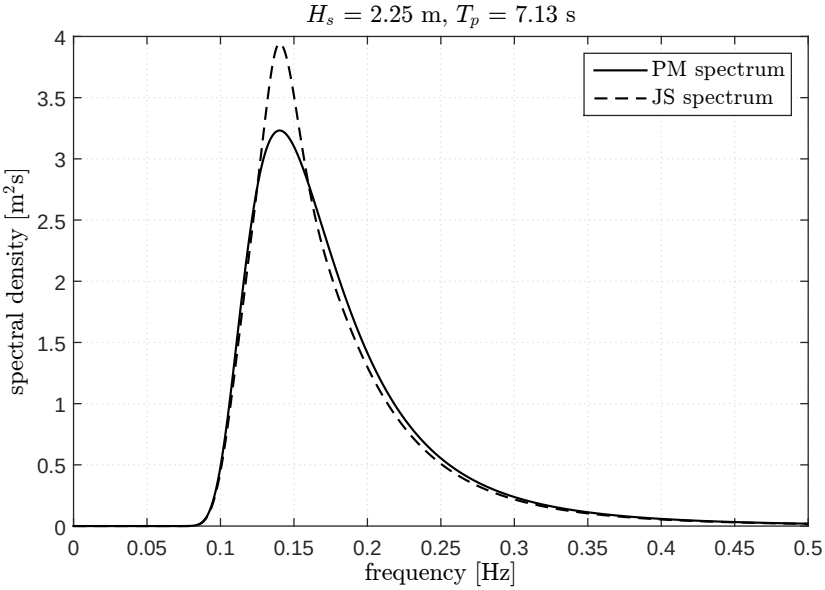

Figure 4.7: Comparison between the Pierson-Moskowitz and Jonswap spectra.

In absence of more detailed information, the parameters can be established as follows[15] [42]:

$$\alpha = \exp\left[-\frac{(f-f_p)^2}{2\sigma^2 f_p^2}\right] \tag{4.56}$$

$$\sigma = \begin{cases} 0.07 & \text{for} \quad f \leq f_p \\ 0.09 & \text{for} \quad f > f_p \end{cases} \tag{4.57}$$

$$\gamma = \begin{cases} 5 & \text{for} \quad \frac{T_p}{\sqrt{H_s}} \leq 3.6 \\ \exp\left[5.75 - 1.15\frac{T_p}{\sqrt{H_s}}\right] & \text{for} \quad 3.6 < \frac{T_p}{\sqrt{H_s}} \leq 5 \\ 1 & \text{for} \quad \frac{T_p}{\sqrt{H_s}} > 5 \end{cases} \tag{4.58}$$

$$C(\gamma) = 1 - 0.287 \cdot \ln\gamma \tag{4.59}$$

4.4 First-order theory

The linear wave theory is based on the solution of the Laplace equation associated with linearised kinematic and dynamic free surface boundary conditions on the mean surface

[15] The peak period T_p might be expressed in seconds and the significant wave height H_s in meters.

and the seabed condition[16], namely [29, 68]:

$$\mathbf{v} = \nabla\Phi \tag{4.60}$$

$$\frac{\partial\eta}{\partial t} = \frac{\partial\Phi}{\partial x_3^I} \qquad \text{on} \quad x_3^I = 0 \tag{4.61}$$

$$g\eta + \frac{\partial\Phi}{\partial t} = 0 \qquad \text{on} \quad x_3^I = 0 \tag{4.62}$$

$$\frac{\partial\Phi}{\partial x_3^I} = 0 \qquad \text{on} \quad x_3^I = -d \tag{4.63}$$

The same solution can be also derived by solving the differential problem with a first-order perturbation scheme [29]. In linear theory, the potential of the velocity is proportional to the wave amplitude, which should be small with respect to the characteristic wavelength and the dimension of the body [29, 46]. For further discussions on the topics presented in this section the reader is addressed to the references [4, 29, 50, 66, 68].

4.4.1 Reference frame

The first-order hydrodynamics is usually formulated with respect to a favourite reference frame related to the mean free surface of the fluid. Hence, let's consider an inertial (fixed) reference frame $\{O; x, y, z\}$ defined by the orthonormal basis $\mathcal{S} = \{\mathbf{e}_i^I\}$, with the origin O located in the mean free surface, the z-axis pointing vertically upwards, and the x-axis aligned with the direction of the wave. The physical quantity $(\bullet)$ observed in this frame is indicated with the notation $(\bullet)^I$ and is always implicitly expressed with respect to the canonical basis[17] $\mathcal{S}$. Alternatively, if the indication of the reference frame is not significant (for instance for forces), the physical quantity $(\bullet)$ expressed with respect to the basis of the fixed frame is indicated with the notation $(\bullet)^{\mathcal{S}}$.

4.4.2 Wave kinematics

The kinematics of a long-crested[18] irregular sea propagating along the positive x-axis can be expressed as the superimposition of a number N (sufficiently large) of monochromatic (regular) waves, which are solutions of the differential problem associated with the linear wave theory, in particular the wave elevation $\eta^{(1)}$ is given by [29, 68]:

$$\eta^{(1),I}(x_1^I, t) = \sum_{m=1}^{N} \zeta_m \cos(k_m x_1^I - \omega_m t + \varepsilon_m) \tag{4.64}$$

The wave number k_m is related to the circular frequency ω_m through the dispersion relation; the amplitude ζ_m of each harmonic can be expressed by the wave spectrum, and

[16] The seabed is assumed horizontal and of infinite extension.

[17] In order to not weigh the notation down, the double indication of the reference frame and the basis is removed, namely:

$$\mathbf{x}^I = \mathbf{x}^{I,\mathcal{S}}$$

[18] By contrast, in the case of a short-crested irregular sea, i.e. when the waves propagate in different directions, the formulation should account for the spread of the spectrum along different directions [68].

the random phases ε_m should be independent and uniformly distributed in the interval $[0, 2\pi]$ in order to ensure that the process is Gaussian [68]. The previous equation, if restricted to the particles P along the vertical line passing through the origin of the reference frame, i.e. $\mathbf{x}_P^I = [0\ 0\ x_{P,3}^I]^T$, becomes as follows [4, 29, 68]:

$$\eta^{(1),I}(t) = \sum_{m=1}^{N} \zeta_m \cos(\omega_m t - \varepsilon_m) \tag{4.65}$$

The autocorrelation and the variance of the process defined by the Equation (4.65) are given by [68]:

$$R_{\eta\eta}(\tau) = E[\eta(t)\eta(t+\tau)] = \sum_{i=1}^{N} \frac{\zeta_i^2}{2} \cos(\omega_i \tau) \tag{4.66}$$

$$\sigma_\eta^2 = \int_0^\infty S_{\eta\eta}(\omega) d\omega \approx \sum_{i=1}^{N} \frac{\zeta_i^2}{2} \tag{4.67}$$

The Equation (4.67) can be rearranged by using the properties of integrals and the mean-value theorem, as done in [68], as follows:

$$\sum_{i=1}^{N} \int_{\omega_i - \Delta\omega/2}^{\omega_i + \Delta\omega/2} S_{\eta\eta}(\omega) d\omega = \sum_{i=1}^{N} \frac{\zeta_i^2}{2} \tag{4.68}$$

$$\int_{\omega_i - \Delta\omega/2}^{\omega_i + \Delta\omega/2} S_{\eta\eta}(\omega) d\omega = \frac{\zeta_i^2}{2} = S_{\eta\eta}(\omega_i^*)\Delta\omega \qquad \text{for} \quad \omega_i^* \in \left[\omega_i - \frac{\Delta\omega}{2}, \omega_i + \frac{\Delta\omega}{2}\right] \tag{4.69}$$

Therefore, the amplitude of each harmonic is given by [68]:

$$\zeta_i = \sqrt{2 S_{\eta\eta}(\omega_i^*)\Delta\omega} \qquad \text{with} \quad \omega_i^* \in \left[\omega_i - \frac{\Delta\omega}{2}, \omega_i + \frac{\Delta\omega}{2}\right] \tag{4.70}$$

In practice ω_i^* is approximated with ω_i; therefore, the resulting realisation of the process is periodic of period $2\pi/\Delta\omega$. However, if ω_i^* is randomly chosen within the interval $[\omega_i - \Delta\omega/2, \omega_i + \Delta\omega/2]$, the fundamental period increases [68].

4.4.2.1 Potential, velocity, and acceleration

Let d be the depth of the seabed with respect to the mean free surface, the velocity potential $\Phi^{(1)}$ associated with the first-order theory is given by[19] [4]:

$$\Phi^{(1)} = \sum_{m=1}^{N} \frac{\zeta_m g}{\omega_m} \frac{\cosh[k_m(d + x_3^I)]}{\cosh(k_m d)} \sin(\varepsilon_m - \omega_m t) \tag{4.71}$$

[19] Let's refer to regular waves, sometimes the expression of the velocity potential $\Phi^{(1)}$ is simplified on the basis of the ratio between the water depth d and the wave length λ. In particular, the potential for deep-water waves ($d/\lambda > 0.5$) is given by:

$$\Phi^{(1)} = \frac{\zeta g}{\omega} e^{k x_3^I} \sin(k x_1^I - \omega t)$$

The horizontal water particle velocity $v_1^{(1)}(x_3^I, t)$ and the horizontal water particle acceleration $\dot{v}_1^{(1)}(x_3^I, t)$ can be obtained by differentiating the velocity potential as follows [4]:

$$v_1^{(1),I}(x_3^I, t) = \frac{\partial \Phi^{(1)}}{\partial x_1^I} \tag{4.72}$$

$$\dot{v}_1^{(1),I}(x_3^I, t) = \frac{\partial v_1^{(1),I}(x_3^I, t)}{\partial t} \tag{4.73}$$

Note that the random phase angles ε_m, uniformly distributed in the interval $[0, 2\pi]$, do not vary with time, and, for a given harmonic, they are the same for each kinematic quantity, either $\Phi^{(1)}$, or $\eta^{(1)}$, or $v^{(1)}$, or $\dot{v}^{(1)}$ [29].

4.4.2.2 Dispersion relation

Given the water depth d, the wave number k and the circular frequency ω are related by the dispersion relationship, namely [50]:

$$\omega^2 = gk \tanh(kd) \tag{4.74}$$

The previous equation is nonlinear and could be solved with an iterative scheme, even if it can be approximated either when d is very large (deep water) or, on the contrary, when d is very small (shallow water). For each regular wave, the wave number k is also related to the wave length λ, as follows [50]:

$$k\lambda = 2\pi \tag{4.75}$$

4.4.3 Numerical approach

Irregular first-order waves can be generated as a finite sum of harmonic functions with amplitude related to the power spectral density of the wave. The numerical simulation can be efficiently performed by the Inverse Fast Fourier Transform (IFFT) algorithm starting from the Fourier coefficients (i.e. the spectrum) of the kinematic physical quantities, namely [4]:

$$X^{\eta}(\omega_m) = \zeta_m \exp(-j\varepsilon_m) \tag{4.76}$$

$$X^{v_1}(d, x_3^I, \omega_m) = \frac{gk_m}{\omega_m} \frac{\cosh[k_m(d + x_3^I)]}{\cosh(k_m d)} X^{\eta}(\omega_m) \tag{4.77}$$

$$X^{\dot{v}_1}(d, x_3^I, \omega_m) = -X^{v_1}(d, x_3^I, \omega_m)\omega_m \tag{4.78}$$

Whereas for transitional-water waves ($0.05 \leq d/\lambda \leq 0.5$) the potential is given by the complete expression, namely:

$$\Phi^{(1)} = \frac{\zeta g}{\omega} \frac{\cosh[k(d + x_3^I)]}{\cosh(kd)} \sin(kx_1^I - \omega t)$$

Whereas for shallow-water waves ($d/\lambda < 0.05$) the potential is given by:

$$\Phi^{(1)} = \frac{\zeta g}{\omega} \sin(kx_1^I - \omega t)$$

Pierson-Moskowitz spectrum		
significant wave height, H_s	2.25	m
peak period, T_p	7.13	s
environment		
gravity acceleration, g	9.81	m/s^2
seabed depth, d	100.0	m

Table 4.3: Parameters used for the generation of the wave time histories.

The quantities described with a cosine law, i.e. sea surface elevation and particle velocity, are simply the real part of the inverse discrete Fourier transform, whereas the quantities related to a sine law, i.e. particle acceleration, are the imaginary part of the inverse transform. The random phases ε_m ensure that each monochromatic wave is independent and cannot be neglected (see Figure 4.8) without significantly deteriorating the time series. The water particle horizontal velocity and acceleration (see Figure 4.9) decrease with the depth and are negligible below a certain depth threshold. The parameters used for the generation of the wave time histories are reported in Table 4.3.

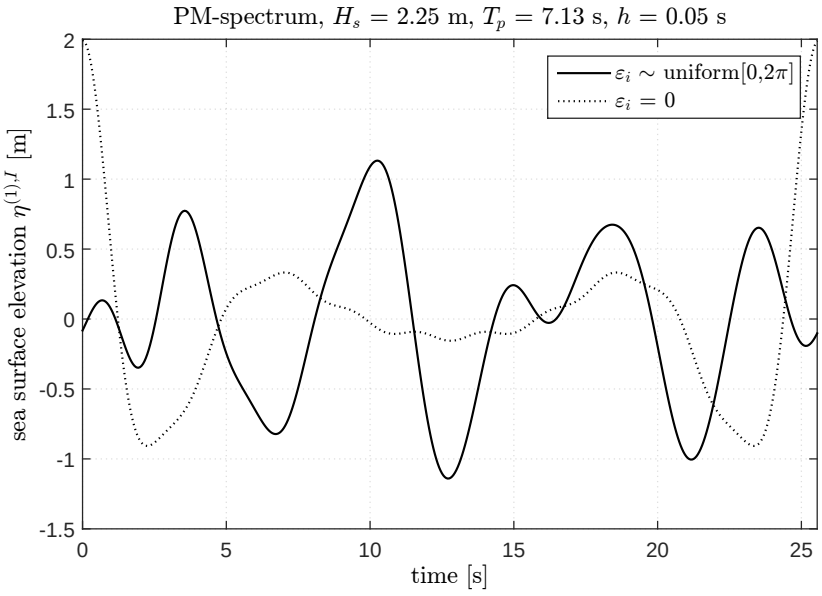

Figure 4.8: Linear wave theory; sea surface elevation generated on the basis of the Pierson-Moskowitz spectrum, comparison between the time series obtained with random phases ε_i and without the random terms.

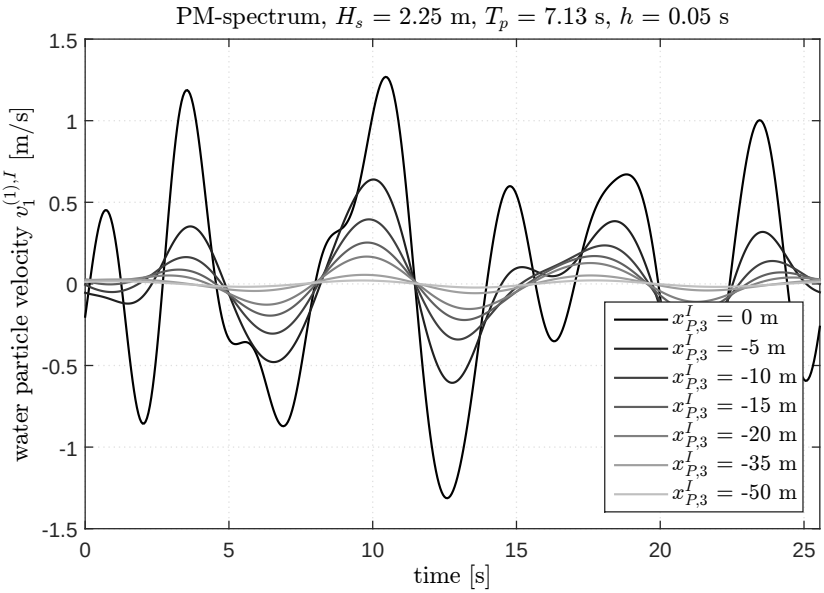

(a) particle velocity

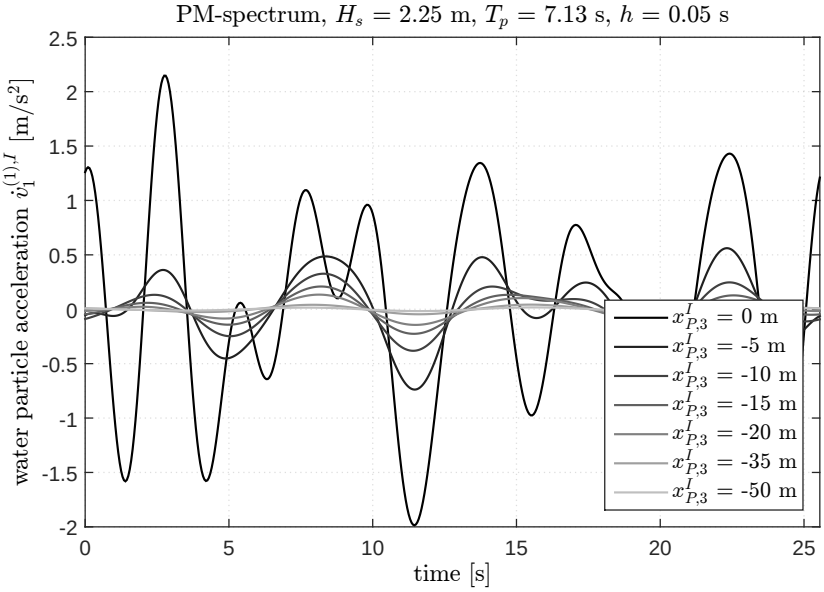

(b) particle acceleration

Figure 4.9: Linear wave theory; particle horizontal velocity and acceleration generated on the basis of the Pierson-Moskowitz spectrum.

4.4.3.1 Simulation strategy

An irregular (aperiodic) wave can be generated by a Fourier series of N monochromatic waves, which is a periodic signal. Therefore, the time series should have a period at least as long as the total simulation time T_{sim}, i.e. the circular-frequency-step size cannot be randomly chosen, namely [68]:

$$\Delta\omega \leq \frac{2\pi}{T_{sim}} \tag{4.79}$$

The harmonics could be selected with pitch $\Delta\omega$ only in the range of frequency where the spectrum is significant, restricting the number of significant components. Moreover, the amplitude can be computed with respect to ω_i^* obtaining a time series with $T > T_{sim}$ [68].

4.4.4 Hydrodynamic loads

As discussed in the previous sections, the linear wave theory consists in the solution of the Laplace equation with linearised kinematic and dynamic sea surface boundary conditions and implies that the wave amplitude is small with respect to the wavelength. Moreover, the displacements (translations) of the floating platform should be small with respect to a characteristic dimension of the body (body length) [46]. The linear theory also implies that the hydrodynamic problem can be addressed as the linear superimposition of separate sub-problems [29]:

- floating body fixed (restrained) subjected to incident waves. This diffraction[20] sub-problem returns the *wave-excitation loads*, composed of Froude-Kriloff and scattering loads;
- moving floating body without incident waves. The body is forced to oscillate with the same frequency of the incoming wave in each rigid-body degree of freedom (separately). This sub-problem returns the loads related to the hydrostatics (restoring) and to the radiation problem, i.e. hydrodynamic added mass and damping matrices.

The linear theory is generally adequate for the description of the most waves in deep water [46]. The formulation described in this section neglects the loads due to the currents or the presence of ice and debris.

4.4.4.1 Cummins approach

The Cummins approach is suitable for any bounded excitation load [68] (diffraction sub-problem) including both regular and irregular sea states. The latter can be generated as the superimposition of a number (finite) of monochromatic waves. Let $\mathbf{q} = [\Delta\mathbf{x}_C^I; \Delta\boldsymbol{\psi}]$ be the vector collecting the displacement of the reference point[21] C of the floating body

[20] Note that some authors use the term *diffraction* to indicate only the scattering loads. By contrast, in this thesis the diffraction sub-problem is understood to include both scattering and Froude-Kriloff loads, as also done in [46].

[21] The reference point C depends on the code used for computing the hydrodynamic added mass and damping matrices, and hydrostatic matrix. It could be the center of mass of the body as well as the projection of the center of mass onto the mean free surface plane. The code could employ the nautical angle parametrization in place of the rotational vector; moreover, the angular velocity (and acceleration) vector could be replaced by the time derivatives of the Euler angles (or Tait-Bryan).

and the rotational vector (or another minimal parametrization) with respect to the reference configuration[22], and let $\mathbf{v} = [\mathbf{v}_C^I; \boldsymbol{\omega}]$[23] and $\dot{\mathbf{v}} = [\mathbf{a}_C^I; \dot{\boldsymbol{\omega}}]$ be respectively the corresponding velocity and acceleration vectors. Given the hydrodynamic added mass matrix $\mathbf{M}^A$, the hydrodynamic damping matrix $\mathbf{D}$, and thus the radiation-retardation kernel $\mathbf{D}^{ker}$, and the transfer function $\mathbf{X}$ of wave-excitation forces[24], the loads associated with irregular waves can be computed as the superimposition of the loads related to the hydrostatic, diffraction, and radiation problems, as follows[25] [5, 46]:

$$F_i^{hyd} = F_i^{hys} + F_i^{diff} + F_i^{rad} \tag{4.80}$$

$$F_i^{hys}(t) = -K_{ik}^{hys} q_k + \rho_w g V_0 \delta_{i3} \tag{4.81}$$

$$\begin{aligned} F_i^{diff}(t)|_{t=nh} = \mathrm{Re}\Bigg[\frac{1}{\sqrt{N}} \sum_{k=0}^{N/2} \sqrt{\frac{4\pi}{h} S_{\eta\eta}^{1-sided}(\omega)|_{\omega=k\Delta\omega}} \cdot \\ X_i(\omega,\beta)|_{\omega=k\Delta\omega} e^{j\left(\frac{2\pi kn}{N} - \varepsilon_k\right)} \Bigg] \qquad \text{for} \quad n = 0, 1, \ldots, N-1 \end{aligned} \tag{4.82}$$

$$F_i^{rad}(t) = -M_{ik}^A(\omega)|_{\omega=\infty} \dot{v}_k - \int_0^t D_{ik}^{ker}(t-\tau) v_k(\tau) d\tau \tag{4.83}$$

$$D_{ij}^{ker}(t) = \frac{2}{\pi} \int_0^\infty D_{ij}(\omega) \cos(\omega t) d\omega \tag{4.84}$$

$$h = \frac{T_{sim}}{N} = \frac{2\pi}{N\Delta\omega} \tag{4.85}$$

The hydrodynamic added mass matrix does not depend on the frequency but only on the geometry of the floating body, namely [46]:

$$M_{ij}^A(\omega)|_{\omega=\infty} = \lim_{\omega\to\infty} M_{ij}^A(\omega) \tag{4.86}$$

If the two-sided power spectral density is used, the Equation (4.82) should be rewritten as follows[26] [46]:

$$\begin{aligned} F_i^{diff}(t)|_{t=nh} = \frac{1}{\sqrt{N}} \sum_{k=-N/2+1}^{N/2} \sqrt{\frac{2\pi}{h} S_{\eta\eta}^{2-sided}(\omega)|_{\omega=k\Delta\omega}} \cdot \\ X_i(\omega,\beta)|_{\omega=k\Delta\omega} e^{j\left(\frac{2\pi kn}{N} - \varepsilon_k\right)} \qquad \text{for} \quad n = 0, 1, \ldots, N-1 \end{aligned} \tag{4.87}$$

[22] For the dynamic analysis of a floating body, the origin of the inertial reference frame is usually placed in the location of the reference point in the reference configuration, generally the static equilibrium configuration. In this way, the position vector of the reference point and the rotational vector are directly quantities expressed with respect to the reference configuration. However, it is possible to choose arbitrary reference frames provided that the operators are consequently properly modified.

[23] Do not confuse the angular velocity $\boldsymbol{\omega}$ of the rigid-body platform with the circular frequency ω of the monochromatic wave.

[24] The transfer function returns the wave-excitation loads per unit wave amplitude, and it is a function of the wave circular frequency ω and the wave direction β.

[25] Note that in the following expressions N is double the number of superimposed regular waves. Moreover, the symbol F denotes the loads (both forces and torques) correlative to the i-th degree of freedom.

[26] Note that in the Equation (4.87) the random phase should be selected so that $\varepsilon_k = -\varepsilon_{-k}$; otherwise, the imaginary part of the complex number does not vanish. In other words, the monochromatic wave with circular frequency $\omega = k\Delta\omega$ cannot propagate with two different random phases.

Note that the Equation (4.82) includes the regular wave as a particular case, i.e. sum restricted to only one harmonic, as if the spectrum was defined for just one frequency. For further discussions on the hydrodynamic load formulation the reader is addressed to the references [32, 33, 68, 69] where the radiation forces on floating ships are analysed by means of the Cummins approach [24].

4.4.4.2 Steady regular model

The steady regular model is suitable when the incident wave propagates at only one frequency (monochromatic) and the body oscillates at the same frequency of the wave. Such model can efficiently describe steady conditions. Let $\mathbf{q} = [\Delta\mathbf{x}_C^I; \Delta\boldsymbol{\psi}]$ be the vector collecting the displacements of the reference point C of the floating body and the rotational vector with respect to the reference configuration, and let $\mathbf{v} = [\mathbf{v}_C^I; \boldsymbol{\omega}]$ and $\dot{\mathbf{v}} = [\mathbf{a}_C^I; \dot{\boldsymbol{\omega}}]$ be respectively the corresponding velocity and acceleration vectors. Given the hydrodynamic added mass matrix $\mathbf{M}^A$, the hydrodynamic damping matrix $\mathbf{D}$, and the transfer function $\mathbf{X}$ of wave-excitation forces, the loads associated with regular waves can be computed as the superimposition of the loads related to the hydrostatic, diffraction, and radiation problems, as follows [46]:

$$F_i^{hyd} = F_i^{hys} + F_i^{diff} + F_i^{rad} \tag{4.88}$$

$$F_i^{hys}(t) = -K_{ik}^{hys} q_k + \rho_w g V_0 \delta_{i3} \tag{4.89}$$

$$F_i^{diff}(t) = \mathrm{Re}[\zeta X_i(\omega, \beta) e^{j\omega t}] \tag{4.90}$$

$$F_i^{rad}(t) = -M_{ik}^A(\omega)\dot{v}_k - D_{ik}(\omega) v_k \tag{4.91}$$

Note that the hydrodynamic loads are computed in steady conditions, i.e. the effects of the transients associated with the initial conditions are neglected [29]. Moreover, the use of this monochromatic model requires that the body oscillates at the same frequency of the incident wave [46, 58]. Therefore, it can generally be used for the analysis of steady conditions, whereas for the study of the transients it is not reliable, and the radiation sub-problem should be replaced by the Cummins approach.

4.4.4.3 Hydrodynamic added mass and damping matrices

The hydrodynamic added mass $\mathbf{M}^A$ and damping $\mathbf{D}$ matrices are related to the loads due to the harmonic motion of the floating body (at the same frequency of the incoming wave) in absence of waves, i.e. a *radiation* problem. Although there are not incoming waves, the forced oscillations of the body generate outgoing waves all around the floating system [29]. The resultant force and resultant torque (with respect to the reference pole) of the interaction forces (pressures) over the wetted surface are modelled as linear transformations of the velocity vector and acceleration vector. The operators $\mathbf{M}^A$ and $\mathbf{D}$ depends on the oscillation circular frequency, shape of the floating body, and forward speed [29] (significant in the case of non-moored ships). The added mass terms represent the hydrodynamic induced loads and should not be interpreted as an additional oscillating mass attached to the body [29, 68]. Furthermore, the hydrodynamic damping terms do not represent viscous effects because are computed within the hypotheses of the potential theory, i.e. the fluid is inviscid, but are related to a transfer of kinetic energy into the generated waves due to the motion of the body [68].

The symmetry of the floating body with respect to planes or axes simplifies the structure of the added mass matrix. In fact, the higher is the level of symmetry, the

fewer is the number of non-zero terms of the matrix. However, if the hydrodynamic operators are computed by means of the surface panel method, as done in the most common codes, they result non-symmetric (nearly symmetric). A common strategy is to make the operators symmetric, as follows [93]:

$$\mathbf{Z}^{sym} = \frac{1}{2}(\mathbf{Z} + \mathbf{Z}^T) \tag{4.92}$$

For further discussions the reader is addressed to the references [29, 50, 66, 68].

4.5 Higher-order effects

First-order wave theory refers to the solution of the Laplace equation with linear boundary kinematic and dynamic conditions formulated with respect to the mean free surface. The linear theory is accurate enough for a wide range of applications but neglects some phenomena and, in particular, cannot capture the effects of the nonlinearities associated with the waves. Higher-order formulations[27] can improve the accuracy on the description of mean drift forces and slowly-varying wave loads on marine structures, like moored platforms or ships [29, 68]. In particular, hydrodynamic second-order effects appear definitely non-negligible for tension-leg-platforms [72]. Weakly-nonlinear problems can be studied by solving the Laplace equation with a perturbation scheme, which is based on a series expansion, with respect to a small parameter, of the physical quantities that characterize the flow, for instance, the potential, the wave elevation, etc. A second-order theory considers also the terms related to the square of the wave amplitude and can capture the effects associated with both mean loads and sum-frequencies and difference-frequencies oscillating forces, which could cause the resonance of moored structures [29].

In [96, 97], a second-order model, based on a perturbation approach, for coupling numerical and physical wave tanks for 2D irregular waves is developed and experimentally validated. Higher-order weakly nonlinear problems, including the effects of currents and forward speed are discussed in [9, 78]. Other interesting second-order formulations in two dimensions, less recent, are described in [51, 60] while a solution for random interfacial waves at different steady uniform speeds is presented in [85]. In [92], the forces associated with oscillating heave motions of floating or submerged bodies are analysed with a third-order approach obtaining a good agreement with experimental data. Many researches are also focused on fully nonlinear analysis necessary for assessing strongly nonlinear phenomena, like slamming, sloshing, breaking waves. In [88], the fully nonlinear analysis of interactions between solitary waves and structures is addressed by means of the finite element method. The reflection, collision, and propagation of solitary waves are assessed as well as the interaction with rectangular cylinders and a pair of twin cylinders. In [79, 80], the 3D Laplace equation, i.e. the potential flow, is solved

[27] For vertical, slender cylinders Morison's equation is widely used also with nonlinear wave kinematic models. It assumes that the presence of the body does not perturb the flow of the fluid (diffraction sub-problem neglected), and the viscous drag is dominant with respect to the damping associated with the radiation sub-problem (small oscillations of the body) [23]. Such assumptions are no longer valid for moored floating platforms. However, in the case of floating platforms, Morison's equation is often used to estimate the nonlinear viscous drag (by assuming an effective diameter of the structure), which is proportional to the square of the relative velocity between the floating body and the fluid particles, and it is therefore neglected by the linear hydrodynamic theory [46].

with a harmonic polynomial cell method with very promising results in terms of accuracy and efficiency. Some applications are presented, including the interaction of the fully nonlinear waves with bottom-mounted vertical circular cylinders. The research works mentioned are not an exhaustive list but mark the great interest of the scientific community on higher-order hydrodynamic effects.

4.5.1 Second-order wave kinematics

In order to better understand the role of second-order wave kinematics, the numerical model proposed in [4], based on the formulation developed in [81] that solves the Laplace's equation with nonlinear boundary conditions by using a perturbation approach, was implemented and employed for some comparisons with the first-order model described above.

4.5.1.1 Formulation

Let's focus on the particles P along the vertical line passing through the origin of the reference frame, i.e. $\mathbf{x}_P^I = [0\ 0\ x_{P,3}^I]^T$, the nonlinear surface elevation η can be expressed as the superimposition of the first-order $\eta^{(1)}$ and second-order $\eta^{(2)}$ contributions, namely [4]:

$$\eta(t) = \eta^{(1)}(t) + \eta^{(2)}(t) \tag{4.93}$$

$$\eta^{(1),I}(t) = \sum_{m=1}^{N} \zeta_m \cos(\omega_m t - \varepsilon_m) \tag{4.94}$$

$$\eta^{(2),I}(t) = \sum_{m=1}^{N}\sum_{n=1}^{N} \left[\zeta_m \zeta_n \left(B_{mn}^{-} \cos(\phi_m - \phi_n) + B_{mn}^{+} \cos(\phi_m + \phi_n)\right)\right] \tag{4.95}$$

$$\phi_m = \varepsilon_m - \omega_m t \tag{4.96}$$

The wave number k_m is related to the circular frequency ω_m through the dispersion relation; the amplitude ζ_m of each harmonic can be expressed by the wave spectrum, and the random phases ε_m should be independent and uniformly distributed in the interval $[0, 2\pi]$. The second-order transfer functions B_{mn}^{+} and B_{mn}^{-} depend on the frequency and the wave number and are independent of the spectrum. For their formulation see the references [4, 81]. Let d be the depth of the seabed with respect to the mean free surface, even the velocity potential Φ can be written as the superimposition of the first-order $\Phi^{(1)}$ and second-order $\Phi^{(2)}$ components, as follows [4]:

$$\Phi = \Phi^{(1)} + \Phi^{(2)} \tag{4.97}$$

$$\Phi^{(1)} = \sum_{m=1}^{N} \frac{\zeta_m g}{\omega_m} \frac{\cosh[k_m(d + x_3^I)]}{\cosh(k_m d)} \sin(\varepsilon_m - \omega_m t) \tag{4.98}$$

$$\Phi^{(2)} = \frac{1}{4} \sum_{m=1}^{N}\sum_{n=1}^{N} \left[\frac{\zeta_m g}{\omega_m} \cdot \frac{\zeta_n g}{\omega_n} \cdot \frac{\cosh\left(k_{mn}^{\pm}(d + x_3^I)\right)}{\cosh(k_{mn}^{\pm} d)} \frac{D_{mn}^{\pm}}{\omega_m \pm \omega_n} \sin(\phi_m \pm \phi_n)\right] \tag{4.99}$$

$D_{mn}^{\pm}$ is a second-order transfer function defined in [4, 81]. The horizontal water particle velocity $v_1(x_3^I, t)$ and the horizontal water particle acceleration $\dot{v}_1(x_3^I, t)$ can be obtained

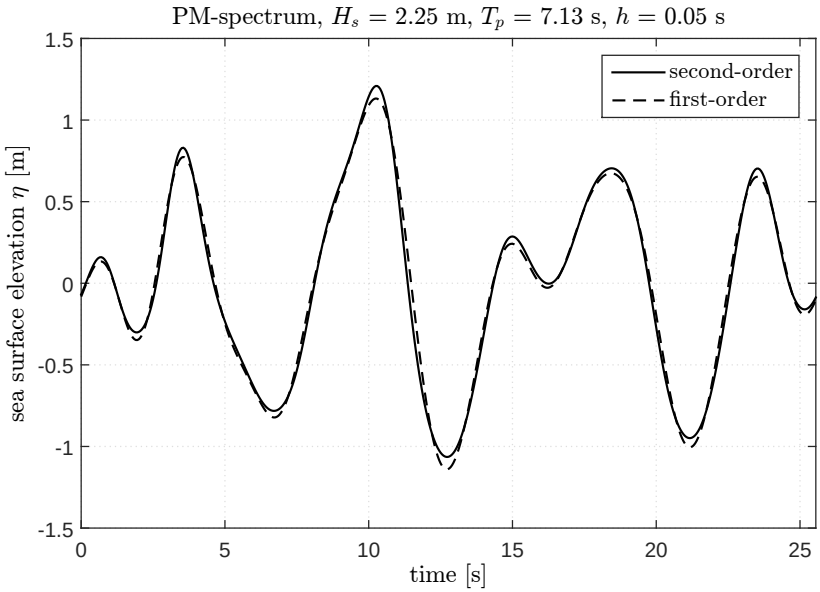

Figure 4.10: Second-order wave theory; sea surface elevation generated on the basis of the Pierson-Moskowitz spectrum, comparison with the first-order wave theory.

by differentiating the velocity potential, namely [4]:

$$v_1^I(x_3^I, t) = \frac{\partial \Phi}{\partial x_1^I} \tag{4.100}$$

$$\dot{v}_1^I(x_3^I, t) = \frac{\partial v_1^I(x_3^I, t)}{\partial t} \tag{4.101}$$

4.5.1.2 Numerical solution

As seen in the previous section, second-order wave kinematic components involve a double summation that do not allow the direct use of the inverse fast Fourier transform (IFFT), as it is possible for the first-order problem. Anyway, the double summation can be rearranged and rewritten as a single summation, which can be efficiently performed with a one-dimensional IFFT procedure. For further details on the numerical approach the reader is addressed to the reference [4]. The second-order sea surface elevation (see Figure 4.10) is characterized by sharper crests and more shallow troughs with respect to the linear wave [29]. The parameters used for the generation of the wave time histories are reported in Table 4.3.

4.5.1.3 Remarks

The second-order wave is quite different from the linear wave. In order to evaluate the second-order effects, the fluid pressures could be integrated all over the wetted surface of the body. In fact, once obtained the potential of the fluid, the pressure field is consequently defined (Bernoulli equation).

4.6 On the use of the linear hydrodynamic theory

The linear hydrodynamic theory implies that incident waves have amplitudes much smaller than their wavelength [46]. This assumption is rather representative of the most waves in deep-water sites (see Figure 4.11 and the references [26, 77]) where linear theory can be used with an acceptable level of accuracy, at least up to a certain dimensionless wave steepness. Since floating platforms for offshore wind turbine purposes are usually installed in deep waters, the linear theory is widely used for the study of such devices [23, 46, 58].

Furthermore, the subdivision of the hydrodynamic problem into the sub-problems of hydrostatics, diffraction, and radiation, associated with the linear theory, implies also that the system undergoes small oscillations about a mean position[28]. The hydrodynamic operators (added mass and damping) are based on the superimposition of the responses associated with the basic displacements of the body. If the displacements are small, the vector of the time derivatives of Euler angles (nautical angles) approximatively coincides with the angular velocity vector regardless of the basis, namely:

$$\frac{d\boldsymbol{\varphi}}{dt} \approx \boldsymbol{\omega}^{\mathcal{M}} \approx \boldsymbol{\omega}^{\mathcal{S}} \tag{4.102}$$

Therefore, also the hydrodynamic added mass (and similarly the damping) matrix can be summed to the structural mass matrix regardless of the bases used for describing the rotational motion, either fixed or body-attached, provided that they coincide in the reference mean configuration.

If the displacements cannot be considered small but the body rotates about an approximately fixed axis, for the sake of simplicity about an axis of the reference frame, the aforementioned equivalence between the time derivative of nautical angles and the components of the angular velocity vectors is still valid. In this case, the linear hydrodynamic theory can be used with a good level of accuracy. Platforms symmetric with respect to their vertical principal planes connected to a mooring system with the same symmetry are a rather typical case in offshore wind turbine industry. Such bodies rotate prevalently about a fixed axis, at least for incident waves parallel to a vertical plane of symmetry. More complex problems include motions of arbitrary magnitude about a variable axis. They should be treated with prudence because the linear theory can lead to very rough errors due to the impossibility to approximate the current configuration of the body with the mean configuration used as reference for the computation of the hydrodynamic operators.

4.6.1 Alternative simulation strategy

In order to overcome the limit related to the small-displacement assumption of the linear theory, a possible alternative approach could be to compute the hydrodynamic operators at each time step with respect to the current configuration or whenever the body displacements are out of the neighbourhood of the reference configuration. However, this approach requires a high computational effort and is not definitely consistent with the linear theory which usually requires a reference configuration in static equilibrium.

[28] In literature there are also some models that consider a forward speed of the floating body [68, 69].

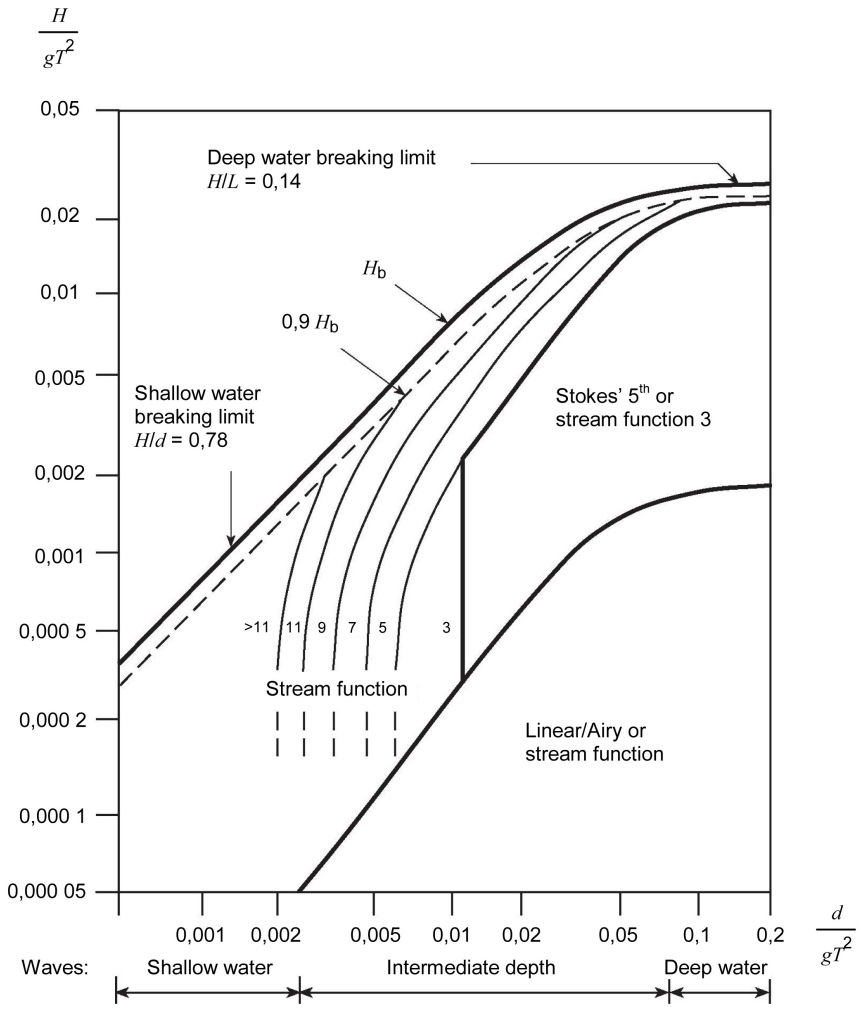

Figure 4.11: Validity of different wave theories. Source: IEC [42].

The validity of the linear hydrodynamic theory for large displacements is an open issue and need further investigations.

Chapter 5

Mooring model

"You have to make the rules,
not follow them."

Isaac Newton

The loads associated with the mooring system are discussed in the framework of quasi-static models. Two different formulations are presented and compared to each other in terms of tension on the single cable and loads on the whole mooring system, with parametric analyses on the role of the different parameters that characterize the models. The chapter aims at providing the reader with a critique overview of the models used in this research to assess the mooring line loads.

5.1 Mooring lines

In many applications, floating systems (platforms, ships, hulls) should be kept in a fixed position, mainly for operational reasons. In order to guarantee precise positions or motion control, under the action of wind, waves, and currents, it is necessary to connect the floating body to other external systems, such as mooring lines, or to equip the floating body with devices able to contrast the environmental loads, such as thrusters. A mooring system consists of a set of cables with their upper end (fairlead) connected to the floating structure and their lower end anchored to the seabed. The mooring system should provide the constraints to the translation in the water plane and to the rotation about the vertical axis, which cannot be provided by the buoyancy. Depending on how the overall stability is reached, the system of cables can be ascribed to the following main concepts or a combination of them [29]:

- *tension leg.* This concept is employed when the buoyancy is designed to exceed the weight of the floating body; the tension of the cables equilibrates the net vertical thrust. This concept considers vertical forces also at the anchor points, which are secured to the seabed by dead-weights or drilled-in piles;
- *spread moorings.* The cables do not have to equilibrate any unbalanced buoyancy and the tension forces are mainly due to the self-weight. This concept usually considers a portion of the cable lying on the seabed (catenary moorings), which implies the absence of vertical forces at the anchor points, but it is also possible to design a spread mooring system capable to withstand vertical loads (taut moorings) at the anchors.

The tension forces in the moorings, due to the self-weight, elastic properties, and geometry, provide the restraints of the floating structure with an effectiveness that depends on the configuration of the whole mooring system. As the moored body moves, the geometric configuration of the cables changes, and thus their tension; the mooring system behaves as a spring with elastic and geometric stiffness [29].

5.2 Quasi-static models

Quasi-static models are widely used in offshore wind energy applications since they can reach an acceptable level of accuracy with a reduced computational effort. In dynamic analyses, quasi-static formulations can be accurate enough if and only if the mass of the mooring lines is small with respect to the overall mass of the system, which means of the order of 8% [46]. A quasi-static model considers the cable in static equilibrium at each time step, in other words, the interaction forces between the floating body and the mooring system can be computed only with static considerations. For further discussions on the topics presented in this section the reader is addressed to the references [29, 45, 46].

5.2.1 Reference frame

The static deformed shape of a mooring line secured to the seabed and subjected to the action of its weight, the buoyancy, and the force at the suspended end due to the interaction with a floating body connected to the line, is contained in a vertical plane passing through the anchor and the fairlead, which defines a favoured reference frame for the mathematical formulation of the quasi-static model. Hence, let's consider a local

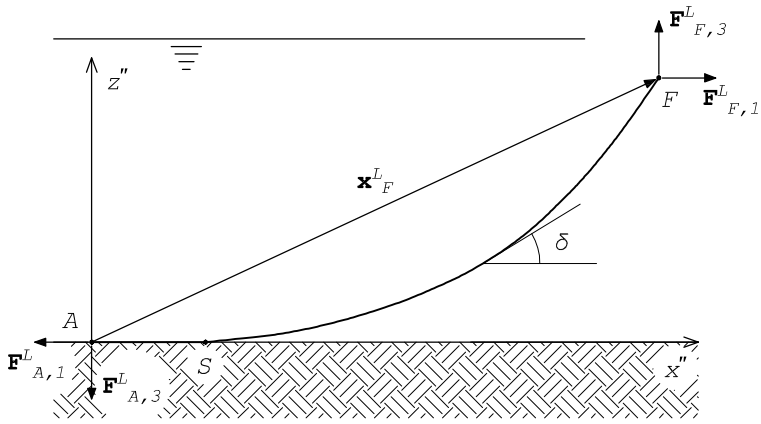

Figure 5.1: Quasi-static model.

(inertial[1]) reference frame $\{A; x'', y'', z''\}$ defined by the orthonormal basis $\mathcal{L} = \{\mathbf{e}_i^L\}$. The origin is located at the anchor A of the mooring line and the cable is contained in the $x''z''$ vertical plane (see Figure 5.1). The physical quantity $(\bullet)$ observed in this frame is indicated with the notation $(\bullet)^L$ and is always implicitly expressed with respect to the canonical basis[2] $\mathcal{L}$. Alternatively, if the indication of the reference frame is not significant (for instance for forces), the physical quantity $(\bullet)$ expressed with respect to the basis of the local frame is indicated with the notation $(\bullet)^{\mathcal{L}}$.

5.2.2 Hypotheses

Quasi-static models consider the cable in static equilibrium, ignoring the dynamic effects due to the application of external loads. The models presented in this section are based on the following hypotheses:

- horizontal seabed. If the sea floor is sloping, the static formulation is accurate only when the cable does not lie on the seabed; otherwise, the static configuration is not properly described by the model;
- cable contained in a vertical plane. It is a direct consequence of the catenary model and implies that the forces acting along the moorings are contained in a vertical plane, i.e. the self-weight, the buoyancy, and an external tension at the fairlead;
- bending stiffness negligible. It corresponds to moorings made of chains, but it is also a good approximation for wires with large radius of curvature [29];

[1] The model described in this section refers to static equilibrium equations; hence, the time derivative of the system configuration does not have any role, and all the reference frames can be considered inertial.

[2] In order to not weigh the notation down, the double indication of the reference frame and the basis is removed, namely:

$$\mathbf{x}^L = \mathbf{x}^{L,\mathcal{L}}$$

- absence of currents. The quasi-static models cannot account for current loads, which require a dynamic approach; in this case, current and wave loads can be computed with Morison's equations [19, 43, 95];
- inertia of the mooring line negligible. It is implied in the quasi-static approach that does not consider the dynamic equilibrium of the cable;
- damping of the mooring line negligible. Ignoring the mooring system damping is usually a conservative approach [46];
- infinite axial stiffness (only for the quasi-static model of Faltinsen). It corresponds to neglecting the extension of the cable;
- line tangent to the seabed at the anchor (only for the quasi-static model of Faltinsen), i.e. a portion (even infinitesimal) of the mooring line rests on the seabed. It is the usual working range of spread catenary moorings, but if the displacements are large or other mooring system concepts are employed, this assumption can be no longer valid;
- mooring line completely submerged in an homogeneous fluid, usually the water, but the formulation can be used also for other fluids (for instance, air).

In offshore wind energy applications the position of the anchors and the fairleads are usually a data of the problem. The unknown is generally the tension vector of each mooring line connected to the floating body, which can be used in an iterative procedure for updating the configuration of the floating system. The quasi-static approach considers the nonlinear behaviour of the cable with respect to the displacements of the fairlead and, if the model is properly coupled with the dynamic solver of the floating body, it also considers the nonlinear geometric restoration of the complete mooring system.

5.2.2.1 Apparent weight in fluid

Let μ_c be the mass of the line per unit length, ρ_w the water density, D_c the effective diameter of the mooring line, and g the gravitational acceleration constant; the quasi-static models usually refers to the apparent weight in fluid per unit length w defined as follows [46]:

$$w = \left(\mu_c - \rho_w \frac{\pi D_c^2}{4}\right) g \tag{5.1}$$

The apparent weight (or weight in water) takes into account the vertical force due to the weight of the cable and the buoyancy.

5.2.3 Faltinsen model

The quasi-static model proposed in [29] is based on the equilibrium equation that defines the shape of catenary. For instance, the model is suitable for mooring systems with gravity anchors but can be used also with other types of seabed connections provided that a portion (even infinitesimal) of the cable lies on the sea floor. Let's consider a cable anchored to the seabed at point A (the origin of the local frame) and assume that a segment of cable lies on the seabed from point A to point S after that the cable is

raised up to the fairlead F. The suspended portion of the cable has a catenary shape, its length l_s and the vertical coordinate $x^L_{F,3}$ of the fairlead, i.e. the deepness of the anchor with respect to the upper end, are given by [29]:

$$l_s = \frac{F^{\mathcal{L}}_{F,1}}{w} \sinh\left[\frac{w}{F^{\mathcal{L}}_{F,1}}(x^L_{F,1} - x^L_{S,1})\right] \tag{5.2}$$

$$x^L_{F,3} = \frac{F^{\mathcal{L}}_{F,1}}{w}\left[\cosh\Big(\frac{w}{F^{\mathcal{L}}_{F,1}}(x^L_{F,1} - x^L_{S,1})\Big) - 1\right] \tag{5.3}$$

If $A \equiv S$, the Equation (5.2) defines the minimum length of the cable, which can be computed with an iterative procedure, such as the Newton-Raphson method. The location of the fairlead can be related to the components of the tension on the cable as follows [29]:

$$x^L_{F,1} = l - x^L_{F,3}\left(1 + \frac{2F^{\mathcal{L}}_{F,1}}{wx^L_{F,3}}\right)^{\frac{1}{2}} + \frac{F^{\mathcal{L}}_{F,1}}{w}\cosh^{-1}\left(1 + \frac{wx^L_{F,3}}{F^{\mathcal{L}}_{F,1}}\right) \tag{5.4}$$

$$F^{\mathcal{L}}_{F,3} = wl_s \tag{5.5}$$

These nonlinear equations can be used for computing the tension components on the cable at the fairlead given the location of the upper end with respect to the anchor; otherwise, if the tension vector is known, it is possible to establish the corresponding configuration of the cable. In offshore wind energy applications the first problem is usually addressed. The nonlinear problem can be solved with an iterative procedure, such as the Newton-Raphson method.

5.2.3.1 Mooring stiffness

Let's assume that the cable is in static equilibrium and let $\mathbf{x}^{L,\star}_F$ be the corresponding position vector of the fairlead. Let's suppose that the fairlead location changes in the neighbourhood of the equilibrium point; thus, it is possible to consider the first-order series expansion of the horizontal tension at the fairlead about the equilibrium configuration $x^{L,\star}_{F,1}$, which defines the mooring geometric stiffness, as follows [29]:

$$F^{\mathcal{L}}_{F,1} = F^{\mathcal{L}}_{F,1}\Big|_{\mathbf{x}^{L,\star}_F} + \frac{d}{dx^L_{F,1}}F^{\mathcal{L}}_{F,1}\Big|_{\mathbf{x}^{L,\star}_F} dx^L_{F,1} = F^{\mathcal{L}}_{F,1}\Big|_{\mathbf{x}^{L,\star}_F} + k dx^L_{F,1} \tag{5.6}$$

$$k = \frac{d}{dx^L_{F,1}}F^{\mathcal{L}}_{F,1}\Big|_{\mathbf{x}^{L,\star}_F} = w\left[-2\Big(1 + \frac{2F^{\mathcal{L}}_{F,1}}{wx^L_{F,3}}\Big)^{-\frac{1}{2}} + \cosh^{-1}\Big(1 + \frac{wx^L_{F,3}}{F^{\mathcal{L}}_{F,1}}\Big)\right]^{-1}\Bigg|_{\mathbf{x}^{L,\star}_F} \tag{5.7}$$

The linearisation described above could be used in an iterative time integration procedure, where at each time step the differential equilibrium equations are linearised about the previous balanced configuration.

5.2.4 Jonkman model

The quasi-static model developed in [45] overcomes some simplifying hypotheses of the model described in the previous section; in particular, it considers the axial stiffness

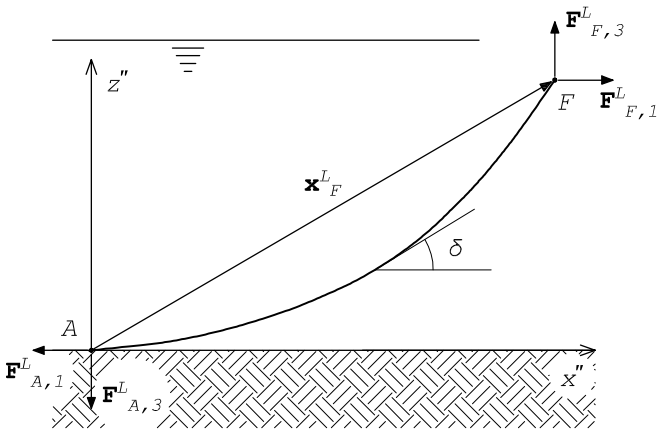

Figure 5.2: Quasi-static model, suspended cable.

of the cable EA, the seabed friction coefficient ξ_b, and the possibility that the angle between the line and the seabed at the anchor is non-zero, i.e. the presence of a vertical reaction at the anchor. The formulation assumes that the elastic modulus of the mooring line is much greater than the hydrostatic pressure [46]. Depending on the static configuration of the mooring line, or rather if a portion of the cable rests or not on the seabed, two different mathematical formulations should be considered [45, 46, 57].

5.2.4.1 Cable suspended

Let's consider a cable completely suspended between the anchor A and the fairlead F (see Figure 5.2), without any segment in contact with the seabed, the analytical formulation that relates the location of the fairlead to the tension components (in the local frame) is given by [45, 46, 57]:

$$x^L_{F,1} = \frac{F^{\mathcal{L}}_{F,1}}{w}\left[\sinh^{-1}\left(\frac{F^{\mathcal{L}}_{F,3}}{F^{\mathcal{L}}_{F,1}}\right) - \sinh^{-1}\left(\frac{F^{\mathcal{L}}_{F,3} - wl}{F^{\mathcal{L}}_{F,1}}\right)\right] + \frac{F^{\mathcal{L}}_{F,1} l}{EA} \tag{5.8}$$

$$x^L_{F,3} = \frac{F^{\mathcal{L}}_{F,1}}{w}\left[\sqrt{1+\left(\frac{F^{\mathcal{L}}_{F,3}}{F^{\mathcal{L}}_{F,1}}\right)^2} - \sqrt{1+\left(\frac{F^{\mathcal{L}}_{F,3} - wl}{F^{\mathcal{L}}_{F,1}}\right)^2}\right] + \frac{1}{EA}\left(F^{\mathcal{L}}_{F,3} l - \frac{wl^2}{2}\right) \tag{5.9}$$

These nonlinear equations can be used for computing the components of the tension vector at the fairlead with an iterative procedure. The components of the constraint reaction at the anchor are given by:

$$F^{\mathcal{L}}_{A,1} = -F^{\mathcal{L}}_{F,1} \tag{5.10}$$

$$F^{\mathcal{L}}_{A,3} = -F^{\mathcal{L}}_{F,3} + wl \tag{5.11}$$

5.2.4.2 Cable lying on the seabed

Let's consider a mooring line anchored at point A with a portion lying on the seabed between the points A and S, the equations that relate the location of the fairlead F to

the tension components (in the local frame), including also the terms representing the friction force shared at the seabed interface, are given by[3] [45, 57]:

$$x^L_{F,1} = l - \frac{F^{\mathcal{L}}_{F,3}}{w} + \frac{F^{\mathcal{L}}_{F,1}}{w}\sinh^{-1}\left(\frac{F^{\mathcal{L}}_{F,3}}{F^{\mathcal{L}}_{F,1}}\right) + \frac{F^{\mathcal{L}}_{F,1} l}{EA} + \frac{\xi_b w}{2EA}\left[-\left(l - \frac{F^{\mathcal{L}}_{F,3}}{w}\right)^2 + \right.$$
$$\left. + \left(l - \frac{F^{\mathcal{L}}_{F,3}}{w} - \frac{F^{\mathcal{L}}_{F,1}}{\xi_b w}\right)\max\left(l - \frac{F^{\mathcal{L}}_{F,3}}{w} - \frac{F^{\mathcal{L}}_{F,1}}{\xi_b w}, 0\right)\right] \tag{5.12}$$

$$x^L_{F,3} = \frac{F^{\mathcal{L}}_{F,1}}{w}\left[\sqrt{1 + \left(\frac{F^{\mathcal{L}}_{F,3}}{F^{\mathcal{L}}_{F,1}}\right)^2} - 1\right] + \frac{(F^{\mathcal{L}}_{F,3})^2}{2EAw} \tag{5.13}$$

The previous equations embed the elastic stretching of the mooring line through the terms depending on the axial stiffness EA. The deformation of the portion of the line resting on the seabed is also affected by the friction force (modelled with a constant friction coefficient ξ_b), which modifies the distribution of the horizontal tension. If the cable resting on the seabed is long enough to let the friction force overcome the horizontal tension, the reaction force at the anchor is zero [46]. The unstretched portion l_b of the mooring line resting on the seabed is given by [45]:

$$l_b = l - \frac{F^{\mathcal{L}}_{F,3}}{w} \tag{5.14}$$

The components of the constraint reaction at the anchor are given by:

$$F^{\mathcal{L}}_{A,1} = \min(-F^{\mathcal{L}}_{F,1} + \xi_b w l_b, 0) \tag{5.15}$$

$$F^{\mathcal{L}}_{A,3} = 0 \tag{5.16}$$

5.2.4.3 Lying condition

In order to establish which formulation might be used, it is necessary to formulate a mathematical condition as a function of either the configuration or the tension on the cable. If a portion of the mooring line rests on the seabed, the first derivative of the equation describing the elevation of the line as a function of the line abscissa s [45], calculated at the anchor ($s = 0$), should be lesser than zero:

$$\left.\frac{\partial z}{\partial s}\right|_{s=0} = \left[1 + \left(\frac{ws - F^{\mathcal{L}}_{A,3}}{F^{\mathcal{L}}_{F,1}}\right)^2\right]^{-\frac{1}{2}} \left.\frac{ws - F^{\mathcal{L}}_{A,3}}{F^{\mathcal{L}}_{F,1}}\right|_{s=0} + \left.\frac{ws - F^{\mathcal{L}}_{A,3}}{EA}\right|_{s=0} < 0 \tag{5.17}$$

5.3 System of moorings

Moored floating bodies are usually connected to a number of mooring lines in order to achieve the desired stability of the floating structure. The system of moorings provides the restraints by means of the tension forces at the fairleads. Given the configuration of the cables, it is of interest to find the net load acting on the floating structure due to the lines.

[3] The Equation (5.13) can be obtained from the Equation (5.9) considering that the mooring line is suspended between the points S and F (see Figure 5.1).

5.3.1 Reference frames

As seen in the previous section, the static deformed shape of a mooring line subjected to its apparent weight is contained in a vertical plane passing through the anchor and the fairlead, which defines a favoured reference frame for the mathematical formulation of the static problem. The best strategy is first to solve the statics of each mooring line in this local frame (different for each cable) and then to transform the tension vector at the fairlead with respect to a common reference frame. Therefore, let's consider the following right-handed orthogonal Cartesian systems:

- spatial (fixed) inertial reference frame $\{O; x, y, z\}$ with the z-axis pointing upwards and defined by the orthonormal basis $\mathcal{S} = \{\mathbf{e}_i^I\}$. The physical quantities $(\bullet)$ observed in this frame are indicated with the notation $(\bullet)^I$ and are always implicitly expressed with respect to the canonical basis $\mathcal{S}$;

- local (inertial) reference frame $\{A; x'', y'', z''\}$ with the z''-axis pointing upwards (in the same direction of the z-axis) and defined by the orthonormal basis $\mathcal{L} = \{\mathbf{e}_i^L\}$. The origin is located at the anchor A of the mooring line, and the axes are oriented so that the cable is contained in the $x''z''$ vertical plane. The physical quantities $(\bullet)$ observed in this frame are indicated with the notation $(\bullet)^L$ and are always implicitly expressed with respect to the canonical basis $\mathcal{L}$.

Since the z-axis and the z''-axis have got the same direction, the orientations of the spatial and local frames differ of a rotation about the vertical axis. If the indication of the reference frame is not significant (for instance for forces and torques), the physical quantity $(\bullet)$ expressed with respect to the basis of the inertial frame is indicated with the notation $(\bullet)^{\mathcal{S}}$, whereas if the quantity is expressed with respect to the basis of the local frame, the notation is $(\bullet)^{\mathcal{L}}$.

5.3.2 Restoring loads

Let's consider a floating rigid body connected to a number n of moorings and focus on the related local frames. The orientation of each local frame with respect to the spatial frame can be measured by means of the angle φ between the positive x-axis and the negative x''-axis, as follows[4]:

$$\varphi = \pi + \tan^{-1}\left(\frac{x^I_{F,2} - x^I_{A,2}}{x^I_{F,1} - x^I_{A,1}}\right) \qquad \text{if} \quad x^I_{F,1} - x^I_{A,1} > 0 \tag{5.18}$$

$$\varphi = \tan^{-1}\left(\frac{x^I_{F,2} - x^I_{A,2}}{x^I_{F,1} - x^I_{A,1}}\right) \qquad \text{if} \quad x^I_{F,1} - x^I_{A,1} < 0 \tag{5.19}$$

The mooring lines interact with the floating (rigid) body by means of the tension forces at the fairleads. The overall load, usually called *restoring* load, due to the whole system of moorings is equivalent to a resultant force $\mathbf{F}^{moor}$ and a resultant torque $\mathbf{T}^{moor}$ about

[4] In this special case, since the rotation axis is fixed, the Euler angles (or Tait-Bryan angles) coincide with the rotational vector components. Moreover, it can be demonstrated that the rotation belongs to a vector space, i.e. compound rotations can be defined with the classic sum composition rule.

a point P, namely:

$$F_{P,1}^{\mathcal{S},moor} = \sum_{i=1}^{n} F_{F_i,1}^{\mathcal{L}_i} \cos\varphi_i \tag{5.20}$$

$$F_{P,2}^{\mathcal{S},moor} = \sum_{i=1}^{n} F_{F_i,1}^{\mathcal{L}_i} \sin\varphi_i \tag{5.21}$$

$$F_{P,3}^{\mathcal{S},moor} = -\sum_{i=1}^{n} F_{F_i,3}^{\mathcal{L}_i} \tag{5.22}$$

$$\mathbf{T}_{P}^{\mathcal{S},moor} = -\sum_{i=1}^{n} (\mathbf{x}_{F_i}^{I} - \mathbf{x}_{P}^{I}) \times \mathbf{F}_{F_i}^{\mathcal{S}} \tag{5.23}$$

where $\mathbf{F}_{F_i}$ is the tension at the fairlead of the i-th mooring line. Alternatively, the resultant force can also be computed as follows:

$$\boldsymbol{\psi}_i = (\varphi + \pi)\mathbf{e}_3^I \tag{5.24}$$

$$\mathbf{F}^{\mathcal{S},moor} = -\sum_{i=1}^{n} \mathbf{R}(\boldsymbol{\psi}_i)\mathbf{F}_{F_i}^{\mathcal{L}_i} \tag{5.25}$$

5.3.3 Restoring stiffness

Let's assume that the floating body (and thus the moorings) is in static equilibrium and suppose that the body oscillates in the neighbourhood of the equilibrium point. It is possible to consider the first-order series expansion of the restoring loads about the equilibrium configuration, which defines the restoring geometric stiffness of the whole mooring system, as follows (simplified) [29]:

$$K_{11}^{t} = \sum_{i=1}^{n} k_i \cos^2\varphi_i \tag{5.26}$$

$$K_{22}^{t} = \sum_{i=1}^{n} k_i \sin^2\varphi_i \tag{5.27}$$

$$K_{66}^{t} = \sum_{i=1}^{n} k_i (x_{F_i,1}^{I} \sin\varphi_i - x_{F_i,2}^{I} \cos\varphi_i)^2 \tag{5.28}$$

$$K_{12}^{t} = K_{21}^{t} = \sum_{i=1}^{n} k_i \sin\varphi_i \cos\varphi_i \tag{5.29}$$

$$K_{16}^{t} = K_{61}^{t} = \sum_{i=1}^{n} k_i (x_{F_i,1}^{I} \sin\varphi_i - x_{F_i,2}^{I} \cos\varphi_i) \cos\varphi_i \tag{5.30}$$

$$K_{26}^{t} = K_{62}^{t} = \sum_{i=1}^{n} k_i (x_{F_i,1}^{I} \sin\varphi_i - x_{F_i,2}^{I} \cos\varphi_i) \sin\varphi_i \tag{5.31}$$

Where the stiffness k_i of the i-th mooring line can be computed with the Equation (5.7).

5.4 Numerical analysis

Quasi-static models are widely used in the study of moored floating bodies because of their effectiveness with an acceptable lack of accuracy. In the most applications the position of both anchors and fairleads are data of the problem, and the unknown is the tension vector on the moorings. As seen in the previous sections, the mathematical formulations consist of a set of nonlinear equations that relate the geometry to the tension.

5.4.1 Initial condition

The set of nonlinear equations should be solved with a proper method (usually iterative), such as the Newton-Raphson scheme, which involves the linearisation of the problem about successive approximate configurations close to the equilibrium until the inaccuracy is below a certain threshold[5]. In order to reach the convergence, the numerical method should start from a proper initial point (configuration) that could be either the variables known from previous analyses[6] or, otherwise, the values calculated as follows [45]:

$$F_{F,1}^{\mathcal{L},0} = \left| \frac{w x_{F,1}^{L}}{2\lambda_0} \right| \tag{5.32}$$

$$F_{F,3}^{\mathcal{L},0} = \frac{w}{2}\left[\frac{x_{F,3}^{L}}{\tanh(\lambda_0)} + l \right] \tag{5.33}$$

where the coefficient λ_0 is defined as follows [45]:

$$\lambda_0 = \begin{cases} 10^6 & \text{for} \quad x_{F,1}^{L} = 0 \\ 0.2 & \text{for} \quad \sqrt{(x_{F,1}^{L})^2 + (x_{F,3}^{L})^2} \geq l \\ \sqrt{3\left(\frac{l^2 - (x_{F,3}^{L})^2}{(x_{F,1}^{L})^2} - 1\right)} & \text{otherwise} \end{cases} \tag{5.34}$$

5.4.2 Single mooring line

The quasi-static models presented in Sections 5.2.3 and 5.2.4 are analysed in terms of tension vector (at the fairlead or at the anchor) for different configurations of the mooring. Let's consider a mooring line anchored to the seabed and completely submerged in water; the features of the cable and of the environment are reported in Table 5.1. Since the tension on the cables depends on a number of parameters, in order to better understand both the influence of the variables and the potentialities of the models, the tension components are computed for different admissible configurations with the variation of one parameter only (for every test), namely:

[5] The method requires the calculation of the Jacobian of the analytical model, namely:

$$J = \begin{bmatrix} \frac{\partial x_{F,1}^{L}}{\partial F_{F,1}^{\mathcal{L}}} & \frac{\partial x_{F,1}^{L}}{\partial F_{F,3}^{\mathcal{L}}} \\ \frac{\partial x_{F,3}^{L}}{\partial F_{F,1}^{\mathcal{L}}} & \frac{\partial x_{F,3}^{L}}{\partial F_{F,3}^{\mathcal{L}}} \end{bmatrix}$$

[6] For instance, if the quasi-static model is used in a time integration procedure, the variables can be initialized with the values computed at the previous time step.

environment		
gravity acceleration, g	9.81	m/s^2
water density, ρ_w	1 025	kg/m^3
mooring		
diameter, D_c	0.1454	m
mass density per unit length, μ_c	130.4	kg/m
extensional stiffness, EA	$589{\cdot}10^6$	N

Table 5.1: Parameters adopted for the single-mooring analysis.

- effect of the mooring length[7] (see Figures 5.3, 5.8);
- effect of the horizontal location of the fairlead with respect to the anchor (see Figure 5.4);
- effect of the vertical location of the fairlead with respect to the anchor (see Figure 5.5);
- effect of the seabed friction coefficient, for various mooring lengths (see Figures 5.6, 5.7, 5.9).

5.4.2.1 Results

An increase of the length (see Figure 5.3) has an effect on the tension vector similar to a reduction of the horizontal distance of the fairlead (see Figure 5.4). In fact, the two cases are somehow equivalent because the effects on the deformed shape of the line due to an increase of its length or to a reduction of the fairlead horizontal distance are qualitatively equivalent. Moreover, since the Faltinsen model assumes an infinity extensional stiffness, the associated tension at the upper end of the cable is coherently greater than the tension estimated by the Jonkman model, although the models can be considered equivalent without any significant loss of accuracy in the actual range of mooring axial stiffness. The difference between the two numerical solutions is much more relevant when the ratio between the horizontal distance of the fairlead and length of the mooring increases. By contrast (see Figure 5.8), if the extensional stiffness is very weak, even if this case is not very common in practical cases, the difference between the two models obviously becomes much more evident, and the Faltinsen model cannot be considered reliable. Since the slope of the curves of Figure 5.4 represents the horizontal-translational stiffness of the fairlead, as the cable approaches its minimum length the mooring is stiffer. An elevation of the fairlead (see Figure 5.5) increases the tension in the cable, but the impact on the vertical-translational stiffness is quite weak. The reason can be ascribed to the fact that a reduction (or increase) in length of the minor cathetus of a right triangle causes a change of the hypotenuse length lesser than the variation caused by the same reduction (or increase) of the major cathetus.

The magnitude of the seabed friction (see Figure 5.6) does not significantly affect the tension vector at the upper end of the cable regardless of the length of the mooring.

[7] The minimum length of the cable (anchor 150 m deep) associated with the Faltinsen model is 435.32 m.

At the anchor (see Figure 5.7) the behaviour is similar, but if the cable is long enough to lie on the seabed, the horizontal component of the reaction significantly depends on the friction magnitude. In particular, for higher values of the seabed friction coefficient, the horizontal friction drag can balance the horizontal component of the tension without stressing the anchor restraint. By contrast (see Figure 5.9), if the extensional stiffness is very weak, the magnitude of the seabed friction becomes more relevant, and the tension at the fairlead smoothly increases as the friction coefficient growths.

5.4.2.2 Remarks

The length of the mooring, or equivalently the location of the fairlead with respect to the anchor, significantly affects the tension at the upper end of the cable. The smaller is the ratio between the length and the distance of the fairlead from the anchor, the larger is the tension. Close to its minimum length the mooring appears very stiff, so a small perturbation of the fairlead location can cause a large variation of the tension.

The moorings usually employed for offshore floating supports have a high extensional stiffness (for instance, steel cables are currently used); therefore, the quasi-static model developed in [29] can be used in place of the model developed in [46] without any significant loss of accuracy provided that the mooring line is long enough to ensure that a portion of the line (even infinitesimal) always lies on the seabed. Moreover, for current extensional stiffness, the seabed friction coefficient does not significantly affect the tension at the fairlead, so it is possible to use a rough approximation.

5.4.3 Loads on a floating rigid body

As seen in the previous sections, a floating body can achieve the stability through a system of moorings. The cables interact with the structure by means of the tension forces at the fairleads; their resultant is the restoring load. The quasi-static approach implies that the tension in the moorings depends on the geometry (location of anchors and fairleads) as well as on the environmental conditions and the features of the cables. Since a lot of practical cases consider the floating structure modelled as a rigid body, it is of interest to analyse the effects on the restoring load (resultant force and torque) due to rigid movements of the fairleads[8].

Let's consider a system of four moorings completely submerged in water and anchored to the seabed at the vertexes of the square inscribed in a circle of radius r_A. Let's assume that the fairleads are rigidly connected together and arranged along the vertexes of the square (oriented as the lower one) inscribed in a circle of radius r_F. The features of cables and of the environment are reported in Table 5.2. According to a rigid body motion, the location of the upper ends of the cables is completely defined by six parameters, namely the translation $\mathbf{x}_P^{I,\mathcal{S}}$ of a point (generally the center of mass) of the hypothetical rigid body and the rotation $\boldsymbol{\psi}$ about that point. Although the problem is nonlinear and a complete description requires a high number of numerical analyses, for the sake of simplicity, the restoring loads are computed for a set of admissible configurations obtained with the variation of one parameter only (for every test), namely[9]:

- translation along the x-axis, for symmetry equivalent to a translation along the

[8] The anchor points are usually kept in a fixed location by a proper foundation, for instance gravity ballast or drilled piles.

[9] The origin of the spatial reference frame $\{O; x, y, z\}$ is located at the fairlead geometric center G_f.

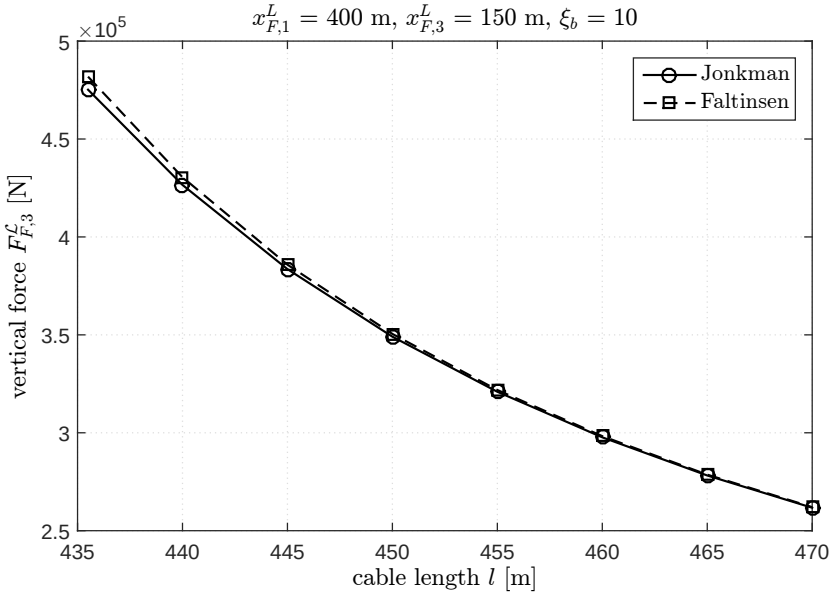

(a) vertical component

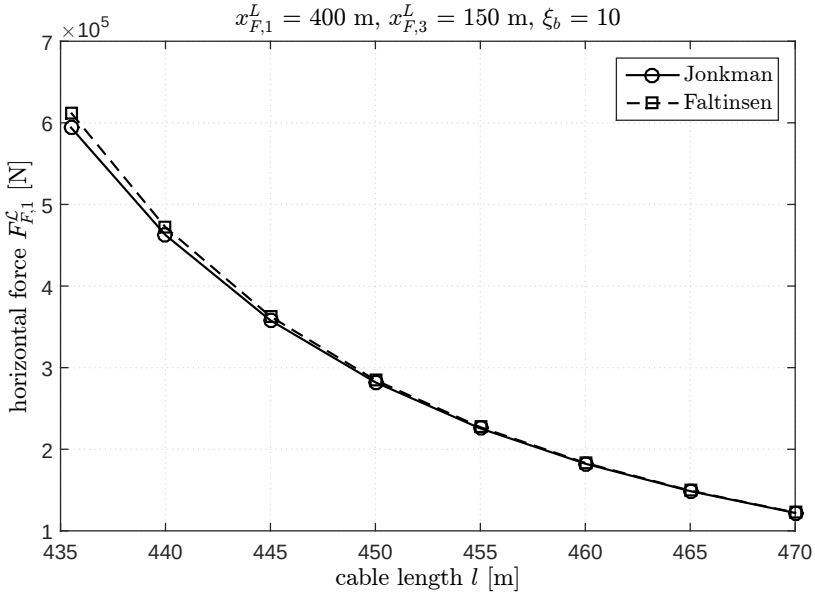

(b) horizontal component

Figure 5.3: Tension components at the fairlead for different mooring lengths; comparison between the quasi-static models of Jonkman and Faltinsen.

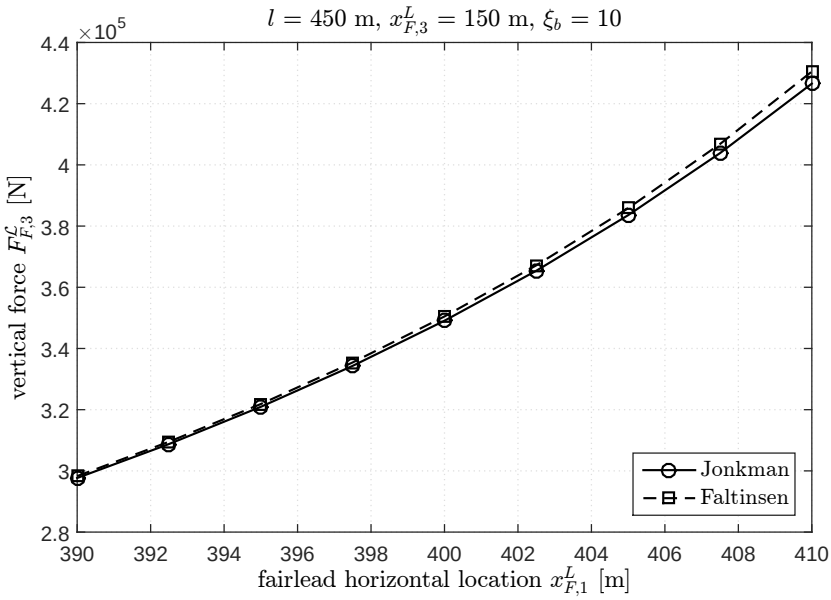

(a) vertical component

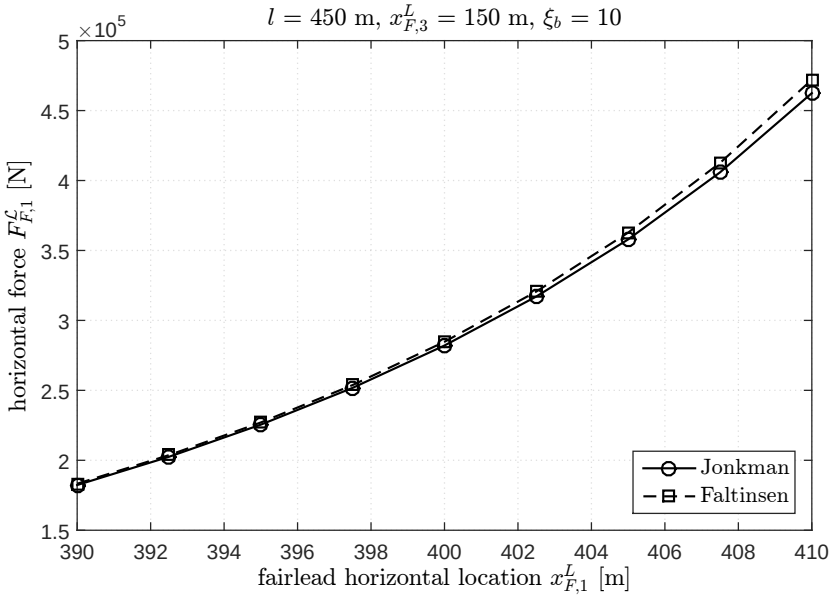

(b) horizontal component

Figure 5.4: Tension components at the fairlead for different horizontal locations of the fairlead with respect to the anchor; comparison between the quasi-static models of Jonkman and Faltinsen.

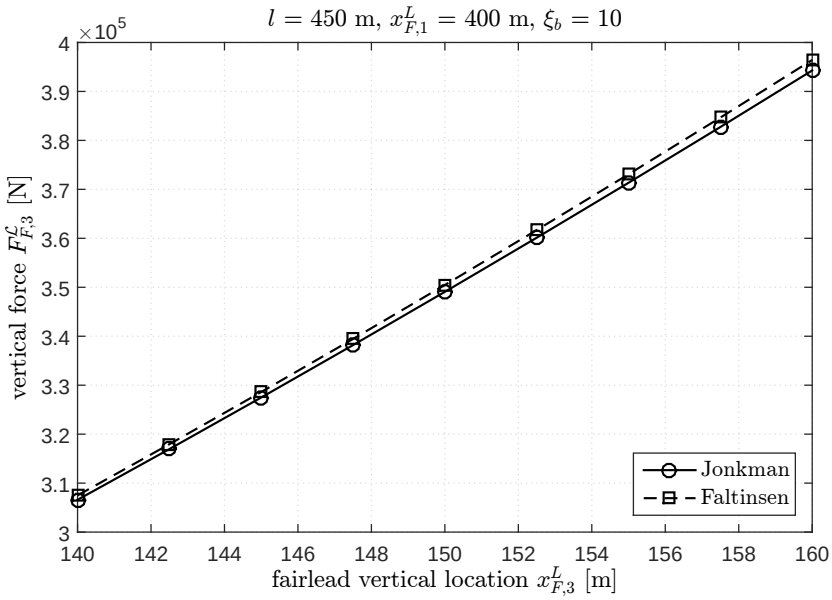

(a) vertical component

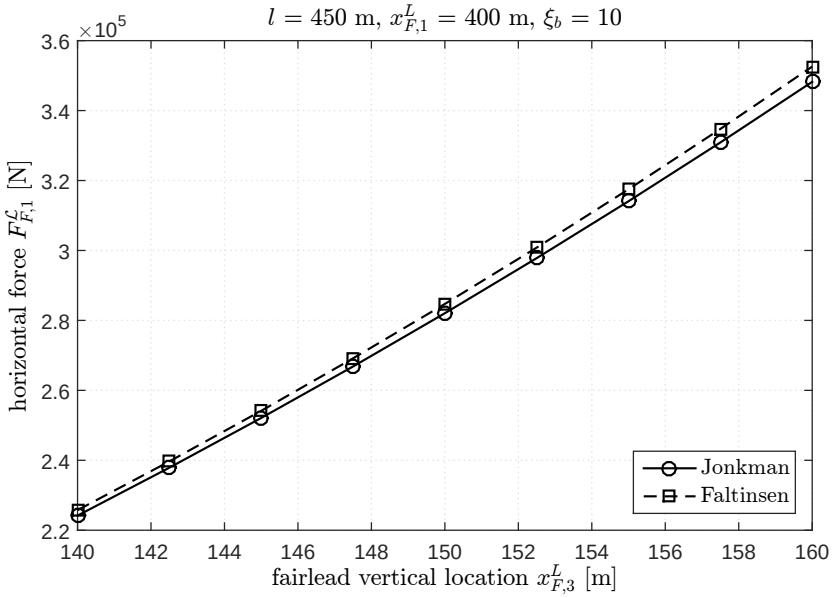

(b) horizontal component

Figure 5.5: Tension components at the fairlead for different vertical locations of the fairlead with respect to the anchor; comparison between the quasi-static models of Jonkman and Faltinsen.

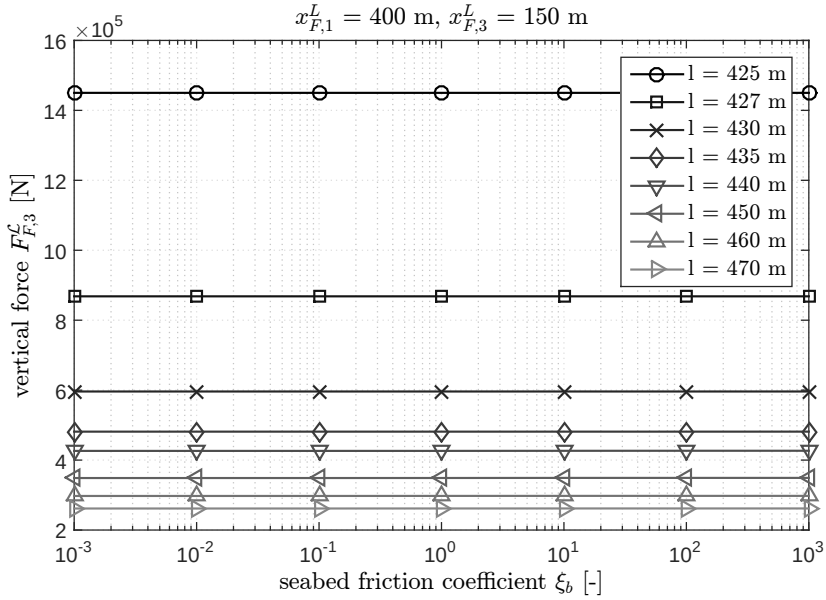

(a) vertical component

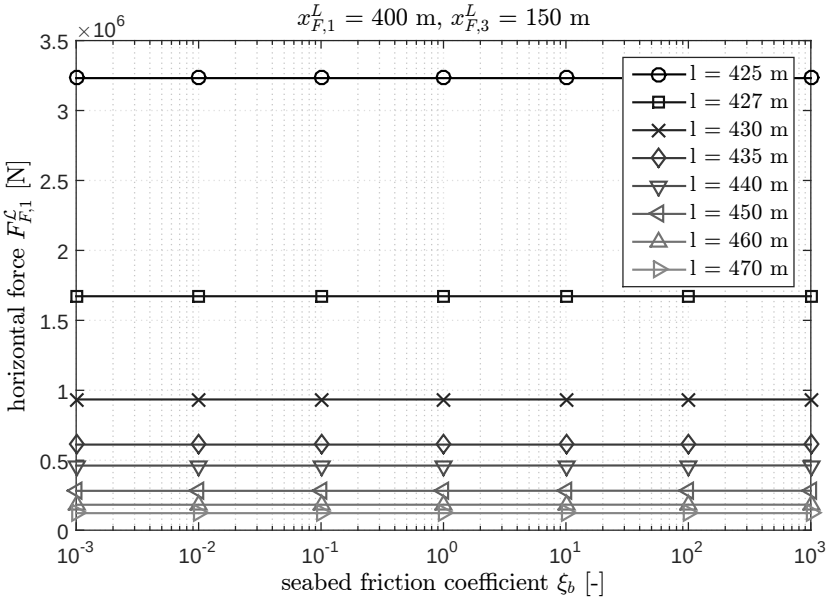

(b) horizontal component

Figure 5.6: Tension components at the fairlead for different mooring lengths and seabed friction coefficients (Jonkman model).

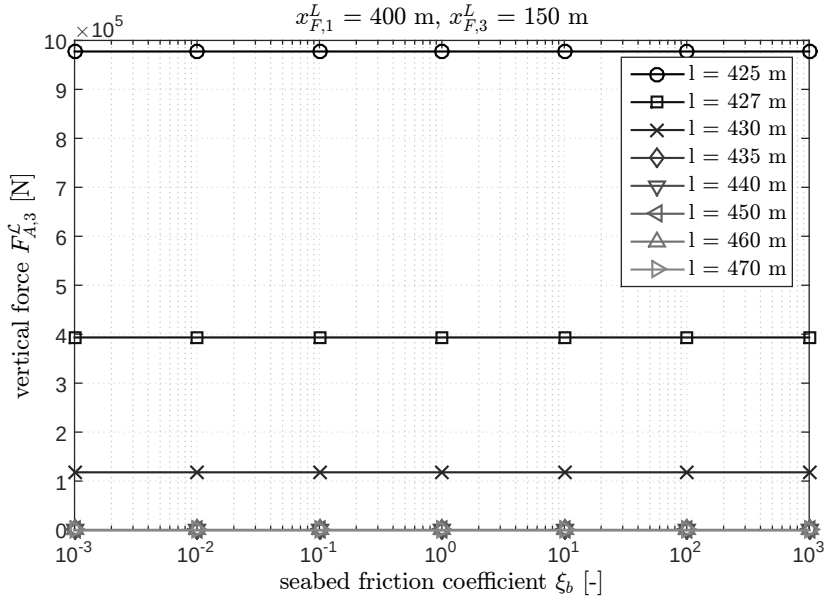

(a) vertical component

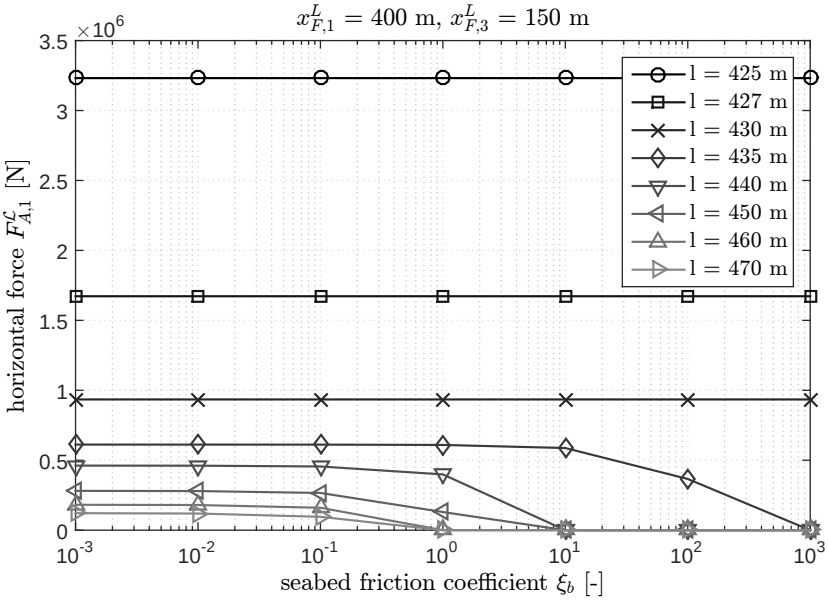

(b) horizontal component

Figure 5.7: Tension components at the anchor for different mooring lengths and seabed friction coefficients (Jonkman model).

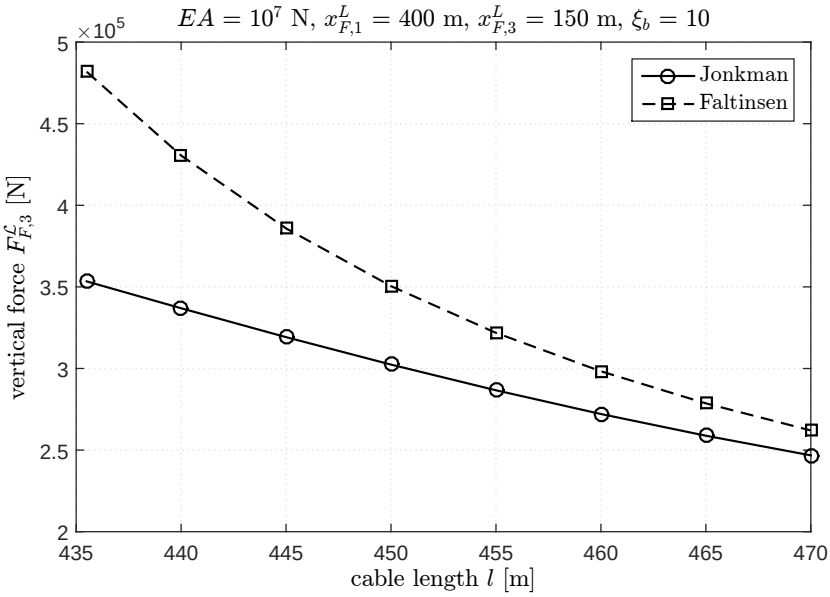

(a) vertical component

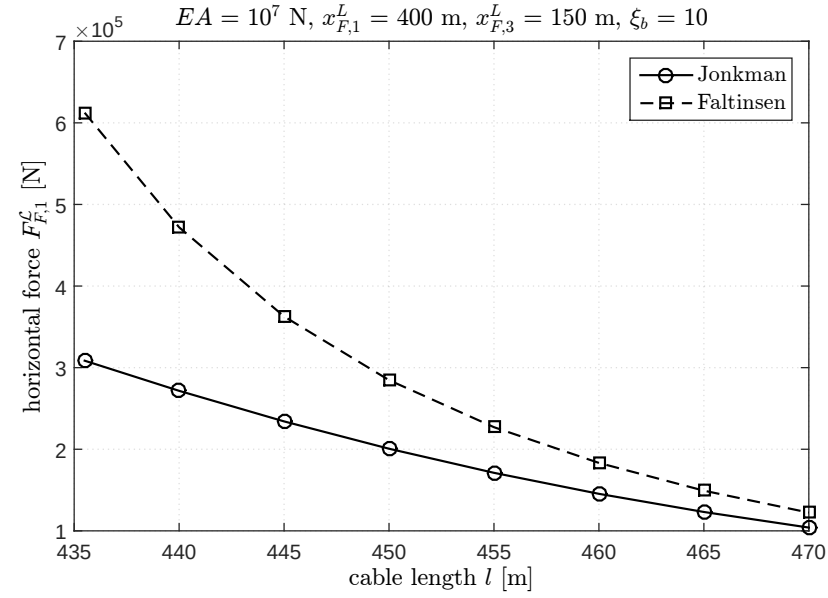

(b) horizontal component

Figure 5.8: Tension components at the fairlead for different mooring lengths in the case of small axial stiffness; comparison between the quasi-static models of Jonkman and Faltinsen.

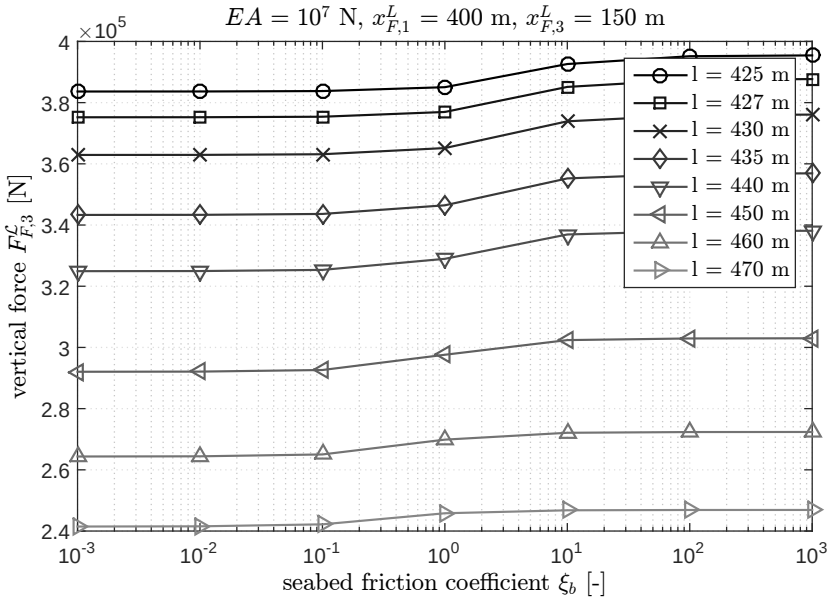

(a) vertical component

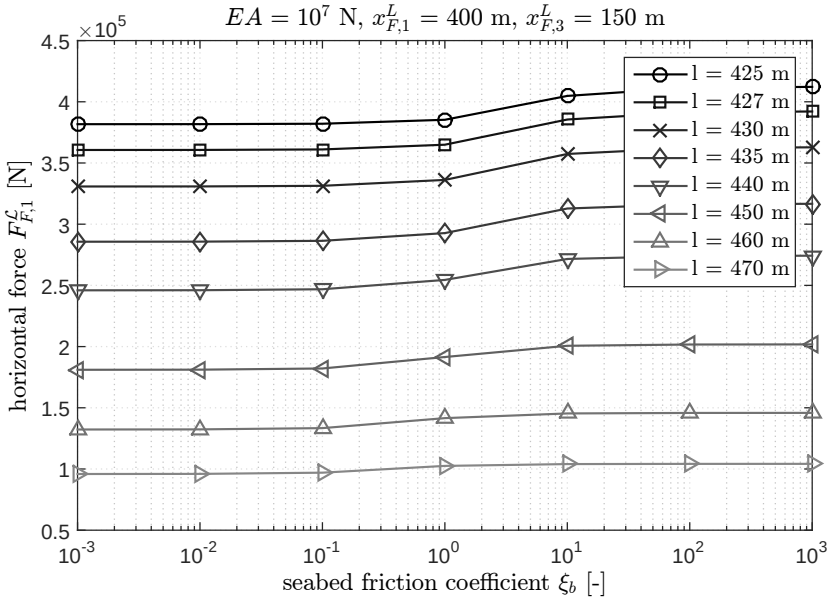

(b) horizontal component

Figure 5.9: Tension components at the fairlead for different mooring lengths and seabed friction coefficients in the case of small axial stiffness (Jonkman model).

environment		
gravity acceleration, g	9.81	m/s^2
water density, ρ_w	1 025	kg/m^3
seabed friction coefficient, ξ_b	1.0	-
moorings		
number, n_c	4	-
diameter, D_c	0.1454	m
unstretched length, l	450	m
mass density per unit length, μ_c	130.4	kg/m
extensional stiffness, EA	$589{\cdot}10^6$	N
fairlead elevation, $x^L_{F,3}$	150	m
radius to fairleads, r_F	25	m
radius to anchors, r_A	425	m

Table 5.2: Parameters adopted for the analysis of a mooring system with the fairleads rigidly connected together.

y-axis (see Figure 5.10);

- translation along the z-axis (see Figure 5.12);
- rotation about the x-axis, for symmetry equivalent to a rotation about the y-axis (see Figure 5.11);
- rotation about the z-axis (see Figure 5.13).

The displacements and the resultant loads are referred to the geometric center of the fairleads G_f.

5.4.3.1 Results

The mooring system analysed is symmetric with respect to the two principal vertical planes; this is a particular configuration that is usually used for practical purposes unless specific challenges require a non-symmetric layout. An elementary rigid movement of the fairleads affects the correlative restoring loads but could also modify the loads corresponding to other displacements; Table 5.3 depicts the scenario. Any displacement implies that the geometry of each cable changes and thus their tension vector. However, the overall restoring loads depend on the combination of the forces at the fairlead of each mooring; thus, if the varied configuration maintains a symmetry with respect to a certain vertical plane, all the restoring loads acting out of that plane are not affected by the motion.

If the fairleads rigidly translate along the x-axis (see Figure 5.10), the correlative restoring force and the resultant moment about the y-axis change according to an approximately linear law, whereas the overall vertical force exhibits a nonlinear trend characterized by a constant sign of the response regardless of the sign of the displacement. Similarly, a rotation about the x-axis (see Figure 5.11) implies an approximately linear variation of both the correlative torque and the restoring force along the y-axis.

	$F_1^{\mathcal{S},moor}$	$F_2^{\mathcal{S},moor}$	$F_3^{\mathcal{S},moor}$	$T_1^{\mathcal{S},moor}$	$T_2^{\mathcal{S},moor}$	$T_3^{\mathcal{S},moor}$
$\Delta x_{G_f,1}^{I,\mathcal{S}}$	x		x		x	
$\Delta x_{G_f,2}^{I,\mathcal{S}}$		x	x	x		
$\Delta x_{G_f,3}^{I,\mathcal{S}}$			x			
$\Delta\psi_1$		x	x	x		
$\Delta\psi_2$	x		x		x	
$\Delta\psi_3$			x			x

Table 5.3: Effect of a pure (only one degree of freedom) rigid motion of the fairleads, with respect to the mean undisplaced equilibrium configuration, on the restoring loads for a double-symmetric system of moorings; the symbol x indicates the loads affected by the motion.

An approximately linear trend is also observed for the vertical reaction when the fairleads are forced to move upward and downward (see Figure 5.12), whereas a rotation about the z-axis (see Figure 5.13) is associated with a slightly nonlinear trend of the correlative restoring torque.

The approximately linear trend of some components of the restoring load, observed in the numerical analyses, cannot be generalized since it depends on a wide number of parameters, such as the lengths of the cables, the geometry of the mooring system (location of anchors and fairleads), the number of excited degrees of freedom, the magnitude of the displacements, which are strongly case-dependent.

5.4.3.2 Remarks

The mooring system reacts to any perturbation of the fairlead location with an opposite load that tends to restore the previous configuration, i.e. the system acts as an imperfect constraint because provides the restoring loads only if the system changes its initial configuration. The code developed to compute the tension in each cable and then the restoring loads can be successfully coupled with the main solver and used for the dynamic analysis of moored floating structures. Note also that the operation of the mooring system generally implies the coupling of different degrees of freedom, since a displacement that involves only one degree of freedom is usually associated with mooring loads along some of the unperturbed degrees of freedom.

5.5 Other approaches

The quasi-static approach can be employed in a wide range of problems, generally for slowly varying motion of the system [23] and provided that the mass of the moorings is small with respect to the overall mass of the system [46]. However, more accurate models are available. The catenary model developed in [35], even though it maintains a quasi-static approach, considers also the hydrodynamic drag due to viscous phenomena (mooring damping), which could be important in deep-water applications. A much more accurate dynamic approach is discussed in many research works both theoretically and numerically, with also good agreement with experimental data [8, 59, 71]. Another interesting dynamic model is proposed in [90, 91] for the analysis of high-extensible cables; the developed governing equations consider a nonlinear stress-strain relation and include the bending stiffness of the cables (lines). The problem is solved with

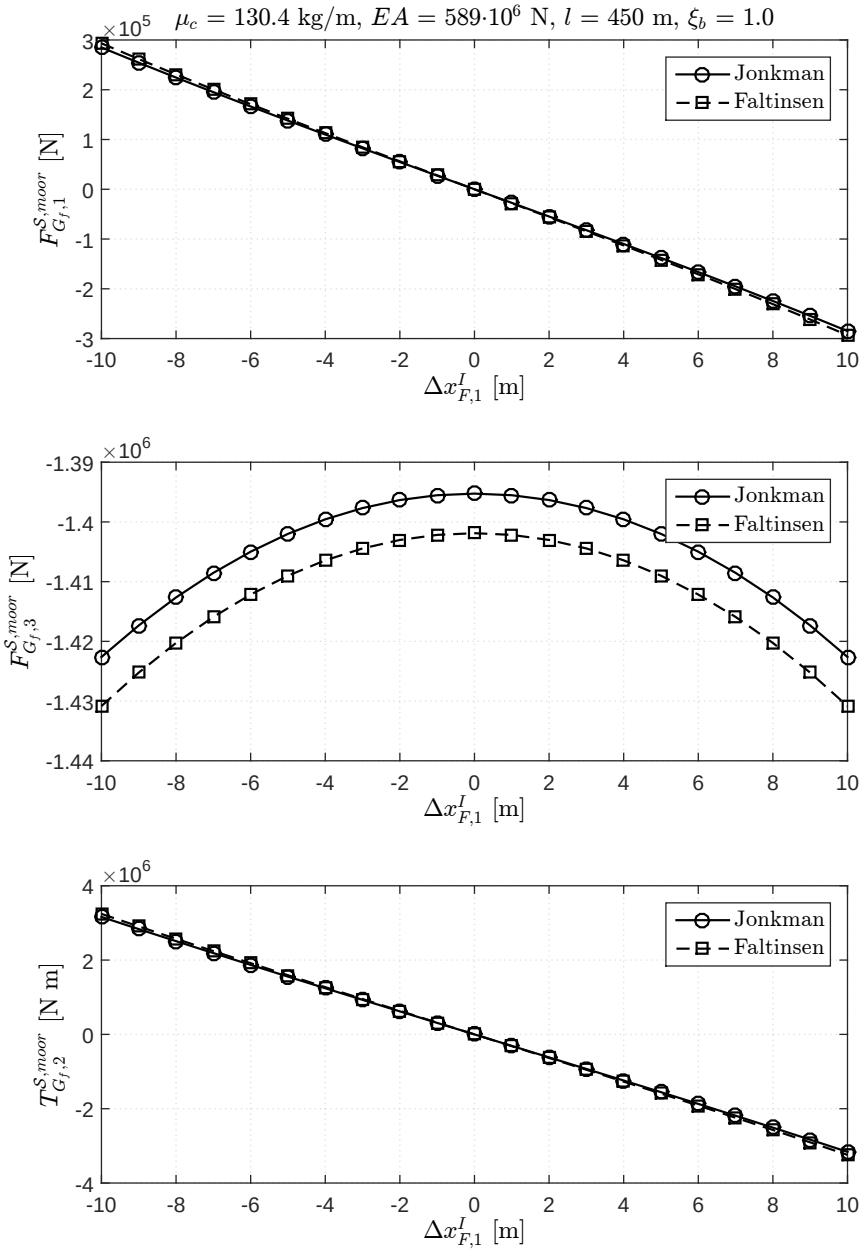

Figure 5.10: Effect on the restoring loads of rigid displacements of the fairleads along the x-axis.

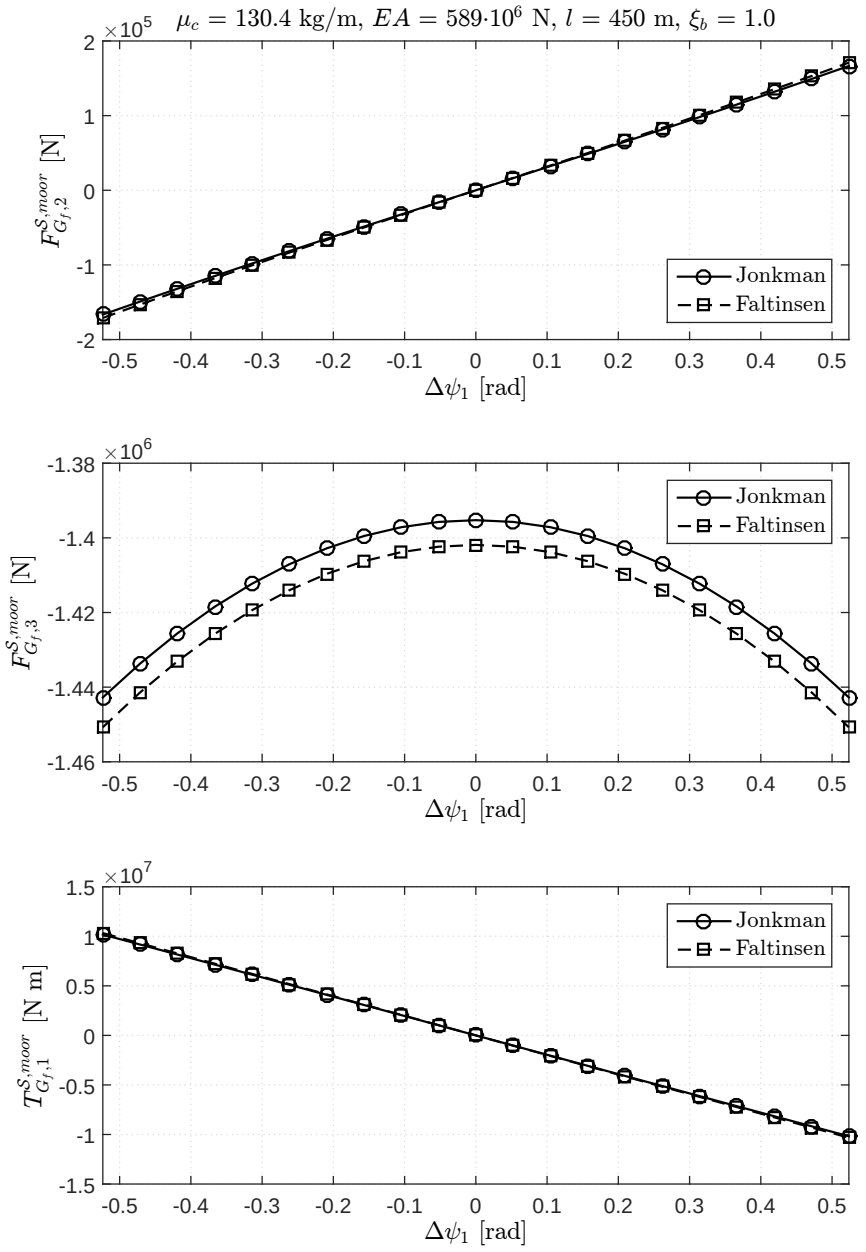

Figure 5.11: Effect on the restoring loads of rigid displacements of the fairleads about the x-axis.

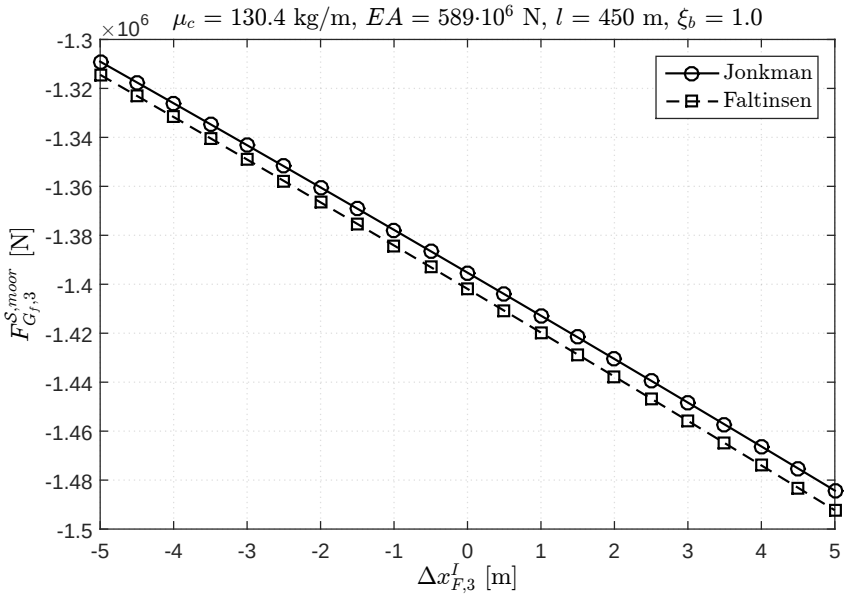

Figure 5.12: Effect on the restoring loads of rigid displacements of the fairleads along the z-axis.

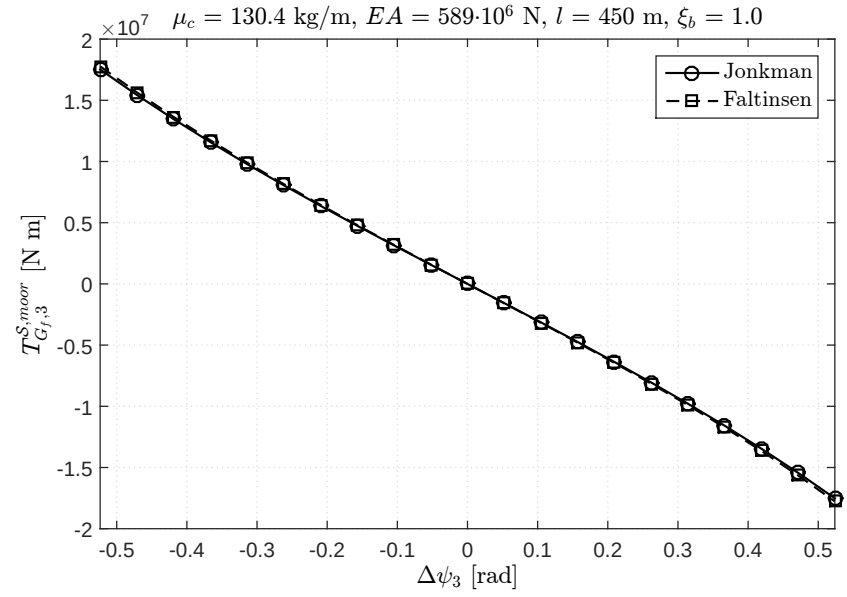

Figure 5.13: Effect on the restoring loads of rigid displacements of the fairleads about the z-axis.

a finite difference approach. On the other hand, also simpler models could be used, as those based on the so called force-displacement representation, which consists in modelling the mooring system as a nonlinear spring for each degree of freedom at the fairlead location, eventually including also a damping term [23]. However, this approach neglects the inertia of the mooring lines and does not usually consider the coupling of different degrees of freedom to each other.

Chapter 6

Coupled dynamic response

"Limits, like fears, are often just an illusion."

Michael Jeffrey Jordan

The coupled response of a moored floating platform is assessed by coupling the main solver with the load models. Different coupling and simulation strategies are introduced and discussed in order to reduce the computational effort. The coupled code is evaluated with a series of perturbation tests to ensure the correct functionality of the system in restoring the equilibrium. The dynamics of a moored floating platform is finally analysed with the main objective to better understand the role of some parameters as the wave period, wave amplitude, mass of the platform, length of the cables. The chapter aims at discussing the potentiality of the method together with some applications to floating offshore platforms.

6.1 Coupling problem

The dynamic solver (main code) can analyse the dynamics of a non-constrained[1] rigid body subjected to a wide range of loads, both follower and non-follower, in time domain. The study of particular systems, such as a floating platform, should properly consider that the motion is generally affected by specific sources of loads that are related both to the features of the system and to the environment, but also to the current configuration of the body, i.e. the state variables. Therefore, at each time step, the actual load depends on the unknown configuration, and the modules (codes) addressing specific issues, such as the evaluation of mooring loads or hydrodynamic actions, should be properly coupled with the main code. This step is crucial to get a reliable solution.

One possibility is to embed the formulation of the load model into the differential problem of the rigid-body dynamics, but this approach requires to modify the algorithm of the main code whenever the system or the sources of load change. By contrast, a weak coupling strategy refers to the estimation of the current loads on the basis of the values of the state variables at the previous time step. This approach could be accurate enough for small time step sizes, but the dynamic equilibrium is not verified at each time step because the loads are not computed with respect to the current configuration, which is unknown. The procedure can be improved by using an explicit iterative approach: the state variables at the previous time step are just used for the first estimation of the actual loads, then an iterative procedure, involving the updated configuration, is carried out until the convergence of an opportune residual is reached; thus, also the dynamic equilibrium is verified.

6.1.1 Mooring system

The mooring system provides the constraints to the translation of the floating body in the water plane and to the rotation about the vertical axis, namely against surge, sway, and yaw motions. Restoring loads (force and torque) are related both to the features of the moorings (mass, length, initial configuration) and to the displacements of the floating body, which define the actual configuration of the mooring system, in particular the location of the fairleads. Therefore, the mooring action[2] can be regarded as a nonlinear[3] function of the configuration of the rigid body, i.e. of the translation of the center of mass and of the rotation about the center of mass.

The mooring line model is implemented as an independent code, which should be coupled with the main dynamic solver in terms of external non-follower loads[4]. In particular, the codes are coupled together by means of an explicit procedure. The convergence on the residual is based either on the norm of the mooring loads (see

[1] The degrees of freedom could be constrained through a linear spring (both translational and rotational) with very large stiffness. In this way, of course, the constraint is not ideal, but the approximation is usually acceptable.

[2] It is considered a quasi-static model of the mooring lines. More complex models could also be related to the time derivatives of the displacements of the floating body.

[3] As discussed in the previous chapter, mooring system loads could be approximated by a linear spring if the displacements are limited within a certain range. However, such an approximation should properly consider also the coupling of different degrees of freedom due to the operation of the mooring system.

[4] The developed code computes the resultant load (force and torque) with respect to a fixed point of the body and expressed with respect to the basis of the inertial (fixed) reference frame. Also the tangent stiffness matrix is calculated with the same convention. Therefore, the restoring loads associated with the mooring system are treated as non-follower.

Algorithm 6.1: Coupling of the mooring code; residual evaluated with respect to the mooring loads.

input : h, α_f, α_m, β, γ, tol, n_{max}, m, $\mathbf{J}$, $\mathbf{g}$, $\hat{\mathbf{q}}_n$, $\hat{\mathbf{v}}_n$, $\hat{\dot{\mathbf{v}}}_n$, $\mathbf{a}_n$, $\mathbf{F}^{(\bullet)}$, $\mathbf{T}^{(\bullet)}$, $\mathbf{A}^{(\bullet)}$, $\mathbf{B}^{(\bullet)}$, …, ρ_w, ξ_b, n_c, l, w, EA, $\mathbf{x}^B_{F_j}$, $\mathbf{x}^I_{A_j}$

output: $\hat{\mathbf{q}}_{n+1}$, $\hat{\mathbf{v}}_{n+1}$, $\hat{\dot{\mathbf{v}}}_{n+1}$, $\mathbf{a}_{n+1}$

$\mathbf{F}^{moor} = \mathbf{F}^{moor}(\hat{\mathbf{q}}_n, \rho_w, \xi_b, n_c, l, w, EA, \mathbf{x}^{B,\mathcal{M}}_{F_j}, \mathbf{x}^{I,\mathcal{S}}_{A_j})$;
$\mathbf{T}^{moor} = \mathbf{T}^{moor}(\hat{\mathbf{q}}_n, \rho_w, \xi_b, n_c, l, w, EA, \mathbf{x}^{B,\mathcal{M}}_{F_j}, \mathbf{x}^{I,\mathcal{S}}_{A_j})$;
$\mathbf{K}^{t,moor} = \mathbf{K}^{t,moor}(\hat{\mathbf{q}}_n, \rho_w, \xi_b, n_c, l, w, EA, \mathbf{x}^{B,\mathcal{M}}_{F_j}, \mathbf{x}^{I,\mathcal{S}}_{A_j})$;
for $i \leftarrow 1$ **to** n_{max} **do**
  $\mathbf{F}^{*,moor} = \mathbf{F}^{moor}$;
  $\mathbf{T}^{*,moor} = \mathbf{T}^{moor}$;
  solve $\hat{\mathbf{q}}_{n+1}$, $\hat{\mathbf{v}}_{n+1}$, $\hat{\dot{\mathbf{v}}}_{n+1}$, $\mathbf{a}_{n+1} = f(\hat{\mathbf{q}}_n, \hat{\mathbf{v}}_n, \hat{\dot{\mathbf{v}}}_n, \mathbf{a}_n, \ldots, \mathbf{F}^{moor}, \mathbf{T}^{moor}, \mathbf{K}^{t,moor})$, Algorithm 3.1;
  $\mathbf{F}^{moor} = \mathbf{F}^{moor}(\hat{\mathbf{q}}_{n+1}, \rho_w, \xi_b, n_c, l, w, EA, \mathbf{x}^{B,\mathcal{M}}_{F_j}, \mathbf{x}^{I,\mathcal{S}}_{A_j})$;
  $\mathbf{T}^{moor} = \mathbf{T}^{moor}(\hat{\mathbf{q}}_{n+1}, \rho_w, \xi_b, n_c, l, w, EA, \mathbf{x}^{B,\mathcal{M}}_{F_j}, \mathbf{x}^{I,\mathcal{S}}_{A_j})$;
  $\mathbf{K}^{t,moor} = \mathbf{0}$;
  $\delta r = \max(||\mathbf{F}^{*,moor} - \mathbf{F}^{moor}||, ||\mathbf{T}^{*,moor} - \mathbf{T}^{moor}||)$;
  if $\delta r < tol$ **then**
    break;
  end
end

Algorithm 6.1) or on the norm of the system state variables (see Algorithm 6.2). The last one is usually preferable when in the same iterative procedure other modules are coupled together or with the main code, such as a code addressing the hydrodynamic problem. Note that if the procedure is stopped at the first iteration, the aforementioned weak coupling is performed[5]. As said before, an alternative approach is to embed the nonlinear mooring equations in the differential problem of the rigid-body dynamics.

6.1.2 Hydrodynamic action

The hydrodynamic action results from the dynamic pressures of the fluid all over the wetted surface and is evaluated on the basis of the linear theory, which basically splits the problem into three main sub-problems: radiation, diffraction, and hydrostatics [46]. In the case of the steady regular model the coupling is very simple since the radiation, diffraction, and hydrostatic problems are assessed by means of linear transformations of the state variables, namely, the hydrodynamic added mass $\mathbf{M}^A$ and damping $\mathbf{D}$ matri-

[5]The stiffness of the mooring system, i.e. the first-order expansion of the mooring loads about the equilibrium configuration at the previous time step, is used as a suitable predictor of the variation of load due to the change of configuration at the current time step. The following iterations consider a zero mooring stiffness because it would have been defined about the updated configuration, whereas the dynamic problem is always solved starting from the state variables of the previous time step. However, the procedure can be improved including the first-order expansion of the mooring loads about the updated configuration, but it is necessary to keep track of the new state variable, which should be an additional input of the main code.

Algorithm 6.2: Coupling of the mooring code; residual evaluated with respect to the system state variables.

input : h, α_f, α_m, β, γ, tol, n_{max}, m, $\mathbf{J}$, $\mathbf{g}$, $\hat{\mathbf{q}}_n$, $\hat{\mathbf{v}}_n$, $\hat{\dot{\mathbf{v}}}_n$, $\mathbf{a}_n$, $\mathbf{F}^{(\bullet)}$, $\mathbf{T}^{(\bullet)}$, $\mathbf{A}^{(\bullet)}$, $\mathbf{B}^{(\bullet)}$, $\ldots$, ρ_w, ξ_b, n_c, l, w, EA, $\mathbf{x}^B_{F_j}$, $\mathbf{x}^I_{A_j}$

output: $\hat{\mathbf{q}}_{n+1}$, $\hat{\mathbf{v}}_{n+1}$, $\hat{\dot{\mathbf{v}}}_{n+1}$, $\mathbf{a}_{n+1}$

$\mathbf{F}^{moor} = \mathbf{F}^{moor}(\hat{\mathbf{q}}_n, \rho_w, \xi_b, n_c, l, w, EA, \mathbf{x}^{B,\mathcal{M}}_{F_j}, \mathbf{x}^{I,\mathcal{S}}_{A_j})$;
$\mathbf{T}^{moor} = \mathbf{T}^{moor}(\hat{\mathbf{q}}_n, \rho_w, \xi_b, n_c, l, w, EA, \mathbf{x}^{B,\mathcal{M}}_{F_j}, \mathbf{x}^{I,\mathcal{S}}_{A_j})$;
$\mathbf{K}^{t,moor} = \mathbf{K}^{t,moor}(\hat{\mathbf{q}}_n, \rho_w, \xi_b, n_c, l, w, EA, \mathbf{x}^{B,\mathcal{M}}_{F_j}, \mathbf{x}^{I,\mathcal{S}}_{A_j})$;
for $i \leftarrow 1$ **to** n_{max} **do**
  if $i \neq 1$ **then**
    $\hat{\mathbf{q}}^* = \hat{\mathbf{q}}_{n+1}$;
    $\hat{\mathbf{v}}^* = \hat{\mathbf{v}}_{n+1}$;
    $\hat{\dot{\mathbf{v}}}^* = \hat{\dot{\mathbf{v}}}_{n+1}$;
  else
    $\hat{\mathbf{q}}^* = \hat{\mathbf{q}}_n$;
    $\hat{\mathbf{v}}^* = \hat{\mathbf{v}}_n$;
    $\hat{\dot{\mathbf{v}}}^* = \hat{\dot{\mathbf{v}}}_n$;
  end
  solve $\hat{\mathbf{q}}_{n+1}$, $\hat{\mathbf{v}}_{n+1}$, $\hat{\dot{\mathbf{v}}}_{n+1}$, $\mathbf{a}_{n+1} = f(\hat{\mathbf{q}}_n, \hat{\mathbf{v}}_n, \hat{\dot{\mathbf{v}}}_n, \mathbf{a}_n, \ldots, \mathbf{F}^{moor}, \mathbf{T}^{moor}, \mathbf{K}^{t,moor})$, Algorithm 3.1;
  $\delta r = \max(||\hat{\mathbf{q}}^* - \hat{\mathbf{q}}_{n+1}||, ||\hat{\mathbf{v}}^* - \hat{\mathbf{v}}_{n+1}||, ||\hat{\dot{\mathbf{v}}}^* - \hat{\dot{\mathbf{v}}}_{n+1}||)$;
  if $\delta r < tol$ **then**
    break;
  end
  $\mathbf{F}^{moor} = \mathbf{F}^{moor}(\hat{\mathbf{q}}_{n+1}, \rho_w, \xi_b, n_c, l, w, EA, \mathbf{x}^{B,\mathcal{M}}_{F_j}, \mathbf{x}^{I,\mathcal{S}}_{A_j})$;
  $\mathbf{T}^{moor} = \mathbf{T}^{moor}(\hat{\mathbf{q}}_{n+1}, \rho_w, \xi_b, n_c, l, w, EA, \mathbf{x}^{B,\mathcal{M}}_{F_j}, \mathbf{x}^{I,\mathcal{S}}_{A_j})$;
  $\mathbf{K}^{t,moor} = \mathbf{0}$;
end

ces, and the hydrostatic restoring matrix $\mathbf{K}^{hys}$, plus a time-dependent wave-excitation load. These transformations are generally non-follower, but it depends on the code used for computing the operators.

On the other hand, if the floating body is subjected to an irregular wave or whenever the steady regular model is not suitable (for instance for a detailed analysis of transients), the coupling can be similarly achieved referring to the Cummins approach by means of the superimposition of different external loads. In this case the time-dependent wave-excitation loads should include all the harmonics of the incident wave, whereas the radiation sub-problem is assessed by a constant linear transformation (infinite-frequency limit of the added mass matrix) of the acceleration of the body and the convolution integral that involves the wave-radiation-retardation kernel matrix and the time history of the velocity vector of the system. If the time step size is small enough, such integral can be evaluated on the basis of the time series of the velocity up to the previous time

step, even if it is possible to improve the coupling with an iterative procedure in order to always preserve the dynamic equilibrium.

6.1.3 On the use of the steady regular model

The steady regular model for the evaluation of the hydrodynamic loads due to monochromatic waves, presented in Section 4.4.4.2, requires that the system oscillates at the same frequency of the incident wave. Such requirement is surely satisfied when the system is modelled as a linear oscillator (after the initial transient). By contrast, if the system is nonlinear, the response could be rather different depending on the weight of the nonlinear character. For strongly nonlinear systems the analysis should be carried out modelling the radiation loads with the Cummins approach (see Section 4.4.4.1).

Moored floating platforms are usually weakly nonlinear. If the system is forced by regular waves parallel to a vertical plane of symmetry of the moored system, the steady response is still an oscillatory motion practically at the same frequency of the incident wave. Even if the nonlinearities associated with the operation of the mooring system (quasi-static model) could cause additional mean forces and oscillations at about double the frequency of the wave, they do not significantly contribute to the spectrum of the response[6]. Even when the waves are misaligned with respect to a vertical plane of symmetry of the floating system, the response to regular waves can still be considered monochromatic, although there are also nonlinearities related to the rotational motion and the follower or non-follower interpretation of loads, which, as happen for the mooring system, causes harmonic loads at higher frequencies, usually at double the frequency of the incident wave, and with a non-zero mean value. However, also in this case the contribution of such oscillations to the spectrum of the response is usually negligible.

In this context the steady regular model can be used without a significant loss of accuracy with the benefit of a reduced computational effort. On the other hand, the Cummins approach is mandatory for a detailed study of transients, or when the incident wave is not monochromatic, or whenever the response has not a dominant frequency. However, it requires the computation at each time step of a convolution integral between the radiation-retardation kernel operator[7] and the time series of the velocity, which is generally time consuming. For this reason whenever is possible, i.e. when the response has a dominant frequency identical to that one of the incoming wave, it is preferable the use of the steady regular model.

6.2 Calibration of the coupled model

This section describes the calibration of the initial conditions to ensure that the moored floating system is in static equilibrium in absence of incident waves and any other time-dependent external load, together with a simulation strategy to limit the initial

[6] The system steady response obtained with the steady regular model is practically the same obtained by modelling the radiation loads with the more general Cummins approach. It can be easily verified by performing both the analyses, or simply by analysing the spectrum of the response, which still maintains a dominant frequency.

[7] The radiation-retardation kernel operator is computed by integrating the hydrodynamic damping matrix over the frequencies. The accuracy is usually affected by the frequency resolution of the damping matrix and the interpolations over the time, necessary to have a time series with the same discretization of the response when the radiation-retardation kernel is computed with a fast Fourier transform, as usual. Moreover, if the damping matrix is interpreted as either follower or non-follower operator, it should be updated at each time step considering the actual orientation of the body (only for rotations about a fixed axis it can be avoided).

transient related to the initial conditions. Moreover, the effects on the motion of the extra-diagonal terms of the hydrodynamic added mass matrix are verified, and the equivalence of the mooring quasi-static models of Jonkman and Faltinsen is discussed.

6.2.1 Reference frames

The reference frames and the notations adopted in this chapter are the same used for the formulation of the main dynamic model (see Section 3.1.1). The inertial frame $\{O; x, y, z\}$ has the origin O in the location of the center of mass in the free floating equilibrium configuration, i.e. without the mooring lines and any other external load except the weight and the buoyancy, z-axis pointing vertically upwards, and x-axis directed along one of the principal directions of the system. The body-attached frame $\{G; x', y', z'\}$ is a principal reference frame that coincides with the inertial frame in the free floating equilibrium configuration.

6.2.2 Initial configuration

Hydrostatic forces are usually computed when the platform is free to float without any external load (only the weight). When the mooring lines are connected to the floating body, the additional forces due to the tension on the lines perturb the static equilibrium. The system needs a transient to reach a new equilibrium configuration. However, this transient can be avoided, or limited, with an appropriate initial condition on the displacements[8].

Let's consider a homogeneous parallelepiped platform connected to a system of eight moorings (two for each vertex of the bottom) anchored to the seabed on a circle of radius r_A with the layout described in Figure 6.1. Let's assume that the floating body is subjected to gravity and mooring forces, whereas the hydrodynamic problem, in the framework of the linear theory, is restricted to the hydrostatic and radiation sub-problems (absence of incident waves). The features of the system and of the environment are reported in Table 6.1[9]. The transient is evaluated for different conditions, namely:

- zero initial conditions, the configuration of the floating body is equilibrated only with the weight but not with the mooring loads. The hydrodynamic[10] added mass and damping matrices[11] are evaluated at the frequency of free heave oscillations;
- initial heave displacement established on the basis of the resultant loads of the mooring system evaluated with respect to the initial configuration (before the

[8] The initial condition depends both on the floating body and on the features of the mooring system, in particular its geometry. If both the systems have the same symmetry properties, i.e. the mooring load, the weight, and the buoyancy are aligned along the same vertical line, it is sufficient an initial condition on the heave displacement, as it happens in the most common cases.

[9] The features of the system in terms of geometry and materials (mass, stiffness, etc.) are more or less the same used in [46] for the floating support of an offshore wind turbine. Such features are the reference for all the examples reported in this chapter in order to analyse a system as realistic as possible.

[10] For the examples discussed in this chapter, the hydrostatic and hydrodynamic (added mass, damping, and wave-excitation) operators were computed by AQWA code [5] and should be considered as non-follower operators applied to the center of mass G.

[11] Although in this example there are not incident waves, the system oscillates in still water; thus, it seems reasonable to consider the hydrodynamic operators associated with the radiation problem and evaluated at the frequency of heave oscillations. Such frequency depends, among others, on the hydrodynamic added mass and damping operators, which in turn are related to the oscillating frequency itself. A rough estimation can be done on the basis of the (undamped) natural frequency including the

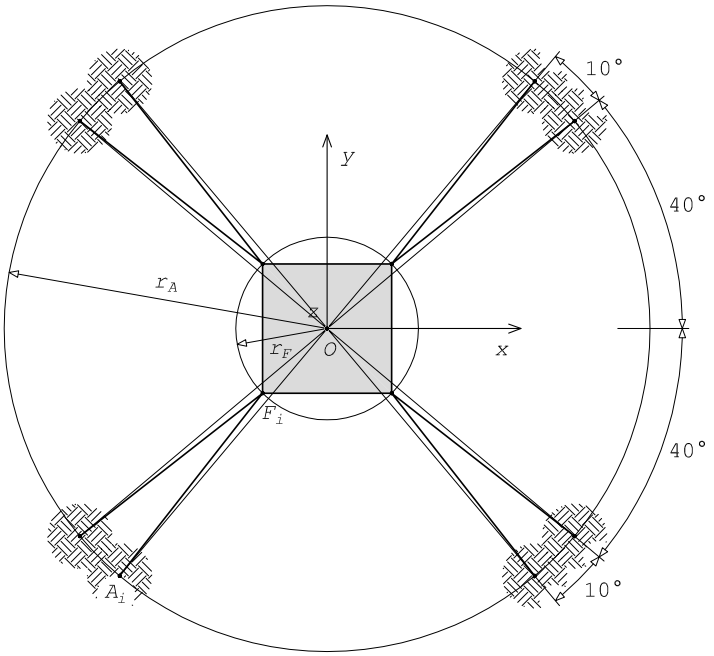

Figure 6.1: Layout of the mooring system in the static equilibrium configuration [71].

transient), namely:

$$\hat{q}_3|_{t=0} = \frac{F_{G,3}^{\mathcal{S},moor}}{K_{33}^{hys}} \tag{6.1}$$

The hydrodynamic added mass and damping matrices are evaluated at the frequency of free heave oscillations;

- zero initial conditions without hydrodynamic added mass and damping operators.

contribution of the added mass, namely:

$$\omega_n = \sqrt{\frac{K_{33}^{hys}}{m + M_{33}^A}}$$

which corresponds to a period $T_n = 7.3185$ s. A more comprehensive estimation of the frequency of free oscillations should also include the contribution of the hydrodynamic damping, namely:

$$\omega = \sqrt{\frac{K_{33}^{hys}}{m + M_{33}^A}} \sqrt{1 - \left[\frac{D_{33}}{2\omega_n(m + M_{33}^A)}\right]^2}$$

which corresponds to a period $T = 7.4519$ s. The added mass and damping terms can be estimated with an iterative procedure starting from the natural frequency of the system in absence of radiating waves, i.e. $\omega_n = \sqrt{K_{33}^{hys}/m}$, which corresponds to a period $T_n = 3.8372$ s.

environment		
gravity acceleration, g	9.807	m/s^2
water density, ρ_w	1 025	kg/m^3
water depth, d	150.0	m
seabed friction coefficient, ξ_b	0.5	-
floating platform		
length along x', a	40.0	m
length along y', b	40.0	m
height, c	10.0	m
mass, m	5 998.538	t
moment of inertia about x', J_{11}	$8.4979 \cdot 10^5$	$t{\cdot}m^2$
moment of inertia about y', J_{22}	$8.4979 \cdot 10^5$	$t{\cdot}m^2$
moment of inertia about z', J_{33}	$1.5996 \cdot 10^6$	$t{\cdot}m^2$
draft, h_{imm}	3.6576	m
location of the center of mass with respect to the sea water level, $\mathbf{x}_G$	$[0\ 0\ 1.3424]^T$	m
moorings		
number, n_c	8	-
diameter, D_c	0.1454	m
unstretched length, l	460	m
mass density per unit length, μ_c	130.4	kg/m
extensional stiffness, EA	$589{\cdot}10^6$	N
radius to fairleads, r_F	28.28	m
radius to anchors, r_A	423.4	m

Table 6.1: Parameters adopted for the analysis of the initial transient due to the coupling of the mooring system.

6.2.2.1 Results

If the mooring system is coupled with zero initial conditions (see Figure 6.2), the static equilibrium is no longer verified, and a transient is required to reach a new equilibrium configuration. Because of the symmetry of the coupled system, the transient concerns only the heave motion. If a non-zero initial condition (see Figure 6.3), evaluated on the basis of the initial unbalanced force of the moorings, is imposed to the system, the transient is limited in terms of amplitude of oscillations. This approach seems a good strategy to limit the time window where the perturbation of data is significant. In particular, in the case of mooring lines modelled by the Jonkman formulation[12], the estimation leads to an initial heave of about -0.1326 m in front of an equilibrated displacement of -0.13234970 m. If the hydrodynamic operators are neglected, in particular the damping matrix, the system indefinitely vibrates without any attenuation, according to a simple undamped oscillator.

[12]By contrast, in the case of the Faltinsen model the estimation leads to an initial heave of about -0.1328 m, in front of an equilibrated displacement of -0.13258159 m.

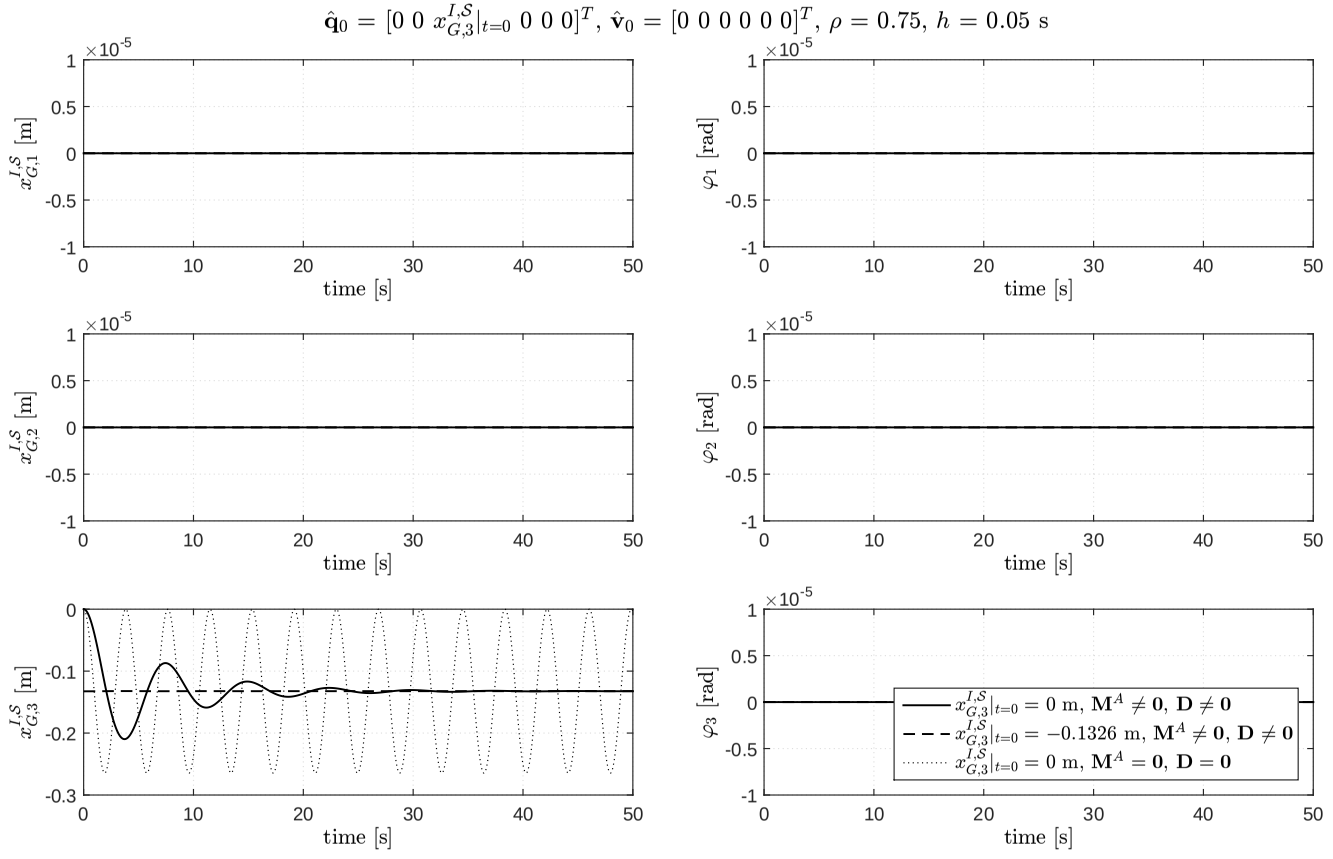

Figure 6.2: Transient due to the coupling of the mooring system; comparison between different initial conditions and hydrodynamic properties. Analyses carried out with the Jonkman model for mooring lines and the steady regular model for the radiation and hydrostatic sub-problems.

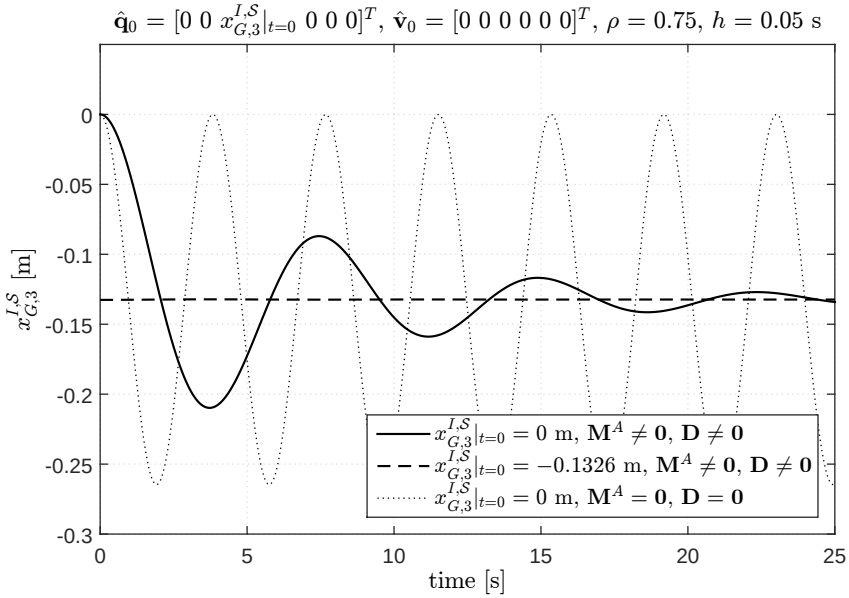

Figure 6.3: Transient due to the coupling of the mooring system; close-up of the heave motion evaluated for different initial conditions and hydrodynamic properties. Analyses carried out with the Jonkman model for mooring lines and the steady regular model for the radiation and hydrostatic sub-problems.

6.2.2.2 Remarks

When the mooring line code is coupled with the dynamic solver with zero initial conditions, the system is not in an equilibrium configuration because of the forces originating from the tension on the mooring lines. Therefore, the system requires a transient to reach a new equilibrium configuration. The transient becomes negligible after a time that depends both on the initial displacement and on the damping factor; the higher the damping the higher the amplitude attenuation. If the initial heave displacement is evaluated on the basis of the initial unbalanced force due to the mooring system, the transient is strongly reduced even if this estimation of the additional draft does not guarantee the equilibrium. In fact, if the configuration of the mooring system changes, also the associated loads vary. It is necessary an iterative procedure to evaluate the initial displacement that guarantees the static equilibrium.

However, a small initial transient is usually acceptable considering also that an initial window of the time series is usually discarded because it is affected by other transients due to the initial conditions (let's think to the general solution of a homogeneous differential problem) and to the nonlinear coupling of some degrees of freedom associated with the operation of the mooring system and the combination of the rotational motion with a follower or non-follower interpretation of loads.

The case of absence of hydrodynamic operators seems to be not realistic because of the nature of the fluid. Only in the case of quasi-static motions the hydrodynamic damping could be neglected. Note also that this static configuration can be different

from the mean dynamic configuration because of the aforementioned nonlinear coupling of different degrees of freedom. In fact, a pure harmonic motion can cause loads with non-zero mean value that bring the system into a new mean configuration[13].

6.2.3 Effect of the added mass matrix

Let's consider the structure of the added mass matrix[14] (see Equation (6.2)) of a rigid body symmetric with respect to the principal planes, the extra-diagonal elements correspond to loads not directly associated with the correlative displacements. For example the term M^A_{15} means that a rotational motion about the y-axis causes a force along the x-axis.

$$\mathbf{M}^A = \begin{bmatrix} M^A_{11} & 0 & 0 & 0 & M^A_{15} & 0 \\ 0 & M^A_{22} & 0 & M^A_{24} & 0 & 0 \\ 0 & 0 & M^A_{33} & 0 & 0 & 0 \\ 0 & M^A_{24} & 0 & M^A_{44} & 0 & 0 \\ M^A_{15} & 0 & 0 & 0 & M^A_{55} & 0 \\ 0 & 0 & 0 & 0 & 0 & M^A_{66} \end{bmatrix} \tag{6.2}$$

Let's consider a homogeneous parallelepiped platform without any mooring line; the features of the system and of the environment are reported in Table 6.2. In order to verify if the code is well implemented, three very simple tests are performed:

- non-moored platform subjected to a regular-wave-like force[15] and free to translate only along the z-axis (heave motion) and to rotate only about the y-axis (pitch motion);
- non-moored platform subjected to a regular-wave-like force and free to translate along the x and z axes (surge and heave motions) and to rotate only about the y-axis (pitch motion);
- non-moored platform subjected to a regular-wave-like torque and free to translate along the x and z axes (surge and heave motions) and to rotate only about the y-axis (pitch motion).

In the first case, after an initial transient, the heave and pitch motions should be oscillations at the same frequency of the incoming wave and, in absence of the torque components, the system should only translate along the z-axis. On the other hand, in the second case, the introduction of a further degree of freedom (translation along the x-axis) should guarantee pitch motions even in absence of the torque forcing load, due to the aforementioned cross-element $M^A_{51} = M^A_{15}$. In the third case, a torque about the y-axis should also cause surge motions.

[13] For instance a pure harmonic rotational motion about the x-axis (see Figure 5.11) causes an harmonic torque about the x-axis, an harmonic force along the y-axis, and an oscillatory vertical force with a non-zero mean value (at about double frequency) that brings the system into a new mean configuration.

[14] Also the damping matrix has a similar structure.

[15] The force applied to the center of mass is that of a regular wave directed along the x-axis, but the torque is neglected.

environment		
gravity acceleration, g	9.807	m/s^2
water density, ρ_w	1 025	kg/m^3
water depth, d	150.0	m
seabed friction coefficient, ξ_b	0.5	-
wave		
wave amplitude, ζ	1.0	m
wave period, T	7.5	s
wave direction, β	0	rad
floating platform		
length along x', a	40.0	m
length along y', b	40.0	m
height, c	10.0	m
mass, m	5 998.538	t
moment of inertia about x', J_{11}	$8.4979 \cdot 10^5$	$t{\cdot}m^2$
moment of inertia about y', J_{22}	$8.4979 \cdot 10^5$	$t{\cdot}m^2$
moment of inertia about z', J_{33}	$1.5996 \cdot 10^6$	$t{\cdot}m^2$
draft, h_{imm}	3.6576	m
location of the center of mass with respect to the sea water level, $\mathbf{x}_G$	$[0\ 0\ 1.3424]^T$	m
moorings		
number, n_c	none	-

Table 6.2: Parameters adopted for the analysis of the effect of the added mass matrix.

6.2.3.1 Constraints

The code, as it is structured, does not permit to suppress some degrees of freedom (in this case the system has six d.o.f.). A constrained system is modelled by means of a proper stiffness matrix, i.e. a non-follower linear transformation of the displacements $\mathbf{A^q}$. The constraints obtained are not perfect but with high values of the spring stiffness the behaviour could be adequate for the purposes. For instance, in order to let the body translate only along the z-axis and rotate only about the y-axis, the transformation of the displacement is given by[16]:

$$\mathbf{A^q} = \begin{bmatrix} 10^{16} & 0 & 0 & 0 & 0 & 0 \\ 0 & 10^{16} & 0 & 0 & 0 & 0 \\ 0 & 0 & 0 & 0 & 0 & 0 \\ 0 & 0 & 0 & 10^{16} & 0 & 0 \\ 0 & 0 & 0 & 0 & 0 & 0 \\ 0 & 0 & 0 & 0 & 0 & 10^{16} \end{bmatrix} \tag{6.3}$$

[16]The terms should be as large as possible but not too large because otherwise the operator could affect the convergence process of the Newton-Raphson scheme (performed at each time step).

By contrast, in order to let the system move also along the x-axis, the transformation of the displacements is given by:

$$\mathbf{A}^{\mathbf{q}} = \begin{bmatrix} 0 & 0 & 0 & 0 & 0 & 0 \\ 0 & 10^{16} & 0 & 0 & 0 & 0 \\ 0 & 0 & 0 & 0 & 0 & 0 \\ 0 & 0 & 0 & 10^{16} & 0 & 0 \\ 0 & 0 & 0 & 0 & 0 & 0 \\ 0 & 0 & 0 & 0 & 0 & 10^{16} \end{bmatrix} \tag{6.4}$$

6.2.3.2 Results

The loads associated with the diffraction problem (see Figure 6.4) of a wave directed along the positive x-axis have dominating components in the xz-plane. In this example the system is forced either by the wave force or by the wave torque. If the translations of the center of mass along the x-axis are constrained (see Figure 6.5), a regular-wave-like force makes the floating body translate along the z-axis without any rotation. By contrast, if the translation along the x-axis is released, the system oscillates about the y-axis (pitch rotations), even if the wave-like load is not eccentric because of the resultant torque associated with the structure of the added mass matrix. A similar behaviour is observed in the case of system subjected to a regular-wave-like torque (see Figure 6.6), where the system undergoes surge motions as a consequence of the coupling of some degrees of freedom associated with the radiation problem. These results are definitely compatible with the initial expectations.

6.2.3.3 Remarks

All the numerical results correspond to the expected behaviour of the floating body. Further investigations are required to establish if the time histories correspond exactly to those associated with the incident regular wave, even though the hydrodynamic operators were generated by a reliable available code.

The strategy used to constrain the body seems as effective as reliable. However, the corresponding constraints are not ideal. As an alternative, the differential problem could be rewritten including also the constraint equations, for example at the position level. The Lie group time integrator is suitable also for constrained bodies [11].

6.2.4 Initial transient

Because of the initial conditions, the system obeys an initial transient rather far from the operation state. This initial transient is similar to the transient associated with the general solution of a system of homogeneous linear differential equations[17]. Generally, the environment and the corresponding sea state do not suddenly change but gradually develop in time until the stationary condition. However, the dynamic model has not memory of the previous history of the loads, which result suddenly applied and associated with non compatible initial conditions. The consequent initial transient is usually undesired and discarded from the time series.

[17] Although the coupled model is generally nonlinear, the actual range of displacements and the specific load models make the differential problem weakly nonlinear so that some considerations can be qualitatively extended from the linear case.

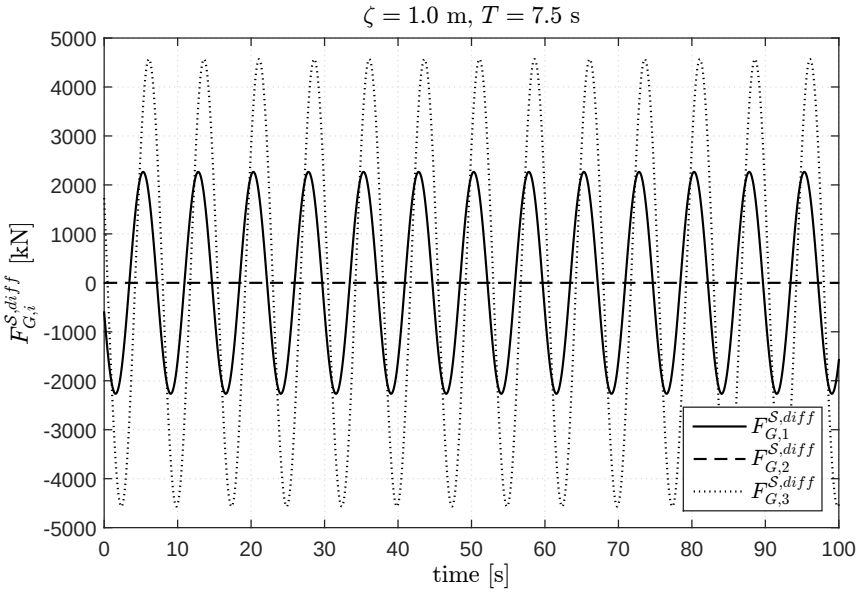

(a) forces associated with the diffraction problem

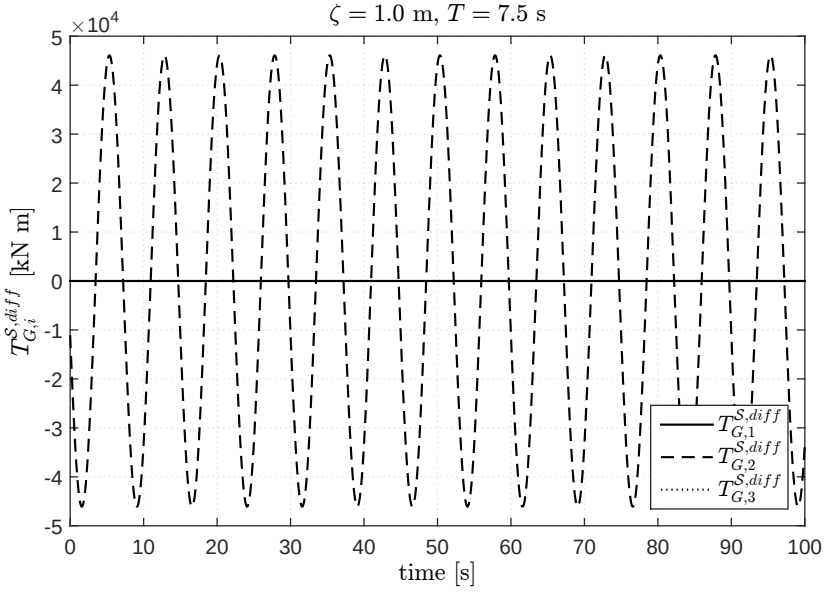

(b) torques associated with the diffraction problem

Figure 6.4: Effect of the added mass matrix; wave-excitation loads.

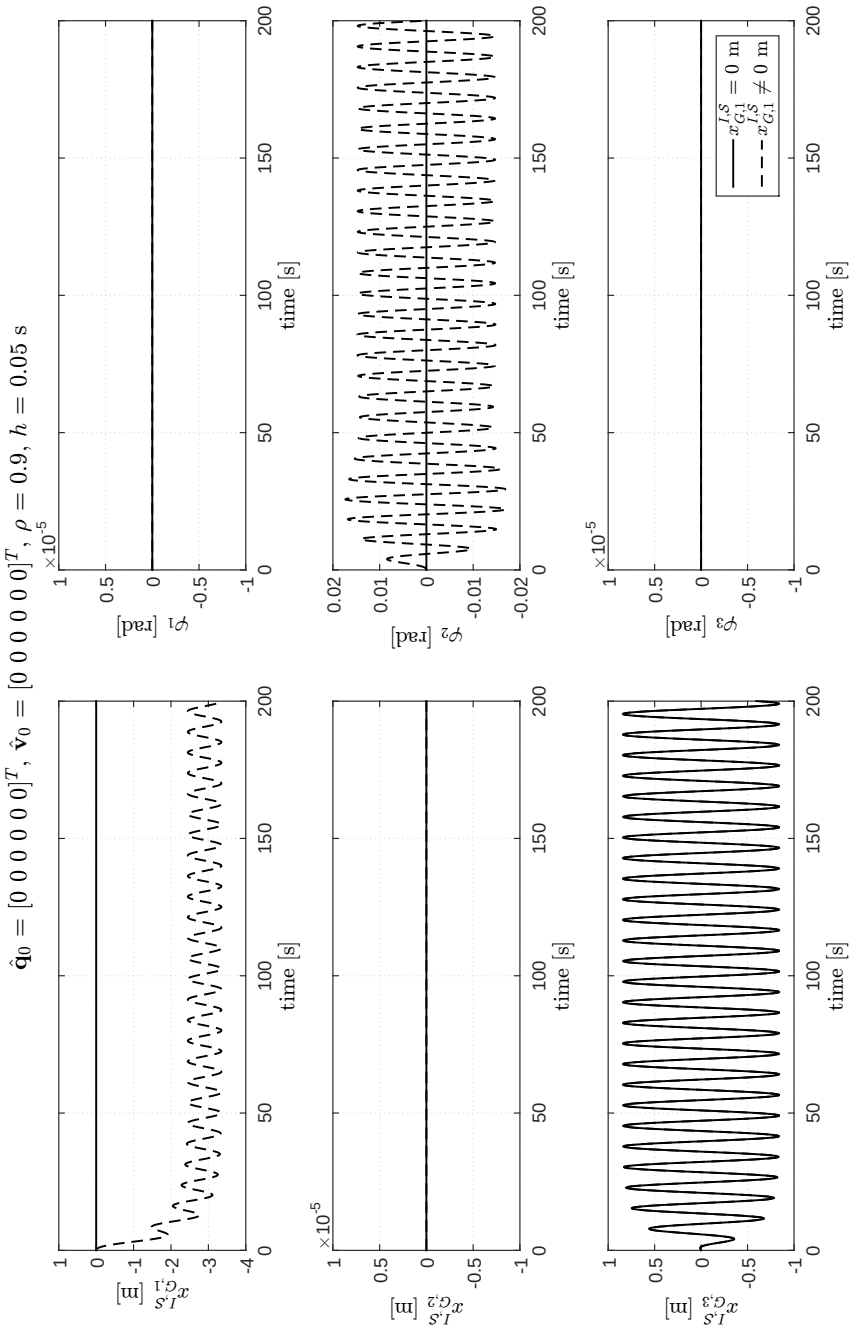

Figure 6.5: Effect of the added mass matrix with a regular-wave-like force; comparison between different constraint conditions. Analyses carried out with the steady regular model.

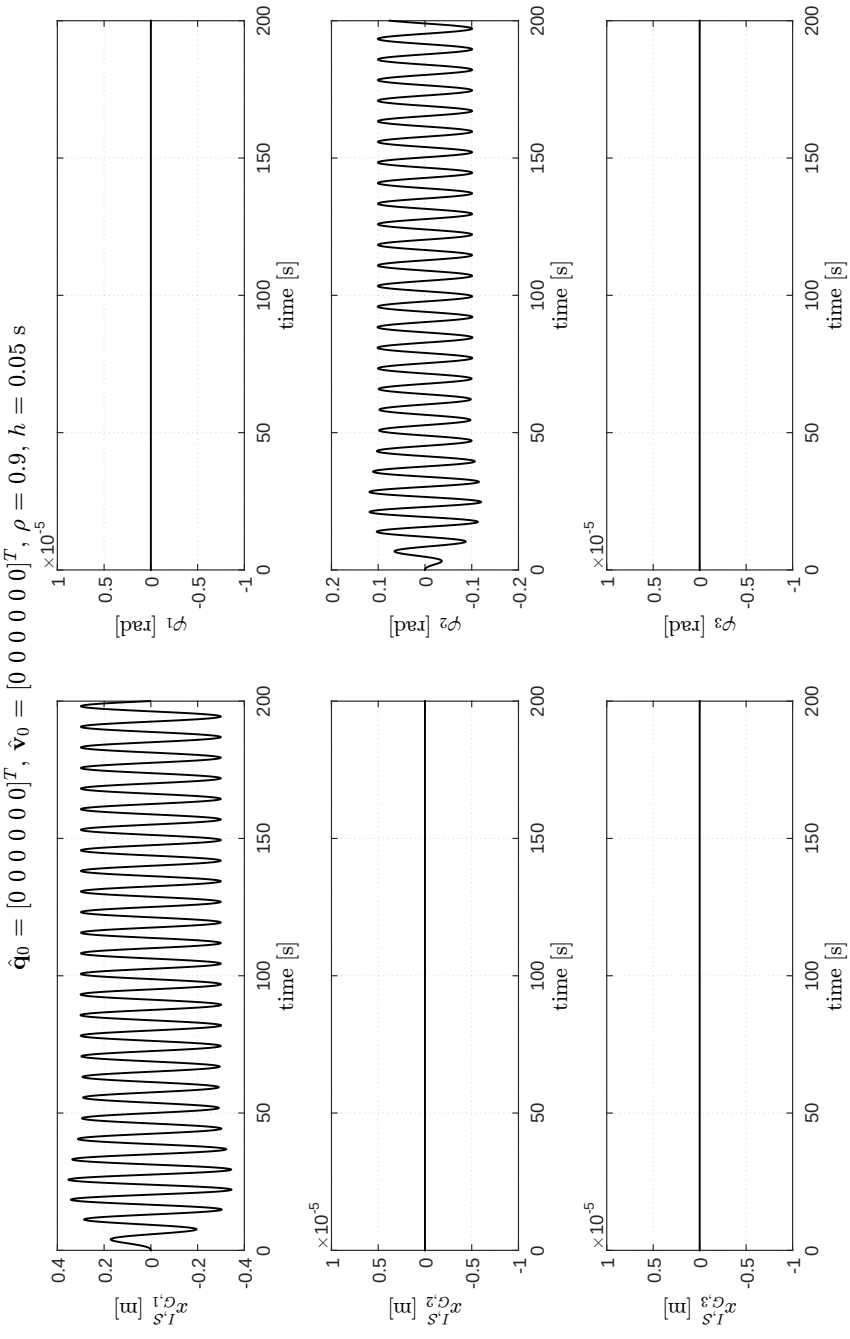

Figure 6.6: Effect of the added mass matrix with a regular-wave-like torque. Analysis carried out with the steady regular model.

environment		
gravity acceleration, g	9.807	m/s^2
water density, ρ_w	1 025	kg/m^3
water depth, d	150.0	m
seabed friction coefficient, ξ_b	0.5	-
wave		
wave amplitude, ζ	1.0	m
wave period, T	variable	s
wave direction, β	0	rad
floating platform		
length along x', a	40.0	m
length along y', b	40.0	m
height, c	10.0	m
mass, m	5 998.538	t
moment of inertia about x', J_{11}	$8.4979 \cdot 10^5$	t·m^2
moment of inertia about y', J_{22}	$8.4979 \cdot 10^5$	t·m^2
moment of inertia about z', J_{33}	$1.5996 \cdot 10^6$	t·m^2
draft, h_{imm}	3.6576	m
location of the center of mass with respect to the sea water level, $\mathbf{x}_G$	$[0\ 0\ 1.3424]^T$	m
neutral configuration (Jonkman mooring model), $\hat{q}_3\|_{t=0}$	-0.13235	m
moorings		
number, n_c	8	-
diameter, D_c	0.1454	m
unstretched length, l	460	m
mass density per unit length, μ_c	130.4	kg/m
extensional stiffness, EA	$589{\cdot}10^6$	N
radius to fairleads, r_F	28.28	m
radius to anchors, r_A	423.4	m

Table 6.3: Parameters adopted for the analysis of the transient associated with the initial conditions.

Let's consider a homogeneous parallelepiped platform connected to a system of eight moorings (two for each vertex of the bottom) anchored to the seabed on a circle of radius r_A with the layout described in Figure 6.1. The features of the system and of the environment are reported in Table 6.3. The initial transient, associated with regular waves of periods $T = 7.5$ s and $T = 12.0$ s and directed along the x-axis, is qualitatively studied by using the steady regular model, and a simulation strategy to limit such transient is proposed.

6.2.4.1 On the interpretation of the transients

The transients described in this section should be interpreted only qualitatively because they are obtained with the steady regular model for monochromatic waves (see Section 4.4.4.2), which is reliable only for the steady response. For a more comprehensive analysis of the transient it is necessary the use of the Cummins approach, which considers vibrations of the body at different frequencies. However, the main aim of this section is the reduction of the transient in order to limit the discarded data for the analysis of the operating (steady) response.

By contrast, if the goal is the study of the transients, such procedure should be avoided, and the use of the more complete hydrodynamic load model becomes mandatory even if it generally increases the computational effort. Note also that the use of the steady regular model contributes to limit the transient associated with translational motions, in particular when they have long natural periods[18], because of the higher damping.

6.2.4.2 Simulation strategy

The initial transient associated with the initial conditions can be limited by properly modifying the wave-excitation load (diffraction problem) so that it gradually reaches its amplitude. The strategy proposed is very simple and consists in scaling the load with a linear function so that after a period of T_t seconds the load reaches its final amplitude, namely:

$$\mathbf{F} = f(t)\mathbf{F}^{diff} \qquad \text{where} \tag{6.5}$$

$$f = \frac{t}{T_t} \qquad \text{if} \quad t < T_t, \qquad f = 1 \qquad \text{if} \quad t \geq T_t \tag{6.6}$$

The system is therefore gradually brought into the oscillatory motion without the perturbation due to a sudden application of the load. The window T_t should be calibrated on the basis of the period of the incident wave.

6.2.4.3 Results

The duration of the initial transient depends on the hydrodynamic damping, which is related to the period of the incident wave. If the system is forced by a regular wave of period $T = 7.5$ s (see Figure 6.7), the consequent transient is rather short. By contrast, for a wave period $T = 12.0$ s (see Figure 6.8) the transient is much longer and consequently more than five hundred seconds should be discarded. The strategy proposed[19] can reduce the initial transient regardless of the period of the incoming wave, limiting the data discarded and thus saving computational time.

6.2.4.4 On the time step size and the coupling of moorings

In order to verify other different possible approaches, the system was also simulated with a reduced time step size ($h = 0.01$ s) and by using a weak coupling strategy of

[18] If the same system is analysed computing the radiation loads either with constant added mass and damping matrices (evaluated at the wave frequency) or with the Cummins approach (infinite frequency added mass and convolution integral), the transient associated with the second approach is much more long because of the low damping associated with long-period oscillations. However, the simulation strategy proposed in this section has the same effectiveness regardless of the model used.

[19] The simulations are carried out with $T_t = 30.0$ s.

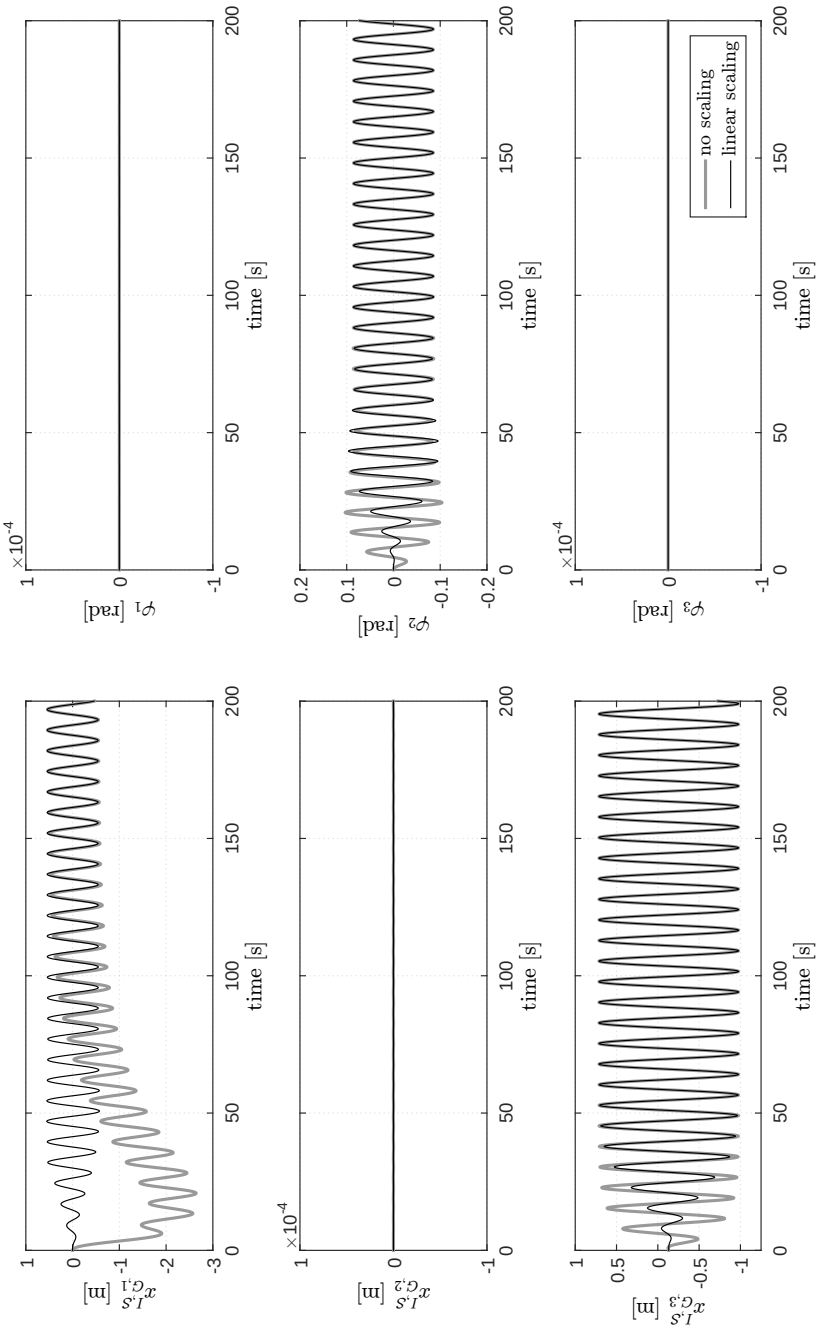

Figure 6.7: Initial transient; comparison between the time series obtained with and without a linear scaling strategy of the wave-excitation loads for a regular wave with period of 7.5 s directed along the x-axis. Analyses carried out with the Jonkman model for mooring lines and the steady regular model for waves.

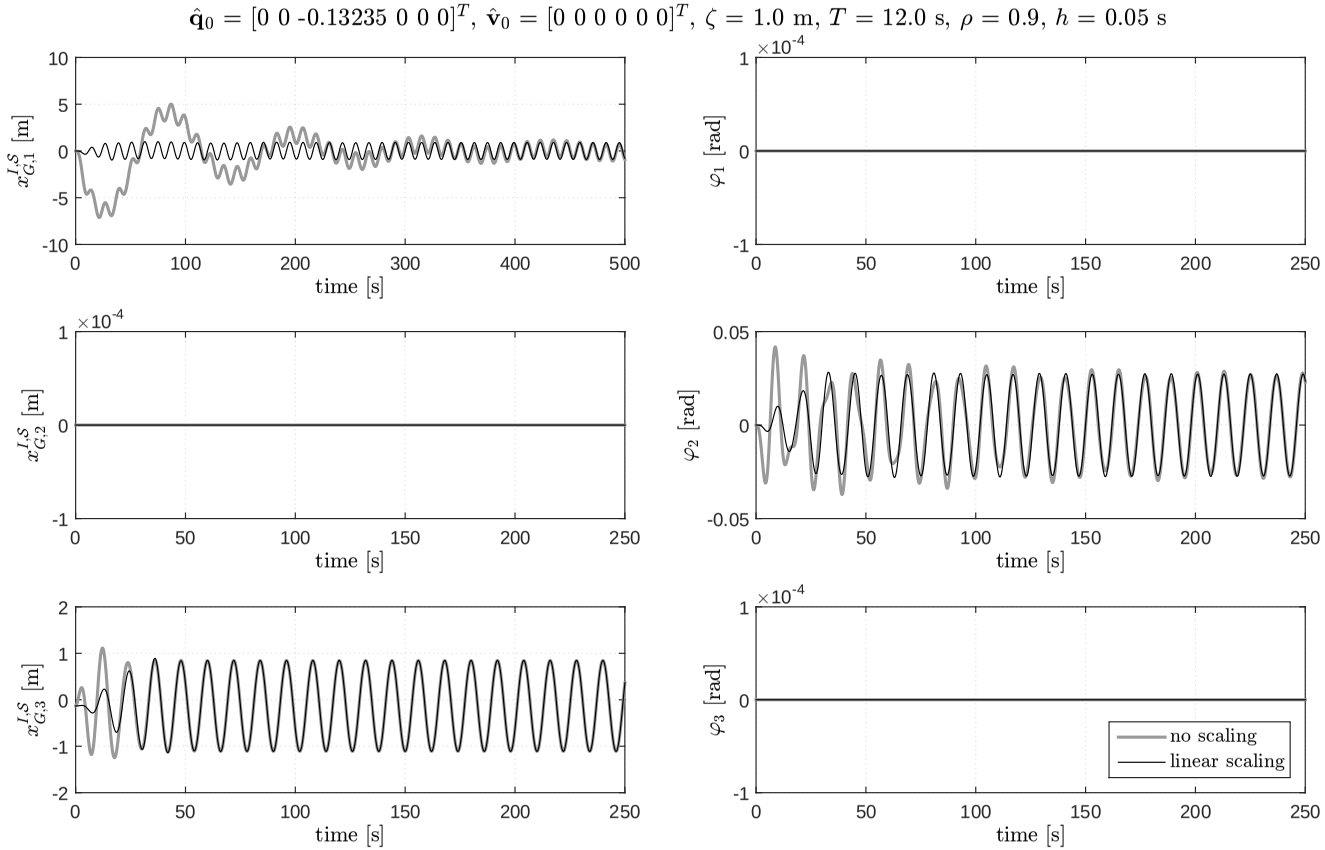

Figure 6.8: Initial transient; comparison between the time series obtained with and without a linear scaling strategy of the wave-excitation loads for a regular wave with period of 12.0 s directed along the x-axis. Analyses carried out with the Jonkman model for mooring lines and the steady regular model for waves.

the model assessing the mooring system loads, i.e. the loads at time t_{i+1} are computed only on the basis of the configuration at time t_i. The results (see Figure 6.9) are very interesting. In particular, a reduced time step size does not qualitatively improve the accuracy of the solution, so that a time step size $h = 0.05$ s seems to be a good compromise between the accuracy of the model and the computational effort, at least for the most practical cases. Moreover, the solution associated with a weak coupling strategy matches the time series obtained with a full coupling strategy without any appreciable loss of accuracy (after 1000 s of simulation the difference is on the third significant figure).

6.2.4.5 Remarks

The analysis of the operating behaviour of a floating platform should not include the initial transient associated with the initial conditions[20]. The duration of such transient depends on the period of the incoming waves and, in particular, on the corresponding hydrodynamic damping. Generally, long periods are associated with low damping, and the consequent transient expires after several seconds (hundreds). The strategy proposed can limit such undesired transient within the initial seconds of the time series and simply consists in scaling the forcing load in the first seconds of the simulation, making the load gradually reach its actual amplitude. Further tests revealed that such strategy is efficient also in the case of waves not directed along a principal axis of the system (see Figure 6.10) as well as for irregular waves or regular waves analysed assessing the radiation sub-problem by means of the Cummins approach. However, this strategy cannot avoid the transient due to the nonlinear coupling of some degrees of freedom associated with the operation of the mooring system and the combination of the rotational motion with the follower and non-follower interpretation of loads (see Section 6.4.1.2).

Furthermore, as known, the reduction of the time step size theoretically improves the accuracy of the numerical solution against an increase of the computational effort. However, for the most applications, a time step size of about 0.05 s can be considered sufficiently reliable. On the other hand, a weak coupling strategy, even if it seems to be rather reliable, should be used much more carefully because at each time step it implies an unbalanced dynamic equilibrium. Only for slowly varying motions a weak coupling can be considered sufficiently reliable.

6.2.5 Mooring line model

In Chapter 5 two different quasi-static models for the assessment of mooring line loads are discussed. In particular, considering the actual extensional stiffness of the lines together with the common range of displacements, and provided that the mooring line is long enough to ensure that a portion of the line (even infinitesimal) always lies on the seabed, the Faltinsen model (which assumes an infinite axial stiffness) and the Jonkman model exhibit just slight differences in terms of loads at the fairlead, so that they can be considered more or less equivalent. It is interesting to evaluate if such equivalence is valid also for the dynamic response of the coupled system.

Let's consider a homogeneous parallelepiped platform connected to a system of eight moorings (two for each vertex of the bottom) anchored to the seabed on a circle of

[20] If the hydrodynamic action is computed with the steady regular model, the initial transient should be discarded for sure because such model is not suitable for a detailed analysis of transients.

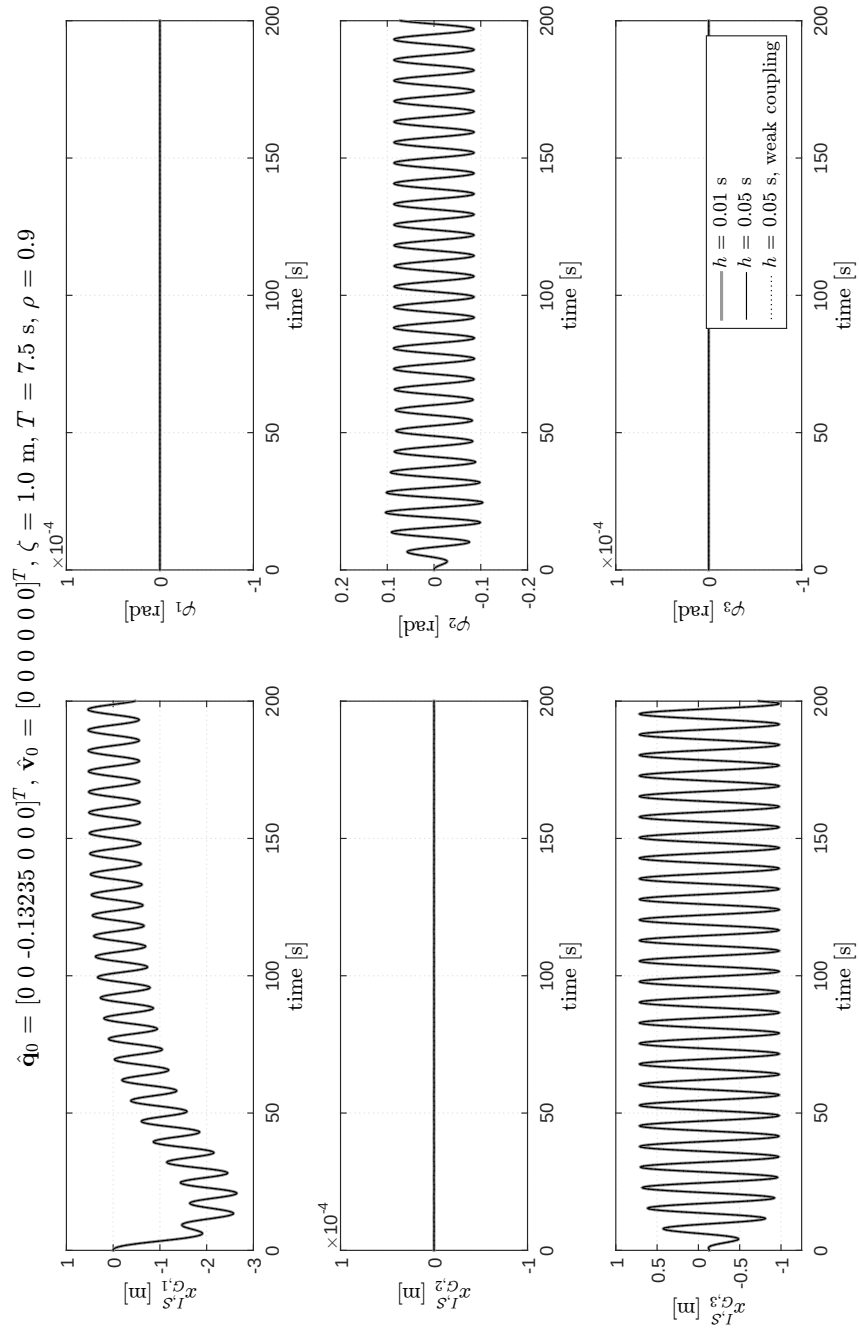

Figure 6.9: Effect on the dynamic response of the time step size and a weak coupling of the mooring system model. Analyses carried out with the Jonkman model for mooring lines and the steady regular model for waves.

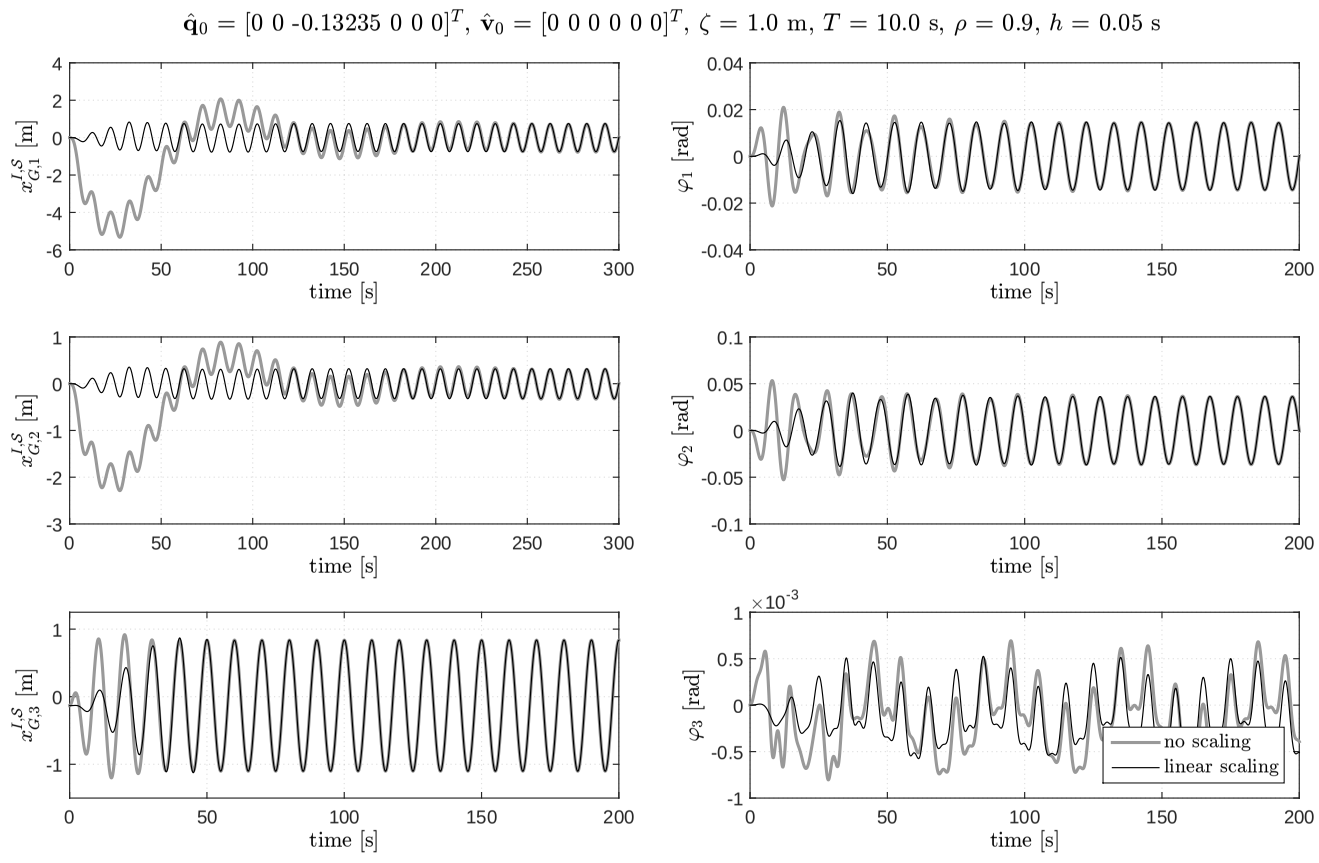

Figure 6.10: Initial transient; comparison between the time series obtained with and without a linear scaling strategy of the wave-excitation loads for a regular wave with period of 10.0 s directed 22.5 degrees with respect to the x-axis. Analyses carried out with the Jonkman model for mooring lines and the steady regular model for waves.

radius r_A with the layout described in Figure 6.1. The features of the system and of the environment are the same of the previous example, except the period $T = 8.0$ s of the incident regular wave, and are reported in Table 6.3. The effect of the mooring model on the dynamic response of the overall system is analysed in terms of displacements.

6.2.5.1 Results

The time histories of the displacements (see Figure 6.11) match to each other without any appreciable difference. Therefore, the two quasi-static models of the mooring lines can be considered equivalent also in terms of response of the coupled system, at least for ordinary extensional stiffness of the lines.

6.2.5.2 Remarks

Considering the current stiffness of the mooring lines, the quasi-static models of Jonkman and Faltinsen are definitely equivalent also in terms of dynamic response of the coupled system and can be indifferently used. The difference between the two time histories is on the fourth significant figure and can be considered negligible for the most purposes in civil engineering. However, if the lines have a weak stiffness the model of Jonkman is preferable even if it is slightly more time consuming.

6.3 Perturbation tests

In this section some perturbation tests are presented in order to prove the reliability and effectiveness of the coupled code. Both non-zero initial conditions, rectangular loads, and triangular loads are considered. The system must be stable to the perturbations, i.e. if the system is distanced from its static equilibrium configuration, the forces acting on the system itself should tend to restore the equilibrium. For a floating body, the restoring loads are associated with the mooring system (surge, sway, and yaw) and the hydrostatic action (heave, roll, and pitch)[21].

The main aim of this section is the verification of the stability of the system rather than a detailed study of the transients. Perturbations could always occur, for instance because of numerical errors, bad evaluation of the initial conditions, or an error in the computation of the loads. The stability to such perturbations ensures that the response is altered just within a transient. For these reasons the radiation sub-problem is simply modelled with constant hydrodynamic added mass and damping matrices (steady regular model). Therefore, the transients should be interpreted only qualitatively. With this approach, the perturbation tests are also useful to verify the reliability of the steady regular model and the mooring system model in restoring the steady condition.

6.3.1 Initial imposed displacements

A non-equilibrated initial condition on the displacements originates a transient motion that should run out in the neutral (unperturbed) equilibrium configuration. Let's consider a homogeneous parallelepiped platform connected to a system of eight moorings

[21] When the equilibrium configuration is perturbed, the system obeys a dynamic transient to return into the initial configuration. Since the body moves in absence of incident waves, in the framework of the linear theory, this is a radiation problem. For this reason in the following tests the hydrodynamic added mass and damping matrices are always considered. For the sake of simplicity they are estimated for a period of 9.0 s, just to somehow consider at least some damping necessary to limit the duration of the transients. However, because of the nature of the motion a rigorous approach requires the evaluation of the radiation sub-problem by means of the Cummins approach.

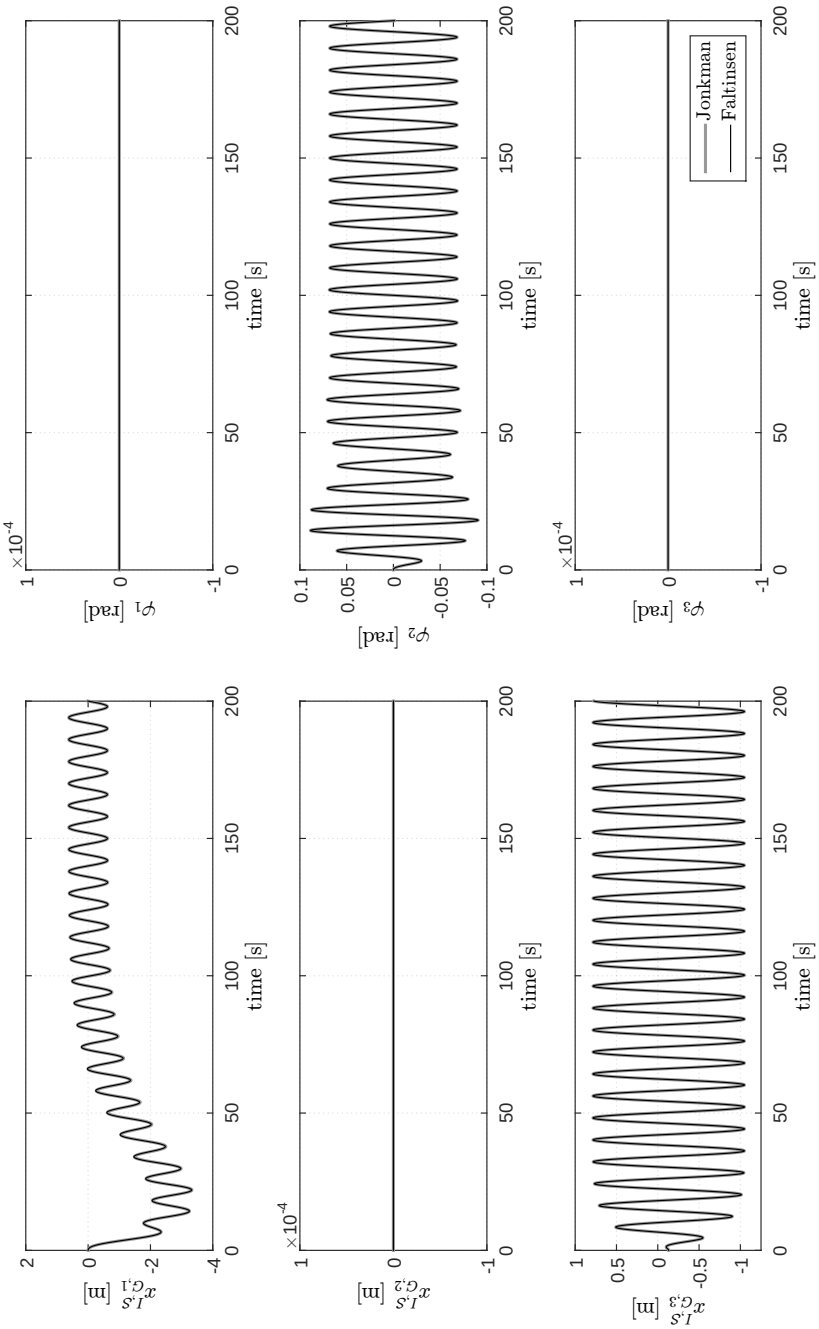

Figure 6.11: Mooring line model; comparison between the time series obtained with the coupling of different quasi-static models for mooring lines in the case of a regular wave directed along the x-axis. Analyses carried out with the steady regular model for waves.

(two for each vertex of the bottom) anchored to the seabed on a circle of radius r_A with the layout described in Figure 6.1. Let's assume that the floating body is subjected to gravity and mooring forces, whereas the hydrodynamic problem, in the framework of the linear theory, is restricted to the hydrostatic and the radiation sub-problems (absence of incident waves). The features of the system and of the environment are reported in Table 6.4. In order to have a much more comprehensible scenario, two different initial conditions on the displacements are analysed without mixing up translations with rotations, namely[22]:

- $\hat{\mathbf{q}}|_{t=0} = [0.5\ 0.5\ -0.13235\ 0\ 0\ 0]^T$ m|rad;
- $\hat{\mathbf{q}}|_{t=0} = [0\ 0\ -0.13235\ 0.05\ 0.05\ 0]^T$ m|rad.

Note that these perturbations are rather small in magnitude.

6.3.1.1 Results

The system after a transient (see Figure 6.12) due to the initial conditions returns in the neutral equilibrium configuration exhibiting a stable behaviour. Note that the initial condition on the rotational vector produces a non null initial yaw angle even if the term ψ_3 is zero. The consequent yaw perturbation attenuates very quickly. The interpretation of such a transient is rather complex because of the nature of the rotational motion. The stronger attenuation of the yaw angle with respect to roll and pitch angles is also due to geometrical reasons; in particular, it should be noted that if the initial rotational vector is doubled, the corresponding yaw angle has a larger increment. Moreover, the yaw motion has a residual oscillation (not appreciable in the plot) associated with the small hydrodynamic damping term D_{66}, even if such oscillations are very small in amplitude and negligible in practical cases.

6.3.1.2 Remarks

Generally, the stable behaviour to non-equilibrated (in static terms) initial conditions is very important to ensure that any numerical perturbation do not strongly affect the solution. Moreover, the corresponding transients should be reasonably short because are like a background noise that cannot always be easily filtered. The results reported in this section should be interpreted also considering the effective magnitude of the perturbations employed in the analysis (expected numerical errors are usually smaller).

The system, in the framework of the steady regular model, exhibits a stable behaviour. The transients require at least one hundred seconds to reasonably run out, even if the yaw motion has a residual oscillation that needs a long transient to expire. Maybe the hydrodynamic damping is not sufficient to ensure a complete restoring of the equilibrium. Furthermore, because of such small damping, the yaw motion could be affected by numerical amplification (negative damping). Although such amplification is very small, it can be avoided by increasing the numerical damping or reducing the time step size.

6.3.2 Rectangular function

Another interesting perturbation test deals with a sudden increase of the load (both force and torque) acting on the system, modelled as a rectangular function. Let's

[22] The initial conditions on the vertical location of the center of mass correspond to the neutral heave of the coupled system. Moreover, the stability to heave unbalanced initial conditions is analysed in Section 6.2.2 together with the calibration of the initial configuration.

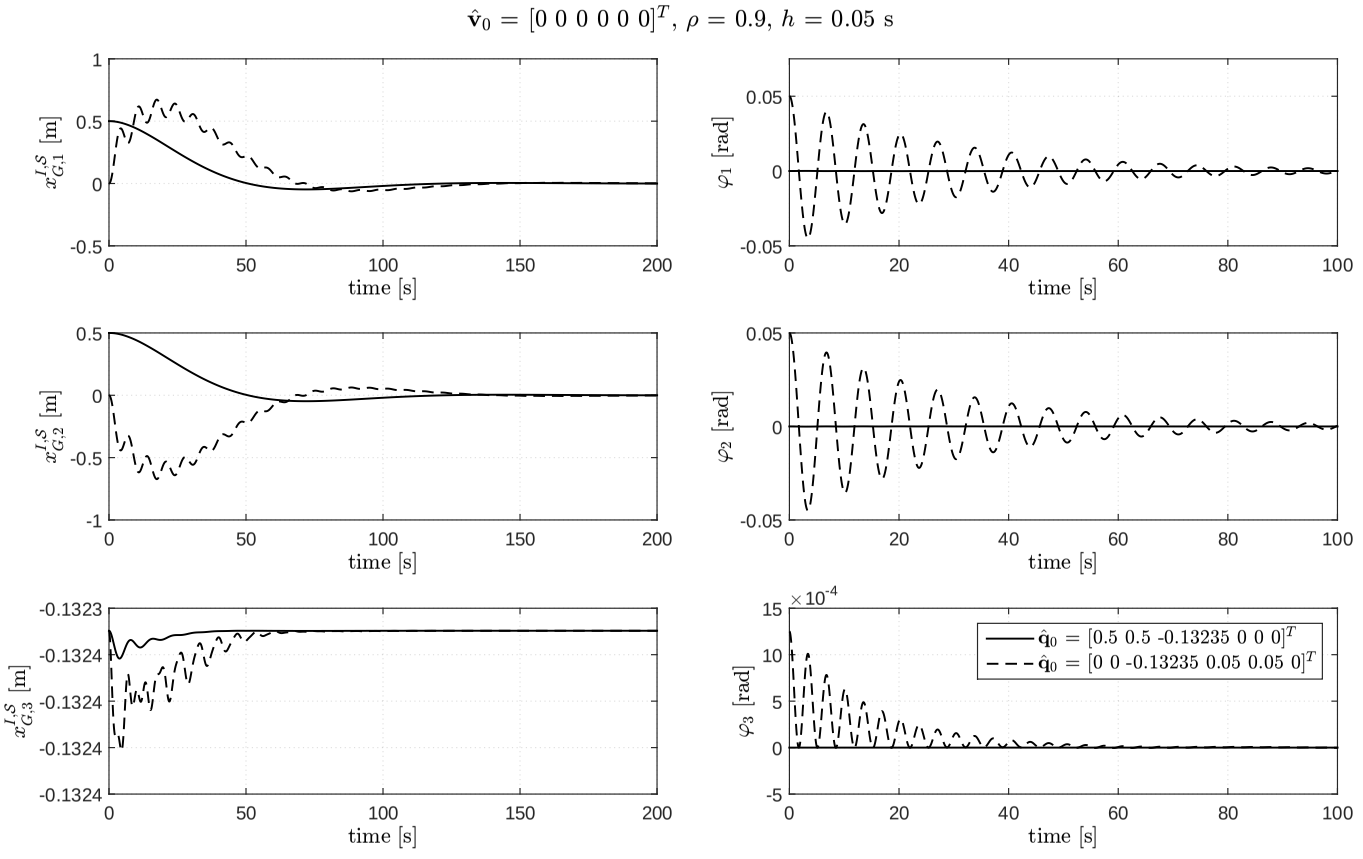

Figure 6.12: Perturbation with initial imposed displacements; transients of the system to restore the equilibrium when either the location of the center of mass or the orientation of the body are varied. Analyses carried out with the Jonkman model for mooring lines and the steady regular model for the radiation and hydrostatic sub-problems.

environment		
gravity acceleration, g	9.807	m/s^2
water density, ρ_w	1 025	kg/m^3
water depth, d	150.0	m
seabed friction coefficient, ξ_b	0.5	-
hydrodynamic operators		
period, T	9.0	s
floating platform		
length along x', a	40.0	m
length along y', b	40.0	m
height, c	10.0	m
mass, m	5 998.538	t
moment of inertia about x', J_{11}	$8.4979 \cdot 10^5$	$t{\cdot}m^2$
moment of inertia about y', J_{22}	$8.4979 \cdot 10^5$	$t{\cdot}m^2$
moment of inertia about z', J_{33}	$1.5996 \cdot 10^6$	$t{\cdot}m^2$
draft, h_{imm}	3.6576	m
location of the center of mass with respect to the sea water level, $\mathbf{x}_G$	$[0\ 0\ 1.3424]^T$	m
neutral configuration (Jonkman mooring model), $\hat{q}_3\|_{t=0}$	-0.13235	m
moorings		
number, n_c	8	-
diameter, D_c	0.1454	m
unstretched length, l	460	m
mass density, μ_c	130.4	kg/m
extensional stiffness, EA	$589{\cdot}10^6$	N
radius to fairleads, r_F	28.28	m
radius to anchors, r_A	423.4	m

Table 6.4: Parameters adopted for the perturbation tests.

consider a moored floating rigid body with the same features described in Section 6.3.1 (see Table 6.4). The perturbations considered are given by:

- non-follower rectangular force $F^{\mathcal{S}}_{G,1}$ along the x-axis applied to the center of mass G (see Figure 6.13(a));
- follower rectangular torque $T^{\mathcal{M}}_{G,2}$ about the y'-axis applied to the center of mass G (see Figure 6.13(b)).

6.3.2.1 Results

If the system is perturbed by a rectangular external force (see Figure 6.14), it returns to the initial equilibrium configuration after a transient of about two hundred seconds, whereas in the case of rectangular torque the transient is of about one hundred seconds. These differences are mainly due to the different hydrodynamic damping factors of

surge and pitch motions. Although the system is not forced along the z-axis, the operation of the mooring system, in particular the modification of the configuration of the lines associated with surge and pitch motions, causes an unbalanced vertical load that produces heave displacements. The system, in the framework of the steady regular model, exhibits a stable behaviour.

6.3.3 Triangular function

In this case the sudden increase of the loads is substituted with a ramp; therefore, the loads are modelled as triangular functions. Let's consider a moored floating rigid body with the same features described in Section 6.3.1 (see Table 6.4). The perturbations considered are given by:

- non-follower triangular force $F^{\mathcal{S}}_{G,2}$ along the y-axis applied to the center of mass G (see Figure 6.15(a));
- follower triangular torque $T^{\mathcal{M}}_{G,1}$ about the x'-axis applied to the center of mass G (see Figure 6.15(b)).

6.3.3.1 Results

If the system is perturbed by a triangular external force (see Figure 6.16), it returns to the initial equilibrium configuration after a transient of about two hundred seconds, whereas in the case of triangular torque the transient is of about one hundred seconds. The duration of the transients is definitely similar to those observed for a rectangular load. In fact, the hydrodynamic damping factors of sway and roll motions are equal respectively to the damping factors of surge and pitch motions, because of the symmetry of the floating body. The system, in the framework of the steady regular model, exhibits a stable behaviour.

6.3.3.2 Remarks

The main dynamic model, coupled with the mooring system model and the steady regular model for the evaluation of the hydrostatic and radiation loads, exhibits a stable behaviour when subjected to load perturbations of both rectangular and triangular shape. The duration of the transients is strongly affected by the hydrodynamic damping, which generally depends on the frequency of the oscillations.

For the sake of simplicity the tests were carried out with a constant hydrodynamic damping (and added mass) matrix in the framework of the steady regular model, regardless of the oscillatory frequencies of the system. However, for a detailed analysis of the transients it is necessary the use of the Cummins approach.

6.4 Moored floating platform

In this section the coupled code is used to analyse the influence of some parameters, which characterize both the system and the environment, on the dynamic response of a moored floating platform. Let's consider a parallelepiped platform with square basis connected to a system of eight moorings (two for each vertex of the bottom) anchored to the seabed on a circle of radius r_A with the layout described in Figure 6.1, the same of the previous examples. In particular, the effect of different periods, amplitudes, and directions of the incident regular wave is analysed together with the effect of the mass of the floating body, its distribution (homogeneous or ballast-like), and the length of

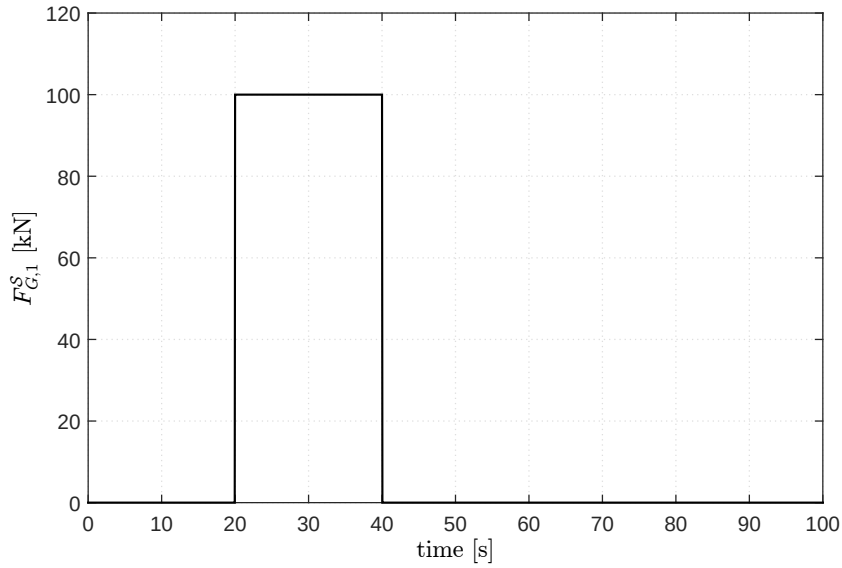

(a) force

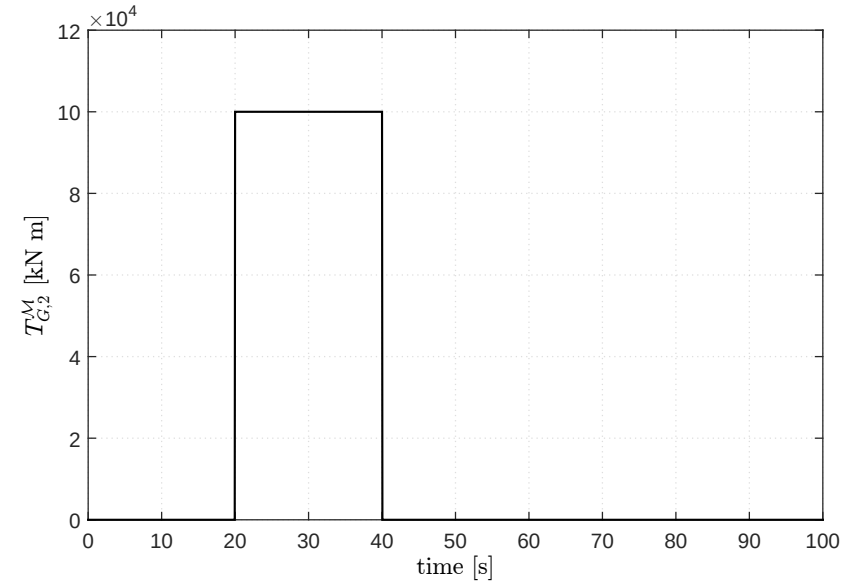

(b) torque

Figure 6.13: Time series of the loads modelled as rectangular functions.

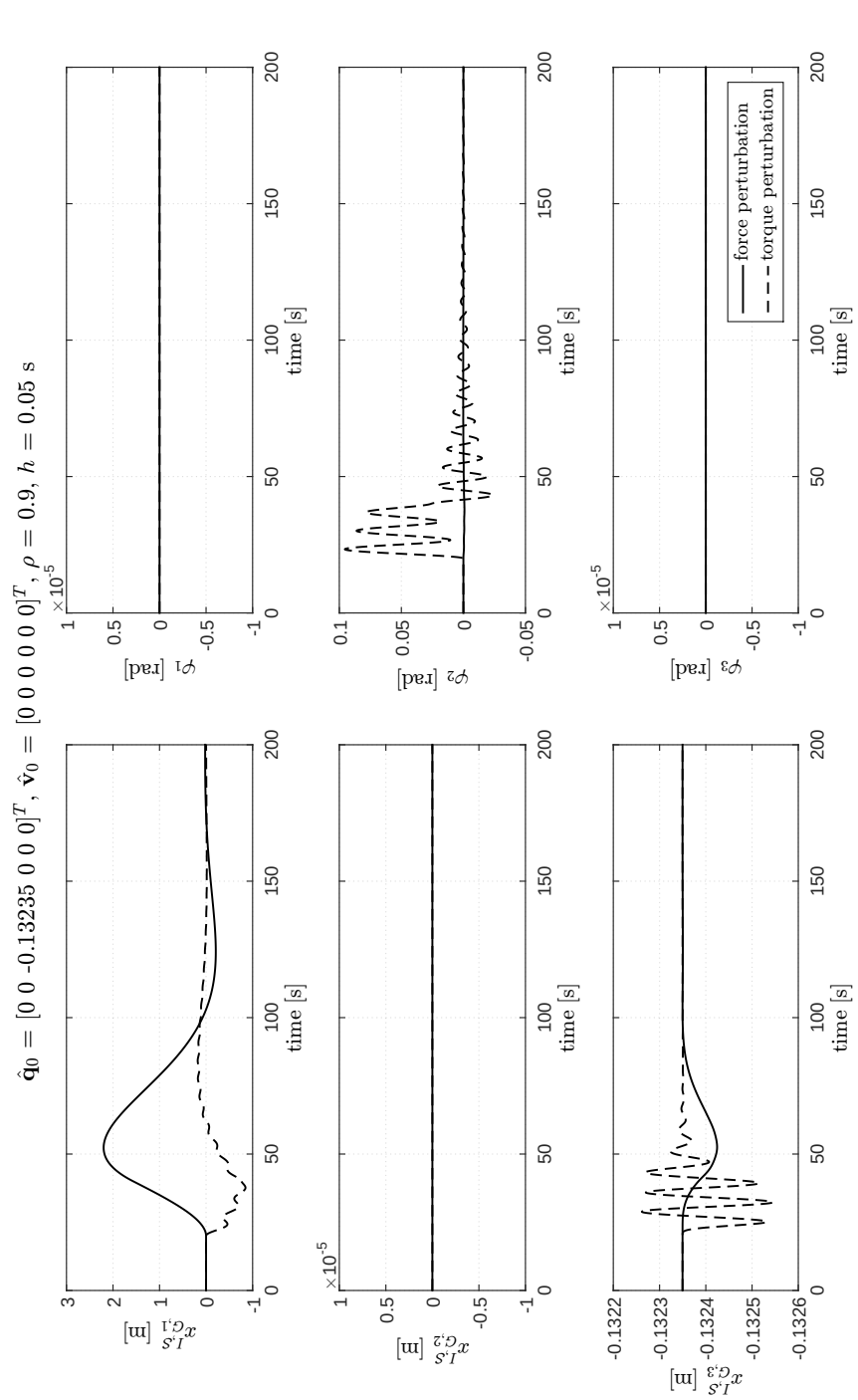

Figure 6.14: Perturbation with a rectangular load; transients of the system to restore the initial equilibrium. Analyses carried out with the Jonkman model for mooring lines and the steady regular model for the radiation and hydrostatic sub-problems.

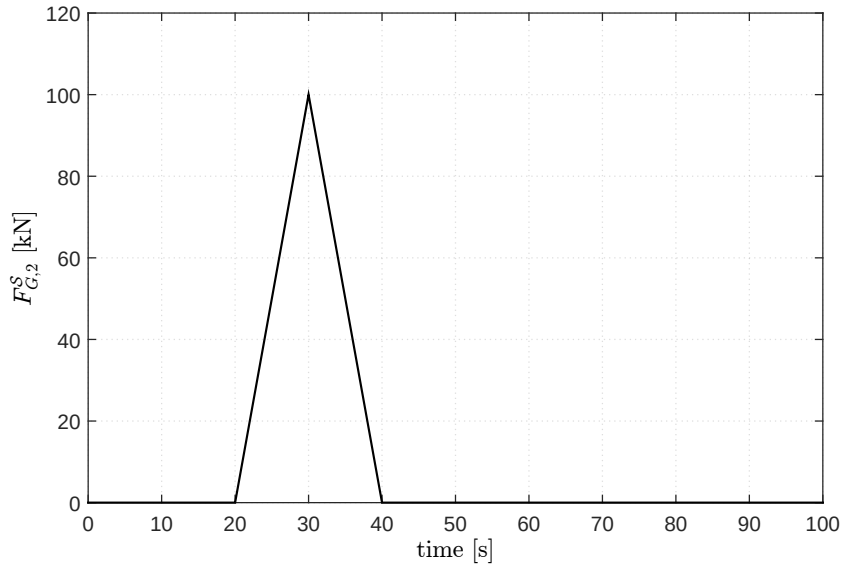

(a) force

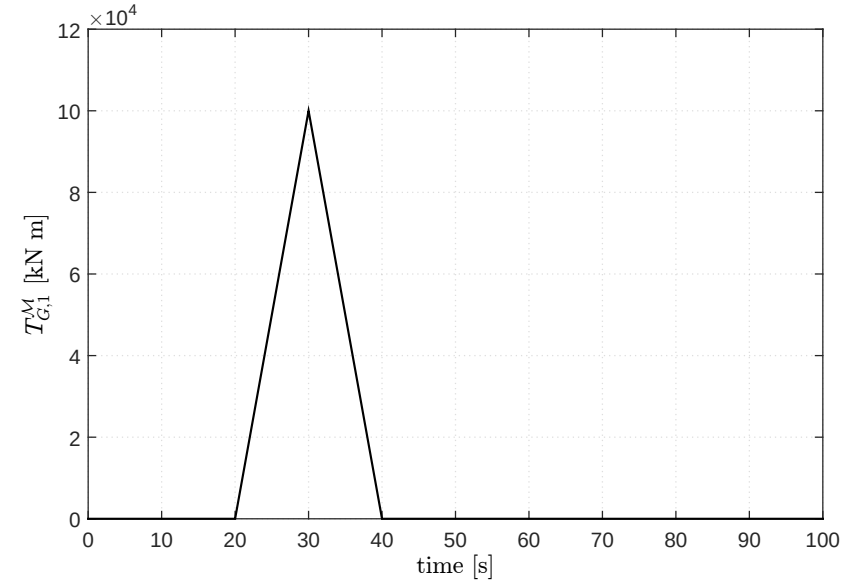

(b) torque

Figure 6.15: Time series of the loads modelled as triangular functions.

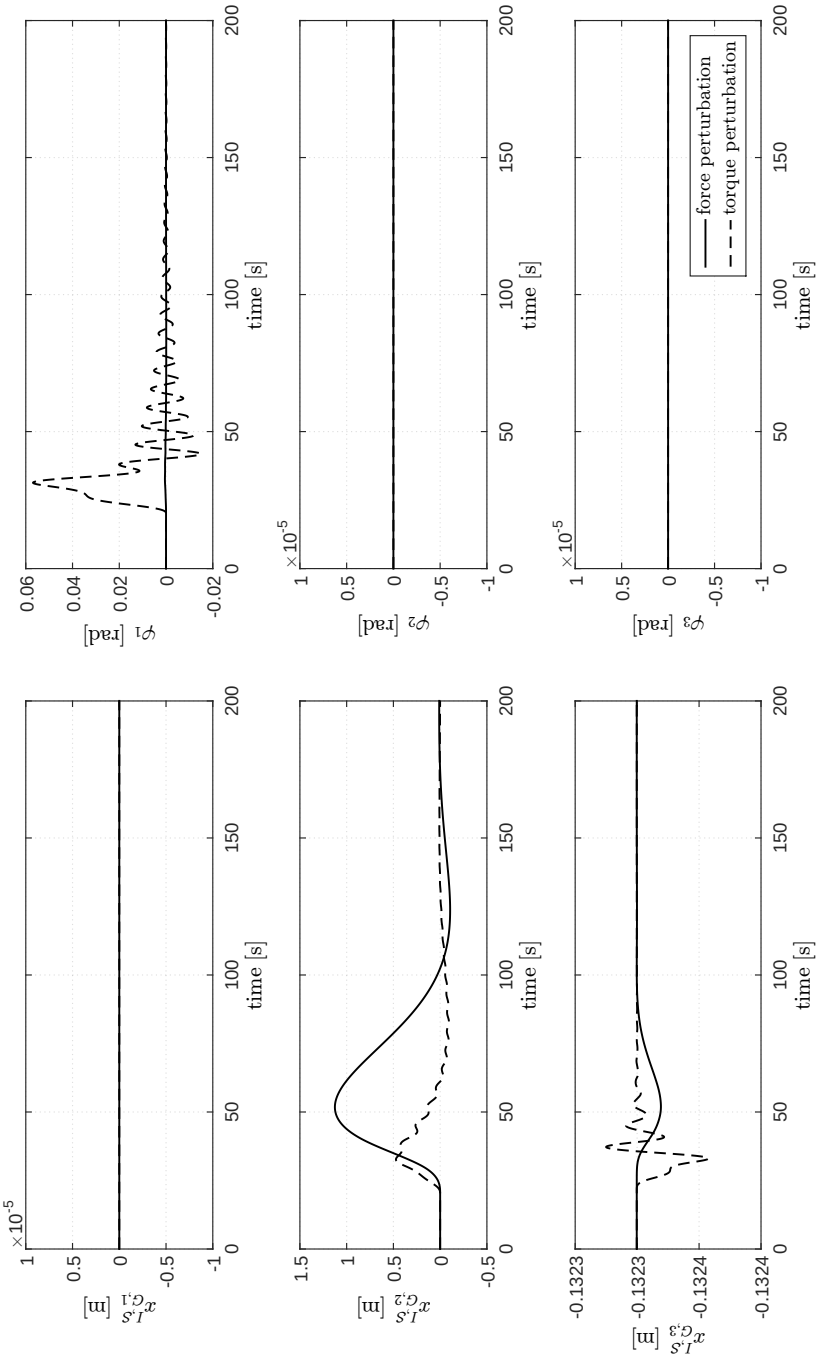

Figure 6.16: Perturbation with a triangular load; transients of the system to restore the initial equilibrium. Analyses carried out with the Jonkman model for mooring lines and the steady regular model for the radiation and hydrostatic sub-problems.

environment		
gravity acceleration, g	9.807	m/s^2
water density, ρ_w	1 025	kg/m^3
water depth, d	150.0	m
seabed friction coefficient, ξ_b	0.5	-
floating platform		
length along x', a	40.0	m
length along y', b	40.0	m
height, c	10.0	m
moorings		
number, n_c	8	-
diameter, D_c	0.1454	m
mass density per unit length, μ_c	130.4	kg/m
extensional stiffness, EA	$589{\cdot}10^6$	N
radius to fairleads, r_F	28.28	m
radius to anchors, r_A	423.4	m

Table 6.5: Common parameters adopted for the parametric analysis of the moored floating platform.

the lines. All the analyses refer to the same geometry of the platform and the same layout of the mooring system (location of fairleads and anchors) as well as the same depth of the seabed and the same material of the lines, reported in Table 6.5[23].

The response of the system is evaluated in terms of maximum displacements (translations and rotations) per unit wave amplitude about the static equilibrium configuration, which is usually called *response amplitude operator RAO*, namely[24]:

$$RAO_i = \frac{\max_{t>T_w} |\hat{\mathbf{q}}(t) \circ (-\hat{\mathbf{q}}_0)|_i}{\zeta} \tag{6.7}$$

where T_w is the discarded initial window. The *RAO* undoubtedly depends on the frequency of the incident regular wave and should be evaluated after the end of initial transients.

6.4.1 Period, direction, and amplitude of the wave

The influence of the wave period on the dynamic response of a moored floating platform is evaluated for a series of regular waves, together with the effect of the direction of the incident wave and its amplitude[25]. Let's consider a mooring system made of lines

[23] Note that these common features are the same adopted in the previous examples and correspond (more or less) to the characteristics of the floating support used in [46] for an offshore wind turbine.

[24] Note that the *RAO* is usually defined for linear systems. However, in this context, the definition is extended also to nonlinear systems (moored floating platforms) as a measure of the absolute maximum steady response in the case of regular waves.

[25] Almost all the periods and the amplitudes of the waves used for the analyses are selected in or close to the range of validity of the linear wave theory (see Figure 4.11). Just for the smaller periods or larger amplitudes the sea state is out of the linear limit.

of length $l = 460$ m connected to a homogeneous platform with weight established so that the mass of the overall mooring system is the 8% of the mass of the platform, i.e. $m = 5\,998.538$ t.

6.4.1.1 Results

For the sake of simplicity let's assume that the system is weakly nonlinear (small displacements) and that the displacements are uncoupled to each other. In this scenario, each displacement can be associated with its own natural frequency, which depends on the properties of the floating body (mass and inertia), on the hydrodynamic added mass (generally frequency-dependent), and on the stiffness of the coupled system provided by hydrostatic and mooring restoring loads. Although the real system is not exactly linear[26] and some motions are coupled to each other because of the hydrodynamic action, the mooring system, and the combination of the rotational motion with a follower or non-follower interpretation of loads, such an estimation of the natural frequency can be considered rather reliable[27] and useful for many qualitative analyses.

In this context, the results should be interpreted considering the amplification effect due to resonant-like phenomena close to the natural frequencies of the system. The stiffness related to surge motions is given only by the mooring system and is generally relatively weak, i.e. large natural period. The corresponding RAO_1 grows with the period of the incoming wave (see Figure 6.17(a)), except at high frequencies where the response has a minimum (typical of barge platforms). By contrast the stiffness related to pitch motions is mainly given by the diagonal term of the hydrostatic stiffness matrix, which is generally rather large (barge platforms). The resonant-like phenomena are therefore observed in the typical range of wave frequencies (about 0.1 Hz); for instance, the system analysed has a strong amplification of the pitch response at about 6.0 s (see Figure 6.17(b)). The behaviour of the system against different amplitudes of the waves (see Figure 6.17) is nearly linear as long as the displacements can be considered small, i.e. in the range of validity of the linear wave theory. However, because of the coupling of the platform motions, the response highlights some slight nonlinearities which could become non-negligible when the system undergoes large motions, especially large rotations.

Finally, the excited degrees of freedom depend on the direction of the incident regular wave. If the wave is parallel to the xz-plane, only surge, heave, and pitch motions are excited. By contrast, a wave directed 22.5 degrees with respect to the x-axis (see Figure 6.10) excites all the degrees of freedom.

6.4.1.2 Coupling of platform motions

Different degrees of freedom of the system are coupled to each other because of the hydrodynamic action, i.e. extra-diagonal terms of the added mass and damping matrices, the mooring system model, and the combination of the rotational motion with a

[26] The nonlinear character of the differential problem of the coupled system is due to the mooring line model and the non-follower interpretation of the hydrodynamic operators, together with the nonlinearities associated with the rotational motion about an arbitrary axis and the conservation of the angular momentum. However, for small oscillations, in particular for small rotations, the system can be considered weakly nonlinear with good approximation, at least in the neighbourhood of the mean configuration.

[27] Note that if some motions are coupled to each other, it is much more proper to talk about natural frequencies of the system, which can involve more than an elementary motion.

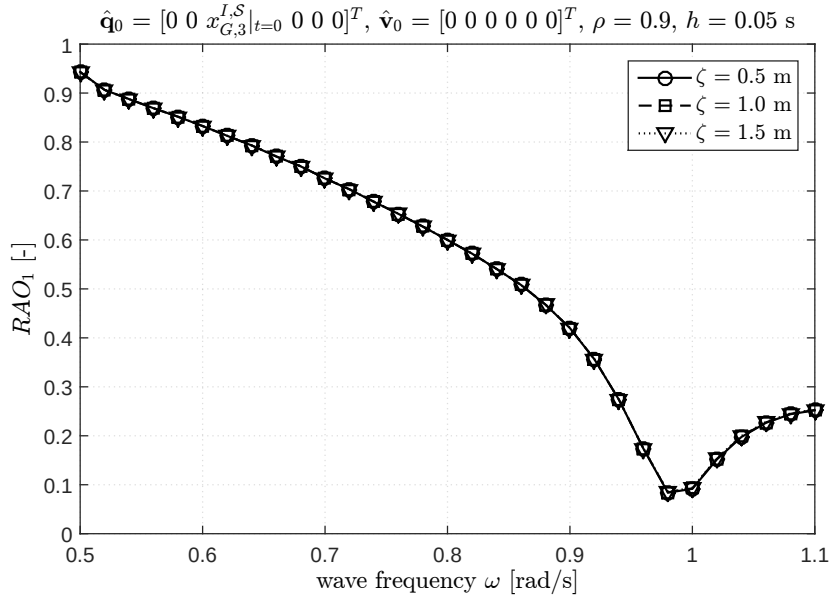

(a) surge

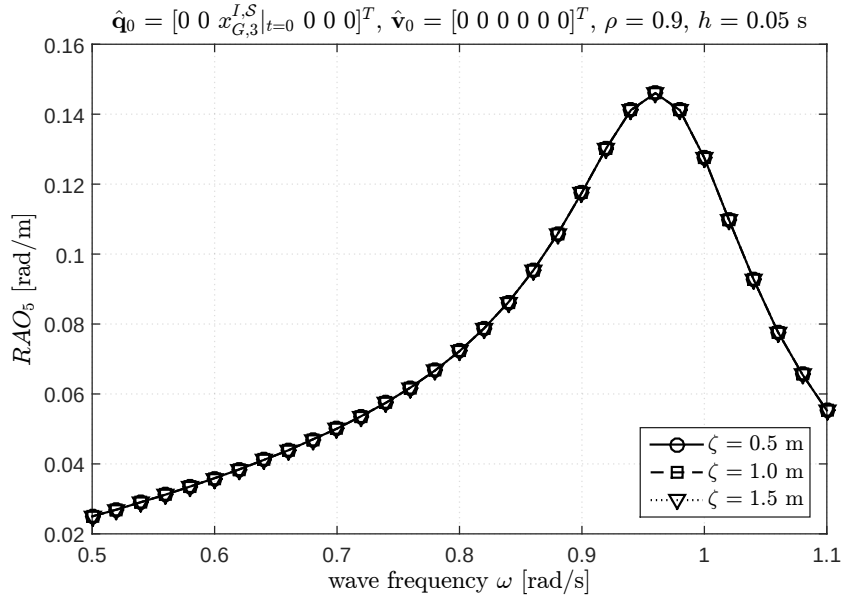

(b) pitch

Figure 6.17: Response of the moored floating platform against the frequency of the incident wave for different wave amplitudes. Waves directed along the x-axis.

follower or non-follower interpretation of loads[28]. The coupling effect associated with the mooring system and the rotational motion is very insidious to understand because of its nonlinear character.

Let's consider the mooring lines, the coupling effect can be explained considering that the restoring action of the mooring system (in the framework of quasi-static models) depends on the location of the fairleads with respect to the anchors. Even in the case of an elementary displacement involving only one degree of freedom, the resulting restoring loads can excite also the unperturbed degrees of freedom (see Section 5.4.3), i.e. different motions are coupled to each other. The coupling becomes misleading if, for reason of symmetry, the load does not change its sign according to the displacement[29] with a consequent unbalanced mean value that, for oscillating motions, forces the system into a new mean equilibrium configuration. The behaviour of the mooring system becomes much more complex to explain if different motions occur simultaneously, and consists of two main coupling effects: a variation of the stiffness for positive and negative excursions of some degrees of freedom and the aforementioned change of the mean configuration. For instance, if the body contemporary undergoes oscillating heave and surge motions at the same frequency, the elevation of the fairleads for positive excursions along the x-axis is always different from the elevation associated with negative excursions, resulting into an asymmetric stiffness of the mooring system (and consequent asymmetric response). Similar considerations can be made also including other motions.

Let's consider the rotational motion. A follower force changes its components with respect to the fixed reference frame according to the rotation of the body. In the case of sinusoidal rotations and sinusoidal follower forces at the same frequency, the components of the force with respect to the inertial frame could be rather different from the original load because the rotation is a nonlinear operation[30]. The resulting load mainly depends on the amplitude of the rotation and the out-of-phase between the rotation and the force. Typical effects of such coupling are harmonic forces with non-zero mean value, an approximately doubling of the frequency, a variation of the shape of the load. However, these effects are strongly reduced for small amplitudes of the rotation. Similar considerations can be made for non-follower torques. Of course this coupling is very complex because also the loads affect the rotational motion and becomes even more complex in the case of the direct coupling of different degrees of freedom due to the extra-diagonal terms of the main operators[31].

[28] The degrees of freedom could be coupled to each other also if the body-attached frame has not its origin in the center of mass. In fact, in this condition the static moment does not vanish. Moreover, even when the origin is in the barycentre of the body, the reference frame should be principal to ensure that the inertia tensor is diagonal.

[29] For instance see the parabolic trend of the vertical force in Figures 5.10 and 5.11.

[30] Let's think to a sinusoidal follower force along the x'-axis combined with a sinusoidal rotation (with amplitude less than $\pi/10$ rad) about the y-axis at the same frequency. The resulting load with respect to the inertial frame is a sinusoidal-like force along the x-axis with the same frequency of the original load and a sinusoidal-like force along the z-axis with a double frequency and a mean value that can be rather different from zero (depending on the out-of-phase between the rotation and the force). This combination of the rotational motion with follower forces couples different degrees of freedom. Similar considerations can be made in the case of non-follower torques and involving more components and more degrees of freedom.

[31] Note that because of the coupling associated with the extra-diagonal terms of the hydrodynamic added mass and damping matrices, the angular velocity and angular accelerations are similar to follower forces even if this interpretation is rather complex because such quantities are somehow related to the rotation of the body.

For moored floating platforms in ordinary conditions, the effects of such couplings are mainly unbalanced forces that bring the system into a new mean dynamic configuration different from the static one, whereas the contribution to the response spectrum of the oscillations at higher frequencies is usually negligible. The coupling effect due to the mooring system and the rotational motion is much more relevant when all the degrees of freedom are excited, i.e. wave misaligned with respect to the vertical plane of symmetry of the system (see figure 6.18[32]) and can be accentuated by the non-diagonal system operators.

6.4.2 Mass of the platform

Let's consider a mooring system made of lines of length $l = 460$ m connected to a platform with the weight established so that the mass of the entire mooring system is either the 4%, or 8%, or 12% of the mass of the platform. Let's consider also three different distributions of the mass, namely:

- (case 1) body made of two homogeneous parts, the lower part takes up one-third of the height and contains the 60% of the overall mass, as if in the platform there is a sort of ballast;
- (case 2) homogeneous body;
- (case 3) body made of two homogeneous parts, the lower part takes up two-third of the height and contains the 40% of the overall mass, as if the platform supports an additional body rigidly connected to the top surface.

Note that these distributions are associated with different locations of the overall center of mass.

6.4.2.1 Results

An increase of the mass (see Figure 6.19) of the platform is always associated with a shifting of the resonant-like phenomena towards the low frequencies (high periods). In this sense, the increase of the weight could be considered to distance the natural frequencies of the system from the typical periods of the incident wave. However, only small adjustments are possible without changing the geometry of the platform[33].

Different distributions of the mass within the same geometry (see Figure 6.20) have relevant effects in the neighbourhood of the resonance of pitch motions. In particular, an heavier bottom can reduce the maximum rotation, even if the surge displacement is slightly amplified.

6.4.3 Length of the lines

The length of the lines influences the stiffness of the mooring system and thus the natural frequencies of the floating body. Generally, shorter lines are associated with stiffer moorings. Let's consider a homogeneous platform of mass $m = 5\,998.538$ t connected to a mooring system made of lines of three different lengths, namely 450 m, 460 m, and 470 m (see Figure 6.21).

[32] In Figure 6.18 the coupling effect is amplified because the forcing torque is very close to the natural frequency of the system involving pitch and roll rotations. Generally such a relocation of the mean configuration is not so evident. For the sake of comparison see Figure 6.10.

[33] The buoyancy should always balance the weight; therefore, there is an upper limit on the increase of the mass. If the geometry of the platform changes, also the hydrostatic stiffness changes, and the benefits associated with the variation of the mass can vanish.

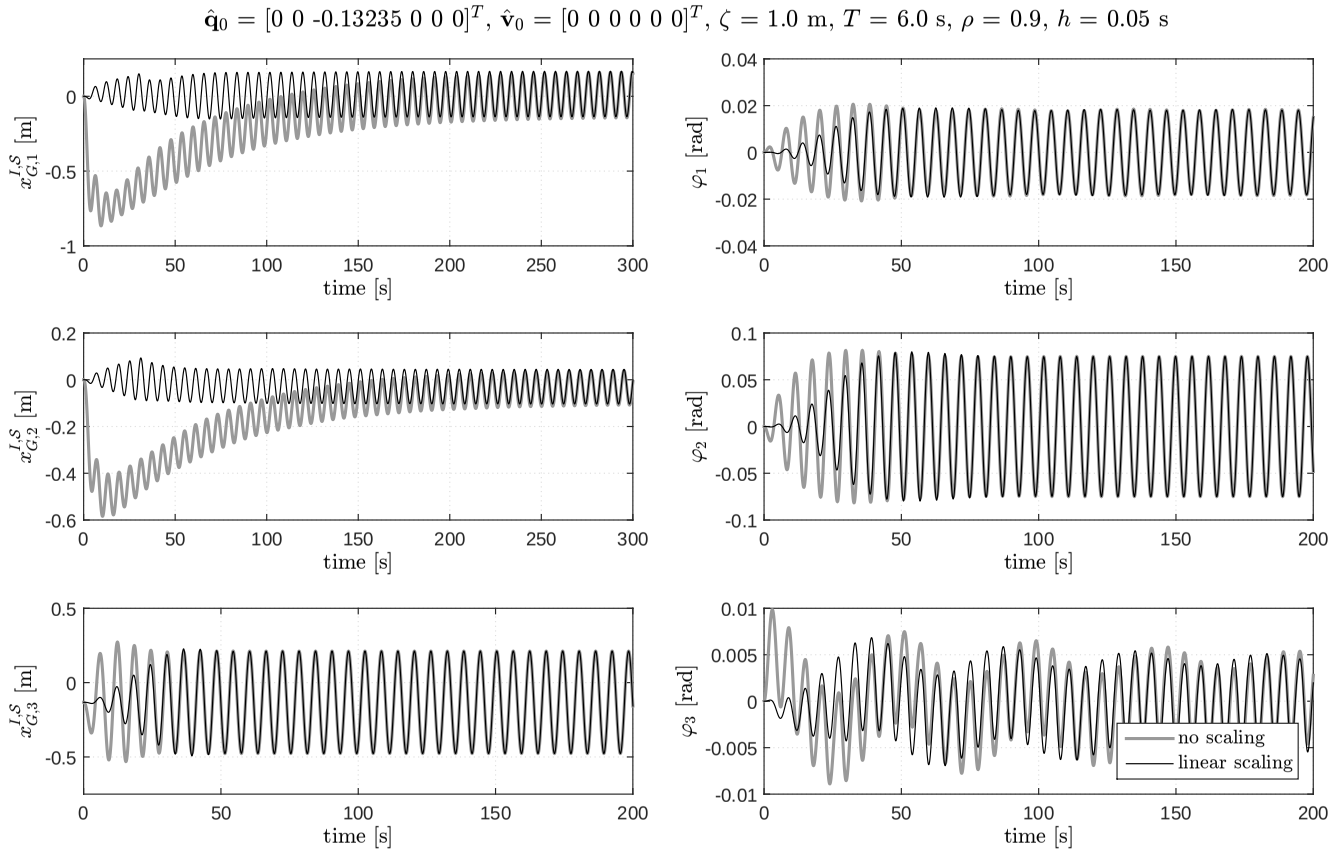

Figure 6.18: Transient due to both the initial conditions and the unbalanced loads associated with the coupling of different degrees of freedom; comparison between the time series obtained with and without a linear scaling strategy of the wave-excitation loads for a regular wave with period of 6.0 s directed 22.5 degrees with respect to the x-axis. Analyses carried out with the Jonkman model for mooring lines and the steady regular model for waves.

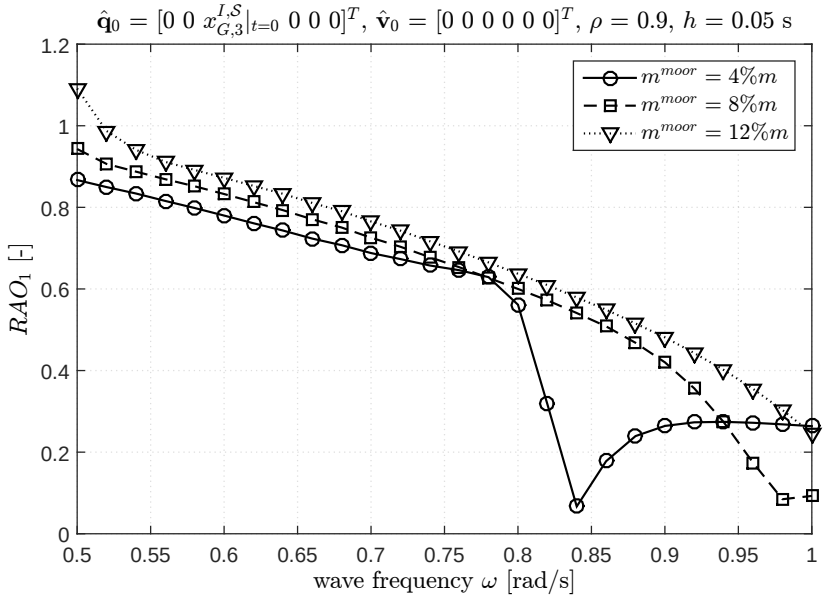

(a) surge

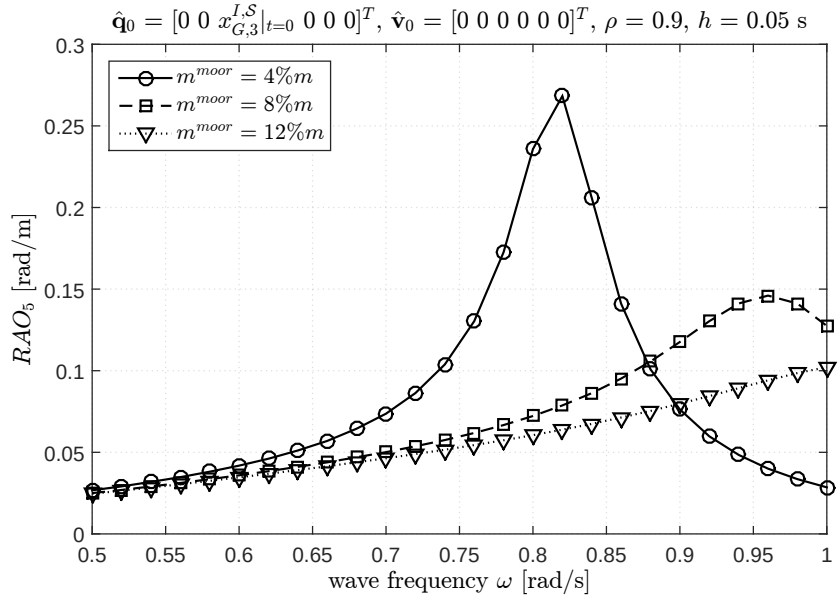

(b) pitch

Figure 6.19: Response of the moored floating platform against the frequency of the incident wave for different masses of the floating body. Case of homogeneous platforms with waves directed along the x-axis.

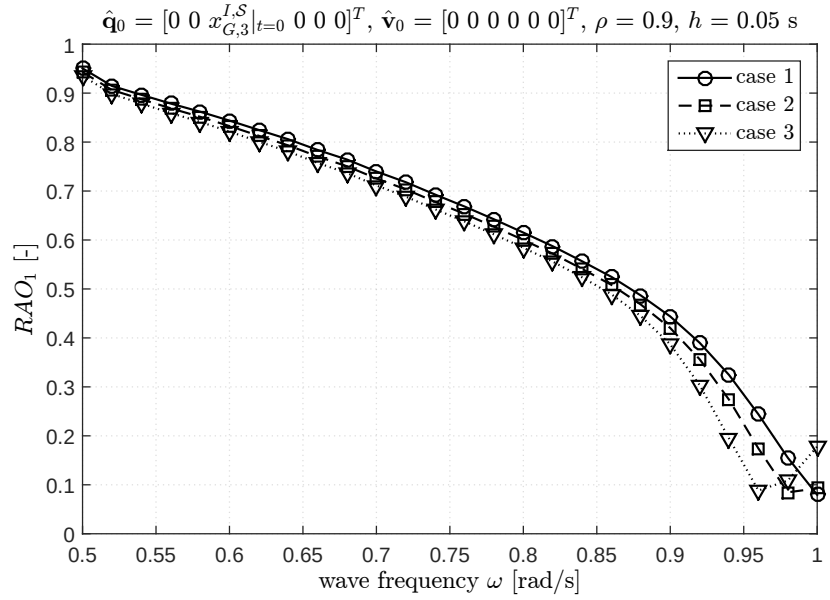

(a) surge

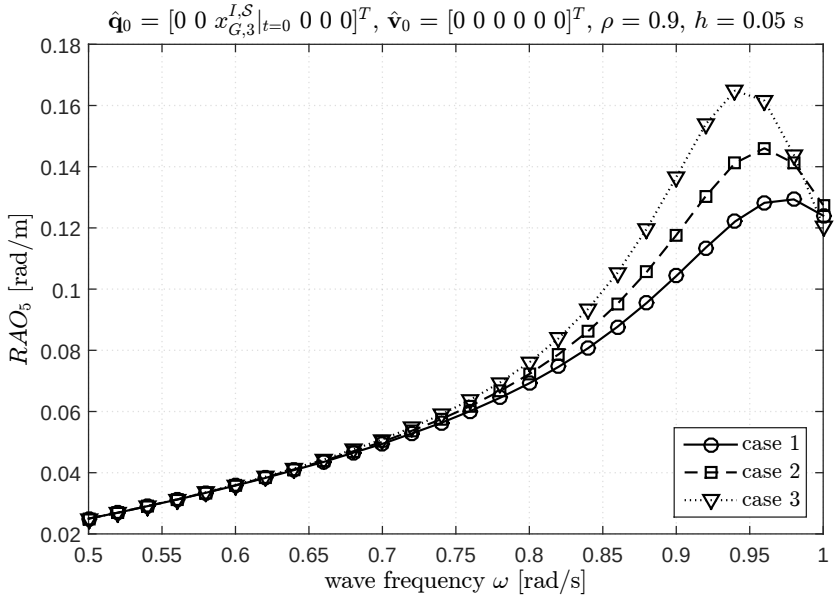

(b) pitch

Figure 6.20: Response of the moored floating platform against the frequency of the incident wave for different distributions of the mass of the floating body. The mass of the mooring system is the 8% of the mass of the platform and the waves are directed along the x-axis.

6.4.3.1 Results

The choice of the optimum length of the lines should consider two different aspects. The first one is related to the response of the system in terms of excited natural frequencies; an increase of the length is generally associated with larger natural periods. The second aspect is much more related to technological and technical issues of the connection of the lines to the platform and to the seabed. In particular if the lines are not long enough to rest on the seabed, the anchor is subjected also to vertical actions that need a proper design of the foundations. Moreover, a shorter line is also subjected to higher tensions, which should be considered in the design of the connection devices. By contrast, a reduction of the length of the lines providing that a portion still rests on the seabed can improve the economical framework of the project.

6.4.4 Remarks

Although it is not possible to draw general conclusions because of the strong case-dependence of such devices, some indications for their design can be addressed. The dynamic response of a moored floating platform is affected by the natural frequencies of the system, which could be in the typical range of frequencies of the incident wave. This is the case of barge floating platforms for which heave, roll, and pitch motions are usually excited by rather small periods because of the extended surface (in terms of aerial projection) interacting with the fluid (large hydrostatic stiffness). In fact, the natural period related to such motions mainly depends on the geometry of the body (inertia and dimensions) and the interaction with the fluid through the hydrodynamic added mass matrix and hydrostatic stiffness (in a first-order model). By contrast, surge, sway, and yaw motions are generally excited by longer natural periods because the only source of stiffness is the mooring system, and it is usually not so high.

In this context, an increase of the overall mass of the system shifts the resonance frequency towards lower frequencies and should evaluated on the basis of the specific features of the environment. On the other hand, a reduction of the length of the cables increases the stiffness of the mooring system. The dependence of the system response on the wave amplitude is rather complex to understand. It can be considered nearly linear for the most cases for which the weight of the nonlinearities is negligible. Only in the neighbourhood of the resonance frequency and for incident waves misaligned with respect to a vertical plane of symmetry of the system, the nonlinear character of the differential problem seems to become relevant.

6.4.5 Irregular waves

In the framework of the linear hydrodynamic theory, irregular waves can be obtained by a superimposition of an adequate number (at limit infinite) of monochromatic waves, out-of-phase to each other by means of a random phase. The amplitude of each harmonic should be established through the spectrum of the wave. The consequent load associated with the diffraction problem is therefore the superimposition of the loads related to each harmonic. The hydrodynamic damping is considered by the convolution of the radiation-retardation kernel operator and the time history of the velocity vector. The dynamic response loses its regular character even if it is always the result of a superimposition of harmonic forcing signals.

Because of the aforementioned random phase the time series of the wave-excitation load (diffraction problem) are in principle different to each other and yield to differ-

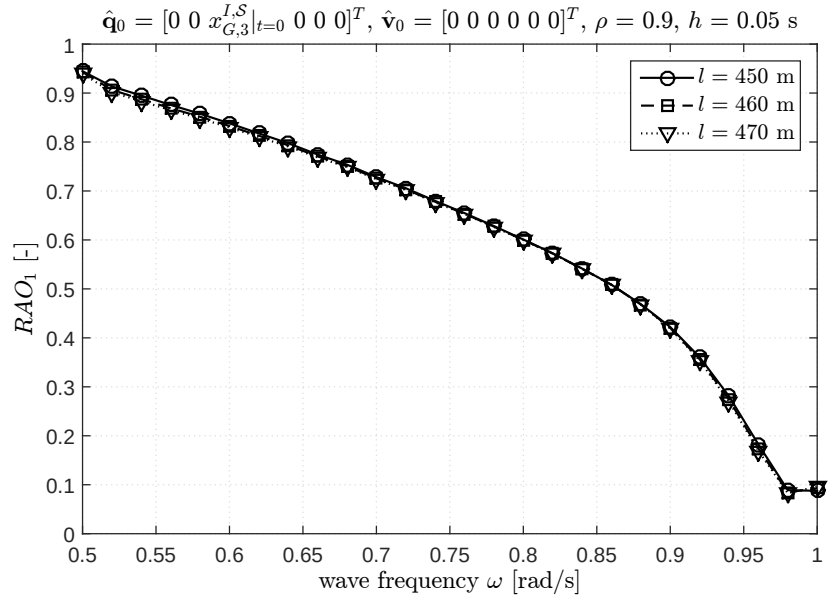

(a) surge

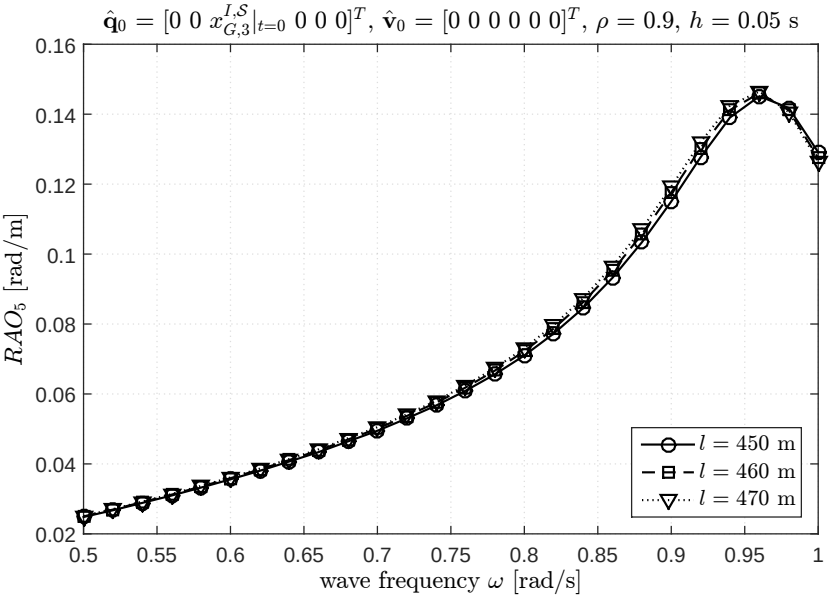

(b) pitch

Figure 6.21: Response of the moored floating platform against the frequency of the incident wave for different lengths of the mooring lines. Waves directed along the x-axis.

ent time histories of the dynamic response, especially if the system is nonlinear. In this context, it would be very interesting to evaluate how many time series should be analysed to have a significant sample of the response. On the other hand, another interesting issue is the selection of the proper spectrum and its parameters. Even when the spectrum is a data of the problem, the parameters (for instance significant wave height H_s and peak period T_p) should be somehow established. Such issue requires the knowledge of the probability joint distribution of the main parameters that characterize the environment and should be pursued with a statistical approach. The final goal is the distribution of the system response, in terms of displacements or stresses.

6.4.5.1 Radiation-retardation kernel

The convolution integral that involves the radiation-retardation kernel keeps track of the influence of the velocity history on the current dynamic equilibrium with a sort of memory effect. In the discrete case, the kernel operator is defined as the superimposition of a finite number of harmonic functions, and therefore it is a periodic function. However, it makes no sense that also the records of the velocity very far from the current time step continue to influence the motion, as it would happen if the kernel operator was considered a periodic function. In practice, the operator should be truncated at half of the first period when its components are almost null (before that they grow up again).

6.5 Final remarks

In order to provide the reader with a critical overview, this section highlights some limitations of the coupled system mainly related to the models adopted. The dynamics of a floating rigid body is modelled as a set of nonlinear differential equations that are solved only numerically[34]. The dynamic solver, as well as the coupled models, uses numerical procedures that always return an approximated solution because of both the nature of the algorithms, in particular the numerical schemes for the solution of nonlinear equations, and the intrinsic finite precision. Anyway, the use of an opportune time step size can limit the errors related to the integration methods. Another aspect, much more limiting, refers to the theoretical models adopted for the system and loads. The dynamics of rigid bodies has been well understood since decades, and the formulation can describe the motion in the Euclidean space without any approximation. Only the rigid-body assumption could give some perplexity because it is an ideal concept, even if in good agreement with the most floating platforms (also ships) [46, 68].

The linear theory, implemented in the hydrodynamic code, is considered a good approximation for deep-water sites [23, 46, 58] but could be replaced by higher-order theories or a fully-nonlinear approach able to capture phenomena due to higher-order hydrodynamic terms. The linear theory implies small oscillations of the floating body and is not suitable for extreme load conditions where the system can undergo large displacements [44, 70]. On the other hand, the quasi-static model, implemented in the mooring line code, does not consider the inertia and the damping of the mooring lines (and their bending stiffness). The approximation is satisfactory for slowly varying motions of the support [23] and if the mass of the cable is small with respect to the overall mass of the system [46]. However, a more complete dynamic model based on finite difference method or finite element method could be considered. Furthermore,

[34] An exact analytic solution has not been developed yet.

even though the aerodynamics of the structure above the support is not considered in this research, this is generally acceptable only in the case of a wind turbine in parked condition, where the wind action is limited by the particular configuration of the rotor and wave loads are dominant. For a more comprehensive study including operating conditions, also the aerodynamic loads should be considered in the analysis.

Moreover, the analysis and the dynamic response of a floating structure depend both on the system properties and on the environmental load features. The problem is strongly case-dependent, and generally it is not possible to establish (or to predict) a priori the behaviour of a particular system, subjected to particular (stochastic) wind and wave loads, not even on the basis of similar cases. This limitation, due to the intrinsic nature of the system and loads, cannot be overcome, and any example should be regarded as an explanation of the method.

Chapter 7

Conclusions

"Joking you can say everything,
even the truth."

Sigmund Freud

A summary of the main achievements of the present research is given together with conclusions and final remarks for future research activities.

Offshore wind energy in deep waters is undoubtedly one of the most important resources in the renewable energy sector and gained over the years a primary role, which is also expected to be maintained in the next future. The design and the optimization of offshore wind turbines require numerical tools that should be very efficient, accurate, and with reduced computational effort. In this research a nonlinear model for the dynamics of moored floating platforms has been developed. Particular attention has been devoted to the evaluation of the capability of the main dynamic solver and its coupling with the models for the assessment of the hydrodynamic action and the mooring system loads. The main code can be further coupled with an aerodynamic model and exploited for the analysis of offshore wind turbines. In the following the main achievements are summarized together with an interesting before-after comparison that highlights the new perspectives related to this research. The conclusions and the recommendations for future research are finally illustrated.

7.1 Main achievements

The research was mainly devoted to the development of a nonlinear model for the dynamics of floating platforms, inside the general framework of rigid bodies. The formulation is developed with a mixed representation of the motion considering several typologies of loads, both follower and non-follower, and including also the transformations of the state variables, i.e. inertia-like, damping-like, and stiffness-like loads. The differential problem is solved by an innovative Lie group time integration scheme, introduced from robotics, overcoming the drawbacks associated with the use of nautical angles and their time derivatives. Such dynamic model should be regarded as the main code. It can solve the dynamics of a rigid body without any restriction and can be coupled with other models for the assessment of specific tasks. The coupling can be achieved in terms of external loads (also as transformations of the state variables) with an explicit procedure.

The numerical model was successfully validated and verified against a series of dynamic problems for which the exact analytic solution is known, including rotating bodies in the Euclidean space and oscillators (simple, damped, and forced). Moreover, the model was also compared with an alternative formulation based on a complete local representation of the motion, with a positive feedback. The main code was coupled with the models that assess the hydrodynamic action and the mooring system loads, based respectively on the linear theory and a quasi-static formulation. On the basis of the response of the coupled system to regular waves, different coupling strategies were proposed to reduce the computational effort, and the role of the main parameters affecting the motion was discussed.

7.1.1 Before and after the thesis

The most of dynamic models in maritime engineering use formulations based on Euler angles (or quaternions) and their time derivatives, which significantly alter the original equations of motion. The resulting formulations are in general highly nonlinear and, in the case of a redundant parametrization, the number of equations and variables increases. Such formulations are rather far from the physics of the problem, cannot easily be interpreted and, above all, they cannot easily be customized for the assessment of specific problems.

The approach proposed, introduced from robotics, is based on the solution of the

differential problem with the so called geometric methods [11, 13, 86, 87], which consider the Lie group structure of the configuration space avoiding the drawbacks associated with classical methods (strong nonlinearities and singularities). Such methods solve the equations directly on the Lie group [13] without the necessity of introducing a parametrization to handle the kinematic compatibility, and therefore preserving the structure of original equations with reduced nonlinearities and no singularity [86]. This approach permits to obtain very efficient numerical models, also in terms of computational effort, without destroying the nature of the equations of motion, which therefore reflect the physics of the problem. The benefits are remarkable especially when it is necessary to modify the dynamic differential problem, with new perspectives also for real-time employments. The wide range of loads analysed and formulated in the framework of the Lie group time integrator based on the mixed representation of the motion is an advanced guideline for the development of further dynamic models.

Moreover, the dynamic formulation considers large displacements (in particular large rotations) without any restriction and can capture any kind of transient. Therefore, the approach proposed in this work appears very promising also for the analysis of extreme operating conditions and operational transients. Future work should focus on the development of improved load models to couple with the main dynamic solver.

7.2 Conclusions

This research activity highlighted the relevance of the nonlinear character of rigid-body motions, generally associated with finite rotations, which should be properly considered as elements of the group $SO(3)$, and therefore require specific formulations and appropriate time integration schemes. The development of the dynamic model as well as the coupling of the main code with the models for the assessment of the hydrodynamic action and the mooring system loads inspired many discussions about the formulation, the accuracy, the computational effort, and thus the best strategies for the simulation of a moored floating platform. The use of a mixed representation of the motion leads to simpler algorithms in terms of composition rule and interpretation of the outputs, but it is usually associated with a loss of symmetry of the main tangent operators, which is however inevitable even with the use of a complete local representation of the motion (because of gyroscopic loads). The validation tests proved the reliability of the formulation and the algorithm in the description of arbitrary motions in the Euclidean space, even for high rotational speeds.

Undoubtedly, the computational effort is one of the parameters that mainly affects the choice of a numerical model. It depends on the convergence velocity of the algorithm but also on the capabilities of the model to reduce discarded data. Generally, an initial window of the time histories of the system response should be discarded because it is affected by the transients of the system. The reduction of such transients without invalidating the accuracy of the solution is therefore a very important issue. In particular, in this research three different kinds of transients were discussed.

The first one is related to the initial conditions of the system and it is accentuated by a sudden application of the external time-dependent loads (as the wave-excitation loads). Such transient (usually undesired) can be justified by considering the general integral of a homogeneous linear differential problem and can be reduced by linearly scaling the external time-dependent forcing loads so that they gradually reach their final amplitude after few seconds (chosen on the basis of the wave period) from the

beginning of the simulation. This method permits to considerably reduce the window of the time history affected by the transient, especially when the hydrodynamic damping is small (low frequencies). Obviously, if the analysis aims at studying the transient of the dynamic response, this strategy should be avoided.

The second transient faced in this work is associated with the coupling of the main code with the mooring system, which provides an additional unbalanced vertical load, due to the tension on the lines, bringing the system into a new static equilibrium configuration. Such transient can be prevented with a proper initial condition on the displacement (increase of the immersion of the body) so that the buoyancy can balance the overall load. Since the load due to the mooring lines is nonlinearly related to the displacement, the initial condition should be established with an iterative procedure, which requires a pre-process of the system. However, in order to avoid such procedure, which is generally time consuming, it is possible to properly reduce the duration of the transient by setting the initial conditions on the basis of the unbalanced load computed with respect to the free floating equilibrium configuration of the body.

The last transient is much more insidious to understand and cannot be avoided or reduced with simple strategies. It is associated with the nonlinear coupling of some degrees of freedom to each other because of both the operation of the mooring system and the combination of the rotational motion with particular sources of loads, for instance those related to a follower interpretation of the forces or a non-follower interpretation of the torques. Such a nonlinear coupling could cause unbalanced forces that bring the system into a mean dynamic configuration different from the static one. In the case of sinusoidal external forcing loads, these loads with non-zero mean value usually have a dominant double frequency.

Another strategy, related to the structure of the algorithm, can reduce the computational effort without affecting the accuracy. At each time step the convergence of the residual (i.e. the satisfaction of the dynamic equilibrium) is achieved by an iterative procedure that involves the linearisation of the dynamic equilibrium equations about the current configuration. In particular, the tangent stiffness operators associated with the transformations of the state variables, both follower and non-follower, are related to the current configuration by the rotation operator $\mathbf{R}$, and thus they should be updated whenever the configuration changes. However, considering that the angular velocity of moored floating platforms (but also ships) is generally limited, so that the rotation increments over a time step should remain small, the series expansion of the exponential map could be truncated without significantly deteriorating the convergence process of the Newton-Raphson iterations. In practical terms, it is not necessary to compute the exact form of the tangent stiffness matrices, but they can be truncated by neglecting all the terms related to the rotational increment. This strategy should be evaluated for each specific problem, and it is suitable if the number of Newton-Raphson iterations does not significantly increase.

Other important aspects related to the time integration scheme are the choice of the time step size and the numerical damping. Both the parameters have a numeric nature and influence the accuracy of the model. On the basis of the analyses carried out in this research activity, some considerations can be drawn. A reduction of the time step size enhances the accuracy of the dynamic model, with a second-order trend. Highly accurate solutions require very small time step sizes with consequent increase of the computational effort. However, if the objective is to obtain a solution reasonably

accurate, for instance with errors on the third significant figure, a time step of 0.05 s can be considered a good compromise and permits to achieve a rather fast code. The numerical damping is often necessary to make the algorithms more stable and is usually associated with an energy dissipation that does not depend on the physics of the problem. The estimation of the impact of the numerical damping on the accuracy of the numerical model is a very arduous task because it is strongly related to the specific problem. For moored floating bodies, the developed model can achieve a stable convergence even with a small numerical damping, for instance the most simulations were carried out with $\rho = 0.9$. The introduction of an amount of numerical damping is considered a reliable strategy to improve the robustness of the coupled code, without significantly compromising the accuracy of the solution.

Finally, some further remarks about the coupling of the dynamic model (main code) with other models developed for the assessment of specific aspects of the dynamic problem, such as the evaluation of particular loads. The dynamic model permits a direct coupling in terms of external loads, also related to the state variables as their transformation. The dynamic equilibrium at each time step can be achieved by an iterative procedure, as that associated with an explicit coupling strategy. However, since for ordinary loads the configuration of the moored floating platform slowly varies in time, even a weak coupling based on the estimation of the loads on the basis of the state variables at the previous time step can be accurate enough.

The dynamics of moored floating bodies is rather complex and is the result of the mutual interaction between the structure and the environment, which is strongly case-dependent. The dynamic response of such systems strongly depends on the frequency range of the incident wave with respect to the natural frequencies of the structure, so that the modification of some parameters such as the mass of the system or the length of the cables can produce opposite or undesired effects. In this sense the platform and the mooring system should be designed so that the natural frequencies of the coupled system are as far as possible from the typical periods of the waves observed in the specific location. Large motions can emphasize the nonlinearities of the dynamic problem and should be carefully analysed. Generally the optimization (also economic) of the design requires a compromise.

7.3 Recommendations for future research

The main dynamic code can be used without any significant restriction to study the dynamic response of systems undergoing large displacements (in particular large rotations), including also the operating transients. The main limitation is the rigid-body assumption, even if it is reliable for the most floating bodies. It could be interesting the evaluation of the code for real-time purposes with the possibility of a continuous updating of the inputs on the basis of field measurements. However, in order to exploit all the potentialities of such dynamic model it is necessary the improvement of the models of loads.

The linear hydrodynamic theory, although rather simple and efficient, has a limited range of validity. It is adequate for the most sea states in deep waters, but for extreme conditions or in shallow waters it becomes very approximate. In particular, the linear hydrodynamic theory implies small oscillations of the floating body and excludes all the phenomena related to higher-order terms of wave kinematics (for instance ringing). Whenever the direction of the regular (or irregular) wave is parallel to a ver-

tical plane of symmetry of the floating system, the formulation is rather reliable, but for misaligned waves the interpretation of the first-order approximation becomes very problematic especially when the oscillations of the body are not small. In particular, a misaligned wave is often associated with a non-negligible torque component about the z-axis, which implies a change of orientation (and direction) during the motion, significant at least for large displacements. There are also some doubts on the explanation of the hydrodynamic operators (added mass, damping, stiffness, wave-excitation) in terms of follower or non-follower transformations. Moreover, misaligned waves amplify the aforementioned transients due to the nonlinear coupling of some degrees of freedom. A three-dimensional fully nonlinear approach seems to be the target for the next developments and can be pursued by means of methods based on computational fluid dynamics computations. In this context the research could consider the use of advanced computational tools for the development of reduced-order models for floating bodies.

On the other hand, the quasi-static model of the mooring lines, even if rather reliable for slowly varying motions of the support [23] and if the mass of the lines is small with respect to the overall mass of the system [46], neglects the inertia and the damping of the mooring lines, the latter associated with the impossibility that the lines can follow instantaneously the motion of the platform [23], as well as the instability phenomena. A more detailed assessment of the dynamics of moored floating bodies requires the use of a dynamic model of the lines, for instance by a finite element method, even if the higher accuracy is paid in terms of computational effort. Reduced-order models seems to be very attractive also for mooring lines.

It is clear that the research should move towards the improvement of the computational efficiency without significantly deteriorating the accuracy of the model. In this context the formulation proposed contributes with its own brick to the simplification of the models of floating platforms preserving their accuracy.

Appendix A

Local formulation

"The shortest path between two truths in the real domain passes through the complex domain."

Jacques Hadamard

The use of a mixed representation of the motion is not the unique possibility to formulate the dynamic problem of a rigid body. A complete local representation of the motion is a suitable alternative approach, especially in multibody dynamics [86]. All the operators defined in Chapter 3 are redefined in this alternative framework. The appendix aims at providing the reader with another point of view on the dynamics of rigid bodies.

A.1 Dynamic problem

The dynamic problem aims at establishing the configuration of the rigid body at any time instant and consists in solving the set of differential equations that defines the motion of the center of mass and the motion about the center of mass when the body is subjected to a certain system of loads. The problem analysed hereafter refers to the local-frame formulation (see Section 2.2.4.2).

A.1.1 Reference frames

The choice of the reference frames used for describing either the displacements of the center of mass or the rotational motion of the body, can lead to different mathematical formulations of the dynamic problem, formally equivalent, and then to different integration formulas[1]. The formulation presented in this appendix refers to two different frames:

- inertial (spatial or fixed) reference frame $\{O; x, y, z\}$ defined by the orthonormal basis $\mathcal{S} = \{\mathbf{e}_i^I\}$. The physical quantities $(\bullet)$ observed in this frame are indicated with the notation $(\bullet)^I$;

- non-inertial (body-attached) reference frame $\{G; x', y', z'\}$ defined by the orthonormal basis $\mathcal{M} = \{\mathbf{e}_i^B\}$. This frame can translate and rotate with respect to the fixed frame according to the motion of the rigid body. Therefore, the associated basis generally changes its orientation during the motion. An observer solidal with the body-attached frame sees the rigid body fixed. The physical quantities $(\bullet)$ observed in this frame are indicated with the notation $(\bullet)^B$.

The velocity of the center of mass is described with respect to the orthonormal basis $\mathcal{M}$, as the motion about the center of mass, resulting in a local formulation. However, in spite of the local approach, the structure of the algorithm, and in particular the kinematic equations associated with the dynamic equilibrium equations, implies that at any time instant the output at the displacement level is the position vector of the center of mass expressed with respect to the orthonormal basis $\mathcal{S}$. This local approach guarantees a quite simple mathematical formulation even if the translational and rotational problems are coupled together because of the gyroscopic forces and the (possible) features of external loads, especially in the case of non-follower loads. Furthermore, since in the body-attached frame the most operators (in particular the inertia tensor) are time-invariant, the conservation of the angular momentum is simplified. By contrast, some complications arise from the aforementioned coupling of the translational and rotational problems that implies, at any time instant, the loss of symmetry of the main system linear operators (damping and stiffness) and their dependence on the actual orientation.

[1] Even if the mathematical formulations are definitely equivalent, the associated time integration algorithms are only approximately equivalent, i.e. the accuracy for a given time step size depends, among others, also on the formulation of the dynamic problem. However, for each formulation, if the time step size tends to zero, also the error tends to zero.

A.1.2 Linear operators

Let $\bar{\mathbf{q}} = [\mathbf{x}_G^{I,\mathcal{S}}; \boldsymbol{\psi}]$ be the position state vector[2], collecting the position vector of the center of mass and the rotational vector, let $\bar{\mathbf{v}} = [\mathbf{v}_G^{I,\mathcal{M}}; \boldsymbol{\omega}^{\mathcal{M}}]$ be the velocity state vector, collecting the velocity vector of the center of mass and the angular velocity vector, let $\dot{\bar{\mathbf{v}}} = [\dot{\mathbf{v}}_G^{I,\mathcal{M}}; \dot{\boldsymbol{\omega}}^{\mathcal{M}}]$ be the acceleration state vector, collecting the acceleration vector of the center of mass and the angular acceleration vector. These three quantities can be regarded as state variables and completely describe the rigid-body motion. In other words, the evolution in time of the state variables offers a complete knowledge about the dynamics of the body. The dynamic equilibrium equations can be written in terms of the state variables, defining the residual vector $\bar{\mathbf{r}}$, as follows:

$$\bar{\mathbf{r}} = \begin{bmatrix} m\mathbf{I}_3 & \mathbf{0}_{3\times3} \\ \mathbf{0}_{3\times3} & \mathbf{J}^{B,\mathcal{M}} \end{bmatrix} \dot{\bar{\mathbf{v}}} + \begin{bmatrix} m\widetilde{\bar{\mathbf{v}}}_{4:6}\bar{\mathbf{v}}_{1:3} \\ \widetilde{\bar{\mathbf{v}}}_{4:6}\mathbf{J}^{B,\mathcal{M}}\bar{\mathbf{v}}_{4:6} \end{bmatrix} - \begin{bmatrix} \mathcal{F}^{\mathcal{M}}(\bar{\mathbf{q}}, \bar{\mathbf{v}}, \dot{\bar{\mathbf{v}}}, t) \\ \mathcal{T}_G^{\mathcal{M}}(\bar{\mathbf{q}}, \bar{\mathbf{v}}, \dot{\bar{\mathbf{v}}}, t) \end{bmatrix} = \mathbf{0}_{6\times1} \quad \text{(A.1)}$$

The linearisation of the Equation (A.1) with respect to the state variables defines the tangent (stiffness, damping, and mass) operators, namely:

$$\mathbf{K}^t \cdot \Delta\bar{\mathbf{q}} = D_{\mathbf{q}}\bar{\mathbf{r}} \cdot \Delta\bar{\mathbf{q}} \quad \text{(A.2)}$$

$$\mathbf{C}^t \cdot \Delta\bar{\mathbf{v}} = D_{\mathbf{v}}\bar{\mathbf{r}} \cdot \Delta\bar{\mathbf{v}} \quad \text{(A.3)}$$

$$\mathbf{M}^t \cdot \Delta\dot{\bar{\mathbf{v}}} = D_{\dot{\mathbf{v}}}\bar{\mathbf{r}} \cdot \Delta\dot{\bar{\mathbf{v}}} \quad \text{(A.4)}$$

A.2 Inertial loads

An accelerating body can be transformed into an equivalent static system by means of the so called inertial loads (D'Alembert's principle), i.e. external forces and torques associated with the accelerating masses, namely:

$$\mathbf{F}_G^{\mathcal{M}} = -m\dot{\bar{\mathbf{v}}}_{1:3} - m\bar{\mathbf{v}}_{4:6} \times \bar{\mathbf{v}}_{1:3} \quad \text{(A.5)}$$

$$\mathbf{T}_G^{\mathcal{M}} = -\mathbf{J}^{B,\mathcal{M}}\dot{\bar{\mathbf{v}}}_{4:6} - \bar{\mathbf{v}}_{4:6} \times \mathbf{J}^{B,\mathcal{M}}\bar{\mathbf{v}}_{4:6} \quad \text{(A.6)}$$

The tangent operators associated with the inertial loads are given by:

$$\mathbf{M}^t_{1:3\times1:3} = m\mathbf{I}_3 \quad \text{(A.7)}$$

$$\mathbf{M}^t_{4:6\times4:6} = \mathbf{J}^{B,\mathcal{M}} \quad \text{(A.8)}$$

$$\mathbf{C}^t_{1:3\times1:3} = m\widetilde{\bar{\mathbf{v}}}_{4:6} \quad \text{(A.9)}$$

$$\mathbf{C}^t_{1:3\times4:6} = -m\widetilde{\bar{\mathbf{v}}}_{1:3} \quad \text{(A.10)}$$

$$\mathbf{C}^t_{4:6\times4:6} = \widetilde{\bar{\mathbf{v}}}_{4:6}\mathbf{J}^{B,\mathcal{M}} - \widetilde{(\mathbf{J}^{B,\mathcal{M}}\bar{\mathbf{v}}_{4:6})} \quad \text{(A.11)}$$

[2] As explained for the mixed formulation, although the state variable associated with the configuration of the body is expressed as a vector $\bar{\mathbf{q}} \in \mathbb{R}^6$, do not confuse the nature of the rotational vector $\boldsymbol{\psi}$, which is a parametrization of the rotation operator $\mathbf{R} \in SO(3)$ as well as do not forget the local representation of the velocity. The position state vector should therefore be treated as an element $\bar{q}$ of the Lie group $SE(3)$, namely $\bar{q} \in \mathbb{R}^3 \rtimes SO(3)$, together with the composition rule proper of such group.

A.3 Non-follower loads

A load is said non-follower if its orientation does not depend on the orientation of the body. The components of a non-follower load, both forces and torques, are referred to the basis $\mathcal{S}$ of the inertial (fixed) frame. Because of the local representation adopted, the components of non-follower loads should be properly modified (change of basis) in order to be coherent with the basis adopted in the formulation of the dynamic problem[3].

A.3.1 Force

Let $\mathbf{F}_P^{nf}$ be a non-follower force, applied to the location (point) P of the rigid body, that can depend on time but not on the state variables. Its contribution to the loads acting on the system in the local-frame formulation is given by:

$$\mathbf{F}_G^{\mathcal{M}} = \mathbf{R}^T \mathbf{F}_P^{nf} \tag{A.12}$$

$$\mathbf{T}_G^{\mathcal{M}} = (P - G) \times \mathbf{R}^T \mathbf{F}_P^{nf} = \widetilde{\mathbf{x}}_P^{B,\mathcal{M}} \mathbf{R}^T \mathbf{F}_P^{nf} \tag{A.13}$$

The tangent operator associated with the non-follower force is given by:

$$\mathbf{K}^t_{1:3\times 4:6} = -\widetilde{\left(\mathbf{R}^T \mathbf{F}_P^{nf}\right)} \tag{A.14}$$

$$\mathbf{K}^t_{4:6\times 4:6} = -\widetilde{\mathbf{x}}_P^{B,\mathcal{M}} \widetilde{\left(\mathbf{R}^T \mathbf{F}_P^{nf}\right)} \tag{A.15}$$

A.3.2 Torque

Let $\mathbf{T}_P^{nf}$ be a non-follower moment, applied to the location (point) P of the rigid body, that can depend on time but not on the state variables. Its contribution to the loads acting on the system in the local-frame formulation is given by:

$$\mathbf{F}_G^{\mathcal{M}} = \mathbf{0} \tag{A.16}$$

$$\mathbf{T}_G^{\mathcal{M}} = \mathbf{R}^T \mathbf{T}_P^{nf} \tag{A.17}$$

The tangent operator associated with the non-follower torque is given by:

$$\mathbf{K}^t_{4:6\times 4:6} = -\widetilde{\left(\mathbf{R}^T \mathbf{T}_P^{nf}\right)} \tag{A.18}$$

A.3.3 Transformations of the state variables

An interesting case is when the loads acting on the rigid body can be modelled as linear transformations of the state variables, $\mathbf{q}$, $\mathbf{v}$, $\dot{\mathbf{v}}$, defined with respect to the basis $\mathcal{S}$ of the inertial frame. The matrices associated with the linear transformation should be properly converted in order to consider that the motion of the center of mass and the rotational motion of the body are referred to the basis $\mathcal{M}$, with the only aforementioned exception of the position vector of the center of mass. The transformation $\mathbf{A}^{(\bullet)}$ of the state variable $(\bullet)$ associated with the local-frame formulation is indicated with the notation $\bar{\mathbf{A}}^{(\bullet)}$.

[3] In the formulations developed in the following sections, as also specified in Chapter 3, the rotation operator $\mathbf{R}$ is considered a function of the rotational vector $\boldsymbol{\psi}$ through the exponential map, i.e. $\mathbf{R} = \mathbf{R}(\boldsymbol{\psi})$. Such dependence should be taken into account in the derivation of the tangent stiffness operators.

A.3.3.1 Configuration operators

Let $\mathbf{A}^{\mathbf{q}}$ be the square matrix of order six associated with a linear transformation of the displacements defined as follows:

$$\begin{bmatrix} \mathbf{F}_G^{\mathcal{S}} \\ \mathbf{T}_G^{\mathcal{S}} \end{bmatrix} = -\mathbf{A}^{\mathbf{q}} \begin{bmatrix} \mathbf{x}_G^{I,\mathcal{S}} \\ \boldsymbol{\psi} \end{bmatrix} \tag{A.19}$$

The transformation expressed in the framework of the local representation of the motion is given by:

$$\begin{bmatrix} \mathbf{F}_G^{\mathcal{M}} \\ \mathbf{T}_G^{\mathcal{M}} \end{bmatrix} = -\bar{\mathbf{A}}^{\mathbf{q}} \begin{bmatrix} \bar{\mathbf{q}}_{1:3} \\ \bar{\mathbf{q}}_{4:6} \end{bmatrix} \tag{A.20}$$

$$\bar{\mathbf{A}}^{\mathbf{q}}_{1:3\times 1:3} = \mathbf{R}^T \mathbf{A}^{\mathbf{q}}_{1:3\times 1:3} \tag{A.21}$$

$$\bar{\mathbf{A}}^{\mathbf{q}}_{1:3\times 4:6} = \mathbf{R}^T \mathbf{A}^{\mathbf{q}}_{1:3\times 4:6} \tag{A.22}$$

$$\bar{\mathbf{A}}^{\mathbf{q}}_{4:6\times 1:3} = \mathbf{R}^T \mathbf{A}^{\mathbf{q}}_{4:6\times 1:3} \tag{A.23}$$

$$\bar{\mathbf{A}}^{\mathbf{q}}_{4:6\times 4:6} = \mathbf{R}^T \mathbf{A}^{\mathbf{q}}_{4:6\times 4:6} \tag{A.24}$$

The new transformation is nonlinear with respect to the state variable $\boldsymbol{\psi}$. The tangent operators associated with the transformation $\bar{\mathbf{A}}^{\mathbf{q}}$ are given by[4]:

$$\mathbf{K}^t_{1:3\times 1:3} = \bar{\mathbf{A}}^{\mathbf{q},\star}_{1:3\times 1:3} \tag{A.25}$$

$$\mathbf{K}^t_{1:3\times 4:6} = \bar{\mathbf{A}}^{\mathbf{q},\star}_{1:3\times 4:6} + \big(\widetilde{\bar{\mathbf{A}}^{\mathbf{q}}_{1:3\times 1:3}\bar{\mathbf{q}}_{1:3}}\big) + \big(\widetilde{\bar{\mathbf{A}}^{\mathbf{q}}_{1:3\times 4:6}\bar{\mathbf{q}}_{4:6}}\big) \tag{A.26}$$

$$\mathbf{K}^t_{4:6\times 1:3} = \bar{\mathbf{A}}^{\mathbf{q},\star}_{4:6\times 1:3} \tag{A.27}$$

$$\mathbf{K}^t_{4:6\times 4:6} = \bar{\mathbf{A}}^{\mathbf{q},\star}_{4:6\times 4:6} + \big(\widetilde{\bar{\mathbf{A}}^{\mathbf{q}}_{4:6\times 1:3}\bar{\mathbf{q}}_{1:3}}\big) + \big(\widetilde{\bar{\mathbf{A}}^{\mathbf{q}}_{4:6\times 4:6}\bar{\mathbf{q}}_{4:6}}\big) \tag{A.28}$$

A.3.3.2 Velocity operators

Let $\mathbf{A}^{\mathbf{v}}$ be the square matrix of order six associated with a linear transformation of the velocities defined as follows:

$$\begin{bmatrix} \mathbf{F}_G^{\mathcal{S}} \\ \mathbf{T}_G^{\mathcal{S}} \end{bmatrix} = -\mathbf{A}^{\mathbf{v}} \begin{bmatrix} \mathbf{v}_G^{I,\mathcal{S}} \\ \boldsymbol{\omega}^{\mathcal{S}} \end{bmatrix} \tag{A.29}$$

[4]The first term of the tangent stiffness operator is indicated with the superscript $\star$ because the matrix $\bar{\mathbf{A}}^{\mathbf{q}}$ does not exactly correspond to the tangent operator. In fact, it should be transformed to consider the structure of the Lie group time integrator and in particular the relations between the increment of the Newton-Raphson procedure and the actual increment of the displacements (translation and rotation).

The transformation expressed in the framework of the local representation of the motion is given by:

$$\begin{bmatrix} \mathbf{F}_G^{\mathcal{M}} \\ \mathbf{T}_G^{\mathcal{M}} \end{bmatrix} = -\bar{\mathbf{A}}^{\mathbf{v}} \begin{bmatrix} \bar{\mathbf{v}}_{1:3} \\ \bar{\mathbf{v}}_{4:6} \end{bmatrix} \tag{A.30}$$

$$\bar{\mathbf{A}}^{\mathbf{v}}_{1:3\times 1:3} = \mathbf{R}^T \mathbf{A}^{\mathbf{v}}_{1:3\times 1:3} \mathbf{R} \tag{A.31}$$

$$\bar{\mathbf{A}}^{\mathbf{v}}_{1:3\times 4:6} = \mathbf{R}^T \mathbf{A}^{\mathbf{v}}_{1:3\times 4:6} \mathbf{R} \tag{A.32}$$

$$\bar{\mathbf{A}}^{\mathbf{v}}_{4:6\times 1:3} = \mathbf{R}^T \mathbf{A}^{\mathbf{v}}_{4:6\times 1:3} \mathbf{R} \tag{A.33}$$

$$\bar{\mathbf{A}}^{\mathbf{v}}_{4:6\times 4:6} = \mathbf{R}^T \mathbf{A}^{\mathbf{v}}_{4:6\times 4:6} \mathbf{R} \tag{A.34}$$

The new transformation is nonlinear with respect to the state variable $\boldsymbol{\psi}$. The tangent operators associated with the transformation $\bar{\mathbf{A}}^{\mathbf{v}}$ are given by:

$$\mathbf{C}^t = \bar{\mathbf{A}}^{\mathbf{v}} \tag{A.35}$$

$$\mathbf{K}^t_{1:3\times 4:6} = \big(\widetilde{\bar{\mathbf{A}}^{\mathbf{v}}_{1:3\times 1:3}\bar{\mathbf{v}}_{1:3}}\big) - \bar{\mathbf{A}}^{\mathbf{v}}_{1:3\times 1:3}\widetilde{\bar{\mathbf{v}}}_{1:3} + \big(\widetilde{\bar{\mathbf{A}}^{\mathbf{v}}_{1:3\times 4:6}\bar{\mathbf{v}}_{4:6}}\big) - \bar{\mathbf{A}}^{\mathbf{v}}_{1:3\times 4:6}\widetilde{\bar{\mathbf{v}}}_{4:6} \tag{A.36}$$

$$\mathbf{K}^t_{4:6\times 4:6} = \big(\widetilde{\bar{\mathbf{A}}^{\mathbf{v}}_{4:6\times 1:3}\bar{\mathbf{v}}_{1:3}}\big) - \bar{\mathbf{A}}^{\mathbf{v}}_{4:6\times 1:3}\widetilde{\bar{\mathbf{v}}}_{1:3} + \big(\widetilde{\bar{\mathbf{A}}^{\mathbf{v}}_{4:6\times 4:6}\bar{\mathbf{v}}_{4:6}}\big) - \bar{\mathbf{A}}^{\mathbf{v}}_{4:6\times 4:6}\widetilde{\bar{\mathbf{v}}}_{4:6} \tag{A.37}$$

A.3.3.3 Acceleration operators

Let $\mathbf{A}^{\dot{\mathbf{v}}}$ be the square matrix of order six associated with a linear transformation of the accelerations defined as follows[5]:

$$\begin{bmatrix} \mathbf{F}_G^{\mathcal{S}} \\ \mathbf{T}_G^{\mathcal{S}} \end{bmatrix} = -\mathbf{A}^{\dot{\mathbf{v}}} \begin{bmatrix} \mathbf{a}_G^{I,\mathcal{S}} \\ \dot{\boldsymbol{\omega}}^{\mathcal{S}} \end{bmatrix} = -\mathbf{A}^{\dot{\mathbf{v}}} \begin{bmatrix} \mathbf{R}(\dot{\mathbf{v}}_G^{I,\mathcal{M}} + \widetilde{\boldsymbol{\omega}}^{\mathcal{M}}_{\mathcal{S}} \mathbf{v}_G^{I,\mathcal{M}}) \\ \dot{\boldsymbol{\omega}}^{\mathcal{S}} \end{bmatrix} \tag{A.38}$$

The resulting load associated with the operator $\mathbf{A}^{\dot{\mathbf{v}}}$ can be split into a linear transformation of the acceleration vector $\bar{\mathbf{A}}^{\dot{\mathbf{v}}}$ and a nonlinear function of the velocity vectors, namely:

$$\begin{bmatrix} \mathbf{F}_G^{\mathcal{M}} \\ \mathbf{T}_G^{\mathcal{M}} \end{bmatrix} = -\bar{\mathbf{A}}^{\dot{\mathbf{v}}} \begin{bmatrix} \bar{\dot{\mathbf{v}}}_{1:3} \\ \bar{\dot{\mathbf{v}}}_{4:6} \end{bmatrix} - \begin{bmatrix} \bar{\mathbf{A}}^{\dot{\mathbf{v}}}_{1:3\times 1:3}\widetilde{\bar{\mathbf{v}}}_{4:6}\bar{\mathbf{v}}_{1:3} \\ \bar{\mathbf{A}}^{\dot{\mathbf{v}}}_{4:6\times 1:3}\widetilde{\bar{\mathbf{v}}}_{4:6}\bar{\mathbf{v}}_{1:3} \end{bmatrix} \tag{A.39}$$

$$\bar{\mathbf{A}}^{\dot{\mathbf{v}}}_{1:3\times 1:3} = \mathbf{R}^T \mathbf{A}^{\dot{\mathbf{v}}}_{1:3\times 1:3} \mathbf{R} \tag{A.40}$$

$$\bar{\mathbf{A}}^{\dot{\mathbf{v}}}_{1:3\times 4:6} = \mathbf{R}^T \mathbf{A}^{\dot{\mathbf{v}}}_{1:3\times 4:6} \mathbf{R} \tag{A.41}$$

$$\bar{\mathbf{A}}^{\dot{\mathbf{v}}}_{4:6\times 1:3} = \mathbf{R}^T \mathbf{A}^{\dot{\mathbf{v}}}_{4:6\times 1:3} \mathbf{R} \tag{A.42}$$

$$\bar{\mathbf{A}}^{\dot{\mathbf{v}}}_{4:6\times 4:6} = \mathbf{R}^T \mathbf{A}^{\dot{\mathbf{v}}}_{4:6\times 4:6} \mathbf{R} \tag{A.43}$$

The new transformation is nonlinear with respect to the state variable $\boldsymbol{\psi}$. The tangent operators associated with the transformation $\mathbf{A}^{\dot{\mathbf{v}}}$, in the framework of the local

[5] Because of the local representation, the code computes the acceleration vector of the center of mass as the time derivative of the velocity vector expressed with respect to the basis $\mathcal{M}$ of the body-attached frame; thus, it misses the contribution of the apparent acceleration. In order to be coherent with the linear transformations defined for the mixed-frame formulation, the transformations $\mathbf{A}^{\dot{\mathbf{v}}}$ and $\mathbf{B}^{\dot{\mathbf{v}}}$ defined hereafter are referred to the acceleration vector $\mathbf{a}_G^I$, which includes the apparent term.

representation of the motion, are given by:

$$\mathbf{M}^t = \bar{\mathbf{A}}^{\dot{\mathbf{v}}} \tag{A.44}$$

$$\mathbf{C}^t_{1:3\times 1:3} = \bar{\mathbf{A}}^{\dot{\mathbf{v}}}_{1:3\times 1:3}\widetilde{\bar{\mathbf{v}}}_{4:6} \tag{A.45}$$

$$\mathbf{C}^t_{1:3\times 4:6} = -\bar{\mathbf{A}}^{\dot{\mathbf{v}}}_{1:3\times 1:3}\widetilde{\bar{\mathbf{v}}}_{1:3} \tag{A.46}$$

$$\mathbf{C}^t_{4:6\times 1:3} = \bar{\mathbf{A}}^{\dot{\mathbf{v}}}_{4:6\times 1:3}\widetilde{\bar{\mathbf{v}}}_{4:6} \tag{A.47}$$

$$\mathbf{C}^t_{4:6\times 4:6} = -\bar{\mathbf{A}}^{\dot{\mathbf{v}}}_{4:6\times 1:3}\widetilde{\bar{\mathbf{v}}}_{1:3} \tag{A.48}$$

$$\begin{aligned}\mathbf{K}^t_{1:3\times 4:6} = {} & \big(\widetilde{\bar{\mathbf{A}}^{\dot{\mathbf{v}}}_{1:3\times 1:3}\bar{\dot{\mathbf{v}}}_{1:3}}\big) - \bar{\mathbf{A}}^{\dot{\mathbf{v}}}_{1:3\times 1:3}\widetilde{\bar{\dot{\mathbf{v}}}}_{1:3} + \big(\widetilde{\bar{\mathbf{A}}^{\dot{\mathbf{v}}}_{1:3\times 4:6}\bar{\dot{\mathbf{v}}}_{4:6}}\big) + \\ & - \bar{\mathbf{A}}^{\dot{\mathbf{v}}}_{1:3\times 4:6}\widetilde{\bar{\dot{\mathbf{v}}}}_{4:6} + \big(\widetilde{\bar{\mathbf{A}}^{\dot{\mathbf{v}}}_{1:3\times 1:3}\widetilde{\bar{\mathbf{v}}}_{4:6}\bar{\mathbf{v}}_{1:3}}\big) - \bar{\mathbf{A}}^{\dot{\mathbf{v}}}_{1:3\times 1:3}\big(\widetilde{\widetilde{\bar{\mathbf{v}}}_{4:6}\bar{\mathbf{v}}_{1:3}}\big)\end{aligned} \tag{A.49}$$

$$\begin{aligned}\mathbf{K}^t_{4:6\times 4:6} = {} & \big(\widetilde{\bar{\mathbf{A}}^{\dot{\mathbf{v}}}_{4:6\times 1:3}\bar{\dot{\mathbf{v}}}_{1:3}}\big) - \bar{\mathbf{A}}^{\dot{\mathbf{v}}}_{4:6\times 1:3}\widetilde{\bar{\dot{\mathbf{v}}}}_{1:3} + \big(\widetilde{\bar{\mathbf{A}}^{\dot{\mathbf{v}}}_{4:6\times 4:6}\bar{\dot{\mathbf{v}}}_{4:6}}\big) + \\ & - \bar{\mathbf{A}}^{\dot{\mathbf{v}}}_{4:6\times 4:6}\widetilde{\bar{\dot{\mathbf{v}}}}_{4:6} + \big(\widetilde{\bar{\mathbf{A}}^{\dot{\mathbf{v}}}_{4:6\times 1:3}\widetilde{\bar{\mathbf{v}}}_{4:6}\bar{\mathbf{v}}_{1:3}}\big) - \bar{\mathbf{A}}^{\dot{\mathbf{v}}}_{4:6\times 1:3}\big(\widetilde{\widetilde{\bar{\mathbf{v}}}_{4:6}\bar{\mathbf{v}}_{1:3}}\big)\end{aligned} \tag{A.50}$$

A.3.3.4 Eccentric transformations

Let's suppose that the linear transformations $\mathbf{A}^{(\bullet)}_P$ of the state variable $(\bullet)$ return a load that is applied to a generic point P of the rigid body. The formulation should account for the torque about the center of mass due to the resultant eccentric force. Given the position vector $\mathbf{x}^{B,\mathcal{M}}_P$ of the point P, the linear operator $\bar{\mathbf{A}}^{(\bullet)}_P$, computed with the formulations described in the previous sections, should transforms as follows:

$$\bar{\mathbf{A}}^{(\bullet)} = \bar{\mathbf{T}}^{\mathbf{A}}_P\bar{\mathbf{A}}^{(\bullet)}_P \tag{A.51}$$

$$\bar{\mathbf{T}}^{\mathbf{A}}_P = \begin{bmatrix} \mathbf{I}_3 & \mathbf{0}_{3\times 3} \\ \widetilde{(\mathbf{x}^{B,\mathcal{M}}_P)} & \mathbf{I}_3 \end{bmatrix} \tag{A.52}$$

The operator $\bar{\mathbf{T}}^{\mathbf{A}}_P$ operates as a linear transformation that transports the load applied to point P into a load applied to the center of mass. The associated linear operators $\mathbf{M}^t_P$, $\mathbf{C}^t_P$, $\mathbf{K}^t_P$ transform with the same rule, namely:

$$\mathbf{M}^t = \bar{\mathbf{T}}^{\mathbf{A}}_P\mathbf{M}^t_P \tag{A.53}$$

$$\mathbf{C}^t = \bar{\mathbf{T}}^{\mathbf{A}}_P\mathbf{C}^t_P \tag{A.54}$$

$$\mathbf{K}^t = \bar{\mathbf{T}}^{\mathbf{A}}_P\mathbf{K}^t_P \tag{A.55}$$

A.4 Follower loads

A load is said follower if it is dragged by the body during the motion (it rotates with the body). The components of a follower load, both forces and torques, are referred to the basis $\mathcal{M}$ of the non-inertial frame. Because of the local representation adopted, the contribution of follower loads to the overall external load acting on the body is quite simple to evaluate.

A.4.1 Force

Let $\mathbf{F}_P^f$ be a follower force, applied to the location (point) P of the rigid body, that can depend on time but not on the state variables. Its contribution to the loads acting on the system in the local-frame formulation is given by:

$$\mathbf{F}_G^{\mathcal{M}} = \mathbf{F}_P^f \tag{A.56}$$

$$\mathbf{T}_G^{\mathcal{M}} = (P - G) \times \mathbf{F}_P^f = \widetilde{\mathbf{x}}_P^{B,\mathcal{M}} \mathbf{F}_P^f \tag{A.57}$$

The follower force gives no contribution to the tangent operators of the system.

A.4.2 Torque

Let $\mathbf{T}_P^f$ be a follower moment, applied to the location (point) P of the rigid body, that can depend on time but not on the state variables. Its contribution to the loads acting on the system in the local-frame formulation is given by:

$$\mathbf{F}_G^{\mathcal{M}} = \mathbf{0} \tag{A.58}$$

$$\mathbf{T}_G^{\mathcal{M}} = \mathbf{T}_P^f \tag{A.59}$$

The follower torque gives no contribution to the tangent operators of the system.

A.4.3 Transformations of the state variables

An interesting case deals with loads applied to the rigid body as linear transformations of the state variables $\mathbf{q}$, $\mathbf{v}$, $\dot{\mathbf{v}}$, defined with respect to the basis $\mathcal{M}$ of the body-attached frame. The matrices associated with the linear transformation should be properly converted in order to consider that the motion of the center of mass and the rotational motion of the body are referred to the basis $\mathcal{M}$, with the only aforementioned exception of the position vector of the center of mass. The transformation $\mathbf{B}^{(\bullet)}$ of the state variable $(\bullet)$ associated with the local-frame formulation is indicated with the notation $\bar{\mathbf{B}}^{(\bullet)}$.

A.4.3.1 Configuration operators

Let $\mathbf{B}^{\mathbf{q}}$ be the square matrix of order six associated with a linear transformation of the displacements defined as follows:

$$\begin{bmatrix} \mathbf{F}_G^{\mathcal{M}} \\ \mathbf{T}_G^{\mathcal{M}} \end{bmatrix} = -\mathbf{B}^{\mathbf{q}} \begin{bmatrix} \mathbf{x}_G^{I,\mathcal{M}} \\ \boldsymbol{\psi} \end{bmatrix} \tag{A.60}$$

The transformation expressed in the framework of the local representation of the motion is given by:

$$\begin{bmatrix} \mathbf{F}_G^{\mathcal{M}} \\ \mathbf{T}_G^{\mathcal{M}} \end{bmatrix} = -\bar{\mathbf{B}}^{\mathbf{q}} \begin{bmatrix} \bar{\mathbf{q}}_{1:3} \\ \bar{\mathbf{q}}_{4:6} \end{bmatrix} \tag{A.61}$$

$$\bar{\mathbf{B}}^{\mathbf{q}}_{1:3\times 1:3} = \mathbf{B}^{\mathbf{q}}_{1:3\times 1:3} \mathbf{R}^T \tag{A.62}$$

$$\bar{\mathbf{B}}^{\mathbf{q}}_{1:3\times 4:6} = \mathbf{B}^{\mathbf{q}}_{1:3\times 4:6} \tag{A.63}$$

$$\bar{\mathbf{B}}^{\mathbf{q}}_{4:6\times 1:3} = \mathbf{B}^{\mathbf{q}}_{4:6\times 1:3} \mathbf{R}^T \tag{A.64}$$

$$\bar{\mathbf{B}}^{\mathbf{q}}_{4:6\times 4:6} = \mathbf{B}^{\mathbf{q}}_{4:6\times 4:6} \tag{A.65}$$

The new transformation is nonlinear with respect to the state variable $\boldsymbol{\psi}$. The tangent operators associated with the transformation $\bar{\mathbf{B}}^{\mathbf{q}}$ are given by:

$$\mathbf{K}^t_{1:3\times 1:3} = \bar{\mathbf{B}}^{\mathbf{q},\star}_{1:3\times 1:3} \tag{A.66}$$

$$\mathbf{K}^t_{1:3\times 4:6} = \bar{\mathbf{B}}^{\mathbf{q},\star}_{1:3\times 4:6} + \mathbf{B}^{\mathbf{q}}_{1:3\times 1:3}\widetilde{(\mathbf{R}^T\bar{\mathbf{q}}_{1:3})} \tag{A.67}$$

$$\mathbf{K}^t_{4:6\times 1:3} = \bar{\mathbf{B}}^{\mathbf{q},\star}_{4:6\times 1:3} \tag{A.68}$$

$$\mathbf{K}^t_{4:6\times 4:6} = \bar{\mathbf{B}}^{\mathbf{q},\star}_{4:6\times 4:6} + \mathbf{B}^{\mathbf{q}}_{4:6\times 1:3}\widetilde{(\mathbf{R}^T\bar{\mathbf{q}}_{1:3})} \tag{A.69}$$

A.4.3.2 Velocity operators

Let $\mathbf{B}^{\mathbf{v}}$ be the square matrix of order six associated with a linear transformation of the velocities defined as follows:

$$\begin{bmatrix} \mathbf{F}^{\mathcal{M}}_G \\ \mathbf{T}^{\mathcal{M}}_G \end{bmatrix} = -\mathbf{B}^{\mathbf{v}} \begin{bmatrix} \mathbf{v}^{I,\mathcal{M}}_G \\ \boldsymbol{\omega}^{\mathcal{M}} \end{bmatrix} = -\mathbf{B}^{\mathbf{v}} \begin{bmatrix} \bar{\mathbf{v}}_{1:3} \\ \bar{\mathbf{v}}_{4:6} \end{bmatrix} \tag{A.70}$$

The matrix $\mathbf{B}^{\mathbf{v}}$ is already formulated in the framework of the local representation of the motion, namely:

$$\bar{\mathbf{B}}^{\mathbf{v}} = \mathbf{B}^{\mathbf{v}} \tag{A.71}$$

The tangent operator associated with the transformation $\bar{\mathbf{B}}^{\mathbf{v}}$ is given by:

$$\mathbf{C}^t = \bar{\mathbf{B}}^{\mathbf{v}} \tag{A.72}$$

A.4.3.3 Acceleration operators

Let $\mathbf{B}^{\dot{\mathbf{v}}}$ be the square matrix of order six associated with a linear transformation of the accelerations defined as follows:

$$\begin{bmatrix} \mathbf{F}^{\mathcal{M}}_G \\ \mathbf{T}^{\mathcal{M}}_G \end{bmatrix} = -\mathbf{B}^{\dot{\mathbf{v}}} \begin{bmatrix} \mathbf{a}^{I,\mathcal{M}}_G \\ \dot{\boldsymbol{\omega}}^{\mathcal{M}} \end{bmatrix} = -\mathbf{B}^{\dot{\mathbf{v}}} \begin{bmatrix} \dot{\mathbf{v}}^{I,\mathcal{M}}_G + \widetilde{\boldsymbol{\omega}}^{\mathcal{M}}\mathbf{v}^{I,\mathcal{M}}_G \\ \dot{\boldsymbol{\omega}}^{\mathcal{M}} \end{bmatrix} \tag{A.73}$$

The resulting load associated with the operator $\mathbf{B}^{\dot{\mathbf{v}}}$ can be split into a linear transformation of the acceleration vector $\bar{\mathbf{B}}^{\dot{\mathbf{v}}}$ and a nonlinear function of the velocity vectors, namely:

$$\begin{bmatrix} \mathbf{F}^{\mathcal{M}}_G \\ \mathbf{T}^{\mathcal{M}}_G \end{bmatrix} = -\bar{\mathbf{B}}^{\dot{\mathbf{v}}} \begin{bmatrix} \bar{\mathbf{v}}_{1:3} \\ \bar{\mathbf{v}}_{4:6} \end{bmatrix} - \begin{bmatrix} \mathbf{B}^{\dot{\mathbf{v}}}_{1:3\times 1:3}\widetilde{\bar{\mathbf{v}}}_{4:6}\bar{\mathbf{v}}_{1:3} \\ \mathbf{B}^{\dot{\mathbf{v}}}_{4:6\times 1:3}\widetilde{\bar{\mathbf{v}}}_{4:6}\bar{\mathbf{v}}_{1:3} \end{bmatrix} \tag{A.74}$$

$$\bar{\mathbf{B}}^{\dot{\mathbf{v}}} = \mathbf{B}^{\dot{\mathbf{v}}} \tag{A.75}$$

The tangent operators associated with the transformation $\mathbf{B}^{\dot{\mathbf{v}}}$, in the framework of the local representation of the motion, are given by:

$$\mathbf{M}^t = \bar{\mathbf{B}}^{\dot{\mathbf{v}}} \tag{A.76}$$

$$\mathbf{C}^t_{1:3\times 1:3} = \mathbf{B}^{\dot{\mathbf{v}}}_{1:3\times 1:3}\widetilde{\bar{\mathbf{v}}}_{4:6} \tag{A.77}$$

$$\mathbf{C}^t_{1:3\times 4:6} = -\mathbf{B}^{\dot{\mathbf{v}}}_{1:3\times 1:3}\widetilde{\bar{\mathbf{v}}}_{1:3} \tag{A.78}$$

$$\mathbf{C}^t_{4:6\times 1:3} = \mathbf{B}^{\dot{\mathbf{v}}}_{4:6\times 1:3}\widetilde{\bar{\mathbf{v}}}_{4:6} \tag{A.79}$$

$$\mathbf{C}^t_{4:6\times 4:6} = -\mathbf{B}^{\dot{\mathbf{v}}}_{4:6\times 1:3}\widetilde{\bar{\mathbf{v}}}_{1:3} \tag{A.80}$$

A.4.3.4 Eccentric transformations

Let's suppose that the linear transformations $\mathbf{B}^{(\bullet)}_P$ of the state variable $(\bullet)$ return a load that is applied to a generic point P of the rigid body. The formulation should account for the torque about the center of mass due to the resultant eccentric force. Given the position vector $\mathbf{x}^{B,\mathcal{M}}_P$ of the point P, the linear operator $\bar{\mathbf{B}}^{(\bullet)}_P$, computed with the formulations described in the previous sections, should transforms as follows[6]:

$$\bar{\mathbf{B}}^{(\bullet)} = \bar{\mathbf{T}}^{\mathbf{B}}_P \bar{\mathbf{B}}^{(\bullet)}_P \tag{A.81}$$

$$\bar{\mathbf{T}}^{\mathbf{B}}_P = \begin{bmatrix} \mathbf{I}_3 & \mathbf{0}_{3\times 3} \\ \widetilde{(\mathbf{x}^{B,\mathcal{M}}_P)} & \mathbf{I}_3 \end{bmatrix} \tag{A.82}$$

The operator $\bar{\mathbf{T}}^{\mathbf{B}}_P$ operates as a linear transformation that transports the load applied to point P into a load applied to the center of mass. The associated linear operators $\mathbf{M}^t_P$, $\mathbf{C}^t_P$, $\mathbf{K}^t_P$ transform with the same rule, namely:

$$\mathbf{M}^t = \bar{\mathbf{T}}^{\mathbf{B}}_P \mathbf{M}^t_P \tag{A.83}$$

$$\mathbf{C}^t = \bar{\mathbf{T}}^{\mathbf{B}}_P \mathbf{C}^t_P \tag{A.84}$$

$$\mathbf{K}^t = \bar{\mathbf{T}}^{\mathbf{B}}_P \mathbf{K}^t_P \tag{A.85}$$

A.5 Time integration algorithm

The dynamic differential problem of the rigid body in the Euclidean space (six degrees of freedom) is solved with an efficient Lie group time integrator [86], suitable both for constrained and unconstrained rigid bodies. At each time step, the scheme solves the set of differential equations with an extension of the classical generalized-α method combined with the Newton-Raphson scheme, necessary for computing the increment of the state variable $\bar{\mathbf{q}}$ (and then $\bar{\mathbf{v}}$, $\bar{\dot{\mathbf{v}}}$) that provides the dynamic equilibrium. The Newton-Raphson algorithm involves the linearisation of the nonlinear differential problem around the previous equilibrium configuration by means of the tangent operators.

[6] The formulation is the same described for non-follower loads. In effect both the operators $\bar{\mathbf{A}}^{(\bullet)}_P$ and $\bar{\mathbf{B}}^{(\bullet)}_P$ return a load expressed in the framework of the local representation of the motion, which should be transformed in the same way, i.e. $\bar{\mathbf{T}}^{\mathbf{B}}_P \equiv \bar{\mathbf{T}}^{\mathbf{A}}_P$.

The rotations are parametrized by the rotational vector, in place of the more common Euler angles (or Tait-Bryan angles).

Let $\bar{\mathbf{q}} = [\mathbf{x}_G^{I,\mathcal{S}}; \boldsymbol{\psi}]$ be the position state vector, where $\mathbf{x}_G^{I,\mathcal{S}}$ is the position vector of the center of mass and $\boldsymbol{\psi}$ is the rotational vector, and let $\bar{\mathbf{v}}$ and $\dot{\bar{\mathbf{v}}}$ be respectively the corresponding velocity vector and acceleration vector expressed in the framework of the local representation of the motion. The state variables at time t_{n+1} can be computed with the Algorithm A.1 [10, 11, 86].

Algorithm A.1: Scheme (single time step) for the solution of the local-frame formulation of the dynamic problem (adapted from [10, 11, 86]).

input : h, α_f, α_m, β, γ, tol, n_{max}, m, $\mathbf{J}$, $\mathbf{g}$, $\bar{\mathbf{q}}_n$, $\bar{\mathbf{v}}_n$, $\bar{\dot{\mathbf{v}}}_n$, $\mathbf{a}_n$, $\mathbf{F}^{(\bullet)}$, $\mathbf{T}^{(\bullet)}$, $\mathbf{A}^{(\bullet)}$, $\mathbf{B}^{(\bullet)}$, ...

output: $\bar{\mathbf{q}}_{n+1}$, $\bar{\mathbf{v}}_{n+1}$, $\bar{\dot{\mathbf{v}}}_{n+1}$, $\mathbf{a}_{n+1}$

$\beta' = \frac{1-\alpha_m}{\beta h^2(1-\alpha_f)}$;

$\gamma' = \frac{\gamma}{\beta h}$;

$\bar{\dot{\mathbf{v}}}_{n+1} = \mathbf{0}$;

$\mathbf{a}_{n+1} = \frac{\alpha_f \bar{\dot{\mathbf{v}}}_n - \alpha_m \mathbf{a}_n}{1-\alpha_m}$;

$\bar{\mathbf{v}}_{n+1} = \bar{\mathbf{v}}_n + h(1-\gamma)\mathbf{a}_n + \gamma h \mathbf{a}_{n+1}$;

$\mathbf{q}^* = \varphi^1_{h^*}(\bar{\mathbf{q}}_n, \bar{\mathbf{v}}_n, \mathbf{a}_n, h, \beta) = \bar{\mathbf{q}}_n$;

$\mathbf{y} = \varphi^1_{hy}(\bar{\mathbf{v}}_n, \mathbf{a}_n, \mathbf{a}_{n+1}, h, \beta) = h\bar{\mathbf{v}}_n + h^2(0.5-\beta)\mathbf{a}_n + \beta h^2 \mathbf{a}_{n+1}$;

for $i \leftarrow 1$ **to** n_{max} **do**

  $\bar{\mathbf{q}}_{n+1,1:3} = \mathbf{x}_{n+1} = \mathbf{q}^*_{1:3} + \mathbf{R}(\mathbf{q}^*_{4:6})[\mathbf{T}(\mathbf{y}_{4:6})]^T \mathbf{y}_{1:3}$;

  $\bar{\mathbf{q}}_{n+1,4:6} = \boldsymbol{\psi}_{n+1} = \log_{\mathbf{R}}\big(\mathbf{R}(\mathbf{q}^*_{4:6})\mathbf{R}(\mathbf{y}_{4:6})\big)$;

  $(\bar{\diamond})^{(\bullet)} = (\bar{\diamond})^{(\bullet)}(\boldsymbol{\psi}_{n+1}, t_{n+1}), \qquad (\diamond) = \mathbf{F}, \mathbf{T}, \mathbf{A}, \mathbf{B}$;

  $\mathbf{res} = \bar{\mathbf{r}}(\bar{\mathbf{q}}_{n+1}, \bar{\mathbf{v}}_{n+1}, \bar{\dot{\mathbf{v}}}_{n+1}, t_{n+1})$;

  if $||\mathbf{res}|| < tol$ **then**

    break;

  end

  $\mathbf{M}^t = \mathbf{M}^t(\bar{\mathbf{q}}_{n+1}, \bar{\mathbf{v}}_{n+1}, \bar{\dot{\mathbf{v}}}_{n+1}, t_{n+1})$;

  $\mathbf{C}^t = \mathbf{C}^t(\bar{\mathbf{q}}_{n+1}, \bar{\mathbf{v}}_{n+1}, \bar{\dot{\mathbf{v}}}_{n+1}, t_{n+1})$;

  $\mathbf{K}^t = \mathbf{K}^t(\bar{\mathbf{q}}_{n+1}, \bar{\mathbf{v}}_{n+1}, \bar{\dot{\mathbf{v}}}_{n+1}, t_{n+1})$;

  $\mathbf{T}^\dagger_{1:3\times 1:3} = \mathbf{I}_3 + \frac{\cos\phi - 1}{\phi^2}\widetilde{\mathbf{y}}_{4:6} + \left(1 - \frac{\sin\phi}{\phi}\right)\frac{\widetilde{\mathbf{y}}_{4:6}\widetilde{\mathbf{y}}_{4:6}}{\phi^2}, \qquad \phi = |\mathbf{y}_{4:6}|$;

  $\mathbf{T}^\dagger_{1:3\times 4:6} = -\frac{\beta^*}{2}\widetilde{\mathbf{y}}_{1:3} + \frac{1-\alpha^*}{\phi^2}(\widetilde{\mathbf{y}}_{1:3}\widetilde{\mathbf{y}}_{4:6} + \widetilde{\mathbf{y}}_{4:6}\widetilde{\mathbf{y}}_{1:3}) - \frac{\alpha^* - \beta^*}{\phi^2}(\mathbf{y}^T_{4:6}\mathbf{y}_{1:3})\widetilde{\mathbf{y}}_{4:6} + \frac{1}{\phi^2}\left[\frac{\beta^*}{2} - \frac{3(1-\alpha^*)}{\phi^2}\right](\mathbf{y}^T_{4:6}\mathbf{y}_{1:3})\widetilde{\mathbf{y}}_{4:6}\widetilde{\mathbf{y}}_{4:6}, \qquad \phi = |\mathbf{y}_{4:6}|,\ \alpha^* = \frac{\sin\phi}{\phi},\ \beta^* = 2\frac{1-\cos\phi}{\phi^2}$;

  $\mathbf{T}^\dagger_{4:6\times 4:6} = \mathbf{I}_3 + \frac{\cos\phi - 1}{\phi^2}\widetilde{\mathbf{y}}_{4:6} + \left(1 - \frac{\sin\phi}{\phi}\right)\frac{\widetilde{\mathbf{y}}_{4:6}\widetilde{\mathbf{y}}_{4:6}}{\phi^2}, \qquad \phi = |\mathbf{y}_{4:6}|$;

  $\mathbf{S}_t = \beta'\mathbf{M}^t + \gamma'\mathbf{C}^t + \mathbf{K}^t\mathbf{T}^\dagger$;

  $\Delta\mathbf{y} = -\mathbf{S}_t^{-1}\mathbf{res}$;

  $\mathbf{y} = \mathbf{y} + \Delta\mathbf{y}$;

  $\bar{\mathbf{v}}_{n+1} = \bar{\mathbf{v}}_{n+1} + \gamma'\Delta\mathbf{y}$;

  $\bar{\dot{\mathbf{v}}}_{n+1} = \bar{\dot{\mathbf{v}}}_{n+1} + \beta'\Delta\mathbf{y}$;

end

$\mathbf{a}_{n+1} = \mathbf{a}_{n+1} + \frac{1-\alpha_f}{1-\alpha_m}\bar{\dot{\mathbf{v}}}_{n+1}$;

Appendix B

Rigid-body oscillators

"Entities should not be multiplied unnecessarily."

William of Ockham

The numerical model based on the mixed-frame formulation is tested on a series of oscillators whose exact analytic solution is well known. Several cases are analysed, which differ to each other on the excited degree of freedom (translational or rotational), or on the stiffness and damping properties of the system, or on the forcing load. The appendix aims at providing the reader with some additional details on the reliability of the numerical dynamic model.

B.1 Undamped oscillators

In this section, the algorithm is tested against undamped harmonic oscillators in order to prove the effectiveness of the approach and the reliability of the dynamic model. Both forced translational and rotational oscillations are considered together with the special case of a completely free body, i.e. without any damper or spring, forced by a harmonic load. The numerical solution obtained with the time integrator based on the mixed-frame formulation is compared with the exact analytic solution.

B.1.1 Rigid body with sinusoidal force

Let's consider a rigid body driven by a sinusoidal non-follower[1] force without any other load (even the weight is null), or stiffness, or damping; the features of the system and of loads are reported in Table B.1. The absence of an external torque together with the zero initial rotational velocity guarantees that the system translates without rotating. This test aims to verify the sensitivity of the numerical model to the initial velocity conditions, in order to well understand the role and the influence of numerical inaccuracies.

environment		
gravity acceleration, g	0.00	m/s^2
rigid body		
mass, m	1.0	kg
natural angular frequency, ω_n	0.0	rad/s
damping factor, ν	0.0	-
loads		
force, $F^f_{G,2}$	$\sin(\pi/5 \cdot t)$	N
initial conditions		
displacement, $\hat{q}_2\|_{t=0}$	0.0	m
velocity, $\hat{v}_2\|_{t=0}$	variable	m/s

Table B.1: Rigid body with sinusoidal force; parameters used for the analysis.

B.1.1.1 Analytic solution

Let's focus on the dynamics of the center of mass forced by an external force, the differential problem is given by:

$$m\dot{\mathbf{v}}_G^{I,\mathcal{S}} = \mathbf{F}_G^{\mathcal{S}} \tag{B.1}$$

[1] Since the system does not rotate, the external force can be considered follower or non-follower without changing the differential problem.

If the external load is a sinusoidal force along the y-axis with circular frequency ω and amplitude F, the previous equations can be simplified as follows:

$$\ddot{x}_{G,1}^{I,\mathcal{S}} = 0 \tag{B.2}$$

$$m\ddot{x}_{G,2}^{I,\mathcal{S}} = F_{G,2}^{\mathcal{S}} = F\sin(\omega t) \tag{B.3}$$

$$\ddot{x}_{G,3}^{I,\mathcal{S}} = 0 \tag{B.4}$$

Let's focus on the Equation (B.3)[2], its general integral is given by:

$$x_{G,2}^{I,\mathcal{S}} = \frac{-F}{m\omega^2}\sin(\omega t) + C_1 t + C_2 \tag{B.5}$$

The general integral should be associated with the initial conditions; thus, the solution of the initial value problem is given by:

$$x_{G,2}^{I,\mathcal{S}}|_{t=0} = x_0 \tag{B.6}$$

$$\dot{x}_{G,2}^{I,\mathcal{S}}|_{t=0} = \dot{x}_0 \tag{B.7}$$

$$x_{G,2}^{I,\mathcal{S}} = \frac{-F}{m\omega^2}\sin(\omega t) + \left(\dot{x}_0 + \frac{F}{m\omega}\right)t + x_0 \tag{B.8}$$

The Equation (B.8) shows that if and only if the initial velocity is $\dot{x}_0 = -F/(m\omega)$ the motion along the y-axis is a limited sinusoidal curve; otherwise, for any other value of the initial velocity, the trajectory indefinitely grows with time (see Figure B.1)[3].

B.1.1.2 Results

In order to verify the sensitivity of the numerical model to the initial velocity conditions, the system is analysed in the neighbourhood of the unique condition that guarantees a limited solution, namely:

- $\hat{v}_2|_{t=0} = -F/(m\omega)$;
- $\hat{v}_2|_{t=0} = -F/(m\omega) \pm 10^{-7}$ m/s;
- $\hat{v}_2|_{t=0} = -F/(m\omega) \pm 10^{-3}$ m/s;
- $\hat{v}_2|_{t=0} = -F/(m\omega) \pm 10^{-2}$ m/s;
- $\hat{v}_2|_{t=0} = -F/(m\omega) \pm 10^{-1}$ m/s.

[2]The other two equations, if associated with the natural initial conditions, have an identically null solution.

[3]The figure illustrates the analytic solution for some values of the constant C_1, which is directly related to the initial velocity as follows:

$$C_1 = \dot{x}_0 + \frac{F}{m\omega}$$

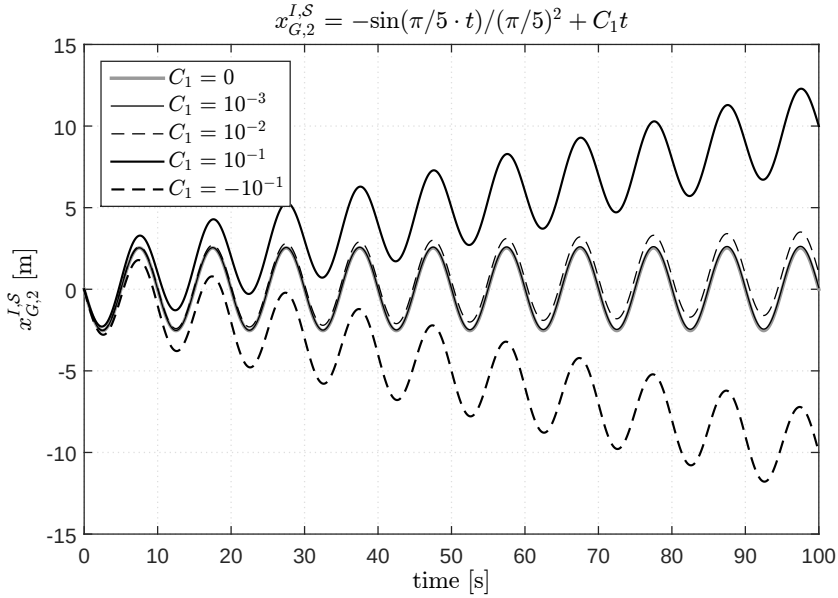

Figure B.1: Rigid body with sinusoidal force; analytic solution for some values of the initial velocity condition.

According to the theory, the center of mass (see Figure B.2) translates only along the y-axis, and if the initial velocity is $\hat{v}_2|_{t=0} = -F/(m\omega)$, the trajectory is rightly a limited curve. The perturbation of the initial velocity (see Figure B.3) causes solutions with a divergent trend, as the analytic solution, but if the perturbation is small, of the order of the numerical error, the solution does not grow (diverge) with appreciable mean velocity.

B.1.1.3 Remarks

The time integrator can properly capture the motion of the center of mass of a driven rigid body. In particular, the numerical solution matches the exact analytic solution for a wide range of initial velocities. When a code works in finite precision, numerical errors ever occur. In this test case the numerical solution obtained by perturbing the initial velocity with an addend of the order of 10^{-7} m/s is reasonably accurate, and indeed the possible numerical errors do not significantly affect the results[4].

B.1.2 Forced harmonic oscillator

Let's consider a system with a linear translational spring, i.e. a simple spring modelled by a diagonal stiffness matrix, placed in the center of mass and forced by a sinusoidal follower force directed along the x-axis without any other external load (even the gravitational field is considered null); the features of the system and of loads are reported in Table B.2. Because of the initial and boundary conditions, the system translates along the x-axis without rotating; therefore, only $\hat{q}_1$, $\hat{v}_1$, and $\hat{\dot{v}}_1$ vary with time, whereas the

[4]For instance, the machine precision of Matlab is $2.2204 \cdot 10^{-16}$.

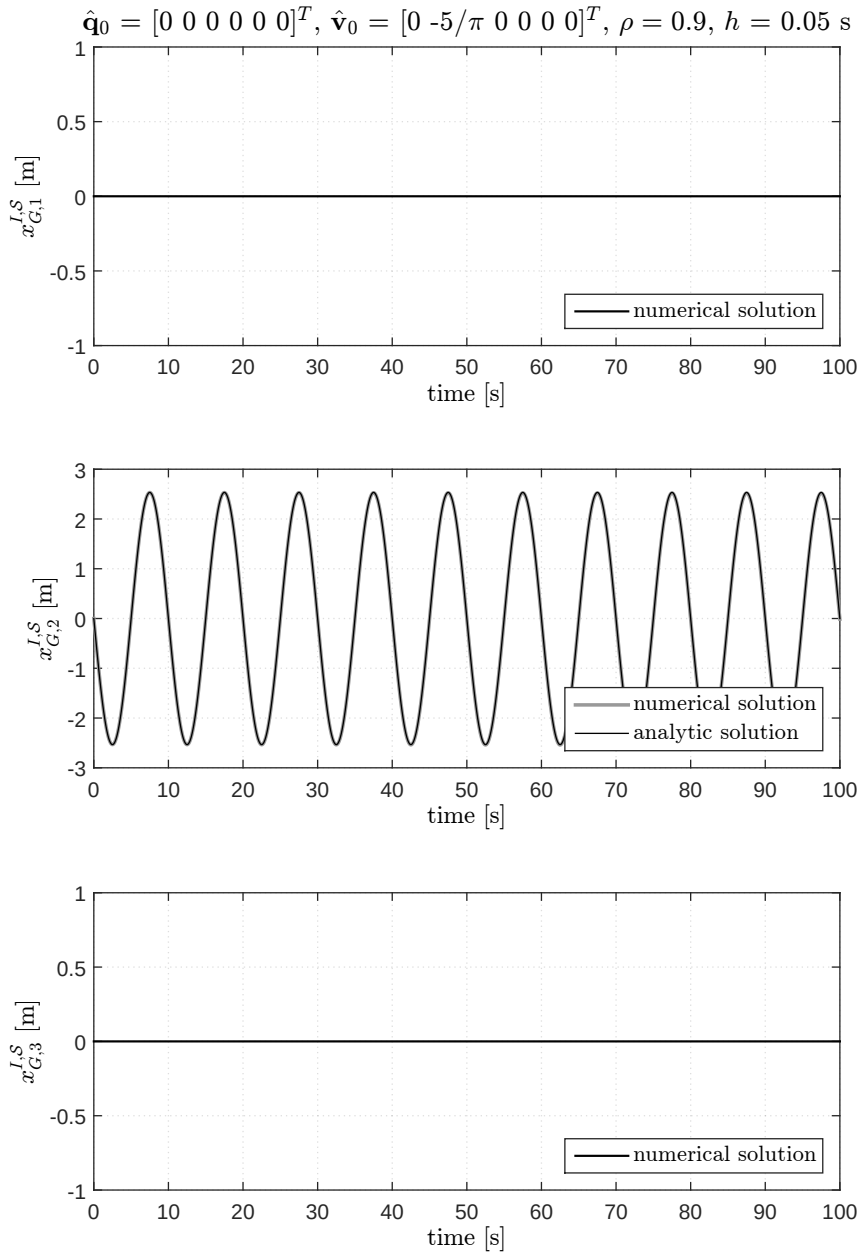

Figure B.2: Rigid body with sinusoidal force; trajectory of the center of mass, $\hat{v}_2|_{t=0} = -F/(m\omega)$.

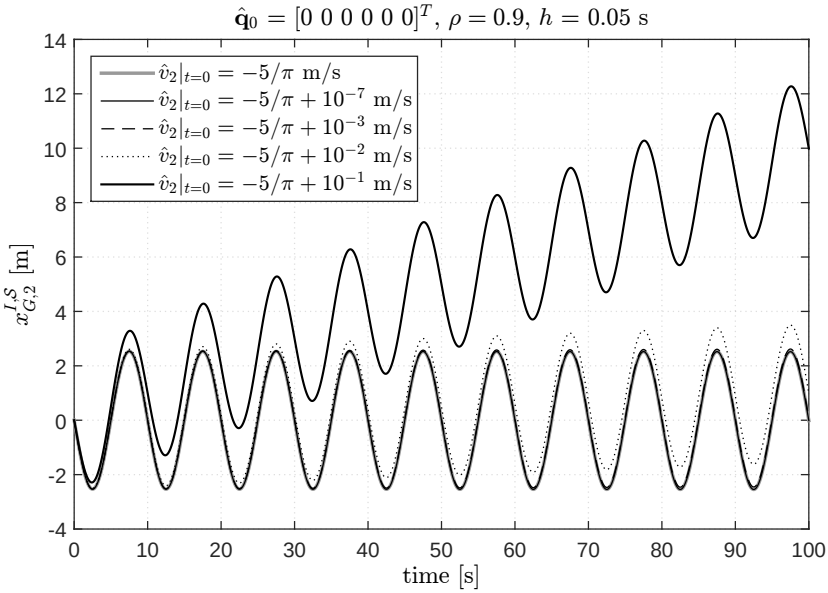

(a) positive perturbation

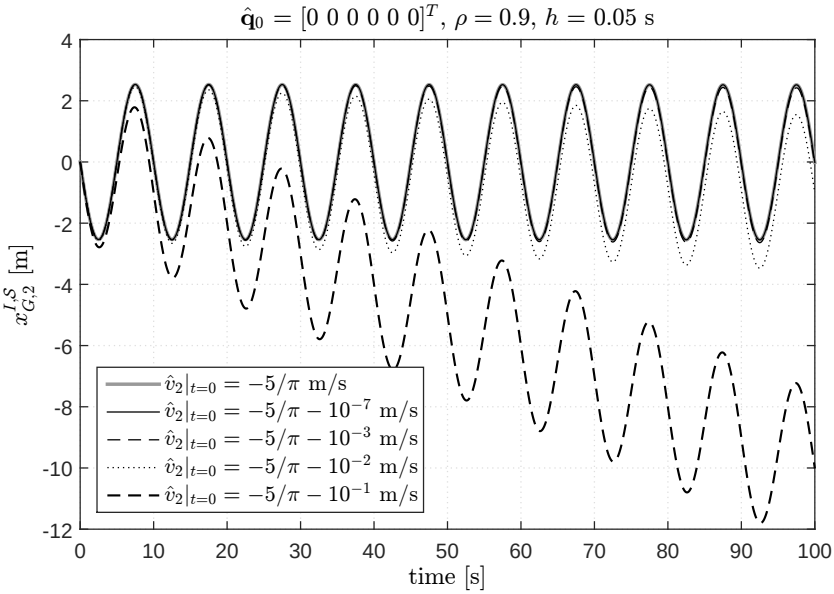

(b) negative perturbation

Figure B.3: Rigid body with sinusoidal force; effect of a perturbation of the initial velocity condition.

environment		
gravity acceleration, g	0.00	m/s^2
rigid body		
mass, m	1.0	kg
natural angular frequency, ω_n	$\pi/5$	rad/s
damping factor, ν	0.0	-
loads		
stiffness, $B^{\mathbf{q}}_{11}$	$m\omega_n^2$	N/m
force, $F^f_{G,1}$	$\sin(\omega t)$	N
initial conditions		
displacement, $\hat{q}_1\|_{t=0}$	0.0	m
velocity, $\hat{v}_1\|_{t=0}$	0.0	m/s

Table B.2: Forced harmonic oscillator; parameters used for the analysis.

other components of the state variables are identically zero. The differential problem can be reduced to the study of a one-dimensional oscillator. This test aims to verify if the algorithm is able to analyse the translational motion at different working fields, depending on the frequency of the forcing force with respect to the natural frequency of the system.

B.1.2.1 Analytic solution

As mentioned before, the six-dimensional differential problem can be reduced to a simple forced harmonic oscillator along the x-axis. The initial value problem is given by[5]:

$$m\ddot{x}_{G,1} + K^t_{11}x_{G,1} = F^{\mathcal{S}}_{G,1} = F\sin(\omega t) \tag{B.9}$$

$$x_{G,1}|_{t=0} = x_0, \qquad \dot{x}_{G,1}|_{t=0} = \dot{x}_0 \tag{B.10}$$

The translational stiffness[6] and the mass of system identify the natural angular frequency ω_n, namely:

$$\omega_n = \sqrt{\frac{K^t_{11}}{m}} \tag{B.11}$$

[5]In order to not weigh the notation down, the indication of both the reference frame and the basis is removed, namely:

$$\mathbf{x} = \mathbf{x}^{I,\mathcal{S}}$$

[6]The translational stiffness can be modelled as a linear transformation of the displacement, i.e. $K^t_{11} \equiv B^{\mathbf{q}}_{11}$.

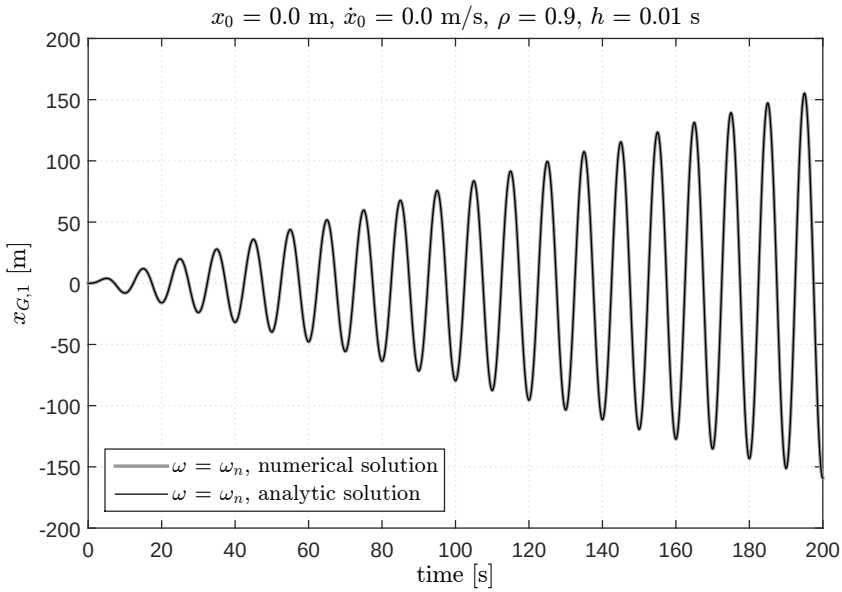

Figure B.4: Forced harmonic oscillator; comparison between the numerical solution (got with the algorithm based on the mixed-frame formulation) and the exact analytic solution in the case of resonance.

The exact analytic solution of the differential problem is given by [36]:

$$x_{G,1} = \frac{1}{1-\left(\frac{\omega}{\omega_n}\right)^2}\frac{F}{K_{11}^t}\sin(\omega t) + \left[\frac{\dot{x}_0}{\omega_n} - \frac{\frac{\omega}{\omega_n}}{1-\left(\frac{\omega}{\omega_n}\right)^2}\frac{F}{K_{11}^t}\right]\sin(\omega_n t) + \\ + x_0\cos(\omega_n t) \qquad \text{if} \quad \omega \neq \omega_n \tag{B.12}$$

In the case of *resonance*, i.e. $\omega = \omega_n$, with natural initial conditions[7], the solution of the differential problem is given by:

$$x_{G,1} = \frac{F}{2K_{11}^t}\left[\sin(\omega_n t) - \omega_n t\cos(\omega_n t)\right] \qquad \text{if} \quad \omega = \omega_n \tag{B.13}$$

B.1.2.2 Results

The solution obtained with the Lie group time integrator (see Figure B.5) matches the exact analytic solution both in the resonance neighbourhood and far from it. According to the theory, closed to the resonance frequency (under or above), the beats phenomenon is observed, whereas at the resonance frequency (see Figure B.4) the system vibrates with an amplitude that grows linearly and indefinitely with time.

[7]The initial conditions are said *natural* when both the position vector and the velocity vector are null.

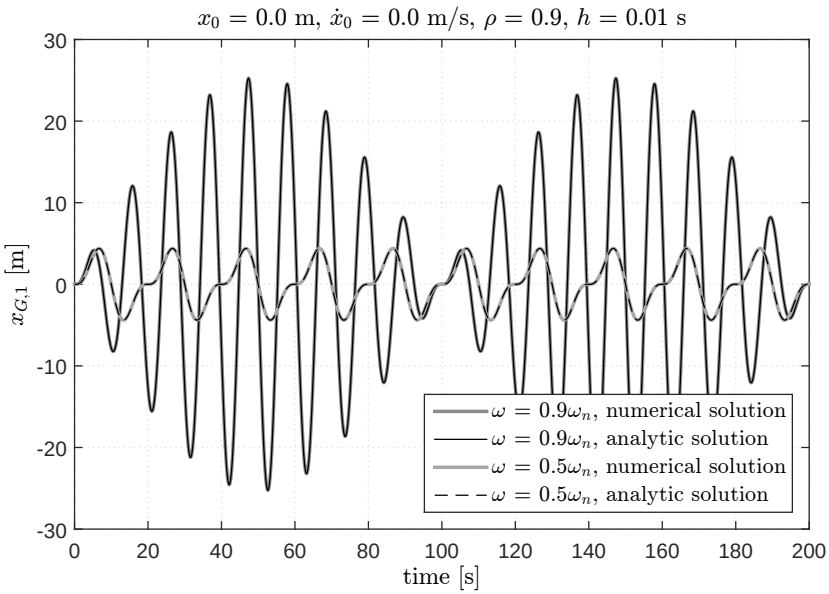

(a) below the resonance

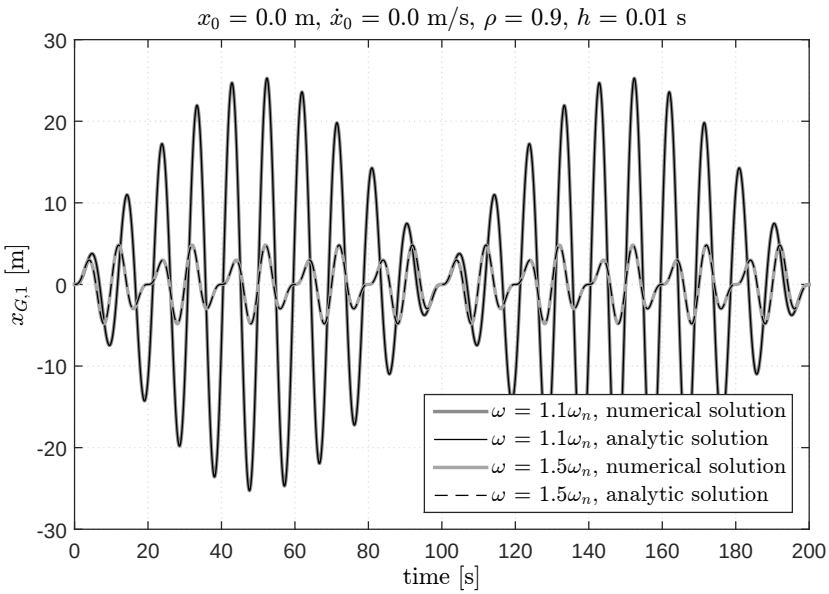

(b) above the resonance

Figure B.5: Forced harmonic oscillator; comparison between the numerical solution (got with the algorithm based on the mixed-frame formulation) and the exact analytic solution for different angular frequencies of the forcing sinusoidal load.

environment		
gravity acceleration, g	0.00	m/s^2
rigid body		
mass, m	10.0	kg
inertia, $\mathbf{J}$	diag(4 4 4)	$kg \cdot m^2$
natural angular frequency, ω_n	5.0	rad/s
damping factor, ν	0.0	-
loads		
stiffness, $B^{\mathbf{q}}_{44}$	$J_{11}\omega_n^2$	$N \cdot m/rad$
torque, T^f_1	$\sin(\omega t)$	$N \cdot m$
initial conditions		
displacement, $\hat{q}_4\|_{t=0}$	0.0	rad
velocity, $\hat{v}_4\|_{t=0}$	0.0	rad/s

Table B.3: Forced rotational harmonic oscillator; parameters used for the analysis.

B.1.2.3 Remarks

The Lie group time integration scheme used to solve the differential problem is able to well describe the motion of the body regardless of the frequency of the forcing force, i.e. the motion is well captured both in resonance, close to resonance, or far from it. Further tests (not reported here) revealed a perfect match between the numerical and analytic solutions also with generic initial conditions, confirming the reliability of the time integrator employed.

B.1.3 Forced rotational harmonic oscillator

Let's consider a system with a linear rotational spring, i.e. a simple spring modelled by a diagonal stiffness matrix[8], placed in its center of mass and forced by a sinusoidal follower[9] torque about the x-axis without any other external load (even the gravitational field is considered null); the features of the system and of loads are reported in Table B.3. Because of the initial and boundary conditions, the system rotates about a fixed axis (the x-axis); therefore, only ψ_1, $\hat{v}_4$, and $\hat{\dot{v}}_4$ vary with time, whereas the other components of the state variables are identically zero. The differential problem can be reduced to the study of a one-dimensional oscillator[10]. This test aims to verify if the algorithm is able to analyse the motion at different working fields, depending on the frequency of the forcing torque with respect to the natural frequency of the system.

[8] The tangent stiffness matrix should be diagonal in order to guarantee that the system is forced (or restored) only along the direction of the displacements.

[9] Since the rotational axis is fixed, i.e. a one-dimensional rotational motion, the external torque can be considered both follower and non-follower without changing the differential problem.

[10] When the rotational axis is fixed, the rotational vector is definitely equivalent to the nautical angles (or any other Euler angle representation), for instance $\psi_1 \equiv \varphi_1$. Moreover, in this very particular case, rotations has a vector character.

B.1.3.1 Analytic solution

As mentioned before, the six-dimensional differential problem can be reduced to a simple forced rotational harmonic oscillator about the x-axis. The initial value problem is given by:

$$J_{11}\ddot{\psi}_1 + K^t_{44}\psi_1 = T_1^{\mathcal{M}} = T\sin(\omega t) \tag{B.14}$$

$$\psi_1|_{t=0} = \psi_0, \qquad \dot{\psi}_1|_{t=0} = \dot{\psi}_0 \tag{B.15}$$

The rotational stiffness[11] and the inertia of system identify the natural angular frequency ω_n, namely:

$$\omega_n = \sqrt{\frac{K^t_{44}}{J_{11}}} \tag{B.16}$$

The exact analytic solution of the differential problem is given by [36]:

$$\begin{aligned}\psi_1 = {} & \frac{1}{1-\left(\frac{\omega}{\omega_n}\right)^2}\frac{T}{K^t_{44}}\sin(\omega t) + \left[\frac{\dot{\psi}_0}{\omega_n} - \frac{\frac{\omega}{\omega_n}}{1-\left(\frac{\omega}{\omega_n}\right)^2}\frac{T}{K^t_{44}}\right]\sin(\omega_n t) + \\ & + \psi_0\cos(\omega_n t) \qquad \text{if} \quad \omega \neq \omega_n\end{aligned} \tag{B.17}$$

In the case of *resonance*, i.e. $\omega = \omega_n$, with natural initial conditions, the solution of the differential problem is given by:

$$\psi_1 = \frac{T}{2K^t_{44}}\left[\sin(\omega_n t) - \omega_n t\cos(\omega_n t)\right] \qquad \text{if} \quad \omega = \omega_n \tag{B.18}$$

Note that the differential problem is formally the same faced in the previous section.

B.1.3.2 Results

Although the numerical problem refers to the part of the code dealing with finite rotations (with its proper algebra), the results are equivalent to those obtained for the translational harmonic oscillator, as expected. The solution obtained with the Lie group time integrator (see Figure B.7) matches the exact analytic solution both in the resonance neighbourhood and far from it. According to the theory, closed to the resonance frequency (under or above), the beats phenomenon is observed, whereas at the resonance frequency (see Figure B.6) the system vibrates with an amplitude that grows linearly and indefinitely with time.

B.1.3.3 Remarks

As far as rotations about a fixed axis are concerned, the Lie group time integration scheme used to solve the differential problem is able to well describe the motion of the body regardless of the frequency of the forcing torque, i.e. the motion is well captured both in resonance, close to resonance, or far from it. Further tests (not reported here) revealed a perfect match between the numerical and the analytic solutions also with generic initial conditions, confirming the reliability of the time integrator employed.

[11] The rotational stiffness can be modelled as a linear transformation of the rotational vector, i.e. $K^t_{44} \equiv B^{\mathfrak{q}}_{44}$.

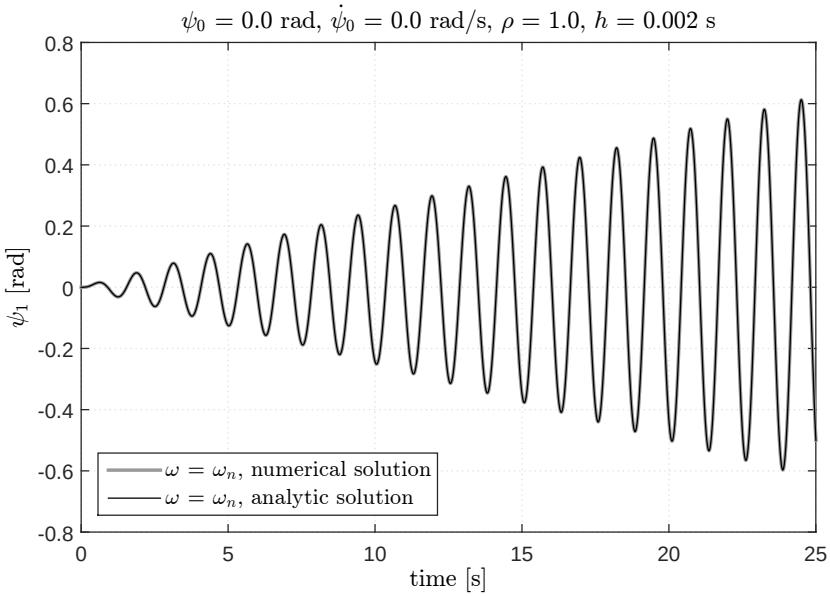

Figure B.6: Forced rotational harmonic oscillator; comparison between the numerical solution (got with the algorithm based on the mixed-frame formulation) and the exact analytic solution in the case of resonance.

B.2 Damped oscillators

In this section, the algorithm is tested against damped oscillators in order to prove the effectiveness of the approach and the reliability of the dynamic model. Both free and forced oscillations are considered. The numerical solution obtained with the time integrator based on the mixed-frame formulation is compared with the exact analytic solution.

B.2.1 Free damped harmonic oscillator

Let's consider a rigid body with a linear spring and a linear damper[12] placed in the center of mass without any external load (even the gravitational field is considered null); the features of the system and of loads are reported in Table B.4. Since the non-zero initial conditions on displacements (and rotations) and velocities include only the translational components along the x-axis, the differential problem can be reduced to the study of a one-dimensional damped oscillator. This test aims to verify if the algorithm is able to capture the motion for different damping factors.

[12] In this case both the spring and the damper should be modelled by diagonal stiffness and damping matrices.

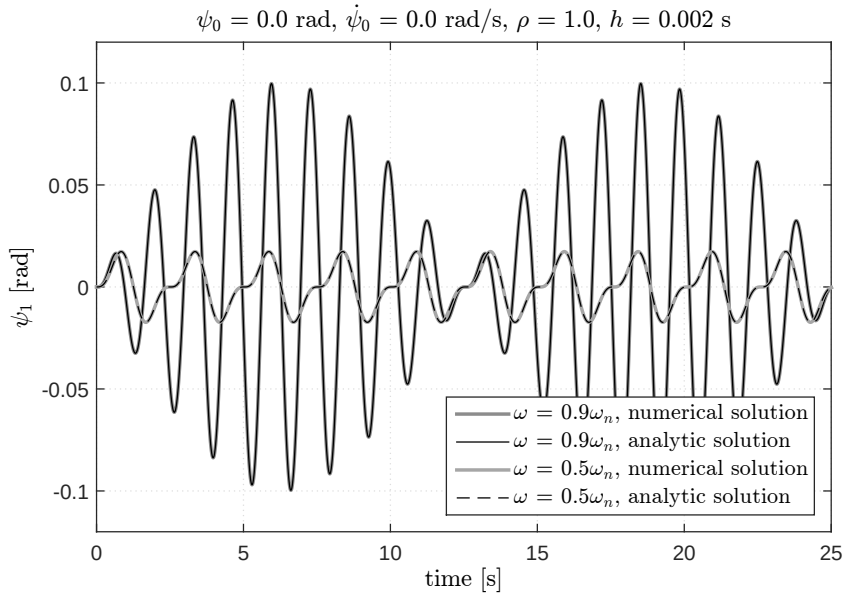

(a) below the resonance

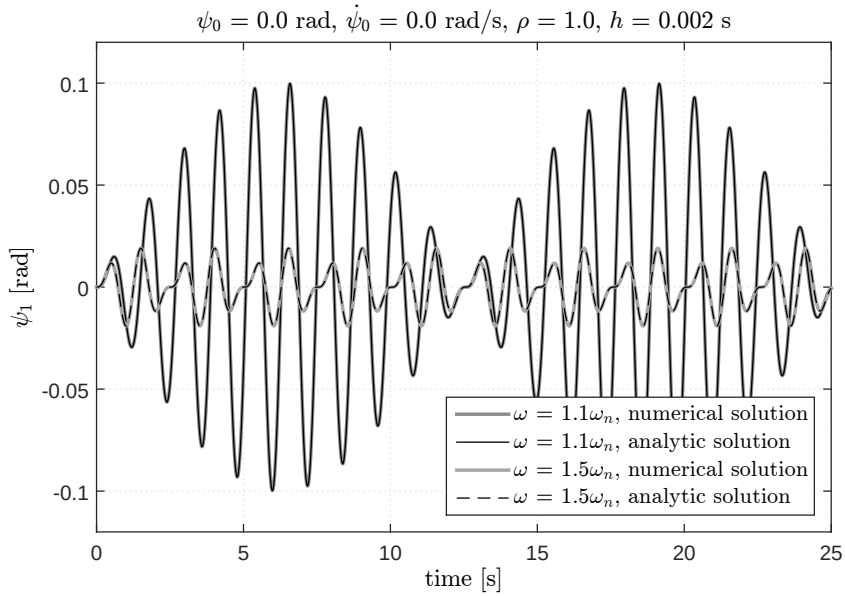

(b) above the resonance

Figure B.7: Forced rotational harmonic oscillator; comparison between the numerical solution (got with the algorithm based on the mixed-frame formulation) and the exact analytic solution for different angular frequencies of the forcing sinusoidal load.

environment		
gravity acceleration, g	0.00	m/s^2
rigid body		
mass, m	1.0	kg
natural angular frequency, ω_n	$\pi/5$	rad/s
damping factor, ν	variable	-
loads		
stiffness, $B^{\mathbf{q}}_{11}$	$m\omega_n^2$	N/m
damping, $B^{\mathbf{v}}_{11}$	$2\nu\omega_n m$	N·s/m
initial conditions		
displacement, $\hat{q}_1\|_{t=0}$	1.0	m
velocity, $\hat{v}_1\|_{t=0}$	0.0	m/s

Table B.4: Free damped harmonic oscillator; parameters used for the analysis.

B.2.1.1 Analytic solution

As mentioned before, the six-dimensional differential problem can be reduced to a simple free damped harmonic oscillator along the x-axis. The initial value problem is given by:

$$m\ddot{x}_{G,1} + C^t_{11}\dot{x}_{G,1} + K^t_{11}x_{G,1} = 0 \tag{B.19}$$

$$x_{G,1}|_{t=0} = x_0, \qquad \dot{x}_{G,1}|_{t=0} = \dot{x}_0 = 0 \tag{B.20}$$

The translational stiffness, the damping[13], and the mass of the system identify the (undamped) natural angular frequency ω_n and the damping factor ν, namely:

$$\omega_n = \sqrt{\frac{K^t_{11}}{m}} \tag{B.21}$$

$$\nu = \frac{C^t_{11}}{2m\omega_n} \tag{B.22}$$

Depending on the damping factor, the exact analytic solution of the differential problem is given by [36]:

$$\begin{aligned} x_{G,1} = {} & \frac{x_0}{2\sqrt{\nu^2-1}}\Big[(-\nu+\sqrt{\nu^2-1})e^{-\sqrt{\nu^2-1}\omega_n t}+ \\ & +(\nu+\sqrt{\nu^2-1})e^{\sqrt{\nu^2-1}\omega_n t}\Big]e^{-\nu\omega_n t} \qquad \text{if} \quad \nu>1 \end{aligned} \tag{B.23}$$

$$x_{G,1} = x_0 e^{-\omega_n t}(1+\omega_n t) \qquad \text{if} \quad \nu = 1 \tag{B.24}$$

$$\begin{aligned} x_{G,1} = {} & x_0 e^{-\nu\omega_n t}\Big[\cos(\omega_n\sqrt{1-\nu^2}t)+ \\ & +\frac{\nu}{\sqrt{1-\nu^2}}\sin(\omega_n\sqrt{1-\nu^2}t)\Big] \qquad \text{if} \quad \nu<1 \end{aligned} \tag{B.25}$$

[13]The stiffness and the damping can be modelled respectively as a linear transformation of the displacement, i.e. $K^t_{11} \equiv B^{\mathbf{q}}_{11}$, and as a linear transformation of the velocity, i.e. $C^t_{11} \equiv B^{\mathbf{v}}_{11}$.

environment		
gravity acceleration, g	0.00	m/s^2
rigid body		
mass, m	1.0	kg
natural angular frequency, ω_n	π	rad/s
damping factor, ν	0.3	-
loads		
stiffness, $B^{\mathbf{q}}_{11}$	$m\omega_n^2$	N/m
damping, $B^{\mathbf{v}}_{11}$	$2\nu\omega_n m$	N·s/m
force, $F^f_{G,1}$	$\sin(2\omega_n t)$	N
initial conditions		
displacement, $\hat{q}_1\|_{t=0}$	0.0	m
velocity, $\hat{v}_1\|_{t=0}$	0.0	m/s

Table B.5: Forced damped harmonic oscillator; parameters used for the analysis.

B.2.1.2 Results

The time integrator (see Figure B.8(a)) properly predicts the exact analytic solution regardless of the damping, confirming once more the effectiveness of the numerical approach and of the algorithm. Depending on the damping factor (see Figure B.8(b)), the free oscillator exhibits different behaviours. If $\nu > 1$ (over-damping), the displacement tends asymptotically to zero without oscillating, as quickly as the damping factor is closer to one. If $\nu = 1$, the system is critically damped. If $\nu < 1$ (under-damping), the system oscillates with amplitudes that decrease to zero with time.

B.2.1.3 Remarks

The time integration scheme used to solve the differential problem is able to well describe the motion of a free damped system independently of the damping factor. Further tests revealed that the presence of damping improve the stability of the algorithm, which can be considered reliable in a wide range of operational states.

B.2.2 Forced damped harmonic oscillator

Let's consider a rigid body with a linear spring and a linear damper placed in the center of mass and forced by a follower sinusoidal force, without any other external load (even the gravitational field is considered null), in the case of natural initial conditions; the features of the system and of loads are reported in Table B.5. The particular initial and boundary conditions make the system translate along the x-axis without rotating, and therefore the differential problem can be reduced to the study of a one-dimensional damped oscillator. This test aims to verify if the algorithm is able to properly describe the motion of forced damped systems.

B.2.2.1 Analytic solution

As previously explained, the six-dimensional differential problem can be reduced to a simple forced damped harmonic oscillator along the x-axis. The initial value problem

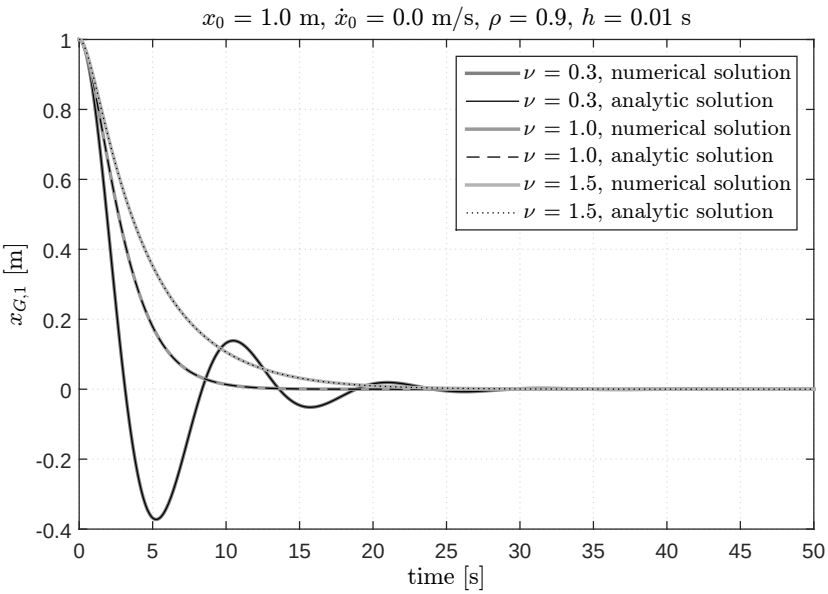

(a) trajectories

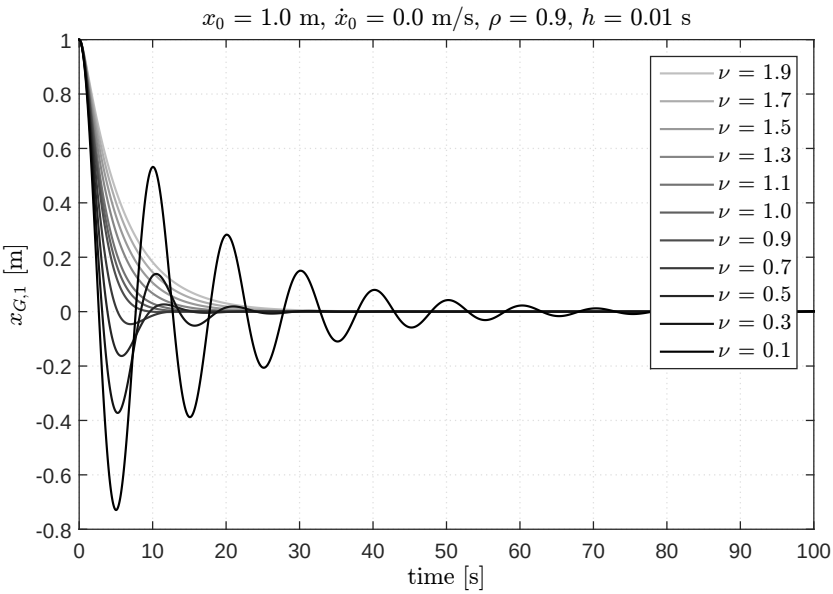

(b) numerical solution for several damping factors

Figure B.8: Free damped harmonic oscillator; comparison between the numerical solution (got with the algorithm based on the mixed-frame formulation) and the exact analytic solution for different damping factors.

is given by:

$$m\ddot{x}_{G,1} + C^t_{11}\dot{x}_{G,1} + K^t_{11}x_{G,1} = F^{\mathcal{S}}_{G,1} = F\sin(\omega t) \tag{B.26}$$

$$x_{G,1}|_{t=0} = x_0 = 0, \qquad \dot{x}_{G,1}|_{t=0} = \dot{x}_0 = 0 \tag{B.27}$$

The translational stiffness, the damping[14], and the mass of the system identify the (undamped) natural angular frequency ω_n and the damping factor ν, namely:

$$\omega_n = \sqrt{\frac{K^t_{11}}{m}} \tag{B.28}$$

$$\nu = \frac{C^t_{11}}{2m\omega_n} \tag{B.29}$$

The exact analytic solution of the differential problem is given by:

$$\begin{aligned} x_{G,1} = {} & \frac{F}{K^t_{11}\sqrt{(1-\alpha^2)^2 + 4\nu^2\alpha^2}}\sin(\omega t - \psi) + \\ & - e^{-\nu\omega_n t}\frac{F}{K^t_{11}\sqrt{(1-\alpha^2)^2 + 4\nu^2\alpha^2}}\left[\sin(-\psi)\cos(\omega_n\sqrt{1-\nu^2}t) + \right. \\ & \left. + \frac{\omega\cos(-\psi) + \nu\omega_n\sin(-\psi)}{\omega_n\sqrt{1-\nu^2}}\sin(\omega_n\sqrt{1-\nu^2}t)\right] \end{aligned} \tag{B.30}$$

$$\mathrm{tg}\psi = \frac{2\nu\alpha}{1-\alpha^2}, \qquad \alpha = \frac{\omega}{\omega_n} \tag{B.31}$$

B.2.2.2 Results

The numerical and analytic solutions are compared in terms of mean absolute error evaluated on the displacement of the center of mass $\mathbf{x}^{I,\mathcal{S}}_G$ at a set of specified times t_k, by using the Equation (3.103). The algorithm (see Figure B.9(a)), as expected, has a second-order convergence, and the numerical damping slightly modifies the accuracy of the time integrator, even if the error does not significantly change.

The trajectory of the center of mass (see Figure B.9(b)), obtained numerically, matches the exact analytic solution without any appreciable difference, and, after an initial transient due to the initial conditions (homogeneous solution), the system is only driven by the forcing load (particular solution).

B.2.2.3 Remarks

The algorithm can properly describe the motion of a translating rigid body with a satisfying level of accuracy. The numerical damping, sometime necessary, can increase the error but without significantly compromising the accuracy. The different mappings of the algorithm do not change the convergence features because they operate on translations with the same composition rule (the classic vector sum). Moreover, the algorithm was compared (not documented here) also with the Newmark method, which, in the case of no numerical damping, is definitely equivalent.

[14] As in the previous example, the stiffness and the damping can be modelled respectively as a linear transformation of the displacement, i.e. $K^t_{11} \equiv B^{\mathbf{q}}_{11}$, and as a linear transformation of the velocity, i.e. $C^t_{11} \equiv B^{\mathbf{v}}_{11}$.

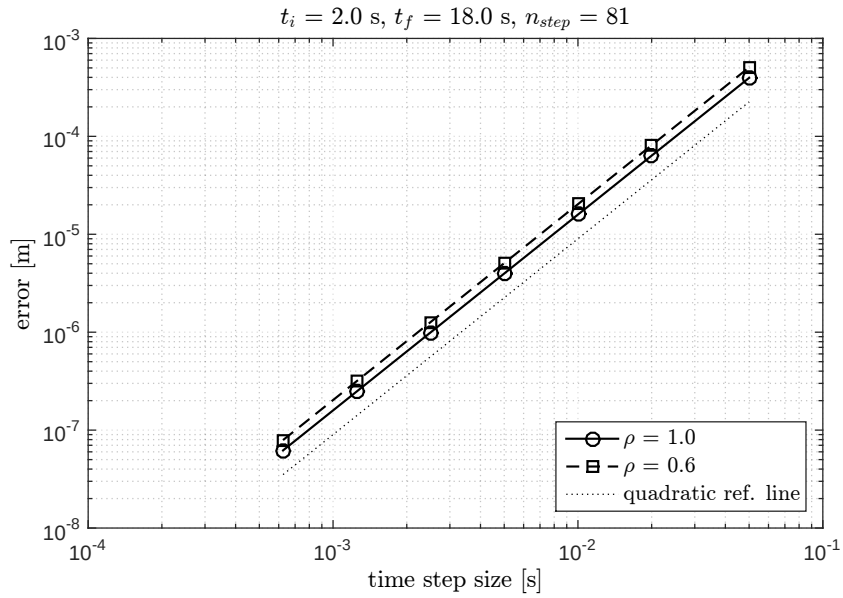

(a) error

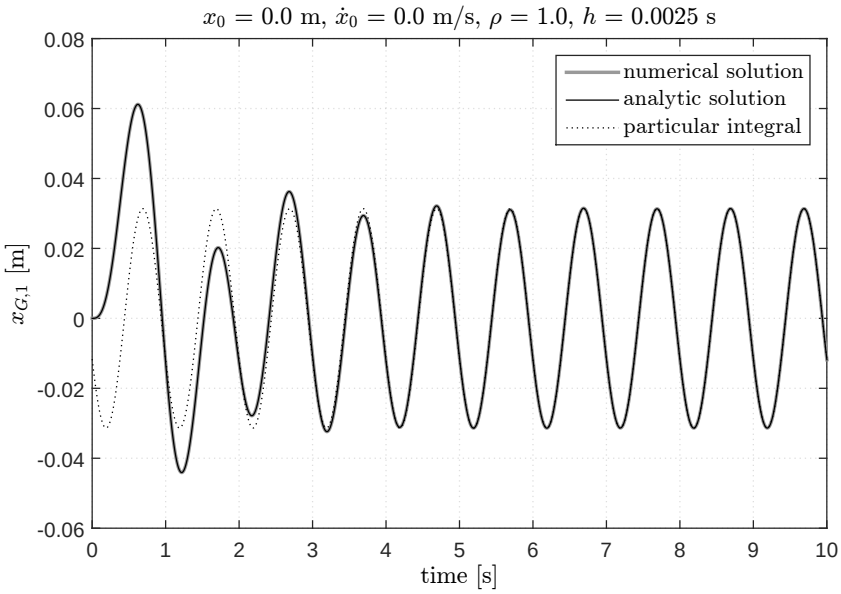

(b) trajectory

Figure B.9: Forced damped harmonic oscillator; comparison between the numerical solution (got with the algorithm based on the mixed-frame formulation) and the exact analytic solution.

Bibliography

[1] Agarwal, P., Manuel, L.: Simulation of offshore wind turbine response for extreme limit states. In: Proceedings of the 26th International Conference on Offshore Mechanics and Arctic Engineering. San Diego, California, USA (2007). Paper OMAE2007-29326

[2] Agarwal, P., Manuel, L.: Extreme loads for an offshore wind turbine using statistical extrapolation from limited field data. Wind Energy **11**, 673–684 (2008)

[3] Agarwal, P., Manuel, L.: Simulation of offshore wind turbine response for long-term extreme load prediction. Engineering Structures **31**, 2236–2246 (2009)

[4] Agarwal, P., Manuel, L.: Incorporating irregular nonlinear waves in coupled simulation and reliability studies of offshore wind turbines. Applied Ocean Research **33**, 215–227 (2011)

[5] ANSYS: Aqwa Theory Manual (2013). Release 15.0

[6] Berner, P., Toms, R., Trott, K., Mamaghani, F., Shen, D., Rollins, C., Powell, E.: Technical concepts - orientation, rotation, velocity and acceleration, and the SRM. Tech. rep., SEDRIS (2008)

[7] Bertin, A., Poli, M., Vitale, A.: Fondamenti di Meccanica. Società Editrice Esculapio (1997)

[8] van den Boom, H.J.J.: Dynamic behaviour of mooring lines. Behaviour of Offshore Structures pp. 359–368 (1985)

[9] Brorsen, M.: Non-linear Waves. Department of Civil Engineering, Aalborg University (2007). DCE Lecture Notes No. 9

[10] Brüls, O., Arnold, M., Cardona, A.: Two Lie group formulations for dynamic multibody systems with large rotations. In: Proceedings of the ASME 2011 International Design Engineering Technical Conferences & Computers and Information in Engineering Conference. Washington, DC, USA (2011). Paper DETC2011-48132

[11] Brüls, O., Cardona, A.: On the use of Lie group time integrators in multibody dynamics. Journal of Computational and Nonlinear Dynamics **5**(3), 031,002 (2010)

[12] Brüls, O., Cardona, A., Arnold, M.: Numerical solution of DAEs in flexible multibody dynamics using Lie group time integrators. In: Proceedings of the First Joint International Conference on Multibody System Dynamics. Lappeenranta, Finland (2010)

[13] Brüls, O., Cardona, A., Arnold, M.: Lie group generalized-α time integration of constrained flexible multibody systems. Mechanism and Machine Theory **48**, 121–137 (2012)

[14] Burton, T., Sharpe, D., Jenkins, N., Bossanyi, E.: Wind energy handbook. John Wiley & Sons (2001)

[15] Butterfield, S., Musial, W., Jonkman, J., Sclavounos, P.: Engineering challenges for floating offshore wind turbines. Conference Paper NREL/CP-500-38776, National Renewable Energy Laboratory, Golden, Colorado (2007)

[16] Cardona, A., Geradin, M.: A beam finite element non-linear theory with finite rotations. International Journal for Numerical Methods in Engineering **26**, 2403–2438 (1988)

[17] Celledoni, E., Marthinsen, H., Owren, B.: An introduction to Lie group integrators - basics, new developments and applications. Journal of Computational Physics **257**, 1040–1061 (2014)

[18] Celledoni, E., Owren, B.: Lie group methods for rigid body dynamics and time integration on manifolds. Computer Methods in Applied Mechanics and Engineering **192**, 421–438 (2003)

[19] Chandler, B.D., Hinwood, J.B.: Combined wave-current forces on horizontal cylinders. In: Coastal Engineering 1982, pp. 2171–2188 (1982)

[20] Chen, J.Q., Ping, J., Wang, F.: Group Representation Theory for Physicists, second edn. World Scientific (2002)

[21] Cheng, P.W., van Bussel, G.J.W., van Kuik, G.A.M., Vugts, J.H.: Reliability-based design methods to determine the extreme response distribution of offshore wind turbines. Wind Energy **6**, 1–22 (2003)

[22] Chung, J., Hulbert, G.M.: A time integration algorithm for structural dynamics with improved numerical dissipation: The generalized-α method. Journal of Applied Mechanics **60**, 371–375 (1993)

[23] Cordle, A.: State-of-the-art in design tools for floating offshore wind turbines. Deliverable report UpWind_WP4_D4.3.5_Floating design tools (2010)

[24] Cummins, W.E.: The impulse response function and ship motions. Schiffstechnik **9**, 101–109 (1962)

[25] Dean, R.G., Dalrymple, R.A.: Water Wave Mechanics for Engineers and Scientists. World Scientific (1991)

[26] DNV-OS-J101: Design of Offshore Wind Turbine Structures. Det Norske Veritas (2011)

[27] DNV/Risø: Guidelines for Design of Wind Turbines, second edn. Det Norske Veritas and Wind Energy Department, Risø National Laboratory (2002)

[28] EWEA: Wind in power: 2015 European statistics. Report, The European Wind Energy Association (2016)

[29] Faltinsen, O.M.: Sea Loads on Ships and Offshore Structures. Cambridge University Press (1990)

[30] Fitzwater, L.M., Cornell, C.A., Veers, P.S.: Using environmental contours to predict extreme events on wind turbines. In: Wind Energy Symposium, AIAA/ASME, pp. 244–258. Reno, Nevada, USA (2003)

[31] Fogle, J., Agarwal, P., Manuel, L.: Towards an improved understanding of statistical extrapolation for wind turbine extreme loads. Wind Energy **11**, 613–635 (2008)

[32] Fossen, T.I.: A nonlinear unified state-space model for ship maneuvering and control in a seaway. International Journal of Bifurcation and Chaos **15**, 2717–2746 (2005)

[33] Fossen, T.I., Smogeli, Ø.N.: Nonlinear time-domain strip theory formulation for low-speed manoeuvring and station-keeping. Modeling, Identification and Control **25**(4), 201–221 (2004)

[34] Freudenreich, K., Argyriadis, K.: Wind turbine load level based on extrapolation and simplified methods. Wind Energy **11**, 589–600 (2008)

[35] Garza-Rios, L.O., Bernitsas, M.M., Nishimoto, K.: Catenary Mooring Lines with Nonlinear Drag and Touchdown. Department of Naval Architecture and Marine Engineering, University of Michigan (1997). No. 333

[36] Gavarini, C.: Dinamica delle strutture. ESA (1986)

[37] Géradin, M., Cardona, A.: Flexible Multibody Dynamics: A Finite Element Approach. John Wiley & Sons (2001)

[38] GWEC: Global wind report: annual market update 2015. Report, Global Wind Energy Council (2016)

[39] Hansen, M.O.L.: Aerodynamics of wind turbines, second edn. Earthscan (2008)

[40] Hansen, M.O.L., Sørensen, J.N., Voutsinas, S., Sørensen, N., Madsen, H.A.: State of the art in wind turbine aerodynamics and aeroelasticity. Progress in Aerospace Sciences **42**(4), 285–330 (2006)

[41] IEC 61400-1: International Standard. Wind turbines - Part 1: Design requirements, third edn. International Electrotechnical Commission (2005)

[42] IEC 61400-3: International Standard. Wind turbines - Part 3: Design requirements for offshore wind turbines, first edn. International Electrotechnical Commission (2009)

[43] Jeon, S.H., Cho, Y.U., Seo, M.W., Cho, J.R., Jeong, W.B.: Dynamic response of floating substructure of spar-type offshore wind turbine with catenary mooring cables. Ocean Engineering **72**, 356–364 (2013)

[44] Jonkman, J., Matha, D.: A quantitative comparison of the responses of three floating platforms. Conference Paper NREL/CP-500-46726, National Renewable Energy Laboratory, Golden, Colorado (2010)

[45] Jonkman, J.M.: Dynamics modeling and loads analysis of an offshore floating wind turbine. Technical Report NREL/TP-500-41958, National Renewable Energy Laboratory, Golden, Colorado (2007)

[46] Jonkman, J.M.: Dynamics of offshore floating wind turbines - model development and verification. Wind Energy **12**, 459–492 (2009)

[47] Jonkman, J.M., Buhl Jr., M.L.: FAST user's guide. Technical Report NREL/EL-500-38230, National Renewable Energy Laboratory, Golden, Colorado (2005)

[48] Jonkman, J.M., Buhl Jr., M.L.: Loads analysis of a floating offshore wind turbine using fully coupled simulation: Preprint. Conference Paper NREL/CP-500-41714, National Renewable Energy Laboratory, Golden, Colorado (2007)

[49] Jonkman, J.M., Sclavounos, P.D.: Development of fully coupled aeroelastic and hydrodynamic models for offshore wind turbines: Preprint. Conference Paper NREL/CP-500-39066, National Renewable Energy Laboratory, Golden, Colorado (2006)

[50] Journée, J.M.J., Massie, W.W.: Offshore Hydromechanics, first edn. Delft University of Technology (2001)

[51] Kyozuka, Y.: 3. Non-linear hydrodynamic forces acting on two-dimensional bodies. Naval architecture and ocean engineering **21**, 23–40 (1983). From J.S.N.A. Japan Vol. 148, Dec. 1980, Vol. 149, June 1981, Vol. 150, Dec. 1981 and Vol. 152, Jan. 1983

[52] Mäkinen, J.: Critical study of Newmark-scheme on manifold of finite rotations. Computer Methods in Applied Mechanics and Engineering **191**, 817–828 (2001)

[53] Marino, E., Borri, C., Peil, U.: A fully nonlinear wave model to account for breaking wave impact loads on offshore wind turbines. Journal of Wind Engineering and Industrial Aerodynamics **99**(4), 483–490 (2011)

[54] Marino, E., Lugni, C., Borri, C.: A novel numerical strategy for the simulation of irregular nonlinear waves and their effects on the dynamic response of offshore wind turbines. Computer Methods in Applied Mechanics and Engineering **255**, 275–288 (2013)

[55] Marino, E., Lugni, C., Borri, C.: The role of the nonlinear wave kinematics on the global responses of an OWT in parked and operating conditions. Journal of Wind Engineering and Industrial Aerodynamics **123**, 363–376 (2013)

[56] Marino, E., Nguyen, H., Lugni, C., Manuel, L., Borri, C.: Irregular nonlinear wave simulation and associated loads on offshore wind turbines. Journal of Offshore Mechanics and Arctic Engineering **137**(2), 021,901 (2015)

[57] Masciola, M., Jonkman, J., Robertson, A.: Implementation of a multisegmented, quasi-static cable model: Preprint. Conference Paper NREL/CP-5000-57812, National Renewable Energy Laboratory, Golden, Colorado (2013)

[58] Matha, D.: Model development and loads analysis of an offshore wind turbine on a tension leg platform, with a comparison to other floating turbine concepts: April 2009. Subcontract Report NREL/SR-500-45891, National Renewable Energy Laboratory, Golden, Colorado (2010)

[59] Mavrakos, S.A., Papazoglou, V.J., Triantafyllou, M.S., Hatjigeorgiou, J.: Deep water mooring dynamics. Marine Structures **9**, 181–209 (1996)

[60] McIver, M.: Second-order wave diffraction in two dimensions. Applied Ocean Research **16**, 19–25 (1994)

[61] Montefusco, L.: Lezioni di idraulica. Pitagora Editrice Bologna (2005)

[62] Moriarty, P.: Database for validation of design load extrapolation techniques. Wind Energy **11**, 559–576 (2008)

[63] Moriarty, P.J., Holley, W.E., Butterfield, S.P.: Extrapolation of extreme and fatigue loads using probabilistic methods. Technical Report NREL/TP-500-34421, National Renewable Energy Laboratory, Golden, Colorado (2004)

[64] Müller, A., Terze, Z.: Is there an optimal choice of configuration space for Lie group integration schemes applied to constrained MBS? In: Proceedings of the ASME 2013 International Design Engineering Technical Conferences & Computers and Information in Engineering Conference. Portland, OR, USA (2013). Paper DETC2013-12151

[65] Musial, W., Butterfield, S., Boone, A.: Feasibility of floating platform systems for wind turbines: Preprint. Conference Paper NREL/CP-500-34874, National Renewable Energy Laboratory, Golden, Colorado (2003)

[66] Newman, J.N.: Marine Hydrodynamics. The MIT Press (1977)

[67] NREL: Wind power today. Brochure, U.S. Department of Energy, Energy Efficiency and Renewable Energy (2006)

[68] Perez, T.: Ship Motion Control: Course Keeping and Roll Stabilisation Using Rudder and Fins. Springer (2005)

[69] Perez, T., Fossen, T.I.: Kinematic models for manoeuvring and seakeeping of marine vessels. Modeling, Identification and Control **28**(1), 19–30 (2007)

[70] Philippe, M., Babarit, A., Ferrant, P.: Modes of response of an offshore wind turbine with directional wind and waves. Renewable Energy **49**, 151–155 (2013)

[71] Qiao, D., Ou, J.: Mooring line damping estimation for a floating wind turbine. The Scientific World Journal **2014** (2014)

[72] Roald, L., Jonkman, J., Robertson, A., Chokani, N.: The effect of second-order hydrodynamics on floating offshore wind turbines. Energy Procedia **35**, 253–264 (2013)

[73] Romano, M.: Exact analytic solution for the rotation of a rigid body having spherical ellipsoid of inertia and subjected to a constant torque. Celestial Mechanics and Dynamical Astronomy **100**, 181–189 (2008). Online version with Errata Corrige

[74] Romano, M.: Exact analytic solutions for the rotation of an axially symmetric rigid body subjected to a constant torque. Celestial Mechanics and Dynamical Astronomy **101**, 375–390 (2008). Online version with Errata Corrige

[75] Saranyasoontorn, K., Manuel, L.: Efficient models for wind turbine extreme loads using inverse reliability. Journal of Wind Engineering and Industrial Aerodynamics **92**(10), 789–804 (2004)

[76] Saranyasoontorn, K., Manuel, L.: On assessing the accuracy of offshore wind turbine reliability-based design loads from the environmental contour method. In: Proceedings of The Fourteenth International Offshore and Polar Engineering Conference, pp. 128–135. Toulon, France (2004)

[77] Sarpkaya, T., Isaacson, M.: Mechanics of Wave Forces on Offshore Structures. Van Nostrand Reinhold Company (1981)

[78] Shao, Y.L.: Numerical potential-flow studies on weakly-nonlinear wave-body interactions with/without small forward speeds. PhD dissertation (2010). NTNU, Norwegian University of Science and Technology

[79] Shao, Y.L., Faltinsen, O.M.: Fully-nonlinear wave-current-body interaction analysis by a harmonic polynomial cell method. Journal of Offshore Mechanics and Arctic Engineering **136**(3), 031,301 (2014)

[80] Shao, Y.L., Faltinsen, O.M.: A harmonic polynomial cell (HPC) method for 3D Laplace equation with application in marine hydrodynamics. Journal of Computational Physics **274**, 312–332 (2014)

[81] Sharma, J.N., Dean, R.G.: Second-order directional seas and associated wave forces. Society of Petroleum Engineers Journal pp. 129–140 (1981)

[82] Simo, J.C.: A finite strain beam formulation. The three-dimensional dynamic problem. Part I. Computer Methods in Applied Mechanics and Engineering **49**, 55–70 (1985)

[83] Simo, J.C., Vu-Quoc, L.: A three-dimensional finite-strain rod model. Part II: computational aspects. Computer Methods in Applied Mechanics and Engineering **58**, 79–116 (1986)

[84] Simo, J.C., Vu-Quoc, L.: On the dynamics in space of rods undergoing large motions - a geometrically exact approach. Computer Methods in Applied Mechanics and Engineering **66**, 125–161 (1988)

[85] Song, J.b.: Second-order solutions for random interfacial waves under steady uniform currents. China Ocean Engineering **19**(2), 333–338 (2005)

[86] Sonneville, V.: A geometric local frame approach for flexible multibody systems. PhD dissertation (2015). Aerospace and Mechanical Engineering Department, Multibody and Mechatronic Systems Lab, Université de Liège

[87] Sonneville, V., Cardona, A., Brüls, O.: Geometrically exact beam finite element formulated on the special Euclidean group SE(3). Computer Methods in Applied Mechanics and Engineering **268**, 451–474 (2014)

[88] Sun, J.L., Wang, C.Z., Wu, G.X., Khoo, B.C.: Fully nonlinear simulations of interactions between solitary waves and structures based on the finite element method. Ocean Engineering **108**, 202–215 (2015)

[89] Terze, Z., Zlatar, D., Müller, A.: Numerical integration algorithm in Lie-group setting for dynamics of mechanical systems. In: Proceedings of 7th International Congress of Croatian Society of Mechanics (7ICCSM 2012). Zadar, Croatia (2012)

[90] Tjavaras, A.A.: The dynamics of highly extensible cables. PhD dissertation (1996). Massachusetts Institute of Technology

[91] Tjavaras, A.A., Zhu, Q., Liu, Y., Triantafyllou, M.S., Yue, D.K.P.: The mechanics of highly-extensible cables. Journal of Sound and Vibration **213**(4), 709–737 (1998)

[92] Vantorre, M.: Third-order theory for determining the hydrodynamic forces on axisymmetric floating or submerged bodies in oscillatory heaving motion. Ocean Engineering **13**(4), 339–371 (1986)

[93] Vernon, T.A., Bara, B., Hally, D.: A surface panel method for the calculation of added mass matrices for finite element models. Technical Memorandum 88/203, Defence Research Establishment Atlantic (1988)

[94] Winterstein, S.R., Ude, T.C., Cornell, C.A., Bjerager, P., Haver, S.: Environmental parameters for extreme response: Inverse FORM with omission factors. In: Proceedings of the ICOSSAR-93. Innsbruck, Austria (1993)

[95] Yang, N., Jeng, D.S., Zhou, X.L.: Tension analysis of submarine cables during laying operations. The Open Civil Engineering Journal **7**, 282–291 (2013)

[96] Yang, Z., Liu, S., Bingham, H.B., Li, J.: Second-order coupling of numerical and physical wave tanks for 2D irregular waves. Part I: Formulation, implementation and numerical properties. Coastal Engineering **92**, 48–60 (2014)

[97] Yang, Z., Liu, S., Bingham, H.B., Li, J.: Second-order coupling of numerical and physical wave tanks for 2D irregular waves. Part II: Experimental validation in two-dimensions. Coastal Engineering **92**, 61–74 (2014)

Vita

"...davanti allo schermo per un'ora,
davanti allo schermo per una vita,
davanti allo schermo per sognare
un mondo che non esiste
ma che si continua inesorabilmente a cercare
come se fosse il primo pensiero
evadere dall'oggi per un domani."

Alessandro Giusti

Alessandro Giusti was born in Figline Valdarno, Italy, on the 30$^{\text{th}}$ of January 1986, and he has lived in Reggello, Italy, since he was born. He graduated from the University of Florence, receiving the Bachelor's degree (*Laurea*) in Civil Engineering on the 16$^{\text{th}}$ of April 2009, and the Master's degree (*Laurea Specialistica*) in Civil Engineering on the 4$^{\text{th}}$ of April 2011. He entered the International Doctoral program joint between the University of Florence and the Technische Universität Braunschweig in 2012.